THE UNIVERSITY
of EDINBURGH

Schwann cell pathology in spinal muscular atrophy (SMA)

Arwin Aghamaleky Sarvestany

A thesis submitted for the degree of Doctor of Philosophy

The University of Edinburgh

2014

Declaration

I declare that the work described in this thesis and its composition are entirely my own.

…….

Arwin Aghamaleky sarvestany

Acknowledgments

There are many people that I would like to thank for supporting me during my PhD time.

I would like firstly to thank my supervisor Prof Tom Gillingwater for believing me and giving me the opportunity to work in his lab. I really appreciate all the support and motivation he has given me, along with all of his ideas for this project. My PhD project would not have been possible without his support and advice over the last two years.

I would like to thank Dr Gillian Hunter for always being motivational and answering all my questions. I would also like to thank other Gillingwater's lab members for being such nice colleagues and make my time in the lab so enjoyable. I would like to especially thank Eilidh, Sarah, Sophie, Rachael and Ross who helped me to do the proof reading for this thesis.

I would like to thank Dr Tom Wishart and his group members for their help with proteomic analysis.

A very special thanks goes to my husband Amir for his sacrifices, helping me all through my academic and personal life. Without his support, I would not able to finish my PhD. There is no word to explain my appreciation to what he did for me.

And last but not least, I would like to thank my parents and my brothers and sister for always being supportive. I would like to thank my father for always being my inspiration and giving me the opportunity to continue my studies abroad. I would

also like to thank my mother for listening to my stories and always giving me motivation in hard times.

Abstract

The childhood neuromuscular disease spinal muscular atrophy (SMA) is caused by low levels of survival motor neuron (SMN) protein. Historically, SMA has been characterised as a disease primarily affecting lower motor neurons. However, recent breakthroughs have revealed defects in other non-neuronal cells and tissues. *In vivo* analysis of peripheral nerve showed defects in Schwann cells, manifesting as abnormal myelination and delayed maturation of axo-glia interactions. The experiments in this thesis were designed to build on these observations and examine whether Schwann cell defects are intrinsic and occur as a primary result of low levels of SMN in that cell type, or rather represent a secondary consequence of pathology in neighbouring motor neurons.

I initially developed a protocol to allow isolation of high-yields of purified, myelination-competent Schwann cells from 'Taiwanese' SMA mice. SMA-derived Schwann cells had significantly reduced SMN levels and failed to respond normally to differentiation cues. Increasing SMN levels restored myelin protein expression in Schwann cells from SMA mice. Perturbations in expression of key myelin proteins were likely due to failure of protein translation and/or stability rather than transcriptional defects. Co-cultures of healthy neurons with SMA Schwann cells revealed a significant reduction in myelination compared to cultures where wild-type Schwann cells were used. The presence of SMA Schwann cells also disrupted neurite stability. Perturbations in the expression of key extracellular matrix proteins, such as laminin $\alpha 2$, in SMA-derived Schwann cells suggests that Schwann cells were influencing neurite stability by modulating the composition of the extracellular matrix.

Previous studies have demonstrated that low levels of SMN lead to disruption of ubiquitin homeostasis and decreased expression of ubiquitin-like modifier activating enzyme (UBA1) in the neuromuscular system, driving neuromuscular pathology via a beta-catenin dependent pathway. Label-free proteomics analysis of SMA and control Schwann cells identified 195 proteins with modified expression profiles. Bioinformatic analysis of these proteins using Ingenuity Pathway Analysis (IPA) software confirmed that major disruption of protein ubiquitination pathways was also present in Schwann cells from SMA mice. Immunolabeling and proteomics data both revealed that UBA1 levels were significantly reduced in SMA-derived Schwann cells. However, loss of UBA1 in Schwann cells did not lead to downstream modifications in beta-catenin pathways. Pharmacological inhibition of UBA1 in healthy Schwann cells was sufficient to induce defects in myelin protein expression, suggesting that UBA1 defects contribute directly to Schwann cell disruption in SMA.

I conclude that low levels of SMN induce intrinsic defects in Schwann cells, mediated at least in part through disruption to ubiquitination pathways.

Table of Contents

List of Figures

List of tables

List of Abbreviations

2'-O-dibutyryladenosine 3': 5' cyclic monophosphate	dbcAMP
β1 integrin	ITGB1
Acetylcholine receptor	AChR
Acid ceramidase	ASAH1
Adenomatous polyposis coli	APC
Amyotrophic lateral sclerosis	ALS
Angiogenin	ANG
Antisense oligonucleotide	ASO
Blood brain barrier	BBB
Brain 2 class III POU-domain protein	BRN2
Brain-derived neurotrophic factor	BDNF
Cardiotrophin-1	CT-1
Caspase 3	CASP3
Central nervous system	CNS
Charcot-Marie-Tooth disease	CMT
Ciliary neurotrophic factor	CNTF
Cyclic adenosine monophosphate	cAMP
Dystrophin related protein-2	DRP2
Dishevelled 2	Dvl2
Dorsal root ganglion	DRG
Dulbecco's modified eagle medium	DMEM
Dystroglycan	DG
Early growth response 2	EGR2/Krox20
Exonic splicing enhancer	ESE
Extracellular matrix	ECM

Geneticin	G418
Glial cell line-derived growth factor	GDNF
Glial fibrillary acidic protein	GFAP
Glycogen synthase kinase-3	GSK3
Hanks balanced salt solution	HBSS
Heat shock protein	HSP
Histone deacetylase inhibitor	HDACi
Horse serum	HS
Human leucocyte-associated antigen A, B, C complement	HLA-ABC
Ingenuity Pathway Analysis	IPA
Insulin-like growth factor 1	IGF-1
Intronic splicing silencer N1	ISS-N1
Inverted formin-2	INF2
Isobaric Tags for Relative and Absolute Quantitation	iTRAQ
Laminin α2	LAMA2
Liquid chromatography–mass spectrometry	LC-MS
Malic enzyme 1	ME1
Bone Morphogenetic protein	BMP
Murine/human survival motor neuron gene/protein	*Smn/SMN*/SMN
Myelin associated glycoprotein	MAG
Myelin basic protein	MBP
Myelin protein zero	MPZ
Nectin-like family	Necl
Nerve growth factor	NGF
Neural precursor cell expressed developmentally down-regulated gene 4	NEDD4
Neuregulin 1	NRG1
Neuromuscular junction	NMJ

Neurosphere-derived neural stem cell	NSC
Neurotrophin-3	NT-3
Nucleolar ribonucleoprotein	snoRNP
Peripheral myelin protein 22	PMP22
Peripheral nervous system	PNS
Phosphatase and tensin homolog deleted on chromosome ten	PTEN
Phosphatidylinositol-3	PI3
Plastin-3	PLS3
Poly-L-lysine	PLL
POU class III homeobox 1	POU3f1/OCT6
Protein-RNA complexes	RNPs
Protein/synaptobrevin-associated membrane protein B	VABP
Reactive oxygen species	ROS
Ribonucleoproteins	snRNPs
Schwann cell precursor	SCP
Schwann cell	SC
Self-complimentary adeno-associated virus 9	scAAV 9
Senataxin	SETX
Spinal muscular atrophy	SMA
Splicing factor 2/ alternative splicing factor	SF2/ASF
SRY (sex determining region Y) box10	SOX10
SRY (sex determining region Y) box2	SOX2
Superoxide dismutase 1 gene	SOD1
transformer-2 protein homolog ß	hTra2ß1
Trichostatin A	TSA
Ubiquitin carboxyl-terminal esterase L1	UCHL1
Ubiquitin-like modifier activating enzyme 1	UBA1

Ubiquitin-proteasome system	UPS
X-linked spinal muscular atrophy	SMAX2

Chapter 1: Introduction

1.1 Spinal muscular atrophy

The term "lower motor neuron" refers to a group of neurons whose cell bodies are located in the spinal cord of the central nervous system (CNS) and whose axons project into peripheral nerves to reach target muscles (Figure 1.1). Degeneration of these motor neurons causes muscle weakness, which is normally progressive and leads to paralysis or death in severe cases (Rezania & Roos, 2013).

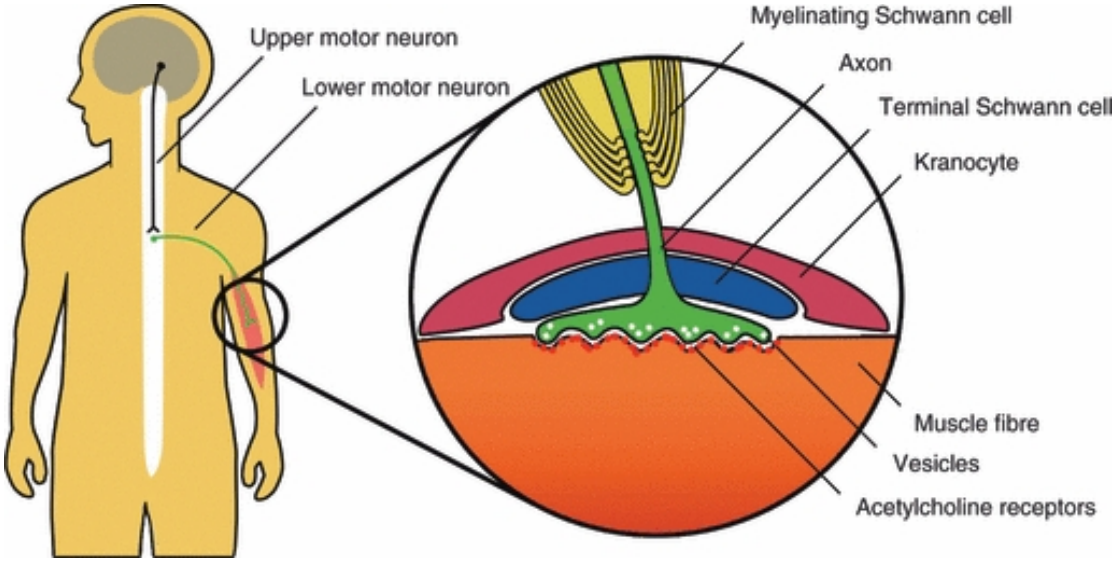

Figure 1.1 Lower motor neuron and neuromuscular junction (NMJ). Figure taken from (Thomson *et al*., 2012) to show how lower motor neurons connect the central nervous system to target muscle fibres. Upper motor neurons synapse onto lower motor neurons in the spinal cord. Lower motor neurons then send their axons out to target skeletal musculature via peripheral nerves. Once a lower motor neuron axon has reached its target muscle (magnified box) it will form neuromuscular synapses with individual muscle fibres. The motor nerve terminal (green) makes up the presynaptic component of the NMJ, and features numerous synaptic vesicles containing the neurotransmitter acetylcholine. The postsynaptic muscle fibre (orange) is also specialised, with accumulations of acetylcholine receptors at the motor endplate (red). The motor nerve terminal is insulated by one or more terminal Schwann cells (blue). A second 'NMJ capping cell'– the kranocyte – also overlies the terminal Schwann cell (pink).

Examples of the most common motor neuron diseases are amyotrophic lateral sclerosis (ALS), which is characterised by degeneration of both upper and lower

motor neurons, and autosomal-recessive spinal muscular atrophy (SMA) that primarily affects lower motor neurons (Lefebvre *et al*., 1995; Bäumer *et al*., 2014). SMA, a predominantly childhood form of motor neuron disease, was first described by Werdnig and Hoffmann in the 1890s. It is the most common genetic cause of infant mortality, with an estimated incidence of around 1 in 6,000 to 1 in 10,000 live births and a carrier frequency of 1 in 50 (Lefebvre *et al*., 1995; Ogino *et al*., 2002).

1.1.2 Clinical classification

SMA is classified into four clinical sub-types based on age of onset and motor functions achieved (Munsat & Davies, 1992). Type I SMA (also known as Werdnig-Hoffmann disease) is the most severe and common type with onset ranging from the prenatal period to the first 6 months of age. Patients never acquire the ability to sit unsupported and they have severe hypotonia, often with no head control and an impaired breathing pattern (Dubowitz, 1999). In the most severe cases, with perinatal onset, reduced intrauterine movement, joint contractures at birth, congenital bone fractures and chest deformities have been observed (Felderhoff-Mueser *et al*., 2002). Patients rarely survive beyond 2 years of age without intervention (D'Amico *et al*., 2011).

Type II SMA is characterised by onset between 7-18 months of age (D'Amico *et al*., 2011). Patients are able to sit unaided, but they do not acquire the ability to walk independently. Joint contractures and kyphoscoliosis, the abnormal curvature of the spine in coronal and sagittal plane, are very common. Chewing ability is affected by weakness of masticatory muscles (D'Amico *et al*., 2011; Haaker & Fujak, 2013).

SMA type III (also known as Kugelberg-Walender disease) is a milder SMA phenotype with the onset after 18 months of age. Patients typically achieve all major motor milestones including independent walking. Based on severity some might need a wheelchair, while others are able to walk and live relatively normal adult lives. However, some patients also develop scoliosis and poor mobility disorders, which leads to obesity and osteoporosis (D'Amico *et al*., 2011; Haaker & Fujak, 2013).

SMA type IV is not a childhood form of the disease with an incidence of <0.5/10000 (Liu *et al*., 2011). Onset occurs in individuals older than 18 years of age and is inherited in either an autosomal dominant or rarely autosomal recessive manner. Adult onset autosomal dominant SMA is caused by different genetic factors from childhood SMA such as vesicle-associated membrane protein/synaptobrevin-associated membrane protein B (VABP) and senataxin (SETX) (Nishimura *et al*., 2004; Rudnik-Schöneborn *et al*., 2012). Motor impairments are mild and patients are able to walk in adulthood without respiratory and nutritional problems. Patients with this type of SMA have a normal life expectancy (D'Amico *et al*., 2011).

1.1.2 Genetics

SMA is caused by mutations in the survival motor neuron gene (*SMN* gene) (Brzustowicz *et al*., 1995). The *SMN* gene has been mapped to chromosome 5q11.2-13.3, where large-scale deletions have been identified, by linkage analysis in all three types of childhood SMA (Brzustowicz *et al*., 1995). Lefebvre *et al*. reported the precise location of the *SMN* gene within the telomeric region of chromosome 5q13, a 20 kb gene encoding a novel protein of 294 amino acids (Lefebvre *et al*., 1995). This

gene was either lacking or interrupted in the majority of SMA patients. The patients that retain this gene carry either point mutations or short deletions in the consensus splice sites of introns 6 or 7. They also found a highly homologous gene in the centromeric region of 95% of their controls (Lefebvre *et al*., 1995). There is one telomeric copy (*SMN1* gene) and several centromeric copies (*SMN2* gene) in the human genome. In SMA patients the *SMN1* gene is deleted or mutated, but at least one copy of *SMN2* is retained (Melki *et al*., 1994).

Although *SMN1* and *SMN2* encode near identical genes, it is the homozygous deletion of *SMN1* gene that causes SMA. The major difference between the two genes occurs in 5 nucleotides, with a single nucleotide C-to-T transition (at codon 280) in an exonic splicing enhancer (ESE) responsible for differential processing of *SMN1* and *SMN2* pre-mRNAs (Lorson *et al*., 1999; Monani *et al*., 1999). Exon 7 is skipped from the *SMN2* mRNA transcripts and results in the generation of an unstable version of the SMN protein, which rapidly degrades (Lorson & Androphy, 2000). However, exon 7 is not spliced out in 10% of the SMN2 mRNA transcripts, resulting in the formation of a small amount of functional, full-length SMN protein (Figure 1.2) (Lefebvre et al., 1995). Complete loss of SMN protein is fatal to all cells and tissues (Wang & Dreyfuss, 2001), but generation of the full-length SMN protein by *SMN2* gene partially compensates for the loss in SMA. The number of *SMN2* copies is variable among individuals and there is correlation between *SMN2* copy number and the severity of disease. The majority of SMA type I patients have one or two copies of the SMN2 gene, while SMA II type patients have three copies. Finally, mild SMA III type patients have 3 or four copies (Feldkötter *et al*., 2002).

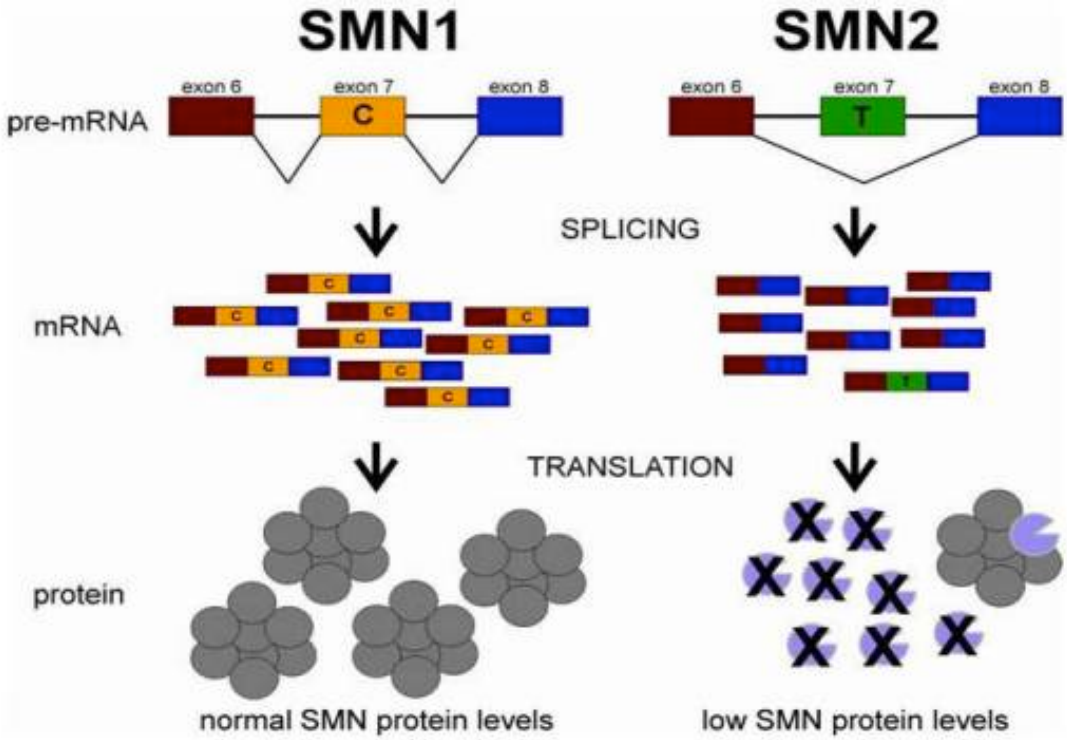

Figure 1.2 *SMN1* and *SMN2* genes, structure and splicing. *SMN1* and *SMN2* have identical gene structure and are 99.9% identical at the sequence level. The essential difference between the two genes is a single nucleotide change in exon 7 (C or T as indicated). This single nucleotide change affects the splicing of the gene. Thus, the majority of *SMN* transcripts from *SMN2* lack exon 7 whereas those from *SMN1* contain exon 7. However, because *SMN2* does produce some full-length *SMN* it can be viewed as a gene with reduced function but not loss of function. The loss of amino acids that are encoded by exon 7 results in the production of *SMN* protein with severely decreased stability. (Burghes & Beattie, 2009)

1.1.3 SMN protein function

Ubiquitous expression of SMN protein suggests it regulates fundamental activities in all cells (Burghes & Beattie, 2009). The SMN protein is a multi-functional protein, but is heavily involved in the assembly of protein-RNA complexes (RNPs) (Eggert *et al*., 2006). SMN is found both in the cell cytoplasm and nucleus, where it is highly enriched within bodies called Gems (Gubitz et al., 2004). Gems are associated with Cajal bodies (Liu & Dreyfuss, 1996), which contain high levels of factors for transcription and processing of many types of nuclear RNAs, such as small nuclear

ribonucleoproteins (snRNPs), nucleolar ribonucleoproteins (snoRNPs), and RNA polymerases (Ogg & Lamond, 2002; Gall, 2003; Gubitz *et al*., 2004). SMN forms a complex with 7 proteins called gemins in the gems. The best-characterised function of SMN is its role in assembly of snRNPs. In eukaryotes, splicing of pre-mRNA transcripts is carried out by snRNPs, which recognise the splice sites of introns and catalyse the splicing reaction to produce mature spliced mRNAs (Nilsen, 2003; Will & Lührmann, 2001). Each snRNP contains a single copy of uridine-rich small-nuclear RNAs (snRNAs) and 7 common core proteins known as Sm proteins. The SMN/gemin complex binds directly to snRNAs and Sm proteins to assemble the Sm core onto the snRNA in an ATP-dependent manner, forming snRNPs (Liu & Dreyfuss, 1996; Pellizzoni *et al*., 2002; Workman *et al*., 2012) (Figure 1.3).

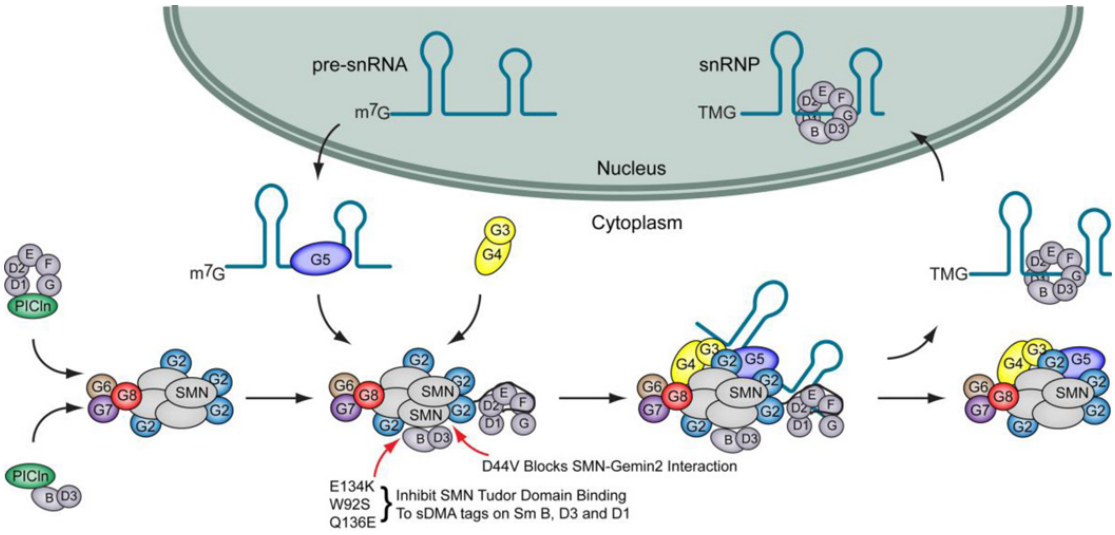

Figure 1.3 The role of SMN in snRNP biogenesis. Following transcription, snRNAs are exported to the cytoplasm where they are bound by Gemin5 and delivered to SMN for Sm core assembly. Sm proteins are methylated in the cytoplasm by PRMT5 and then transferred to pICln, which delivers them to the SMN complex. The SMN complex binds Sm proteins through at least 2 binding modes: 1) SMN binds to sDMA tails on Sm B, D1 and D3, and 2) Gemin2 recognizes the Sm-fold of the Sm D1/D2/E/F/G pentamer. Several SMA patient mutations disrupt these binding activities. SMN forms oligomers and is depicted here as a tetramer for simplicity. The SMN complex then assembles the Sm proteins into a heptameric ring on the snRNA. Assembled snRNPs are then imported into the nucleus for final maturation and function in pre-mRNA splicing (Workman *et al*., 2012).

There are also thought to be specific roles for SMN in motor neurons, the cells most severely affected in SMA. Motor axon-specific pathfindings defects have been observed in zebrafish treated with SMN-specific antisence morpholinos to knockdown SMN protein (McWhorter *et al*., 2003). *In vitro* analysis of motor neurons isolated from a transgenic SMA mouse model has shown reduced axon outgrowth compared to those isolated from wild-type mice (Rossoll *et al*., 2003). SMN has also been reported to involve in transport and trafficking of specific mRNA molecules in motor axons, such as ß-actin mRNA (Rossoll *et al*., 2003). Genome-wide analysis of RNAs present in complexes containing SMN in differentiated NCS-34 cells has identified 200 mRNAs associated with SMN. 30% of identified RNAs have been localised in axons of different neuron types and SMN depletion results in localization deficiencies of mRNAs essential for axogenesis (Rage *et al*., 2013). Furthermore, SMN accumulation has been observed in growth cones and filopodia-like structures in both neuronal- and glial-like cells, suggesting a role for SMN in neurite outgrowth and neuromuscular maturation (Fan & Simard, 2002). These potential motor neuron specific functions of SMN may partly explain the higher sensitivity of this particular cell type to SMN depletion in SMA pathology.

Reduction in SMN levels has also been reported to lead to wider peripheral nerve abnormalities in SMA human patients, including reduced conduction velocities, abnormal axonal membrane conductance and disrupted Schwann cells/myelin (Chien & Nonaka, 1989; Yonekawa *et al*., 2013; Farrar *et al*., 2011).

1.2 Peripheral nerve components and formation

Axons within peripheral nerve are projections of cell bodies located in the dorsal root ganglia (sensory neurons), autonomic ganglia (autonomic neurons) and the ventral horn of the spinal cord or brain stem (motor neurons) (Topp & Boyd, 2006). Three layers of connective tissue protect axons: the endoneurium, the perineurium, and the epineurium. Single large diameter axons are myelinated by myelinating Schwann cells. In contrast, unmyelinating Schwann cells envelop several small diameter axons (Jessen & Mirsky, 2005). Both Schwann cell types are surrounded by a basal lamina of type IV collagen, fibronectin, laminin, and heparan sulfate proteoglycan (Thomas, 1963). Between the axons is a loose connective tissue of type I and type II collagen fibrils in longitudinal orientation, fibroblasts, a few mast cells, macrophages, and endoneurial fluid. These structures are covered by endoneurium and form endoneurial compartments. Capillaries are also present within the endoneurial compartment. Bundles of axons are grouped into fascicles by epineurium and finally, nerve fascicles are held together by epineurium (Topp & Boyd, 2006) (Figure 1.4).

Motor axons are one of the major neural components of peripheral nerves. Motor neuron somas are located in the ventral horn of the spinal cord, from where their axons leave the spinal cord via ventral roots and travel through peripheral nerves to their target muscles. Upon entering the muscle region, single axons undergo intramuscular branching and ultimately innervate between 10-2000 muscle fibres. The neuromuscular junction (NMJ) is a specialised synapse that forms at the contact point of motor neuron and muscle cell (Sanes & Lichtman, 1999) (Figure 1.4).

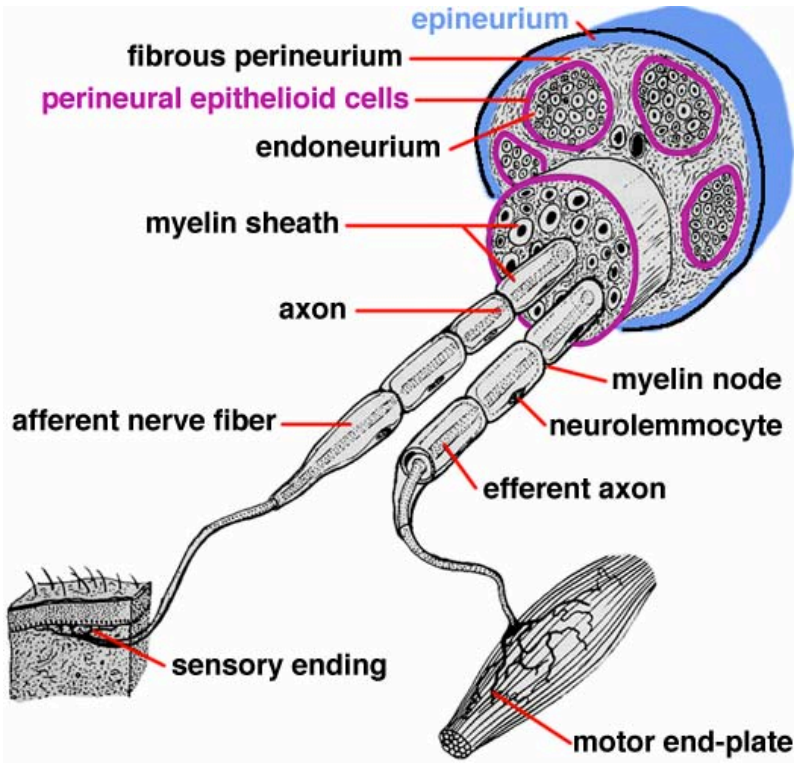

Figure 1.4 Schematic diagram of peripheral nerve. Nerves are composed of nerve fascicles (individual fascicles eventually become branches of the nerve). The entire nerve is enveloped by connective tissue called epineurium. Individual fascicles are delineated by connective tissue called perineurium. Layers of flattened mesodermal cells, called perineural epithelium (epithelioid) cells, line the perineurium and offer a protective barrier. Connective tissue inside perineural epithelium is called endoneurium. It surrounds neurolemmocytes. Axons are either myelinated or non-myelinated (not shown). The latter are ensheathed (by the dozens) by individual neurolemmocytes, in series. Individual myelinated axons are enveloped by a series of myelin internodes, each formed by a single neurolemmocyte (http://vanat.cvm.umn.edu/neurHistAtls/pages/pns1.html).

1.2.1 Motor neuron development

Lower motor neuron development and pathfinding have been shown to be disturbed in models of SMA both *in vitro* (Rossoll et al., 2003) and *in vivo* (McWhorter *et al*., 2003). Lower motor neurons originate in the ventral portion of the neural tube, with developing axons projecting into ventral roots. Growth cones located at the tip of these axonal projections are sensory and motile structures that enable axon pathfinding (Vitriol & Zheng, 2012).

Motor axons make contact with their target muscles as myoblasts are fusing to generate myotubes (Sanes & Lichtman, 1999). Synaptic transmission starts as soon as a motor axon's growth cone contacts its myotube (Sanes & Lichtman, 1999). Initially, transmission efficacy is low due to the lack of both pre- and post-synaptic specialization. At this stage, nerve terminals are bulbous enlargements containing few vesicles and no recognisable active zones. Pre-synaptic specialisations then follow increasing synaptic vesicle number, loss of axonal cytoskeletal elements, generation of active zones, clustering of vesicles at the active zones, and the polarisation of nerve terminals (Sanes & Lichtman, 1999). Stimulation of a motor axon can then lead to depolarisation of pre-synaptic membranes and an influx of Ca^{2+} into the synaptic terminal. Initially, multiple motor axons innervate skeletal muscle fibres. In the first two weeks after birth in rodents, axonal inputs compete with each other and all losing axons are removed in a process known as synapse elimination (Lichtman & Colman, 2000).

1.3 Neuromuscular pathology in SMA

SMA is characterised primarily by disruption of neuromuscular connectivity that precedes degeneration of lower motor neuron soma from the spinal cord and atrophy of skeletal muscle (Dachs *et al*., 2011). However, sensory neuron defects have also been documented (Yonekawa *et al*., 2013). Due to the lack of suitable human tissues either from biopsy or post-mortem, many groups have used animal models of SMA to study these disease processes. Several SMA mouse models have been developed because of the similarities in neuromuscular function between humans and mice (Sleigh *et al*., 2011).

1.3.1 Mouse models of SMA

Unlike humans, mice have only one copy of the *Smn* gene and homozygous deletion of this gene results in embryonic cell death before implantation (Schrank *et al*., 1997). Cre-*loxP* SMA mouse models generated from deletion of *Smn* exon 7 from a conditional allele (Smn^{F7}) produce a complete loss of cellular SMN in all target cells, thereby providing only limited information about SMA pathology (Sleigh *et al*., 2011). In order to better recapitulate the human SMA genotype, the human *SMN2* transgene has been expressed on a *Smn*-null background (Sleigh *et al*., 2011). In these mice the severity of the disease correlates directly with *SMN2* copy number, similar to what has been observed in human patients (Hsieh-Li *et al*., 2000; Feldkötter *et al*., 2002).

'Severe' mice modelling SMA, carrying one or two copies of *SMN2* transgene ($Smn^{-/-}$; $SMN2^{+/+}$), are similar to controls at birth but die before postnatal day 7 (P7) (Monani *et al*., 2000). Extended life span of SMA mice model is essential to study molecular mechanisms of SMA pathogenesis during disease progression and to recapitulate the human SMA pathogenesis. Therefore, a milder mouse model known as *SMNΔ7* ($Smn^{-/-}$; $SMN2^{+/+}$; $SMN\Delta7^{+/+}$) has been generated by inserting an additional *SMN2* gene without exon 7, called the delta7 transgene (Kerr *et al*., 2000). Another milder mouse model of SMA, known as the 'Taiwanese' SMA model, has four copies of the *SMN2* gene (two copies per allele) ($Smn^{-/-}$; $SMN2^{tg/+}$) and can survive for 12 days (Hsieh-Li *et al*., 2000; Riessland *et al*., 2010).

One alternative approach that has been shown to decrease SMN levels in mice is to have a knock-in allele that impairs endogenous *smn* splicing ($Smn^{2B/-}$), which results

in a milder phenotype with life expectancy of around 1 month (Bowerman *et al*., 2009).

1.3.2 Other SMA model organisms

Several other SMA model organisms have been generated due to the high degree of SMN gene evolutionary conservation between different species (Sleigh *et al*., 2011). Depletion of Smn-1, the ortholog of human SMN in *Caenorhabditis elegans* has been shown to induce late larval arrest, reduced lifespan as well as impaired locomotion and pharyngeal activity (Briese *et al*., 2009). *Drosophila* SMA models have been generated by point mutations in Smn similar to those found in SMA patients (Chan *et al*., 2003). These flies show abnormal motor behaviour and defects at the NMJ. The *Drosophila* SMA model has also been used to screen genetic modifiers of Smn (*drosophila SMN* ortholog) phenotype and identify new genes that previously have not been associated with Smn (Chang *et al*., 2008). SMN has been reduced using antisense morpholino in zebrafish, showing for the first time perturbations in motor axon developments *in vivo* (McWhorter *et al*., 2003). However, mouse models are probably the best model to address fundamental questions in SMA pathogenesis, due to the similarities between the neuromuscular system in humans and mice (Sleigh *et al*., 2011).

1.3.3 Motor neuron pathology in SMA

Mouse models with low levels of SMN have been instrumental in defining neuromuscular pathology in SMA. For example, functional motor deficits and degeneration of motor neurons were reported in initial studies (Monani *et al*., 2000).

Several subsequent studies using tissue from these mice reported that reduced SMN protein levels play an important role in neurodevelopmental processes of the lower motor neuron. Primary motor neurons exhibited disrupted actin dynamics in axons and growth cones, resulting in shorter neurites (Rossoll *et al*., 2003). *SMN* knockdown in PC12 cell lines also showed similar defects in cytoskeletal integrity and a subsequent disruption in neuritogenesis (Bowerman *et al*., 2007). Moreover, neurosphere-derived neural stem cells (NSCs) produced from the brains of a hypomorphic series of SMA mice displayed morphological alterations and neuronal differentiation was inhibited (Shafey *et al*., 2008). Similarly, motor neuron pathfinding is deficient in SMN-depleted zebrafish (McWhorter *et al*., 2003). However, early embryonic formation of the neuromuscular system in mice revealed no significant abnormalities in motor axon formation, axonal projection or reduction in outgrowth (McGovern *et al*., 2008). Morphological and genetic analysis of lower motor neuron connectivity in pre-symptomatic severe SMA mice showed no significant disruption in lower motor neuron prior to the onset of symptoms (Murray *et al*., 2010). Therefore SMN depletion can influence neurodevelopmental processes *in vitro* and in lower organisms, but these defects are not sufficient to induce abnormal development in mammalian lower motor neurons (Murray *et al*., 2010).

In mice, the NMJ shows the earliest signs of postnatal pathology in the neuromuscular system (Murray *et al*., 2008). In SMA mice, NMJ defects can be detected when the number of motor neuron cell bodies was not significantly reduced (Dachs *et al*., 2011). Poor terminal arborisations have been shown in two SMA mouse models as well as immature post-synaptic AChRs and intermediate filament aggregates (Kariya *et al*., 2008). Severe SMA NMJs release significant fewer

vesicles (50% reduction) from pre-synaptic terminals, which lead to NMJ functional abnormalities (Kong *et al*., 2009). A GTP-binding protein, Rab3A has been reported to be down-regulated in SMA muscles that are normally innervated (Dachs *et al*., 2011). Rab3A contributes to the targeting of synaptic vesicles to the active zones and induce neurotransmitter release in the synaptic cleft (Dachs *et al*., 2011).

NMJs in human patients have similar structural defects (Kariya *et al*., 2008). Abnormal accumulation of neurofilaments has been observed in nerve terminals of type I SMA patient's diaphragm along with smaller endplates than controls (Kariya *et al*., 2008). Another human SMA study revealed prenatal abnormalities in diaphragm development, pre-terminal accumulation of vesicles and aberrant ultrastructure of nerve terminals (Martínez-Hernández *et al*., 2013).

Widespread heterogeneity has been observed in the susceptibility of individual motor neurons to neurodegeneration in SMA mouse models (Ling *et al*., 2012; Thomson *et al*., 2012). Analysis of motor neurons innervating NMJs across a range of muscles that are affected and resistant to SMA revealed no significant difference in morphological characteristics of neurons. This suggests that either subtle molecular differences between motor neurons, or extrinsic factors from other cell types, possibly determine relative susceptibility in SMA (Thomson *et al*., 2012).

1.3.4 Sensory neuron pathology in SMA

Although motor neuron degeneration is the major hallmark of SMA pathology, sensory neuron involvement has also been observed. Sensory neurons from SMA type I patients have been shown to exhibit wallerian degeneration (Carpenter *et al*.,

1978) as well as reduced fibre density, conduction velocity and sensory nerve action potential amplitude (Rudnik-Schöneborn *et al*., 2003; Yonekawa *et al*., 2013). Sensory neuron degeneration was more significant in large myelinated fibres. Unlike severe SMA patients, SMA type II and III patients showed no abnormalities in sensory neurons (Yonekawa *et al*., 2013). In a *drosophila* model of SMA, restoration of SMN in either muscles or motor neurons did not alter disease phenotype (Imlach *et al*., 2012). However, SMN restoration in proprioceptive neurons and interneurons in the motor circuit corrected neuromuscular defects. Inducing circuit excitability by inhibiting K^+ channels also ameliorated SMN-dependent phenotypes (Imlach *et al*., 2012). It has been reported that SMA motor neurons show reduced proprioceptive reflexes that correlate with decreased number and function of synapses on motor neuron somata and proximal dendrites (Mentis *et al*., 2011). Motor neuron loss followed afferent synapse loss. Treatment with highly specific and potent histone deacetylase inhibitor Trichostatin A (TSA), which increases *SMN2* gene transcription, partially restored spinal reflexes and subsequently improved motor behaviour (Mentis *et al*., 2011). However, a recent study has challenged the causative role for proprioceptive input on motor neurons in SMA pathology (Gogliotti *et al*., 2012). Analysis of sensory neurons in severe SMA mice has demonstrated no widespread loss of sensory neurons in the lumbar dorsal root ganglion at postnatal day 3-5, when motor neuron loss was observed (Jablonka *et al*., 2006). However, cultured sensory neurons had shorter neurites, smaller growth cones and reduced beta-actin mRNA and protein in neurite terminals. Similarly, sensory neuron terminals were smaller in footpads of severe SMA mouse embryos, indicating

that pathological alterations were not restricted to solely motor neurons (Jablonka *et al*., 2006).

1.4 SMA therapy

There is currently no cure for SMA, but there are several approaches being developed to either restore SMN in affected cells, or to protect the most vulnerable cells (e.g. motor neurons). Increasing the amount of full-length SMN protein from the *SMN2* gene is one major focal point for SMA therapeutic development. High levels of SMN can be achieved by inhibiting *SMN2* pre-mRNA splicing, increasing SMN2 transcription, or stabilising SMNΔ7 transcripts (Avila *et al*., 2007; Mattis *et al*., 2009; Passini *et al*., 2011; Ling *et al*., 2012). Similarly, using viral gene therapy, the *SMN* gene can also be reintroduced to restore SMN levels in depleted cells (Valori *et al*., 2010; Foust *et al*., 2010; Dominguez *et al*., 2011). The possibility to replace lost motor neurons by differentiated neural stem cells is another potential approach (Corti *et al*., 2010). From a different perspective, neurotrophic agents have been shown to have a protective role against neurodegeneration, promoting motor neuron survival (Lesbordes *et al*., 2003; Haddad *et al*., 2003). These approaches are covered in more detail in the subsequent sections.

1.4.1 Antisense oligonucleotides

Modulating *SMN2* pre-mRNA splicing is a direct approach to restore proper expression of full-length SMN protein. Antisense oligonucleotides (ASOs) can increase expression of *SMN2* by binding to an intronic splicing silencer (ISS), which leads to inclusion of exon 7 in the *SMN2* transcript, subsequently increasing SMN

protein levels (Hua *et al*., 2010). Off-target effects are limited in this approach by targeting specific nucleotides. ASOSs that block intron 7 ISS in human *SMN2* gene, termed ISS-N1, strongly enhance *SMN2* exon 7 inclusion in cultured patient fibroblasts (Singh *et al*., 2006). Intracerebroventicular (ICV) infusion of ASO-10-27, the 18mer 2'-O-2 methoxyethyl ASO targets ISS-N1 in intron 7, has shown robust and long-lasting increase in *SMN2* exon 7 inclusion in adult mice of type III SMA with no subsequent CNS inflammation (Hua *et al*., 2010). Embryonic ICV administration of ASO-10-27 significantly reduced the tail and ear necrosis in these mice (Hua *et al*., 2010). Furthermore, muscle physiology, motor neuron function and survival have been improved after ASO-10-27 injection into the cerebral lateral ventricles in severe SMA mice (Passini *et al*., 2011). The same study demonstrated that intrathecal infusion of ASO-10-27 into Cynomolgus monkeys delivered ASO to all regions of the spinal cord and therefore can be used as practical route for delivering this therapeutic in the clinic (Passini *et al*., 2011).

Osman *et al.*, has used bifunctional RNAs to obtain more efficient ASO for SMA treatment (Osman *et al*., 2012). They inhibited ISS-N1 through antisense oligonucleotides and at the same time recruit known activators of SMN exon 7 inclusion: splicing factor 2/ alternative splicing factor (SF2/ASF) or transformer-2 protein homolog ß (hTra2ß1) (Osman *et al*., 2012). Both of these exonic splicing factors have shown to promote inclusion of exon 7 to produce full length SMN (Cartegni & Krainer, 2002; Hofmann *et al*., 2000). Bifunctional RNAs elicited induction of SMN protein in the brain and spinal cord of neonatal SMAΔ7 mice, leading to an increase in weight and an extension of lifespan to the extent not achieved by using ISS-N1 antisense alone (Osman *et al.*, 2012).

1.4.2 Histone deacetylase inhibitors

Histones are proteins that promote DNA to form condense chromatin. The post-translational modifications of histones such as methylation, acetylation and phosphorylation determine the accessibility of DNA for transcription (Johnson & Dent, 2013). Histone deacetylases (HDACs) repress transcriptional activity and therefore HDAC inhibitors (HDACi) increase transcription (Johnson & Dent, 2013). HDAC inhibitors have been shown to increase SMN levels by inducing endogenous *SMN2* promoter activity, but this effect is not *SMN2* specific and is likely to have detrimental off-target effects (Ling *et al*., 2012). It has been shown that the HDAC inhibitor, Trichostatin A (TSA) preserves innervation of muscles of SMNΔ7 mice (Ling *et al*., 2012). A single intraperitoneal dose of TSA has been demonstrated to result in modest increase in SMN gene expression in an SMA mouse model. Daily TSA delivery after onset of weight loss and motor deficits improved survival, attenuated weight loss, enhanced motor behaviour, and increased myofiber size (Avila *et al*., 2007). HDAC inhibitors also improve cardiac phenotypes (Heier *et al*., 2010) as well as sensorimotor connectivity in SMA mice (Mentis *et al*., 2011).

1.4.3 SMNΔ7 transcript stabilisation

SMNΔ7 transcript is the main transcript produced by the *SMN2* gene, but it is unstable and rapidly degrades (Lorson & Androphy, 2000). One therapeutic approach for SMA is to stabilize this transcript. Aminoglycosides have been shown to suppress efficient recognition of stop codons, resulting in significantly enhanced levels of SMN protein in SMA patient fibroblasts (Mattis *et al.*, 2009). Geneticin (G418) is a compound acting upon the *SMNΔ7* stop codon sequence and induces

readthrough at this site in a dose dependent manner (Heier & DiDonato, 2009). G418 increased SMN levels in patient cell lines as well as SMA mice. Motor function was improved in the mice treated with G418. However, lifespan was not increased, most likely due to its toxicity (Heier & DiDonato, 2009). TC007, a novel aminoglycoside has been delivered directly to the CNS in an intermediate SMA mouse model, increasing SMN levels in both the brain and spinal cord (Mattis *et al*., 2009). It increased lifespan and ventral horn cell number. TC007 also enhanced SMN protein levels in induced pluripotent stem cell-derived SMA motor neuron cultures (Mattis *et al*., 2009).

1.4.4 Neurotrophic and neuroprotective agents

Developing motor neurons require trophic support from their target, the skeletal muscle. Cardiotrophin-1 (CT-1), an interleukin 6 cytokine is highly expressed in embryonic skeletal muscle (Oppenheim *et al*., 2001). It is secreted by myotubes and increases the survival of embryonic mouse motor neurons. CT-1 deficiency has been shown to increase motor neuron cell death in spinal cord and brainstem nuclei of mice in late embryonic and neonatal stages (Oppenheim *et al*., 2001). Systemic delivery of adenoviral vector expressing CT-1 improves median survival and delays motor defects of mutant mice lacking Smn exon 7 in neurons. It also exerts a protective effect against loss of proximal motor axons and aberrant cytoskeletal organization of motor synaptic terminals (Lesbordes *et al*., 2003).

Glutamate blocking agent Riluzole has a neuroprotective effect and is the only medication demonstrated to be mildly effective in prolonging survival in ALS. Riluzole has improved median survival and exerted its protective effect against

aberrant cytoskeletal organization of motor synaptic terminals but not against loss of proximal axons in post-symptomatic SMA mutant mice model (Haddad *et al*., 2003). Riluzole has been shown to exhibit enhance expression of brain-derived neurotrophic factor (BDNF), which promotes neuronal survival, guides axonal pathfinding, and participates in activity dependent synaptic plasticity (Katoh-Semba *et al*., 2002). It recently has been shown to act via small conductance Ca^{2+}-activated K^{+} (SK) channels to ameliorate defects in both mouse and *C.elegans* SMA models (Dimitriadi *et al*., 2013). However these results should be confirmed in human SMA patients.

1.4.5 Gene therapy

Replacement of *SMN1* is the main focus of gene therapy approaches for SMA. Lentivector expressing human *SMN* has been used to restore SMN protein levels in SMA type 1 fibroblasts (Azzouz *et al*., 2004). *SMN* lentiviral injections to various muscles of SMA mice restored SMN in motor neurons, reduced motor neuron death and increased life expectancy 20-38% (Azzouz *et al*., 2004). The challenge in this field is effective gene delivery to the brain and spinal cord across the blood brain barrier (BBB). Foust *et al*. showed that the self-complementary adeno-associated virus (scAAV) 9 injected intravenously bypasses the BBB and efficiently target cells of the CNS (Foust *et al*., 2009). The same group showed neonatal delivery of *SMN1* with scAAV9 vector rescued motor neuron functions, neuromuscular physiology and improved life span in SMA mice (Foust *et al*., 2010; Valori *et al*., 2010; Dominguez *et al*., 2011). They also observed extensive scAAV9-mediated motor neuron transduction after injection into a newborn Cynomolgus macaque. The fact that AAV9 traverses the blood brain barrier in nonhuman primate emphasises the clinical

potential for scAAV9 gene therapy in SMA (Foust *et al.*, 2010). Delivery of scAAV9 *SMN1* gene has shown to reduce severity of heart defects and improve muscle fibre size in SMA mice (Bevan *et al.*, 2010; Glascock *et al*., 2012).

1.4.6 Stem cell therapy

Corti *et al*. have injected primary neural stem cells from spinal cord as well as ES cell-derived neural cell precursors into the spinal cord of SMNΔ7 model mice (Corti *et al*., 2009; Corti *et al*., 2010). 15% of the injected cells exhibited an astrocyte phenotype and, to a much lesser extent, motor neuron characteristics. The transplant led to an improvement in disease phenotype, with a 50% increase in weight, and 40% increase in lifespan. One of the beneficial effects of transplantation is the release of growth factors from transplanted human motor neurons both *in vivo* and *in vitro*. Although this study demonstrates the feasibility of using stem cells for SMA therapy, the results are not comparable to those obtained by gene and molecular based therapeutic approaches (Corti *et al*., 2010; Zanetta *et al*., 2014).

1.5 SMN-independent pathways contributing to SMA pathology

Recently, extensive progress has been made in understanding the biology of SMA pathogenesis; this includes the identification of new roles and down-stream targets for SMN protein as well as finding new therapeutic approaches to ameliorate disease progression.

1.5.1 Ubiquitination

X-linked spinal muscular atrophy (SMAX2) is a genetically distinct type of SMA with similar clinical characteristics, such as loss of cells in ventral horn of the spinal cord, hypotonia and areflexia (Ramser *et al*., 2008). SMAX2 is caused by mutations in ubiquitin-like modifier-activating enzyme 1 gene (*UBA1*). UBA1 is an enzyme involved in catalysing the initial step of the ubiquitination pathway (Rubinsztein, 2006). The de-ubiquitination enzyme, ubiquitin carboxy-terminal hydrolase L1 (UCHL1) has also been shown to be significantly increased in fibroblasts from SMA type I patients (Hsu *et al*., 2010). Recently, it has been shown that perturbations in ubiquitination pathways are a robust feature of *Drosophila*, mouse and zebrafish models of SMA (Wishart *et al*., 2014). UBA1 levels were shown to be reduced dramatically in a mouse model of SMA, while UCHL1 levels increased. UBA1 and SMN were reported to physically interact in the neuronal cytoplasm while disruption in uba1 mRNA splicing was observed in the spinal cord of SMA mice (Wishart *et al*., 2014). UBA1 perturbations led to beta-catenin accumulation. Pharmacological suppression of beta-catenin significantly ameliorated neuromuscular pathology in different animal models of SMA. However, UBA1-associated disruption of β-catenin was restricted to the neuromuscular system in SMA mice; therefore, pharmacological inhibition of β-catenin in these animals failed to prevent systemic pathology in peripheral tissues and organs, indicating fundamental molecular differences between neuromuscular and systemic SMA pathology (Wishart *et al*., 2014). This study showed that reduction in UBA1 levels induced SMA neuromuscular pathology by modulating downstream effector beta-catenin signalling, confirming a role for the ubiquitination pathway in pathogenesis of SMA.

1.5.2 Plastin-3

Oprea *et al*. reported a case of female individuals with homozygous deletion of *SMN1*, who did not exhibit any SMA symptoms, despite carrying the same number of *SMN2* copies as their affected siblings (Oprea *et al*., 2008). Increased levels of plastin-3 were observed in these individuals (Oprea *et al*., 2008). Plastin-3 is known as an actin binding protein that regulates organisation of actin filaments and colocalises with SMN throughout motor neuron axons. Plastin-3 levels have been reported to be reduced in the brain and spinal cord of SMA mice (Bowerman *et al*., 2009). Furthermore, overexpression of plastin-3 in 'Taiwanese' SMA mice improved neuromuscular defects, suggesting protective role for plastin-3 (Ackermann *et al*., 2013).

1.6 Other non-neuronal cells and tissues contributing to SMA pathology

SMN is a ubiquitously expressed protein, depletion of which clearly leads to pathology in motor neurons. However, other studies have reported SMA pathology in other cells and tissues, such as liver, heart, vasculature and bone (Hamilton & Gillingwater, 2013).

1.6.1 Muscle

Although muscle cells undergo pathological alterations in SMA (Monani, 2005), it is not known whether these alterations are due to intrinsic defects in SMA muscle or as a secondary consequence of motor neuron pathology. It has been shown that muscle biopsy extracts from SMA patients inhibit neurite outgrowth of chick spinal motor

neurons (Henderson *et al*., 1987). Co-cultures of SMA patient muscle with rat spinal cord explants undergo degeneration, suggesting that muscles may play a role in this atrophy (Braun *et al*., 1997). However, analysis of these co-cultures revealed no neurotrophin deprivation or secretion of toxic factors, suggesting intrinsic defects in SMA skeletal muscle (Braun *et al*., 1997).

Myotubes are smaller in SMA patient fetuses, indicating a delay in muscle growth and maturation (Martínez-Hernández *et al*., 2009). Primary cultures of embryonic human skeletal muscle cells from SMA patients are unable to fuse correctly to form myotubes. AChRs are also defective in myotubes from SMA patients (Arnold *et al*., 2004). Fusion defects, as well as reduced proliferation, correlate with SMN levels in myoblast cells (Shafey *et al*., 2005). Satellite cells, skeletal muscle-resident stem cells isolated from severe SMA mice exhibit abnormal differentiation and reduced efficiency in forming myotubes, indicating a role for SMN protein in the intrinsic regulation of muscle differentiation (Hayhurst *et al*., 2012). Analysis of the molecular composition of skeletal muscle in pre-symptomatic severe SMA mice has shown significant increased activity of cell death pathways in the absence of any detectable degenerative changes in innervating lower motor neurons (Mutsaers *et al*., 2011). These molecular changes were also confirmed in skeletal muscles from type II/III SMA patients (Mutsaers *et al*., 2011). Although these data suggest a direct role for SMN in skeletal muscle, the extent to which such intrinsic defects contribute to overall SMA pathology remains unclear.

1.6.2 Liver

Liver-specific deletion of murine Smn exon 7 results in severe impairment of liver development associated with iron overload, dramatic liver atrophy and late embryonic lethality of mutant mice (Vitte *et al*., 2004). Neonatal SMA mice have decreased circulating hepatic insulin-like growth factor 1 (IGF-1), confirming the importance of liver in SMA pathogenesis (Hua *et al*., 2011). IGF-1 is a neurotrophic factor and is necessary for normal postnatal growth, which could be restored by increasing SMN level systemically (Hua *et al*., 2011).

1.6.3 Pancreas

It has been shown that SMN protein has a role in glucose metabolism and pancreatic development (Bowerman *et al*., 2012). SMN-depleted mice ($Smn^{+/-}$) that lack neuromuscular pathology showed abnormal localisation of glucagon-producing alpha cells in the pancreatic islets and increased hepatic insulin and glucagon sensitivity (Bowerman *et al*., 2014). Metabolism abnormalities have also been reported in SMA patients, including metabolic acidosis, abnormal fatty acid metabolism, hyperlipidemia, and hyperglycemia (Bowerman *et al*., 2012).

1.6.4 Heart

Severe SMA patients with a single SMN2 copy develop heart defects such as atrial, ventricular and septal defects, as well as cardiac arrhythmias (Rudnik-Schöneborn *et al*., 2008). SMA mice suffer from severe bradyarrhythmia with progressive heart block and impaired ventricular depolarisation (Heier *et al*., 2010). Structural defects in the heart precede motor neuron dysfunction (Shababi *et al*., 2010). These defects

can exist independently of motor neuron and muscle pathology (Gogliotti *et al*., 2012).

1.6.5 Vasculature

Distal necrosis develops in SMA type I infants due to defects in vasculature (Araujo *et al*., 2009). Vascular defects and subsequent necrosis in tail and ear pinnae have also been observed in mild and severe mouse models of SMA (Hsieh-Li *et al*., 2000; Foust *et al*., 2010). It has been reported that a significant decrease (45%) in the density of the capillary bed is present in skeletal muscles of late symptomatic severe SMA mice (Somers *et al*., 2012). Capillary calibre was increased by 50% in SMA mice, while ramification of capillaries in muscle was reduced. This could have a dramatic influence on oxygen delivery to muscles and the removing of their metabolites, suggesting vasculature defects are likely to contribute to SMA pathogenesis (Somers *et al*., 2012).

Taken together, these studies challenge the notion that SMA is solely a lower motor neuron disorder, indicating that SMA is in fact a multi-system disorder (Hamilton & Gillingwater, 2013). Recently, it has been suggested that there is a gradient of vulnerability to SMN reduction in affected cells in SMA, with motor neurons at one end of spectrum (Sleigh *et al*., 2011). Therefore, therapies aimed to increase SMN levels should be delivered systemically and during specific developmental time points in which SMN delivery could ameliorate the pathology in all affected cells (Sleigh *et al.*, 2011). The identification of new target cells in SMA is of great importance not only for understanding the overall pathogenesis of SMA but also for the design of efficient treatment strategies.

1.7 Axon-Schwann cell interaction

Schwann cells, the major glial cells in the peripheral nervous system (PNS) play a key role in maintenance and regeneration of the PNS and therefore, could be one of the potential target cells contributing to pathogenesis of SMA. Schwann cells are highly specialised glial cells that wrap axons with multi-layered myelin membrane essential for rapid impulse conduction. Investigations have identified the axonal signals that regulate Schwann cell differentiation and myelination. Schwann cells also maintain long-term functional integrity of the axons, which is not always dependent on their myelinating functions (Nave & Trapp, 2008).

Loss of glial support leads to progressive axonal degeneration (Beirowski, 2013). Axonal loss independent of neuronal cell body pathology highlights the critical role of glia in axonal integrity (Beirowski, 2013). However, the underlying mechanisms remain unclear. Microarray analysis of spinal cord in the post-symptomatic SMA mouse model has highlighted a significant disruption in myelination pathways, suggesting that defects in axo-glial interactions may contribute to the pathogenesis of SMA (Murray *et al*., 2010).

1.7.1 Schwann cell differentiation and myelination

Glial cells in the PNS, including satellite cells in peripheral ganglia, myelinating and non-myelinating Schwann cells in nerve trunks, are derived from neural crest cells (Woodhoo & Sommer, 2008). Neural crest-derived stem cells migrate ventrally and differentiate to Schwann cell precursors (SCPs) at embryonic day 12-13 in mice, which are subsequently differentiated to immature Schwann cells at embryonic day

13-15 (Jessen *et al*., 1994; Dong *et al*., 1995). The postnatal fate of immature Schwann cells is determined by which axons they randomly associate with, with myelination being selectively activated in those cells that happen to envelope single large diameter axons (Jessen & Mirsky, 2005). These transitions are strikingly dependent on survival factors, mitogens and differentiation signals from the associating axons (Dong *et al*., 1995). All transitions are reversible except for the transition from SCPs to immature Schwann cells. The onset of myelination is the only step of differentiation that is linked to cell cycle exit (Stewart *et al*., 1993). Numerous molecules have now been implicated in the regulation of Schwann cell development.

SRY (sex determining region Y) box10 (SOX10) is necessary for the generation of all peripheral glia from the neural crest (Britsch *et al*., 2001), whereas bone morphogenetic proteins (BMPs) inhibit glial differentiation (Shah *et al*., 1996). Type III isoform of axon-derived neuregulin 1 (NRG1) is required for the survival of SCPs in embryonic nerves as well as SCP proliferation both *in vitro* and *in vivo*. In mice that selectively lack this isoform, SCPs initially populate spinal nerves, but their numbers are severely reduced, indicating NRG1 type III is important for SCP survival (Wolpowitz *et al*., 2000).

During the transition of SCPs to immature Schwann cells, connective tissue spaces open up within the nerves and become vascularised. Developing perineurium appears at the nerve surface. SCPs are found at the outer margin of the nerves, and inside them. They connect to each other through sheet-like processes that envelope a large number of axons. In contrast, families of immature Schwann cells ensheath large

groups of axons (Wanner *et al*., 2006; Jessen & Mirsky, 2005). Unlike SCPs, immature Schwann cells can support their own survival in an autocrine manner by secreting a cocktail of survival factors (Meier *et al*., 1999). NRG1 accelerates the conversion of SCPs to immature Schwann cells, as well as promoting SCP survival and proliferation (Morrissey *et al*., 1995). Notch has also been shown to promote the generation of Schwann cells from SCPs as well as mediate Schwann cell proliferation (Woodhoo *et al*., 2009)

In a process known as radial axonal sorting, which starts around the time of birth, individual Schwann cells separate from Schwann cell families and adopt a 1:1 relationship with large diameter axons (Jessen & Mirsky, 2005). At the same time, the number of Schwann cells and axons are matched by regulating Schwann cell survival and proliferation. Studies have shown that the amount of NRG1 type III expressed at the axonal surface is an indicator of axonal thickness and determines the fate of associated Schwann cells (Simons & Trotter, 2007). Overexpression of NRG1 leads to hypermyelination of large axons or myelination of small calibre axons (Michailov *et al*., 2004). It has been shown that deletion of various laminin isoforms such as laminin-2 (α2, β1, γ1) and laminin-8 (α4, β1, γ1) impairs radial sorting (Yang *et al*., 2005). Similarly, Schwann cells lacking the laminin receptor, β1integrin show the same phenotype (Feltri *et al*., 2002). It has been reported that laminin/ β1integrin regulates Schwann cell process extension and radial sorting by mediating Rac1 activity (Nodari *et al*., 2007). Another receptor for laminin is dystroglycan (DG), mutations in which lead to infolding of internodal myelin and late onset demyelination similar to that observed in L-periaxin deficient mice (Gillespie *et al*., 2000). L-periaxin has been shown to be necessary for formation of the DG-

dystrophin related protein-2 (DG-DRP2) complex, which is involved in the link between the extracellular matrix (ECM) and the Schwann cell cytoskeleton (Sherman *et al*., 2001). L-periaxin deficient Schwann cells exhibit disruption of Cajal bands and its nutritive function, resulting in reduced Schwann cell length during nerve growth (Court et al., 2004). These observations indicate the important role of the ECM in Schwann cell elongation and process extension involved in radial sorting (Chernousov *et al*., 2008).

There are various signalling pathways that activate or inhibit myelination in immature Schwann cells. Myelination is promoted by the transcription factors early growth response 2 (EGR2, also known as Krox20), POU-domain transcription factor OCT6 (also known as POU3f1) and brain 2 class III POU-domain protein (BRN2) and inhibited by c-Jun, Notch and SRY (sex determining region Y) box 2 (SOX2) (Jessen & Mirsky, 2005). Deletion of OCT6 and its close relative BRN2 has been shown to cause severe but transient arrest at the promyelin stage, resulting in late onset of myelination and hypomyelinated nerves in adult animals (Jaegle *et al*., 2003). OCT6/BRN2 cooperates with SOX10, the master regulator of Schwann cell lineage, to upregulate EGR2 in myelinating cells through the OCT6 Schwann cell enhancer (Jagalur *et al*., 2011). EGR2 is a transcription factor required for the myelinating phase of Schwann cell development. EGR2 null and hypomorphic mice exhibit reduced levels of several major myelin genes with Schwann cell arrested in the promyelinating stage (Le *et al*., 2005). Svaren and Meijer suggested a mechanism for OCT6 regulation, in which CAMP induces PKA signalling, leading to activation of NFκB to upregulate OCT6 (Svaren & Meijer, 2008). However, it is suggested that activation of NFκB regulates OCT6 at the posttranslational level (Svaren & Meijer,

2008). SOX10 can also regulate myelin gene transcription directly through the conserved SOX10 binding sites in several myelin genes such as MPZ (myelin protein 0) and MAG (myelin associated glycoprotein) (LeBlanc *et al*., 2007).

Myelination is also negatively regulated by several transcription factors, such as Notch and c-Jun. It has been shown that EGR2 suppresses Notch signalling in myelinating cells (Woodhoo *et al*., 2009). Notch has been reported to initiate demyelination in demyelinating neuropathies before the onset of neuronal loss. Notch signalling promotes generation of immature Schwann cells and maintains this phenotype (Woodhoo *et al*., 2009). Another negative regulator of Schwann cell myelination is c-Jun, which has been shown to mediate Schwann cell proliferation (Parkinson *et al*., 2004). There is an antagonistic relationship between EGR2 and c-Jun that regulates the transition between nonmyelinating and myelinating Schwann cells (Parkinson *et al*., 2008). Finally, SOX2 is co-expressed with c-Jun in the nuclei of immature Schwann cells as well as dedifferentiated cells. It has been suggested that c-Jun regulates SOX2 expression (Parkinson *et al*., 2008).

At the onset of myelination, Schwann cells establish an axis of polarity, which defines the orientation of the Schwann cell to the extracellular environment and to the axonal membrane (Simons & Trotter, 2007). Cell adhesion molecules of the nectin-like (Necl) family regulate in part the attachment of Schwann cells to the axonal membrane (Maurel *et al*., 2007). Necl4 accumulates with MAG along the axon-glia interface, the region forming the future internode, while neurofascin 155, TAG1 and gliomedin, which are essential for Schwann cell-axon interactions, accumulate at either side of the node of Ranvier (Simons & Trotter, 2007). Polarity is

established by the Par polarity complex, which localises asymmetrically to the inner glial membrane adjacent to the axon and recruits the P75 neurotrophin receptor to the axon-glia junction (Chan *et al*., 2006).

Cholesterol, phospholipids and glycosphingolipids account for 70% of the dry weight of myelin membrane (Simons *et al*., 2000). The synthesis of most of these lipids initiate in the endoplasmic reticulum and because of the propensity of sphingolipids and cholesterol to form tightly packed membrane microdomains (lipid rafts), it is possible that some of the myelin lipids preassemble in the secretory pathway (Simons *et al*., 2000). MBP mRNA in oligodendrocytes (glial cells in the CNS) is transported from cell perikaryon in the form of granules to the myelin membrane, where the response to the stimulus of local translation occurs (Barbarese *et al*., 1999). This mechanism is to ensure that MBP exerts its adhesive function at the appropriate place. MBP seems to act as a clustering agent, inducing myelin membrane formation by bringing together the smaller preassemblies through secretory pathways (Simons & Trotter, 2007).

These observations show that myelination is a complex process that involves precise activation of transcription factors, signals from both the axon and the extracellular matrix.

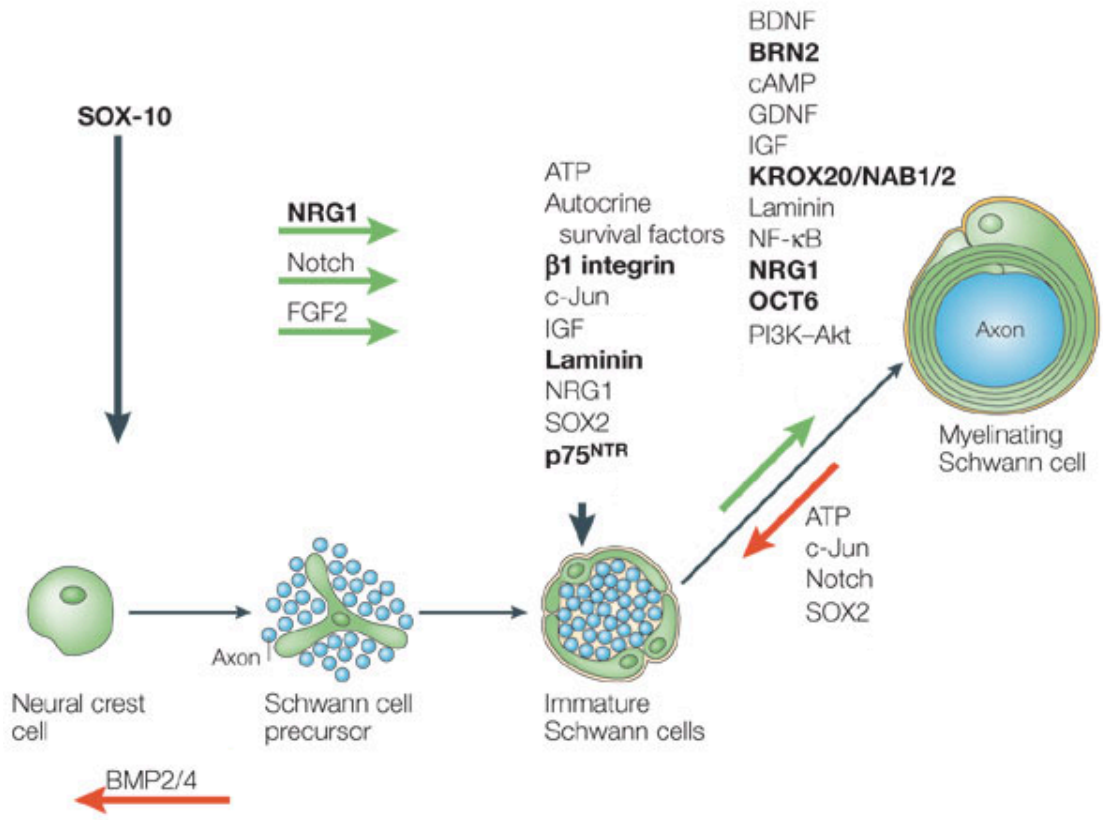

Figure 1.5 Some of the factors that control Schwann cell development and myelination. SOX10 is essential for generation of Schwann cells from the neural crest while BMPs inhibit glial differentiation. NRG1 is necessary for the survival of Schwann cell precursors (SCP). NRG1, fibroblast growth factor 2 (FGF2) and Notch accelerate the SCP-Schwann cell transition. In immature Schwann cells, survival is supported by autocrine survival factors, NRG1 and laminin, whereas p75 neurotrophin receptor ($p75^{NTR}$) induces Schwann cell death. The transcription factors SOX2 and c-Jun support proliferation and ATP inhibits Schwann cell division. Prior to myelination NRG1, BDNF, IGFs and the p38 pathway induce Schwan cell migration and/or association with axons. Radial sorting is mediated by laminin and its receptor ß1 integrin. Myelination is promoted by the transcription factors EGR2 with NGFI-A-binding (NAB) proteins, OCT6 and brain 2 class III POU-domain protein (BRN2), and inhibited by c-jun and SOX2. Cell-extrinsic signals that promote myelination include GDNF, NRG1, IGFs, BDNF and laminin. PI3K-AKT and cyclic AMP (cAMP) activated pathways also promote myelination, whereas it is blocked by ATP and Notch activation (modified from Jessen & Mirsky, 2005).

1.7.2 Terminal Schwann cells

Terminal Schwann cells (also known as teloglia or presynaptic Schwann cells) are synapse-associated non-myelinating Schwann cells. The origin of terminal Schwann cells is similar to the axonal Schwann cells discussed in the previous section. During early postnatal development, terminal Schwann cells proliferate and each NMJ is

associated with several Schwann cells. The number of terminal Schwann cells is tightly regulated in the adult NMJ and depends on the size of the end-plate (Lubischer & Bebinger, 1999). It has been reported that muscle-derived neurotrophin-3 (NT-3) regulates the number of Schwann cells (Hess *et al*., 2007).

Genetic studies have shown that although Schwann cells are present at the beginning of nerve-muscle contact, motor axons can reach target muscle cells in the absence of Schwann cells (Sugiura & Lin, 2011). However, nerves remain defasiculated as Schwann cells are essential for growth and maintenance of the developing synapses (Lin *et al*., 2000; Feng & Ko, 2008).

Terminal Schwann cells can play an important role in restoration of the NMJ after motor nerve injury. They de-differentiate to immature Schwann cells and extend their processes at the site of muscle denervation to guide the growth of nerve sprouts (Reynolds & Woolf, 1992; Son *et al*., 1996). In partial denervation of NMJs, terminal Schwann cells form a 'bridge' from innervated to denervated NMJs to induce axonal sprouting (Kang *et al*., 2003).

Schwann cells (SCs) are shown to play a role during synapse elimination. Their processes separate nerve terminals from each other and from the muscle fibre and contact the plaque of acetylcholine receptors, apposing this surface as closely as the nerve, limiting the area where synaptic transmission occurs. SCs also phagocytose nerve terminals contacting the muscle fibre (Smith *et al*., 2013). Terminal Schwann cells are not direct focus of this study, but its similarities in form and function with myelinating Schwann cells make them a good candidate for future studies of contributing factors in SMA pathogenesis.

1.7.3 Extracellular matrix contribution in Schwann cell development

Extracellular matrix (ECM) plays an important role in peripheral nervous system development. In addition to having structural importance, ECM proteins also regulate cell behaviour through receptor interactions (Chernousov *et al*., 2008). Laminin and collagen are two major ECM proteins that regulate Schwann cell developmental processes in peripheral nerve including proliferation, survival, differentiation, polarisation and morphogenesis (Aszódi *et al*., 2006).

Laminins are heterotrimeric proteins with 15 isoforms of variable numbers of α, β and γ chains. Laminin 2 (α2, β1, γ1), laminin 8 (α4, β1, γ1) and laminin 10 (α5, β1, γ1) play critical roles in Schwann cell myelination (Chernousov *et al*., 2008). Schwann cells express several laminin receptors such as α6β1, α6β4 integrins and dystroglycan (DG) (Previtali *et al*., 2003). Mutations in the laminin α2 gene (LAMA2) have been shown to cause peripheral neuropathy in both humans and mice (Helbling-leclerc *et al*., 1995; Shorer *et al*., 1995). Dystrophic mice, which have mutations in the α2 gene, exhibit hypomyelinated axons most obviously at the proximal region of the peripheral nerve (Stirling, 1975) with reduced conduction velocity (Rasminsky *et al*., 1978). Mouse models with a laminin γ1 mutation lack expression of all laminin isoforms and exhibit tremor, muscle weakness, and hind limb paralysis (Chen & Strickland, 2003; Yu *et al*., 2005). Nerve fibres are significantly smaller than controls and appear hypomyelinated. Schwann cells do not extend processes and therefore are unable to undergo radial sorting (Chen & Strickland, 2003; Yu *et al*., 2005). Radial axonal sorting requires Schwann cell proliferation and process extension. NRG1 mediates Schwann cell proliferation

through ErbB2 and ErbB3 receptors (Morrissey *et al*., 1995). Mutations in laminin γ1 have been shown to inhibit phosphorylation and subsequent activation of these two receptors (Yu *et al*., 2005), leading to a reduced number of Schwann cells. Schwann cells lacking laminins or β1 integrins do not extend processes that interdigitate between axonal bundles through inhibition in Rac1 signalling (Yu *et al*., 2005; Nodari *et al*., 2007). As discussed previously, laminins also induce Schwann cell elongation and are important for the later stages of myelination acting through the dystroglycan receptor by forming a complex between DG, DRP2 and periaxin (Gillespie *et al*., 2000; Sherman *et al*., 2001; Court *et al*., 2004). Finally, it has been shown that laminins play a role in Schwann cell long-term survival (Chernousov *et al*., 2008). PI3-kinase/Akt signalling is important in regulating Schwann cell survival and apoptosis (Maurel & Salzer, 2000). Interestingly, PI3-kinase activation is severely reduced in laminin-deficient Schwann cells (Yu *et al*., 2005). These observations reveal the importance of laminin signalling in Schwann cell differentiation and myelination.

Schwann cells also produce collagens, another ECM component (Chernousov *et al*., 2008). They are classified into three groups: fibril forming collagens (types I, II, and V), basement membrane collagens (type IV) and hybrid proteins with collagen domains such as gliomedin (Chernousov *et al*., 2008). Collagen molecules consist of a rod-like helical domain formed by association of three polypeptides containing repeating proline-rich sequences (Prockop & Kivirikko, 1995). Medium lacking ascorbic acid, an essential co-factor for collagen post-translational modification, fails to induce ECM assembly and myelination in DRG neuron-Schwann cell co-cultures (Chernousov *et al*., 1998). Dominant-negative inhibition or siRNA suppression of

type-V collagen assembly in Schwann cell-DRG neuron co-cultures dramatically inhibits myelin formation (Chernousov *et al*., 2006). However, *in vivo* analysis of mice with homozygous null mutations in α3(V) collagen has not confirmed these findings, suggesting the existence of possible compensatory mechanisms for genetic loss of α3(V) collagen (Chernousov *et al*., 2008). Finally, basement membrane collagen type IV induces Schwann cell attachment and spread through α1β1 and α2β1 integrins on the Schwann cell surface (Chernousov *et al*., 2001).

1.7.4 Axonal signals that recruit glial cells

Axonal NRG1 binds to the Schwann cell tyrosine kinase receptor ErbB3, leading to heterodimerisation of ErbB3 with ErbB2 (Morrissey *et al*., 1995). Although NRG1 plays a role in numerous neural functions, including neuronal migration, synaptogenesis, and glutamatergic neurotransmission, its best-characterised function is neural and axonal regulation of Schwann cell development (Britsch, 2007). The entire Schwann cell lineage is controlled, at least in part, by NRG1. NRG1 as a Schwann cell mitogen secures the necessary number of Schwann cells for normal ensheathment through ErbB2 and ErbB3 receptors (Jessen & Mirsky, 2005). NRG1/ErbB signal is amplified by the phosphatidylinositol-3 (PI3) kinase pathway (Ogata *et al*., 2004). Axon-bound NRG1 type III is required for the differentiation of the myelinating Schwann cell phenotype (Taveggia *et al*., 2005). Myelin sheath thickness is regulated by axonal NRG1. When exposed to the below threshold levels of axonal NRG1 type III, the associated axons are not sorted and myelinated but remain grouped together as a Remak bundle associated with a single nonmyelinating Schwann cell. Experimental NRG1 type III axonal overexpression is sufficient,

however, to trigger axonal sorting and myelination *in vitro* (Taveggia *et al.*, 2005). According to these *in vitro* results, the expression level of NRG1 on the axonal surface may be responsible for lineage decision made by Schwann cells (Nave & Trapp, 2008).

Finally, it has been reported that the axonal release of ATP inhibits Schwann cell differentiation and myelination via purinergic P2 receptor signalling (Fields, 2006). These observations have shown the importance of axonal signals in Schwann cell development and maintenance, but Schwann cells also provide trophic support for axons. This will be discussed in the subsequent section.

1.7.5 Mechanisms of Schwann cell support of axons

Although the presence of Schwann cell precursors is not necessary for the initial guidance and outgrowth of axons to their targets, SCPs are playing a role in late patterning events in the developing nerves (Woodhoo & Sommer, 2008). Genetic ablation of ErbB2 results in the loss of SCPs in the developing nerves. Although initial patterning events are normal, the nerves are poorly de-fasciculated and project abnormally within their final targets as well as making abnormal synaptic connections at the NMJ. In ErbB2 null mice, widespread neuron's death has been observed after initial generation of normal numbers of motor and sensory neurons, indicating a role for SCPs in the trophic support of developing neurons. The same results have been observed as a result of inactivation of the Sox10, ErbB3 and NRG1 type III genes (Woodhoo & Sommer, 2008).

Schwann cells express ciliary neurotrophic factor (CNTF), but the mechanisms of release are unclear because this cytoplasmic cytokine is not exocytosed like other growth factors (Nave & Trapp, 2008). In mice, CNTF is required for motor neuron survival and the long-term integrity of myelinated axons in the PNS (Gatzinsky *et al*., 2003). In 2% of human population, a mutation near exon 3 of the *CNTF* gene results in a truncated and biologically inactive protein without obvious altered phenotype (Takahashi *et al*., 1994). Genotyping the *CNTF* polymorphism in a large group of patients with CMT (Charcot-Marie-Tooth disease) and SALS (sporadic amyotrophic lateral sclerosis) have also revealed no increased frequency of CNTF null alleles. Therefore CNTF does not have an important role in modifying CMT and SALS (Van Vught *et al*., 2007).

Glial cell line-derived growth factor (GDNF) is another growth factor expressed by Schwann cells. Hirschsprungs disease is caused by GDNF mutations, which is characterised by loss of enteric ganglia as a result of early glial and neural crest defects (Nave & Trapp, 2008). GDNF has a survival effect on dopaminergic neurons (Beck *et al*., 1995), embryonic motor neurons (Henderson *et al*., 1994) as well as a beneficial role in neuropathic pain treatment (Boucher *et al*., 2000). GDNF injection into intact peripheral nerves causes Schwann cells to proliferate and to sort and myelinate small-caliber C-fiber axons (Höke *et al*., 2003). Therefore, trophic factors can, in principle, overcome developmental thresholds and change the glial phenotype from nonmyelinating Schwann cells to myelin-forming Schwann cells, similar to axonal NRG1.

A prerequisite for trophic support of axons by Schwann cells is correct physical alignment between these two cell types. The axo-glial junctions are locations of highest probability for delivery of trophic substances (Beirowski, 2013). Axo-glial junctions, between myelinating Schwann cells and their underlying axons, are formed by various adhesion molecules, such as L1, MAG, Necl proteins, Neurofascin, Neural cell adhesion molecule, N-cadherin, Caspr, Contactin, and their associated scaffolding proteins. Deletion of some of these proteins has been shown to induce abnormal axo-glial contact and subsequent axon degeneration (Beirowski, 2013). Progressive unmyelinated sensory axon degeneration has been observed in L1 deficient mice. L1 is specifically required for establishing appropriate contact between non-myelinating Schwann cells and their axons (Haney *et al*., 1999). In contrast, MAG knockout mice develop late-onset axonal detachment from myelinating Schwann cells and neurodegeneration, but exhibit normal myelination (Pan *et al*., 2005)

One of the mechanisms through which Schwann cells protect the axon is through metabolic support. The number of mitochondria is increased in dysmyelinated and demyelinated axons (Andrews *et al*., 2006). ATP is required for membrane repolarisation and for rapid transport of vesicle and organelles including mitochondria (Hollenbeck & Saxton, 2005). Mitochondria have been reported to pause at the nodes of Ranvier, where Na^+/K^+ channels are clustered and more ATP is required (Fabricius *et al*., 1993). Mitochondria are located near paranodes, the site of axo-glial interaction. Caspr is one of the major components of paranodes and mutations in this protein in mice lead to the formation of mitochondria with a swollen morphology, which is abnormally retained at the intra-axonal membrane

beneath disrupted paranodes (Alberti *et al*., 2007). This suggests that myelinating Schwann cells regulate the functioning and transport of axonal mitochondria (Nave & Trapp, 2008). Reduction in axonal ATP also decreases Na^+/K^+ ATPase and ATP-dependent Na^+/Ca^{2+} exchanger activity, which can operate in reverse and exchange axoplasmic Na^+ for extracellular Ca^{2+}, at least under pathological conditions. Elevated axoplasmic Ca^{2+} causes further damage to axonal and mitochondrial proteins, which introduces a second vicious pathological cycle (Li *et al*., 2000).

1.7.6 Glial cell contribution to peripheral nerve pathology

In most neurodegenerative diseases, a subpopulation of neurons is more vulnerable to neurotoxicity. The traditional view was that the mechanism of this action would be cell autonomous that is independent of mutant damage accumulated within other cell types that interact with affected neurons. However recent evidence from different mouse models of neurodegenerative diseases, including amytrophic lateral sclerosis (ALS) and Charcot-Marie-Tooth disease (CMT) has shaken this classic view. Toxicity or mutant protein expression in both neuronal and adjacent non-neuronal glial cells strongly influenced neurodegeneration (Lobsiger & Cleveland, 2007; Berger *et al*., 2006).

ALS is a neurodegenerative disease characterized by degeneration of upper and lower motor neurons. ALS can be induced by mutations in the superoxide dismutase 1 gene (*SOD1*) (Boillée *et al*., 2006). It has been shown that normal motor neurons in chimeric mice, containing a mixture of mutated and normal human SOD1, develop aspects of ALS pathology (Clement *et al*., 2003). The same study showed that non-

neuronal cells that did not express mutant *SOD1* delayed degeneration and dramatically extended survival in mutant-expressing motor neurons (Clement *et al*., 2003). A reduction in mutated SOD1 levels in the microglia and astrocytes slows disease progression (Boillée *et al*., 2006; Yamanaka *et al*., 2008). Co-cultures of mouse-derived, mutant SOD1-expressing astrocytes and mouse wild-type motor neurons have also demonstrated that motor neuron survival reduced over a 2-week period (Di Giorgio *et al*., 2007). Replacing the entire mutant SOD1 myeloid lineage including microglia with normal SOD1 myeloid lineage had no influence on disease onset, but prolonged survival by reducing disease progression (Beers *et al*., 2006). Replacing entire myeloid lineage with mutant SOD1 cells did not produce disease in wild-type mice, indicating that mutant expression within microglia is not sufficient for motor neuron disease, but does drive rapid disease progression (Beers *et al*., 2006). Reactive oxygen species (ROS) and their subsequent oxidative damage are at least part of the microglial-derived component of non-cell autonomous disease (Lobsiger & Cleveland, 2007). Astrocytic glutamate transporters play a key role in neuroprotection against glutamate excitotoxicity (Lobsiger & Cleveland, 2007). In both sporadic and mutant SOD1 mediated ALS, GLT1/EAAT2 glutamate transporters are focally lost (Rothstein *et al.*, 2005). Upregulation of these transporters extend survival in ALS mice (Rothstein *et al*., 2005). It has been suggested that mutant damage in the motor neurons is driving disease initiation and the role of both glial cell types is accelerating disease progression (Lobsiger & Cleveland, 2007). Finally, a decline in Schwann cell-derived IGF1 (insulin growth factor 1) and other growth factors accompanying axon degeneration was reported in SOD1 mice (Lobsiger et al., 2009).

Charcot-Marie-Tooth disease (CMT) represents a large group of inherited peripheral neuropathies, which involves mainly both motor and sensory neurons and induce muscular atrophy and weakness (Juárez & Palau, 2012). More than 40 genes have been identified to be associated with CMT. CMT is caused by mutations in genes that encode proteins involved in Schwann cell functions such as compaction and maintenance of myelin, transport through myelin, cell signalling, cytoskeleton formation, axonal transport, mitochondrial dynamics, vesicle and endosomal trafficking, and chaperones. Autosomal dominant demyelinating CMT or CMT1 is caused by duplication in *PMP22* (peripheral myelin protein 22) that is expressed predominantly in the compact myelin of Schwann cells (Lupski *et al*., 1991). Overexpressed PMP22 reaches late endosomes and forms protein aggregates that are ubiquitinated (Fortun *et al*., 2006). Heat shock response also influences protein aggregation. However, excess PMP22 overloads the protein degradation machinery, leading to a disruption in Schwann cell intracellular sorting of PMP22 and other proteins (Fortun *et al*., 2006). Mouse models with a *PMP22* mutation exhibit minimal or abnormal myelination and reduced axonal diameter (Adlkofer *et al*., 1997). Clinical signs of the disease are demyelination, progressive weakness, reduced axonal conduction velocity and sensory loss (Krajewski *et al*., 2000). CMT1B is caused by mutations in the *MPZ* gene, encoding a major myelination component, myelin protein zero. Patients show two distinct phenotypes: the first group exhibits a delayed motor development, slow nerve conduction and the second group shows late-onset neuropathy that allows myelin production, but eventually leads to axonal degeneration with minimal demyelination (Shy *et al*., 2004). There

are other subtypes for CMT disease that affect both axonal and Schwann cell expressed genes and disrupt axon-Schwann cell interactions (Juárez & Palau, 2012).

Therefore, Schwann cells play key role in axonal survival and maintenance and this makes them a potential suspect in peripheral nerve disorders.

1.8 Aims

Based on the critical role of Schwann cells in regulating peripheral neuropathies, I will address the following questions in this thesis:

1) Are there any intrinsic defects in SMA Schwann cells? (Chapter 4)
2) Do these defects contribute to SMA pathogenesis? (Chapter 4)
3) What molecular pathways control Schwann cell defects in SMA? (Chapter 5)

In order to answer these questions, I developed a technique to isolate primary Schwann cells from SMA mouse model (Chapter 3)

Chapter 2: Materials and methods

2.1 Mouse colony

2.1.1 Ethics statement

All animal experiments were approved by a University of Edinburgh internal ethics committee and were performed under license by the UK Home Office (Project License number 60/3891).

2.1.2 Animal maintenance

'Taiwanese' SMA mice, *Smn*$^{-/-}$; *SMN2*^{tg} mice (originally obtained as breeding pairs from Jackson Labs, strain no. 005058) on a congenic FVB background were maintained as heterozygous breeding pairs under standard SPF conditions in animal care facilities in Edinburgh. All animal procedures and breeding were performed in accordance with Home Office and University of Edinburgh guidelines. The 'Taiwanese' SMA model has two copies of *SMN2* per allele and has a mean age of survival of 11 days (Hsieh-Li *et al*., 2000; Riessland *et al*., 2010). Retrospective genotyping was carried out using standard PCR protocols detailed below.

Wild-type CD1 mice were obtained from in-house breeding stocks at the University of Edinburgh.

2.1.3 Genotyping

5mm tail tips were taken from sacrificed mice for genotyping. Tail tips were digested in Tail Tip Lysis Buffer + 5 µl/ml proteinase K at 55^{o}C overnight. The next

day, the tail tips were further lysed by vortexing before centrifugation at 14000rpm for 5 minutes. The supernatant was added to a new 1.5 ml eppendorf containing 500 µl isopropanol. This mixture was centrifuged at 14000 rpm for 5 minutes to pellet the DNA. The DNA pellet was washed twice in 70% ethanol and then dried for one hour at 37^{o}C to evaporate all traces of ethanol. The DNA was then re-suspended in 200 µl autoclaved deionised water.

SMA mice were genotyped by using the following primers:

SMN wild-type (1,150 bp) Forward (F1): 5'-ATAACACCACCACTCTTACTC-3'

Reverse (R1): 5'-GTAGCCGTGATGCCATTGTCA-3'

SMN knock-out (950 bp) Forward (F1): 5'-ATAACACCACCACTCTTACTC-3'

Reverse (R2): 5'-AGCCTGAAGAACGAGATCAGC-3'

Product was amplified by using the following thermo cycler program (Table 2.1):

Step	Temperature (°C)	Time (Seconds)
1	95	180
2	94	30
3	59	30
4	68 (35 cycles)	60
5	68	300
6	4	Indefinite

Table 2.1 PCR genotyping program

PCR products were separated by gel electrophoresis. Samples were resolved on a 1% agarose gel at 100 V for 30 minutes with a 100 bp DNA ladder (Promega Express) and genotype was assessed by size of bands observed (Figure 2.1)

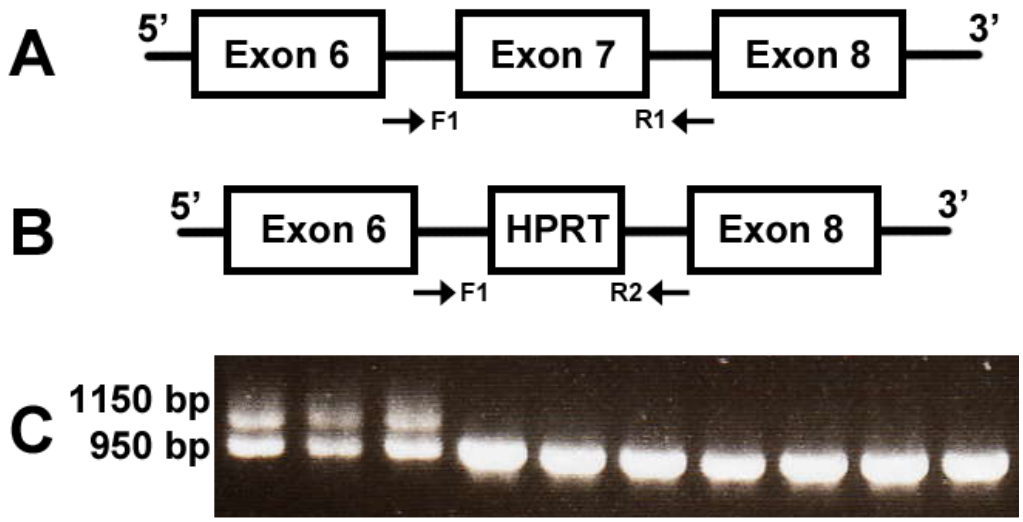

Figure 2.1 Genotyping Taiwanese SMA mice. A) Diagram of a section of wild-type mouse *smn* gene B) *Smn* exon 7 were replaced with Hypoxanthine phosphoribosyltransferase (HPRT) cassette to produce *smn* null allele (Hsieh-Li *et al*., 2000). Three PCR primers were used for genotyping: F1 (5′-ATAACACCACCACTCTTACTC-3′) and R1 (5′-GTAGCCGTGATGCCATTGTCA-3′) were used to detect wild-type allele (1,150 bp), while F1 and R2 (5′-AGCCTGAAGAACGAGATCAGC-3′) were used to detect knockout alleles (950 bp). C) Representative PCR gel scan. Lanes with 2 bands at 950 and 1,150 bp represent control samples and those with one band at 950 bp are SMA samples.

2.2 Isolation of mouse Schwann cells

Mouse Schwann cell isolation was performed by modifying protocols described by Honkanen *et al* (Honkanen *et al*., 2007) and Arthur-Farraj *et al* (Arthur-Farraj *et al*., 2011). Wild type CD1 mice were used to establish modified protocol to isolate Schwann cells (details will be discussed in chapter 3). In order to calculate number of CD1 mouse Schwann cells obtained from each treatment, 12 mice were sacrificed and total number of 24 sciatic nerves was isolated per preparation. Three preparations were used for each treatment and the average number of Schwann cells was used to compare different treatments efficiency.

2.2.1 Dissection and plating nerve fragments

100 μg/ml poly-L-lysine (PLL, Sigma) was deposited to 60 mm dishes and kept for 45 minutes at room temperature. PLL was washed 3 times with sterile water and left to be air- dried. A solution of 30 μl neat laminin (Invitrogen) in 3 ml PBS (Invitrogen) was added to PLL coated dishes and maintained for an hour. Dishes were washed once with PBS and used as wet coating.

Postnatal day 8 (P8) control and SMA mice were sacrificed by cervical dislocation, according to University of Edinburgh guidelines. Sciatic nerves and brachial plexuses were extracted and connective tissues were removed under sterile conditions. Cleaned nerves were shredded in PBS and were lysed with 0.125% trypsin (Invitrogen) and 0.05% Collagenase A (Roche) for 30 minutes at 37°C. Nerves were washed three times with Dulbecco's modified eagle medium (DMEM, Invitrogen) containing 10% horse serum (HS, Invitrogen) and were re-suspended in basic growth medium (Table 2.2). Nerves were plated in PLL/ laminin coated dishes and incubated at 37°C with 5% CO_2 for two days. After two days, medium including any unattached nerves were transferred to another coated dish. Fresh basic growth medium was added to the original dish and left for two additional days in the incubator.

2.2.2 Purification of Schwann cells

Four days after plating nerves, nerve-containing dishes were washed once with Hanks balanced salt solution (HBSS, Invitrogen) in 20 mM Hepes buffer (Invitrogen) and once more with HMEM (Table 2.2). Complement-mediated

cytolysis medium (Table 2.2) was added and incubated for 15 minutes at 37°C in a tissue culture incubator. Human leucocyte-associated antigen A, B, C (HLA-ABC) complement sera (Invitrogen) was then added and dishes were incubated for 2 hours at 37°C. Rinsing the cells twice with HBSS in 20 mM Hepes buffer terminated cytolysis. Schwann cell growth medium was then added.

2.2.3 Expansion of Schwann cells

Schwann cell medium was changed daily for 2 days until cells reached ~80% confluency. Confluency was estimated qualitatively based on the percentage of dish surface area covered by cells. Cells then were rinsed with 20 mM Hepes buffer in HBSS and were detached from the surface of the dish by 1X trypsin versene (Sigma). Trypsinisation was terminated by rinsing cells three times with DMEM containing 10% HS and re-suspended in Schwann cell growth medium. Cell suspension solution was plated on PLL/ laminin coated 60-mm dishes at the density of $1.5 \text{ X } 10^5$.

2.3 Mouse Schwann cell differentiation

The Schwann cell differentiation technique was adapted from a protocol published by Arthur-Farraj *et al*. (Arthur-Farraj *et al*., 2011). Cells were passaged and re-suspended in supplemented defined medium (Table 2.2) containing 10^{-6} M insulin (DM, Roche). They were plated on PLL/Laminin coated 24-well plate dishes and kept at 37°C overnight. The following day, 20 ng/ml NRG-1 (or Heregulin) and

1mM 2'-O-dibutyryladenosine 3': 5' cyclic monophosphate (dbcAMP) were added to cultures and kept for either 72 hours or 120 hours.

Culture medium	
Basic growth medium	High-glucose Dulbecco's modified eagle medium (DMEM, Invitrogen)
	10% v/v inactivated Horse serum (HS, Invitrogen)
	4 mM L-glutamine (Invitrogen)
	100 units/mL penicillin/ streptomycin (Invitrogen)
	0.5 μM forskolin (Sigma)
	2 ng/mL human heregulin-β1 (Sigma)
	10^{-6} M insulin (Roche)
Schwann cell growth medium	High-glucose DMEM (Invitrogen)
	10% v/v inactivated HS (Invitrogen)
	4 mM L-glutamine (Invitrogen)
	100 units/mL penicillin/ streptomycin (Invitrogen)
	0.5 μM forskolin (Sigma)
	2 ng/mL human heregulin-β1 (Sigma)
	10 ng/mL human basic fibroblast growth factor (Invitrogen)
	20 μg/mL bovine pituitary extract (Sigma)
	10^{-6} M insulin (Roche)
HMEM	High-glucose DMEM (Invitrogen)
	20 mM Hepes (Invitrogen)
	10% v/v inactivated HS (Invitrogen)
	4 mM L-glutamine (Invitrogen)
	100 units/mL penicillin/ streptomycin (Invitrogen)
Complement-mediated cytolysis medium	HMEM
	4 μg/ mL anti mouse CD90 anti Thy-1.2 (ABD Serotec)
Schwann cell D-medium	50% v/v High-glucose DMEM (Invitrogen)
	50% v/v Ham F12 (Sigma)

Culture medium	
	1% v/v N2 supplement (Invitrogen)
	1% v/v L-glutamine (Invitrogen)
	1% v/v penicillin/ streptomycin (Invitrogen)
	10^{-6} M insulin (Roche)
Schwann cell differentiation medium	Schwann cell D-medium
	1 mM N6, 2'-O-Dibutyryladenosine 3', 5'-cyclic monophosphate sodium salt (dbcAMP, Sigma)
	20 ng/mL human heregulin-β1 (Sigma)

Table 2.2 Schwann cell media composition and concentrations

2.4 Dorsal root ganglion (DRG) neuron-Schwann cell co-cultures

This technique was modified from the protocol published by Päiväläinen *et al*. (Päiväläinen *et al*., 2008). All media compositions are described in Table 2.3.

2.4.1 DRG dissection and isolation

One part of matrigel (BD biosciences) was diluted in 4 parts of EMEM and a drop of matrigel was deposited on each coverslip (VWR). Matrigel was gelatinised for 45 minutes at 37°C.

Embryonic day 14 (E14) mouse embryos were removed from CD1 female mice, sacrificed with CO_2 exposure and cervical dislocation. DRGs were dissected from spinal cords of the embryos and kept in cold Leibovitz medium (L-15, Life technologies) under sterile conditions. Pooled DRGs were cleaned and were plated on matrigel-coated dishes in DRG growth medium (Table 2.3).

2.4.2 DRG neuron purification

Non-neuronal cells were eliminated from DRG neuron cultures by replacing DRG growth medium with DRG purification medium (Table 2.3) at day 2. Purification medium contained anti-mitotic drugs uridine and deoxyuridine to inhibit proliferation of dividing cells such as fibroblasts and Schwann cells. Non-dividing DRG neurons could survive in this media. After 2 days, cultures were grown in DRG growth medium. This process was repeated 2 more times over a period of 2 weeks. DRG neurons were maintained in DRG growth medium for an additional week before Schwann cell addition. Purity was assessed by immunocytochemistry against anti-S100 and anti-neurofilament 160 kDa (neurofilament medium chain) antibodies (Table 2.4) (Jessen *et al*., 1990; Hyden & McEwen, 1966).

2.4.3 Schwann cell addition, differentiation and myelination

80% confluent Schwann cell cultures were trypsinised and washed (as discussed in 2.2.3). Schwann cell pellets were re-suspended in DRG growth medium. In order to count cells, 10 μl of cell suspension was loaded to haemocytometer (VWR) and cells were counted from 4 selected areas. These data were averaged and rounded to 100. 50000 purified Schwann cells were added to each DRG neuron culture in a 24-well plate in DRG growth medium and were allowed to attach overnight. DRG neuron-Schwann cell co-cultures were then maintained in differentiation medium (Table 2.3) for 7-10 days to induce alignment of Schwann cells.

Differentiation medium was replaced by myelination medium containing L-ascorbic acid (Table 2.3). Ascorbic acid enables Schwann cells to produce components of the

basal lamina necessary for myelination. The medium was changed every other day for 3-4 weeks until luminescent myelin sheaths were observed in cultures under a phase contrast microscope.

Culture medium	
DRG growth medium	EMEM (Sigma)
	4 g/L D-glucose (Sigma)
	50 ng/mL nerve growth factor (NGF, R&D systems)
	10% v/v HS (Invitrogen)
	2 mM L-glutamine (Invitrogen)
	100 U/mL pencillin/ streptomycin (Invitrogen)
DRG purification medium	EMEM (Sigma)
	4 g/L D-glucose (Sigma)
	50 ng/mL NGF (R&D systems)
	10 μM uridine (Sigma)
	10 μM deoxyuridine (Sigma)
	2 mM L-glutamine (Invitrogen)
	1% v/v N2 supplement (Invitrogem)
	100 U/mL pencillin/ streptomycin (Invitrogen)
Differentiation medium	50% v/v high-glucose DMEM (Invitrogen)
	50% v/v F-12 Ham nutrient (Sigma)
	50 ng/mL NGF (R&D systems)
	1% v/v N2 supplement (Invitrogem)
	2 mM L-glutamine (Invitrogem)
	100 U/mL pencillin/ streptomycin (Invitrogem)
Myelinating medium	EMEM (Sigma)
	4 g/L D-glucose (Invitrogem)
	50 ng/mL NGF (R&D systems)
	5% v/v HS (Invitrogem)
	2 mM L-glutamine (Invitrogem)
	1% v/v N2 supplement (Invitrogem)
	50 μg/mL ascorbic acid (Sigma)

Culture medium	
	20 μg/mL bovine pituitary extract (Sigma)
	0.5 μM forskolin (Sigma)
	2 mM L-glutamine (Invitrogen)

Table 2.3 DRG neuron-Schwann cell co-culture media compositions

2.5 Immunocytochemistry

2.5.1 Schwann cell immunocytochemistry

Schwann cells were rinsed 3 times with PBS and fixed with 4% v/v PFA for 10 minutes at room temperature. Cells were then permeabilised with ice-cold methanol for 15 minutes at -20°C. After rinsing cells 3 times with PBS, fixed cells were incubated first with blocking buffer containing 1% v/v Bovine serum albumin (BSA, Invitrogen) in PBS for one hour and then with primary antibody diluted in blocking buffer for 1 hour. Cells were rinsed with blocking buffer for 6 times and incubated with secondary antibody diluted in blocking buffer. For nuclear staining, TOPRO3 (1:500, Life technology) was applied for 10 minutes followed by washing cells 6 times with PBS. Finally, coverslips were mounted with mowiol (Calbiochem) and left to air-dry overnight. Table 2.4 describes all primary and secondary antibodies that were used with applied concentrations.

In order to check Schwann cell proliferation, cells were labelled with 10 μM BrdU (Sigma) 24 hours before fixation. Cells were then fixed, permeabilised and immunostained with mouse anti-BrdU antibody (Table 2.4) and cell marker TOPRO3 as described above. The percentage of BrdU-labelled cells were calculated.

2.5.2 DRG neuron-Schwann cell co-culture immunocytochemistry

DRG neurons are very sensitive to physical disruption; therefore cold methanol was replaced with 0.25 % v/v Triton X-100 (Fisher chemicals) in PBS for 30 minutes as a permeablisation step. Fixation and immunostaining were performed as described in section 2.5.1.

2.6 Immunohistochemistry

Sciatic nerves from SMA 'Taiwanese' mice were fixed for 30 minutes in 4% v/v PFA and incubated overnight in 30% sucrose in 4°C. Sciatic nerves were embedded in a 1:1 solution of 30% sucrose and OCT (CellPath). For immunostaining on intercostal nerves, whole rib cages were fixed, halved at the sternum and each half embedded separately. 10 μm sections were cut with a cryostat and mounted on Superfrost slides.

Sections were permeabilised in 0.025% v/v Triton X-100 solution for 30 minutes to break down cell membranes. Blocking solution of 0.025% v/v Triton X-100 + 1% v/v BSA was added to each section for 30 minutes to minimize non-specific protein binding. Primary antibody was diluted in blocking solution to required concentrations (Table 2.4) and incubated for one hour at room temperature. After 6 times washes (each wash for 5 minutes) in PBS, sections were incubated with secondary antibodies in blocking buffer for 2 hours (Table 2.4). Following 6 times washes (each wash for 5 minutes) in PBS, slides were mounted with Mowiol.

Antibody	Concentration	Host	Company
Sox10	1:50	Goat	Santa Cruz sc-17342
Sox2	1:500	Rabbit	Chemicon AB5603
MPZ	1:1000	Mouse	Gift (Dr. Archelos)
EGR2	1:100	Rabbit	Covance PRB-236P
POU3F1	1:50	Goat	Santa Cruz sc-11661
UbaI	1:50	Mouse	Abcam ab89647
Beta-catenin	1:50	Mouse	BD-transduction 610153
Neurofilament (2H3)	1:200	Mouse	Developmental studies hybridoma bank
Caspase-3	1:50	Rabbit	Cell signalling 9662
BrdU	1:100	Mouse	BD biosciences 347580
LAMA2	1:100	Rat	Abcam AF1060
S100	1:100	Mouse	Abcam ab4066
GFAP	1:1000	Rabbit	Abcam ab7260
MBP	1:1000	Rabbit	Gift (Prof. Brophy)
Collagen type IV	1:100	Rabbit	Millipore AB756P
SMN	1:100	Mouse	BD transduction 610647
Fluorescein (FITC)–anti-rat conjugated IgG (H+L)	1:200	Goat	Jackson Research laboratories 112-095-003
Fluorescein (FITC)–anti- rabbit conjugated IgG (H+L)	1:40	Swine	Dako F0205
Cy3-conjugated anti-mouse IgG (H+L)	1:250	Donkey	Jackson Research laboratories 715-165-151
Cy3-conjugated anti-goat IgG (H+L)	1:250	Donkey	Jackson Research laboratories 705-165-003

Table 2.4 Primary and Secondary antibodies used in this study

2.7 SMN transfection

2.7.1 pMPZ-SMN construct generation

The pMPZ-SMN construct was made by Dr. Gillian Hunter. Briefly a full-length human SMN1 plasmid construct (gift from Prof. Brunhilde Wirth) was amplified and ligated to an intermediate plasmid (pGL4.13, Promega) (Hunter *et al*., 2014). An MPZ-promoter plasmid (gift from Professor Brophy) was used to specifically target Schwann cells. The SMN-containing plasmid and the MPZ-promoter plasmid were digested and ligated to form pMPZ-SMN (Hunter *et al*., 2014). The plasmids were stored at -80°C. Figure 2.2 shows the diagram of plasmids that were used in the SMN transfection experiment.

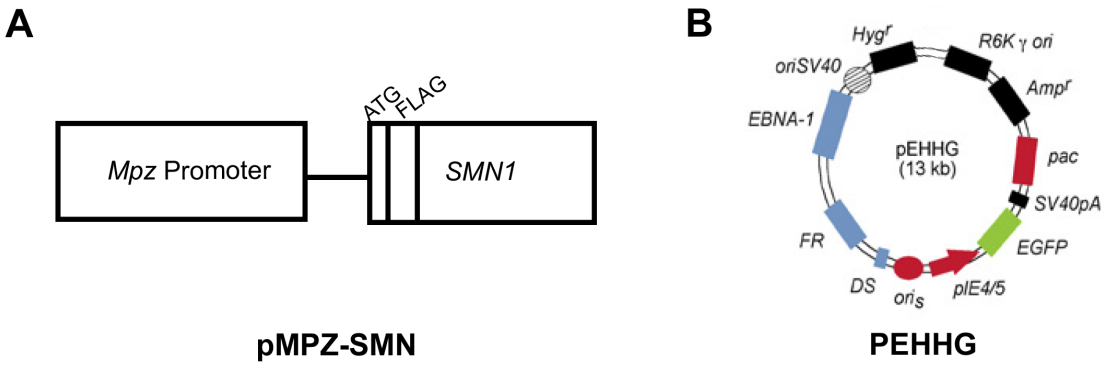

Figure 2.2 Plasmids involved in SMN transfection to Schwann cells. A) SMN1 was expressed under the induction of Schwann cell-specific promoter MPZ (Hunter *et al*., 2014). B) PEHHG plasmid was used as control GFP-expressing (EGFP), non-SMN transgene carrying plasmid to identify transfection efficiency (Hamilton *et al*., 2012).

2.7.2 Plasmid purification

The plasmid colony was transferred to LB-medium containing 100 μg/ml ampicillin and incubated overnight at 37°C with vigorous shaking. The plasmid was purified using a Qiafilter plasmid purification kit (Qiagen). DNA was precipitated with

isopropanol and washed with ethanol. The pellet was air-dried to remove any traces of alcohol. DNA was re-suspended in sterile water. Its concentration and purity were measured using a nanodrop (Thermo Scientific).

2.7.3 Transfection of Schwann cells with pMPZ-SMN

70,000 SMA and control Schwann cells were plated and differentiated as described previously. 90 hours post differentiation, Schwann cells were transfected with either control GFP-expressing, non-SMN transgene carrying plasmid, PEHHG (Hamilton *et al*., 2012) or PEHHG with pMPZ-SMN (Figure 2.2). A total amount of 1 μg DNA was used per reaction, with 2.4 μl Lipofectamine 2000 (Invitrogen) in all transfection studies. 1:1 ratio of PEHHG: pMPZ-SMN construct was used in SMA-derived Schwann cells. Transfection was terminated after 4 hours by changing media to fresh one. Cells were then fixed and immunostained at 120 hours post-differentiation with MPZ and TOPRO3 to measure expression levels.

2.8 Ubiquitin E1 inhibitor UBEI-41 experiment

15,000 Schwann cells were plated in D-media on each 13 mm coverslip and kept overnight to settle down. The next day, D-medium was replaced by differentiation medium and kept for either 72 or 120 hours. 24 hours before termination of differentiation 10 μM UBEI-41 drug (Biogenova) was added to the medium. Control and SMA Schwann cells were fixed and immunostained to study MPZ levels.

2.9 Neurite density

In order to study the stability of DRG neurons in Schwann cell-DRG neuron co-cultures, neurite density was calculated in each culture. Purified DRG neurons cultured for 72 hours either with or without control Schwann cells or SMA Schwann cells. Neurons were immunocytochemically labeled with antibody to NF medium (Table 2.4). Three images were captured approximately 250 μm from the DRG core in each culture. Each image was converted to binary and the total area covered by neurites quantified using ImageJ software.

2.10 Conditioned medium experiment

DRG neurons from wild-type CD1 embryonic mice were purified and grown for 3 weeks. Purified control and SMA Schwann cells were also incubated in Schwann cell D-media (Table 2.2). Conditioned media were collected after 72 hours and 50 ng/ml NGF was added to the media prior to their addition to DRG neurons. Three phase contrast pictures were taken approximately 250 μm from the DRG core in cultures treated with SMA and control condition media after 6, 24 and 72 hours. Each image was converted to binary and the total area covered by neuritis quantified using ImageJ software.

2.11 Microscopy and image analysis

Fluorescent images were taken using a Zeiss 710 laser-scanning confocal microscope (40 X or 20 X objective; 1.4NA) or a standard epi-fluorescence microscope equipped with a chilled CCD camera (20 or 40 X objective; 0.8NA; Nikon IX71 microscope;

Hammamatsu C4742-95). Images were taken at identical confocal microscope settings to compare protein expression levels between control and SMA Schwann cell cultures. To measure protein expression levels for each immunostaining, confocal images were captured from 4 subcultures from single preparation per genotype (N=4). Images were captured from 2 fields of view on coverslip. Pictures with 2 overlaid channels (blue channel: TOPRO3-labeled nuclei, red or green channel: immunostaining of interest) were exported as tif files and opened with ImageJ software. Initially 2 channels were separated and the colour intensities of cells were measured in channel with immunostaining of interest. Colour intensity in ImageJ was measured as mean pixel intensities in a rectangular selection around cell nuclei. Using the same size rectangle, Colour intensity of all cells of both genotypes was measured. The average of colour intensity measurements from each coverslip (2 fields of view) was calculated and therefore 4 readings were obtained per genotype (n= 4 readings). Graph of protein expression levels were plotted using GraphPad prism from the average ± SEM of these 4 readings between SMA and control Schwann cells.

2.12 mRNA expression analysis

2.12.1 Purification of total RNA from Schwann cells

Cells were detached by incubating in pre-warmed Trypsin for up to 5 minutes. Trypsinisation was terminated by washing cells three times in 10% v/v Horse serum in DMEM. Pelleted cells were rinsed with 5ml cold PBS and following

centrifugation were re-suspended in 1ml cold PBS. Cells were centrifuged in 4°C and the supernatant was removed.

mRNA was extracted from Schwann cells using an RNeasy Microkit (Qiagen). 10 μl beta-Mercaptoethanol was added to 1ml RLT buffer prior to its addition to cells. Cells were re-suspended in 350 μl of RLT buffer and homogenised for 30 seconds (pellet mixer, VWR). 350 μl of 70% ethanol was added to the lysate and mixed well. 700 μl of the solution was transferred to an RNease spin column and centrifuged at 10000 rpm for 15 seconds. Flow-through was discarded and 700 μl buffer RW1 was added and centrifuged at 10000 rpm for 15 seconds. 10 μl DNaseI was added to 70 μl RDP buffer (RNase-free DNase set, Qiagen) and mixed gently. The mix was deposited directly onto the column and left to incubate at room temperature for 15 minutes. After centrifugation and discarding the flow-through, 500 μl buffer PPE was added to spin columns. This was repeated and tubes were centrifuged for 2 minutes at 10000 rpm. 30 μl RNase-free water was added directly onto the membrane and centrifuged for 1 minute at 10000 rpm. This eluate was collected and stored at -20°C.

2.12.2 cDNA synthesis

RNA samples were defrosted and quantified using a nanodrop spectrophotometer. A260/230 and A260/280 ratios were recorded as an indication of sample purity.

cDNA was made using a high Capacity cDNA reverse transcription kit (Invitrogen). 100 ng of RNA was added to each tube and made up to 10 μl with RNAse free water. 2 RT-PCR master mixes were made per sample: one with reverse transcriptase and

the other without reverse transcriptase. The master mix composition is described in Table 2.5.

10 μl PCR mix was added to 10 μl RNA tubes. Samples were run in a PCR machine with the following program: 1) 25°C for 10 minutes 2) 37 °C for 2 hours 3) 85 °C for 5 minutes 4) 4°C pause. cDNA samples were quantified using a Nanodrop and were stored at -20°C.

10XRT buffer	2 μl
25X dNTP	0.8 μl
10X RT random primer	2 μl
Reverse transcriptase	1 μl (or 0 μl for negative RT control)
Nuclease free water	4.2 μl (or 5.2 μl for negative RT control

Table 2.5 cDNA synthesis master mix composition

2.12.3 qPCR primer design and optimisation

qPCR primers were designed by Dr. Gillian Hunter. Briefly, each mouse gene cDNA sequence were checked on NCBI website. The corresponding genomic regions (exons) were identified by UCSC genome browser. Couple of exons were selected with their intervening introns. Genomic sequence was downloaded from these areas and those exons that were separated by small intronic sequence were selected so that cDNA and genomic DNA will have significant different PCR product lengths. This strategy will help to identify any cDNA contamination of genomic DNA. cDNA was uploaded into Primer 3 to design primers spanning suitable introns. Table 2.6 shows the forward and reverse primers that were used.

To ensure that primers were amplified correctly and reproducibly between experiments, each cDNA was serially diluted up to 5 orders of magnitude. PCR was performed on cDNA samples. The standard curve is constructed by plotting the log of the starting quantity of template for each dilution (log of dilution/concentration) against the average Ct values obtained during amplification of each dilution. Ideally, the dilution series will produce amplification curves that are evenly spaced and generate a linear standard curve. The slope of a standard curve is indicative of PCR efficiency. Efficiency percentage is calculated using the equation: $E=(10^{(-1/slope)}-1) X 100$. This is the amount of PCR product increased after each cycle and should be between 90-110%.

Gene (Accession number)	Primer sequence	Exon
MPZ (NM_008623)	F: 5'- CTGGTCCAGTGAATGGGTCT -3'	234-400
	R: 5'- ATGACAATGGAGCCATCCTT -3'	401-416
LAMA2 (NM_008481)	F: 5'- CTCGAAGGCTCCCAGACTC -3'	1-246
	R: 5'- GCATTGGTTGTGATGAGTGC -3'	247-417
SOX2 (NM_011443.3)	5'- GAACGCCTTCATGGTATGGT -3'	1-2457
	5'- TCTCGGTCTCGGACAAAGT -3'	1-2457
SOX10 (NM_011437)	5'- GACCAGTACCCTCACCTCCA -3'	210-715
	5'- GGATGGTCCTTTTTGTGCTG -3'	716-984
OAZ1 (NM_008753)	5'-ATCCTCAACAGCCACTGCTT -3'	1-250
	5'- CGGACCCAGGTTACTACAGC -3'	251-396

Table 2.6 qPCR pimers

2.12.4 Quantitative RT-PCR

All cDNA samples and -RT controls were diluted to 5ng/µl. Each sample was amplified in triplicate with primers amplifying gene of interest and two house keeping genes: OAZ1 and GAPDH. Two master mixes were made to minimize

pipetting error between samples. Master mixes composition for one sample is detailed in Table 2.7.

Master mix 1 (10 μl)	Master mix	10 μl
	Forward primer	1 μl
	Reverse primer	1 μl
	Water	2 μl
Master mix 2 (6 μl)	Rox	0.4 μl
	cDNA	1 μl
	Water	4.6 μl

Table 2.7 quantitative RT-PCR master mixes composition

Master mixes were added to 96-well plate. The plate was placed in preheated ABI7000 machine (Applied Biosystems). The appropriate program was selected from computer and the wells to be analysed were chosen. SYBR green was selected as dye and the volume was set. The PCR program was set as follows: a) 95°C for 7 min b) 95°C for 10 s c) 60°C for 30 s (repeat b and c steps 40 times) d) dissociation curve.

2.12.5 Quantitative RT-PCR data analysis

The Ct values were extracted and exported to an excel spread sheet. The standard curve values from section 2.12.3 including slope of the line and Y intercept were also imported to calculate log quantity.

Log quantity=(CT value-Y intercept)/slope.

Anti-log values were calculated by following formulae:

Quantity= $10^{\text{Log quantity}}$

Quantity and Ct means were calculated to measure standard deviation for quantity means and Ct means.

Data was normalised to reference genes OAZ1 and GAPDH. Geometric means (Geomean) for each sample were calculated by averaging the quantity means of OAZ1 and GAPDH. To establish the normalising factor for each sample, the value for each sample Geomean was divided to all Geomeans average. The gene of interest quantity mean was then divided by the normalising factor for each sample to calculate the relative expression levels for the gene of interest.

2.13 Label-free proteomics

2.13.1 Cell preparations

Three separate Control and 3 SMA Schwann cell cultures were differentiated for 120 hours after one passage (P1). To terminate differentiation, cells were trypsinised and washed once with 10% HS in DMEM. After centrifugation, cell pellets were washed twice with ice cold PBS and centrifuged. All PBS was removed from pellets and the samples were snap-frozen on dry ice. Samples were stored at -80°C.

2.13.2 Protein extraction

Protein samples were extracted in SDT lysis buffer containing 100 mM Tris-HCl (pH 7.6), 4% (W/V) Sodium dodecyl sulphate (VWR) and 0.1 M D/L-dithiothreitol (Sigma). For efficient protein extraction, lysates were freeze-thawed and homogenised in SDT buffer several times. Protein concentrations were determined

by bicinchoninic acid assay (BCA; Thermo Scientific Pierce) according to manufacturer's instructions.

Three samples per genotype were sent to Douglas Lamont at the 'Fingerprint' proteomics facility at the University of Dundee for Mass Spectrometry. All three samples for each genotype were pooled together and then separated to three technical replicates to reduce variability between samples. Sample processing steps for the label-free experiment are summarised in Figure 2.3.

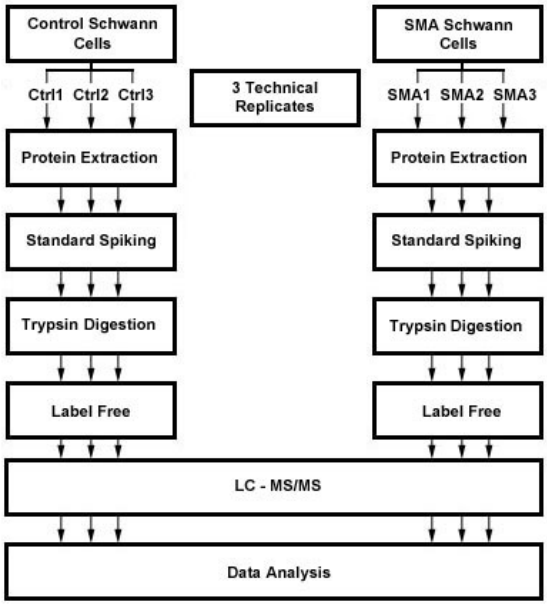

Figure 2.3 Summary of experimental design for label-free proteomics. Picture was modified from (Wang *et al.*, 2012)

2.13.3 Label-free proteomics data analysis

Raw MS data files were sent back for analysis. Progenesis LC-MS (version 4.0) software was used to determine individual peptide sequences and their protein identities.

LC-MS data from 6 samples were imported to Progenesis software and data were aligned automatically. In this process, all experimental runs were compared to every other run. The run with the greatest similarity to all other runs was selected as the alignment reference. Quality of alignment vectors was manually reviewed.

Data were then filtered before starting comparative analysis. The minimum and maximum retention times for ion elution were manually set to more than 16.589 minutes and less than 138.961 minutes. Maximum ion charge was set to 5. These modifications gave 67,883 MS/MS spectra in total. Software automatically established which run was 'least different' from all the other runs for selection as the Normalising reference. The experiment design was set as between-subject design: control versus SMA Schwann cells.

Based on the study done by Mutsaers *et al.*, peptides were filtered initially by their Anova p value of more than 0.05 and power of more than 0.08 (Mutsaers *et al*., 2013). Power is the probability of finding real difference and is calculated based on expression variance, sample size and difference between the means. Application of these filters gave 14,295 peptides. Peptide statistics was performed on selected features to determine existence of any outliers in the data by principal component analysis (PCA). Features were grouped according to the similarity in their expression profiles (Figure 2.4).

MS/MS peak lists were exported to the Mascot (v2.4.0) search engine to perform ion searches and to identify specific peptide sequences. 663 proteins were identified which were re-imported to Progenesis software to resolve conflict by excluding peptides that were associated with more than one protein. Any peptides with Lysine

or Arginine mid-sequence or not having Lysine or Arginine at the end were also removed from data since they were products of improper cleavage by trypsin. 195 proteins remained after further filtering data for p value of less than 0.05, identification of more than 2 peptides and more than 20% up- or down regulation of protein expression compared to control samples.

2.14 Ingenuity pathway analysis (IPA)

Lists of differentially expressed proteins were imported to IPA (Ingenuity systems) software to identify interactions from known relationships between genes, proteins and diseases. The majority of information in the IPA database is extracted from peer-reviewed journals. Proteins with more than 1.2 fold change in their expression compared to wild type (195 proteins) were uploaded to IPA, out of which 12 could not be mapped. IPA generated networks were limited to a maximum of 35 members. The biological interaction scores were defined by p values calculated by right tailed Fisher's exact test. This value is not a direct indicator of biological relevance, but provides a starting point for software to approximate how relevant the network is to the analysis.

2.15 Statistical analysis

All data were exported from Microsoft Excel and analysed by GraphPad Prism software. Statistical tests for each comparison are described in the text. All data are presented as mean ± SEM and P value of less than 0.05 was considered to be significant.

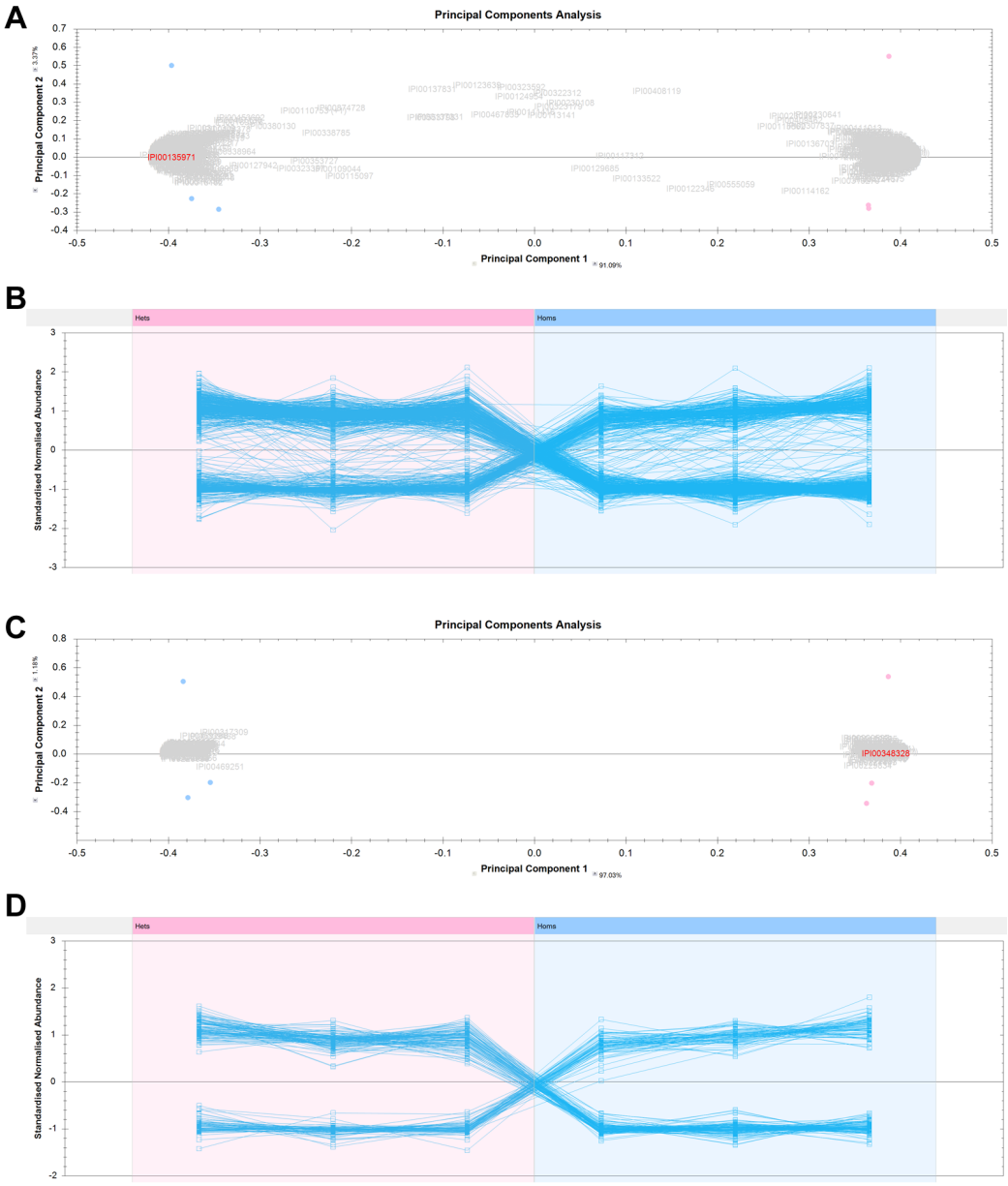

Figure 2.4 Filtering process. A) Principal components analysis before filtering. B) Expression profile before filtering. C) Principal components analysis after filtering. D) Expression profile after filtering. Outliers in the data were removed by filtering and similar expression profiles were grouped.

Chapter 3: Development of primary Schwann cell culture techniques for use with neonatal SMA mice

3.1 Introduction

Spinal muscular atrophy (SMA) is often classified as a motor neuron disease. However, SMN protein is ubiquitously expressed and therefore other cells may contribute to SMA pathology (Hamilton & Gillingwater, 2013). One of the potential cells that may be involved in SMA pathology is the Schwann cell, the predominant glial cell in the peripheral nervous system (PNS). Schwann cells deposit myelin sheaths, which helps neurons to conduct faster electrical pulses (Rasband, 2011). They have also been reported to have protective effects on neurons (Rasband, 2011). Schwann cell defects in development and myelination are observed in several peripheral neuropathies including Charcot-Marie-Tooth disease (CMT) (Berger *et al*., 2006). However, no previous studies have investigated the contribution of Schwann cells in SMA disease pathogenesis.

Primary isolated Schwann cell cultures from SMA mouse models are required in order to study Schwann cell development and differentiation in the absence of neurons. Myelination could then also be studied using co-cultures of wild-type dorsal root ganglion (DRG) with pre-purified SMA Schwann cells. However, to our knowledge, there is no protocol suitable for extraction of Schwann cells from SMA mice. Most studies of PNS myelination have been performed using rat DRG neuron-Schwann cell co-cultures. Kleitman's method is generally used to isolate Schwann cells from sciatic nerves (Kleitman *et al*., 1997). Sciatic nerves are enzymatically dissociated and purified with antibody and complement serum treatment. However,

there is no rat model for SMA. In contrast, several mouse models of SMA have been developed (Bebee *et al*., 2012).

It is difficult to isolate and purify a sufficient amount of myelination competent Schwann cells from mice with existing protocols designed for use with rat models. Therefore, most of the previous work using mouse models has been performed with DRG explant cultures in which Schwann cells and neurons are extracted from the same tissue (Liu *et al*., 2005). Explant cultures therefore limit the potential to generate co-cultures of neurons and Schwann cells from mice with different genetic modifications.

Several protocols have been developed to study myelination in mouse DRG-Schwann cell co-cultures. Although reported Schwann cell purities were satisfactory, the number of Schwann cells generated and their myelination capability were not sufficient for our experiments in SMA mice (Verdú *et al*., 2000; Seilheimer *et al*., 1989; Kim *et al*., 1997). The only protocol suitable for modification for use with SMA mice was published in 2007 by Honkanen *et al* (Honkanen *et al*., 2007). They proposed a co-culture protocol in which they used the basics of the Kleitman method with less harsh treatment for sciatic nerve dissociation. Horse serum was replaced by fetal calf serum and fibroblasts were removed by Thy1.1 antibody instead of Thy1.2 and cytosine arabinoside. The Thy 1.2 antigen is expressed on mouse fibroblasts but not Schwann cells, which provides more efficient and less cytotoxic agent for Schwann cell purification (Dong *et al*., 1999). They also used a Schwann cell mitogenic factor, adenylate cyclase activator forskolin, that was also reported to inhibit fibroblast proliferation (Yamada *et al*., 1995). They compared collagen type

1, poly-L-lysine and laminin as substrata on which cultures were grown. They found that Schwann cells plated on either collagen or PLL had a similar proliferation rate that was higher than that observed using laminin alone. Due to economical reasons they chose to use PLL as coating material. This protocol generated 1.9-3.3 X 10^6 of 95% purified Schwann cells that were myelination competent from sciatic nerves from 12-15 4-day-old wild-type CD1 mice (Honkanen *et al*., 2007).

Although the Honkanen *et al*. study confirmed that it is possible to isolate Schwann cells from mice, further modifications are required to use this protocol for SMA mice. SMA Schwann cell yields would not be sufficient due to the smaller size of sciatic nerves from SMA mice compared to wild-type mice. Older pups are also required to distinguish between healthy and SMA mice before pooling their sciatic nerves for experiments.

In this chapter, I have adapted the Honkanen *et al*. protocol for generating Schwann cells from wild-type CD1 mice with parameters suitable for subsequent use with SMA mice. The number of Schwann cells initially obtained was not sufficient for quantitative studies. I therefore modified the substrata, medium composition, number of pups used, and the age of animals for better Schwann cell yields. Purity of Schwann cells was assessed by double immunostaining with S100 and GFAP antibodies. I adopted this protocol to generate SMA Schwann cells from sciatic nerves of 8-day-old 'Taiwanese' SMA mouse pups. Approximately 400,000 cells per preparation were obtained with around 95-98% purity. Finally, I assessed the capability of the Schwann cells to express myelin markers in DRG neuron-Schwann

cell co-cultures. The resulting protocol was then used for studying Schwann cell development and myelination in subsequent chapters.

3.2 Results

3.2.1 Schwann cell generation from CD1 mice

CD1 mice were used initially because they are more economical to maintain and they produce large litters in which all pups have the same genotype. The protocol by Honkanen *et al* was used (Honkanen *et al*., 2007) as a template that could subsequently be modified. Sciatic nerves were collected from 12 4-day-old mouse pups and plated on 10 μg/ml poly-l-lysine coated dishes. Schwann cells emerged from sciatic nerves after a day in culture. Schwann cells were distinguishable from fibroblasts by their elongated bi- or tri-polar cell morphology with an oval luminescent cell body. Fibroblasts display a round, large non-luminescent nucleus, which is flattened and polymorphic (Kaewkhaw *et al*., 2012). Schwann cells were purified with anti-Thy 1.2 antibody and rabbit complement to remove fibroblasts. Cells were left to become nearly 80% confluent. Schwann cell number was calculated after first passage. 80,000 Schwann cells were obtained by this method, which was not enough for future experiments. Figure 3.1 shows phase contrast pictures of Schwann cells emerging from sciatic nerves, purified and expanded. Modifications were therefore required to generate higher cell yields. Note that in order to calculate number of CD1 mouse Schwann cells obtained from each treatment to modify isolation protocol, 12 mice were sacrificed and total number of 24 sciatic nerves was isolated per preparation. Three preparations were used for each treatment and their average number of Schwann cells was used to compare different treatments efficiency.

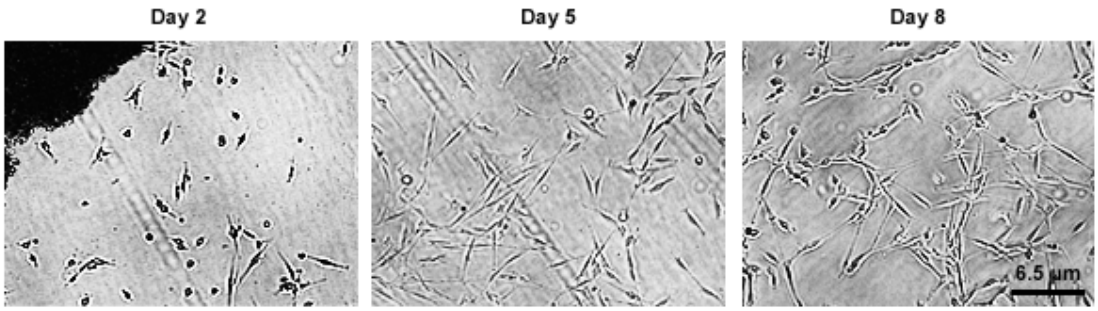

Figure 3.1 Schwann cell isolation, purification and expansion. Schwann cells emerge from sciatic nerves (Day 2), were purified by Thy 1.2 antibody (Day5) and expanded (Day 8).

3.2.2 Coating substrate optimisation

It was observed that the sciatic nerves were loosely attached to the plate and this may have contributed to the low yield of Schwann cells. Higher concentrations of Poly-L-lysine were therefore tested: a 10-fold higher concentration of poly-L-lysine (100 µg/ml) was used. The number of Schwann cells in 60 mm dish was increased to 100,000 cells (Figure 3.2).

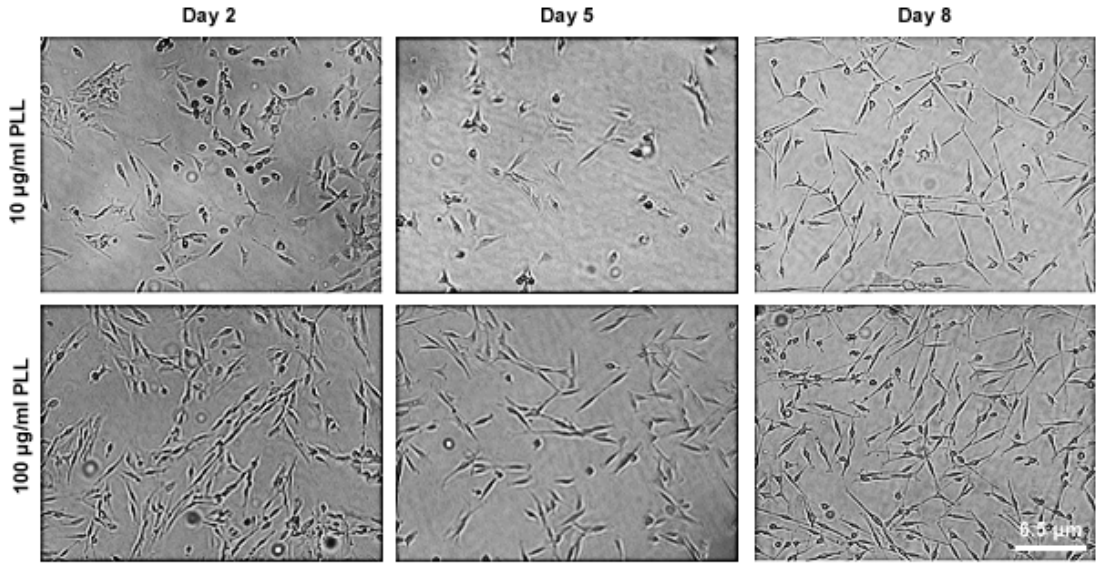

Figure 3.2 Substratum optimisation. Representative phase contrast micrographs of Schwann cell cultures at day 2, 5 and 8. Original poly-L-lysine (PLL) concentration 10 µg/ml (Top panel) was compared to 100 µg/ml (Bottom panel). Applying more concentrated PLL for coating the plates increased the average number of Schwann cells.

For further optimisation of coating substrates, I examined whether concentrated PLL could be used in combination with other coating material. To develop the original protocol, Honkanen *et al*. tried several other substrates and compared the Schwann cell numbers. The coating materials were PLL, laminin and collagen type 1. Although all 3 substrates supported Schwann cell proliferation, they found that cells cultured on collagen type 1 and PLL had significantly higher proliferation rates compared to those grown on laminin. Collagen could not be used with laminin since it needs acidic pH to prepare. The PLL/ laminin coating is also used routinely in rat Schwann cell co-cultures. Therefore, dishes were first coated with concentrated PLL and then with laminin. 198,000 cells were obtained with these coating conditions, representing a notable improvement compared to PLL alone.

3.2.3 Medium composition

In the paper published by Arthur-Farraj *et al*. insulin was used after purification of Schwann cells (Arthur-Farraj *et al*., 2011). Insulin is a hormone that is used as a differentiation factor in Schwann cell cultures. However insulin in combination with forskolin could increase cyclic adenosine monophosphate (cAMP) levels, which was shown to induce Schwann cell proliferation (Stewart *et al*., 1996). 10^{-6} M insulin was therefore added to the Schwann cell growth medium post-purification (Arthur-Farraj *et al*., 2011). Schwann cell number was increased to an average of 245,000 cells.

Based on this success, obtaining higher numbers of Schwann cells upon addition of insulin, it was added to the cultures from day 1. Schwann cell number was nearly doubled; insulin treated cultures had an average of 422,500 cells (Table 3.1).

Treatment	Average Schwann cell number ± SEM
Original protocol	80,000 ± 2309.4
10X Poly-L-lysine	100,000 ± 6110.1
10X Poly-L-lysine/ laminin	198,000 ± 3214.5
Insulin after purification	245,000 ± 4582.6
Insulin before purification	422,500 ± 6427.5

Table 3.1 CD1 mouse Schwann cell culture optimisation. Changing substratum and medium composition increased Schwann cell numbers

3.2.4 Mouse age

The majority of protocols for both rat and mouse Schwann cell cultures use early postnatal pups (day 0-4). Given the need to pool sciatic nerves from several mice of the same genotype for culturing in SMA experiments, there was a need to be able to genotype mouse pups before dissection. However postnatal day 4 SMA mice are pre-symptomatic and do not show significant differences in their gross phenotype compared to wild-type littermates. Postnatal day 7-8 is the time point when I was first able to reliably distinguish between SMA and littermate controls. I initially modified the protocol to use older CD1 mouse pups (day 8) to compare number of Schwann cells compared to previous readings. The average number of cells was approximately 400,000 cells similar to those obtained from P4 mouse pups.

3.2.5 Isolation of Schwann cells from 'Taiwanese' SMA mice

The modified protocol was then tested on litters of SMA 'Taiwanese' mice and littermate controls. SMA mice have reduced body weight, longer righting times and necrosis in their tails (Somers *et al*., 2013; Hsieh-Li *et al*., 2000). Pups were

segregated at P8 based on this phenotype. The number of cells obtained from SMA and littermate animals was calculated after first passage. Given using the whole litter for experiments, the plated number of sciatic nerves from control and SMA mice might be different for each preparation. Therefore in order to compare the number of Schwann cells obtained from each genotype, I calculated Schwann cells per mouse. 68,734 control and 48,478 SMA Schwann cells were obtained per mouse (from 4 separate preparations). The lower number of SMA Schwann cells might be due to their smaller sciatic nerve sizes.

3.2.6 Purity of Schwann cells

Purity of Schwann cells are routinely quantified by double immunostaining with anti calcium-binding protein S100 antibody (Schwann cell marker, (Hyden & McEwen, 1966)) and anti-glial fibrillary acidic protein (GFAP) antibody, an intermediate filament protein in embryonic and non-myelinating Schwann cells (Jessen *et al*., 1990; Honkanen *et al*., 2007). Control and SMA Schwann cells were double-immunostained with these antibodies. Schwann cell purity was calculated as a percentage of cells that were immunostained for all three markers (TOPRO-3 as a % of total cells). Control and SMA Schwann cell purities were 95 and 98% respectively (Figure 3.3).

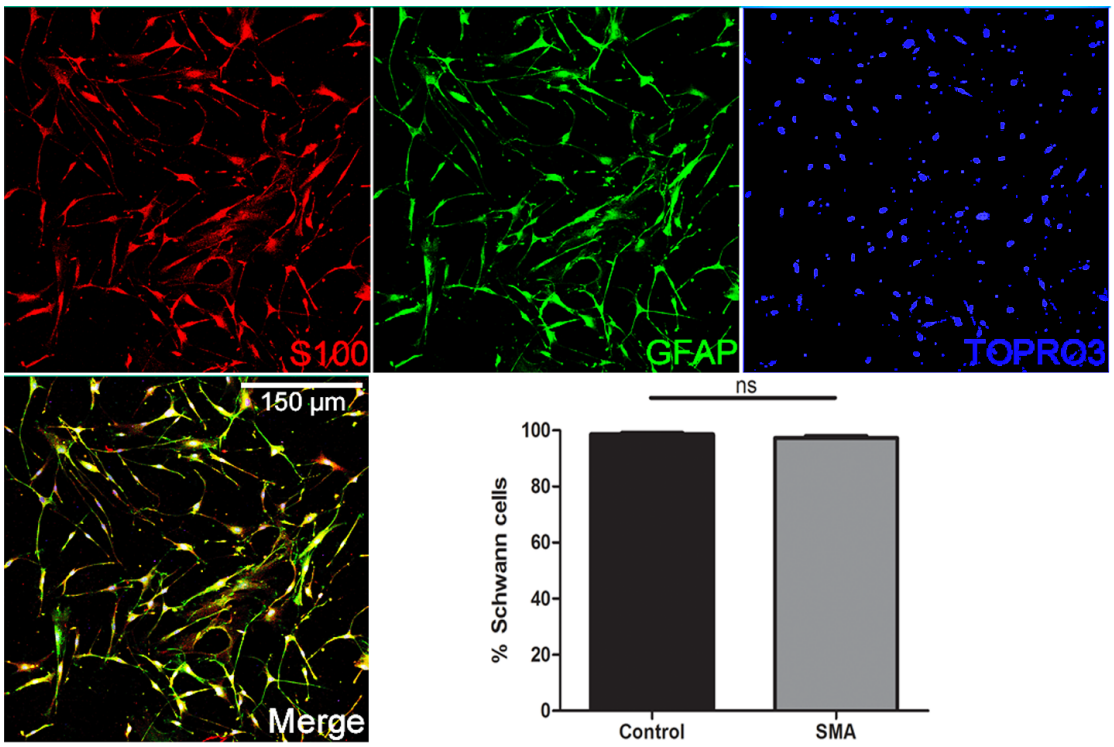

Figure 3.3 Schwann cell purity. Representative confocal micrographs of Schwann cells immunostained with S100 (red), GFAP (green) and TOPRO3 (blue) show that most of the cells in culture were Schwann cells. The graph compares the Schwann cell purification between control and SMA cultures (Two-tailed, unpaired nonparametric t-test; N = 4 subcultures from one preparation per genotype, 2 fields of view imaged per culture, > 150 cells quantified per field of view, n = 4 readings).

3.2.7 Myelination competent Schwann cells

Finally, I needed to establish whether Schwann cells isolated using the new protocol were capable of myelination. Schwann cells from wild-type mice were co-cultured with pre-purified DRG neurons. Myelination was induced by addition of medium supplemented by L-Ascorbic acid. Ascorbic acid induces Schwann cells to produce collagen fibrils necessary for myelination (Eldridge *et al*., 1989). Cells were immunostained after 4 weeks in myelination medium. Myelin basic protein (MBP), a marker for late myelination was expressed around approximately 80% of neurons (Figure 3.4). Therefore the new protocol could be used for isolation of myelination-competent Schwann cells from SMA and wild-type mice.

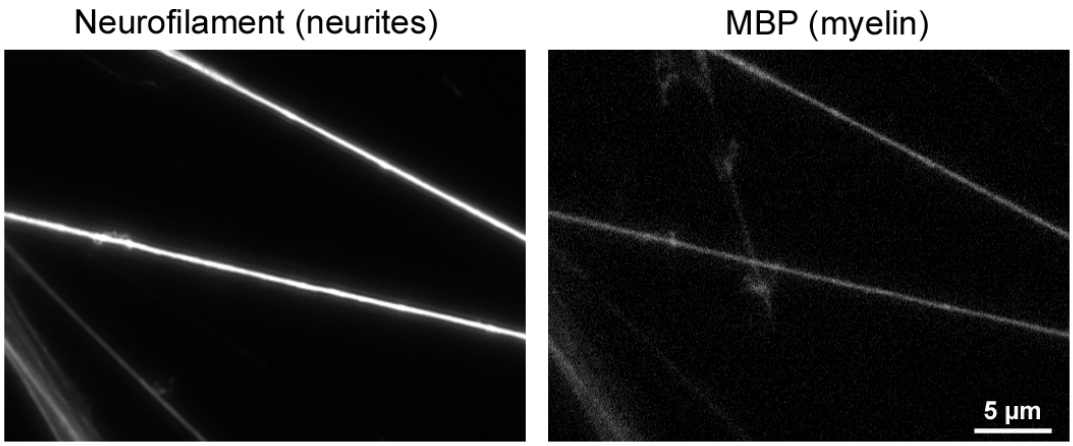

Figure 3.4 Induction of myelination by Taiwanese mouse Schwann cells in DRG neuron-Schwann cell co-cultures. Representative phase-contrast pictures of DRG-neurons immunostained with anti-neurofilament medium antibody show that majority of neurons were co-immunolabled with late myelin marker MBP and therefore capable of myelin production.

3.3 Discussion

In this chapter established protocols were modified to allow isolation of a high yield of Schwann cells from SMA mice. Based on the prior success of the Honkanen *et al*. (Honkanen *et al*., 2007) protocol to achieve high-yield, purified Schwann cells, it was adopted as the basis for this study. However, I could not obtain the same number of Schwann cells using their protocol with our proposed methodology for SMA mice. Therefore modifications were performed on the culture substratum and medium composition. Also I used P8 mice pups instead of P4, in order to distinguish SMA from healthy mice prior to pooling their sciatic nerves. After applying these modifications, I obtained 68,734 control and 48,478 SMA Schwann cells per mouse with 95-98% purity. The generated Schwann cells are capable of myelination and could therefore be used in our subsequent experiments.

Although SMA is often considered as a motor neuron disease, alterations have been demonstrated in both motor and sensory axons (Jablonka *et al*., 2006). Defective myelination was also shown in our previous data in a mixed population of motor and sensory neurons (Hunter *et al*., 2014). Myelination studies are frequently performed in well-established Schwann cell-DRG neuron co-cultures (Honkanen *et al*., 2007). Therefore sensory DRG neurons were considered to be the best source of robust neurons for co-culture experiments.

Here, I developed a protocol for isolation of myelination-competent Schwann cells from SMA mice. This protocol can also be used to study peripheral neuropathies such as Charcot-Marie-Tooth disease. The main advantage of DRG neuron-Schwann cell co-culture is the potential to use Schwann cells and neurons from different

genotypes to study cell type-specific bimolecular and cellular events taking place during normal and pathological myelination. For instance, DRG neuron can be extracted from healthy control mice and Schwann cells from SMA or other peripheral neuropathy mouse models to investigate the intrinsic defects in Schwann cells development and myelination. To my knowledge, no DRG neuron-Schwann cell co-culture experiments have been carried out in mouse models of Charcot-Marie-Tooth disease. Although rat model of human CMT1A has been generated (Nobbio *et al*., 2006), the *in vitro* study of other subtypes of CMT disease was limited to DRG explant cultures (Liu *et al*., 2005). The limitation of this system is that both neurons and Schwann cells are from the same animal and therefore it is impossible to dissect the cell-type specific defects in abnormal myelination. Therefore, the protocol that I developed has the potential to be used in diseases with abnormal Schwann cell myelination.

Chapter 4: SMN-dependent Schwann cell intrinsic defects in mouse models of spinal muscular atrophy

4.1 Introduction

Low levels of SMN are traditionally thought to selectively target lower motor neurons, but SMN has recently been shown to have effects on multiple other cell types (Hamilton & Gillingwater, 2013). Glial cells are essential for the form, function and maintenance of neurons. Defects in glia were observed as a contributing factor in several neurological conditions, such as Parkinson's disease (Fellner *et al*., 2011), Alzheimer's disease (Nagele *et al*., 2004) and amyotrophic lateral sclerosis (Lobsiger & Cleveland, 2007). Genetic defects targeting myelin proteins in Schwann cells, the major glia in the peripheral nervous system (PNS), are also associated with peripheral neuropathies such as Charcot-Marie-Tooth disease (CMT) (Berger *et al*., 2006). Given the importance of Schwann cells for the maintenance of lower motor neurons, I wanted to determine if they contribute to SMA pathology.

Previous microarray analysis on late symptomatic P5 severe *Smn*$^{-/-}$*; SMN2* mouse spinal cord revealed significant alterations in myelin gene expression compared to littermate controls. There was a 6.5 and 3.7 fold decrease in expression of myelin protein zero (MPZ) and peripheral myelin protein 22 (PMP22) in SMA mouse spinal cords, respectively (Murray *et al*., 2010). This suggests disruption in core myelin protein expression in SMA mice.

Myelination has also been examined in the 'Taiwanese' and severe SMA mouse models *in vivo* (Hunter *et al*., 2014). Ultrastructural analysis of myelination in intercostal nerves from P5 severe SMA mice revealed that there were more axons of

large calibre (>1 μm) that remained unmyelinated or had thinner myelin sheaths, with no signs of axonal degeneration. The average G-ratio, the ratio of axon diameter to myelinated axon diameter, was increased in SMA intercostal nerves. No reduction in axonal diameter was observed. Abnormal peripheral myelination was also confirmed in milder 'Taiwanese' SMA mouse models at early (P7) and late symptomatic stages (P11). However upper motor neuron tracts in the spinal cord and distal peripheral nerves did not show any difference in their myelination compared to control littermates. Expression of key myelin proteins such as myelin protein zero (MPZ), peripheral myelin protein 22 (PMP22) and myelin basic protein (MBP) were also disturbed in 'Taiwanese' SMA mice intercostal and sciatic nerves (Hunter *et al*., 2014). Together, these data suggest that myelination is abnormal in SMA mice.

In vivo studies could not rule out the possibility that the observed defects in myelination were occurring as a secondary consequence of pathology in neighbouring motor neurons. Therefore I wanted to isolate Schwann cells from 'Taiwanese' SMA mice in order to examine whether reduced levels of SMN caused intrinsic defects in the absence of pathological neurons. Isolated Schwann cells were extracted from post-symptomatic (P7) mice and so they would have been in association with pathologically affected neurons. There is therefore a possibility that observed defects in Schwann cell differentiation are not intrinsic. However, isolated Schwann cells are thought to be reprogrammed to Schwann cell precursors in culture without differentiation medium (Arthur-Farraj *et al*., 2011) increasing the likelihood that any observed effect is intrinsic.

In this Chapter, I first confirmed that isolated SMA-derived Schwann cells were stable in culture and that SMN protein levels were reduced significantly in these cells. I showed that Schwann cells from SMA mice developed normally at undifferentiated stages. Next, I induced myelination in isolated Schwann cells in the absence of neurons and observed that SMA-derived Schwann cells did not respond normally to myelination cues. Restoring SMN levels was shown to rescue myelination defects. Using co-cultures of wild-type dorsal root ganglion (DRG) neurons with SMA-derived Schwann cells, I showed abnormal myelination with SMA Schwann cells. SMA-derived Schwann cells were also shown to promote instability in neighbouring healthy neurons. Finally, I showed that extracellular matrix (ECM) was disrupted in Schwann cells from SMA mice and it was to some extent responsible for the observed neurite instability.

4.2 Results

4.2.1 Schwann cell stability in culture

Schwann cells derived from SMA 'Taiwanese' mice were de-differentiated to an immature, non-myelinating phenotype *in vitro*.

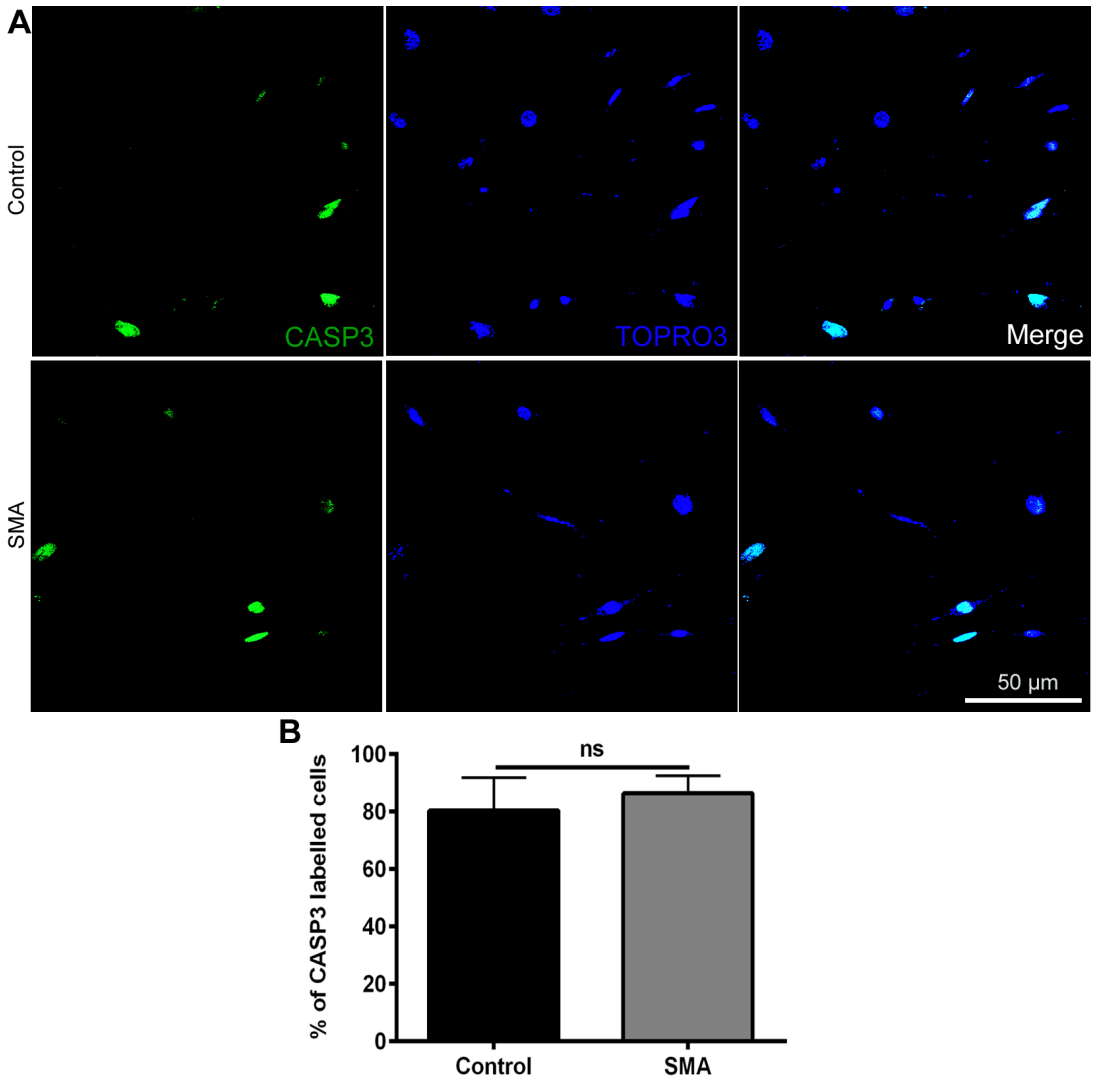

Figure 4.1 (A) Representative confocal micrographs of isolated Schwann cells immunollabeled with antibodies against the apoptotic marker CASP3 (green) and nuclei labeled with TOPRO3 (blue), showing no significant difference in percentage of CASP3 expressed cells between SMA-derived and control Schwann cells pre-differentiation. (B) Bar graph showing no significant difference in percentage of CASP3 of SMA-derived Schwann cells compared to control cells pre-differentiation (two-tailed, unpaired nonparametric t-test; N = 4 subcultures from single preparation per genotype, 2 fields of view imaged per culture, > 150 cells quantified per field of view, total n = 4 readings).

SMA-derived Schwann cells were found to be stable in culture, as immunolabelling for the apoptosis marker caspase 3 (CASP3,Table 2.4) showed no significant change in percentage of apoptotic Schwann cells derived from SMA mice compared with control cells (Figure 4.1).

Cell proliferation was also compared between control and SMA-derived Schwann cells by BrdU labelling (see methods). There was no significant difference in the percentage of BrdU labelled cells between SMA and control Schwann cells (Figure 4.2). These data indicated that immature SMA-derived Schwann cells were stable *in vitro*.

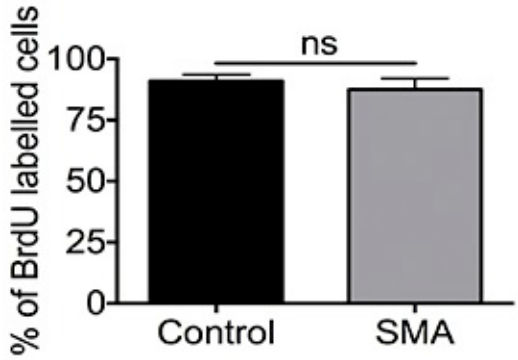

Figure 4.2 Schwann cells proliferation assay. Isolated Schwann cells from control and SMA mice were labelled with mouse BrdU and immunostained with anti-BrdU antibody and nuclei marker TOPRO3 to assess cell proliferation in these two cultures. Number of BrdU labelled cells was quantified in each field of view and percentage of BrdU-labelled cells was compared between two genotypes. Bar graph showed a similar incorporation of BrdU into control and SMA-derived Schwann cells (two-tailed, unpaired nonparametric t-test; N = 4 subcultures from one preparation per genotype, 2 fields of view imaged per subculture, > 25 cells quantified per field of view and total n = 4 readings)

4.2.2 SMN protein levels in vitro

SMN protein expression levels in isolated Schwann cells were examined by immunostaining with an anti-SMN antibody (Table 2.4). SMN expression levels in

cells derived from SMA mice were significantly decreased in comparison with littermate controls (Figure 4.3).

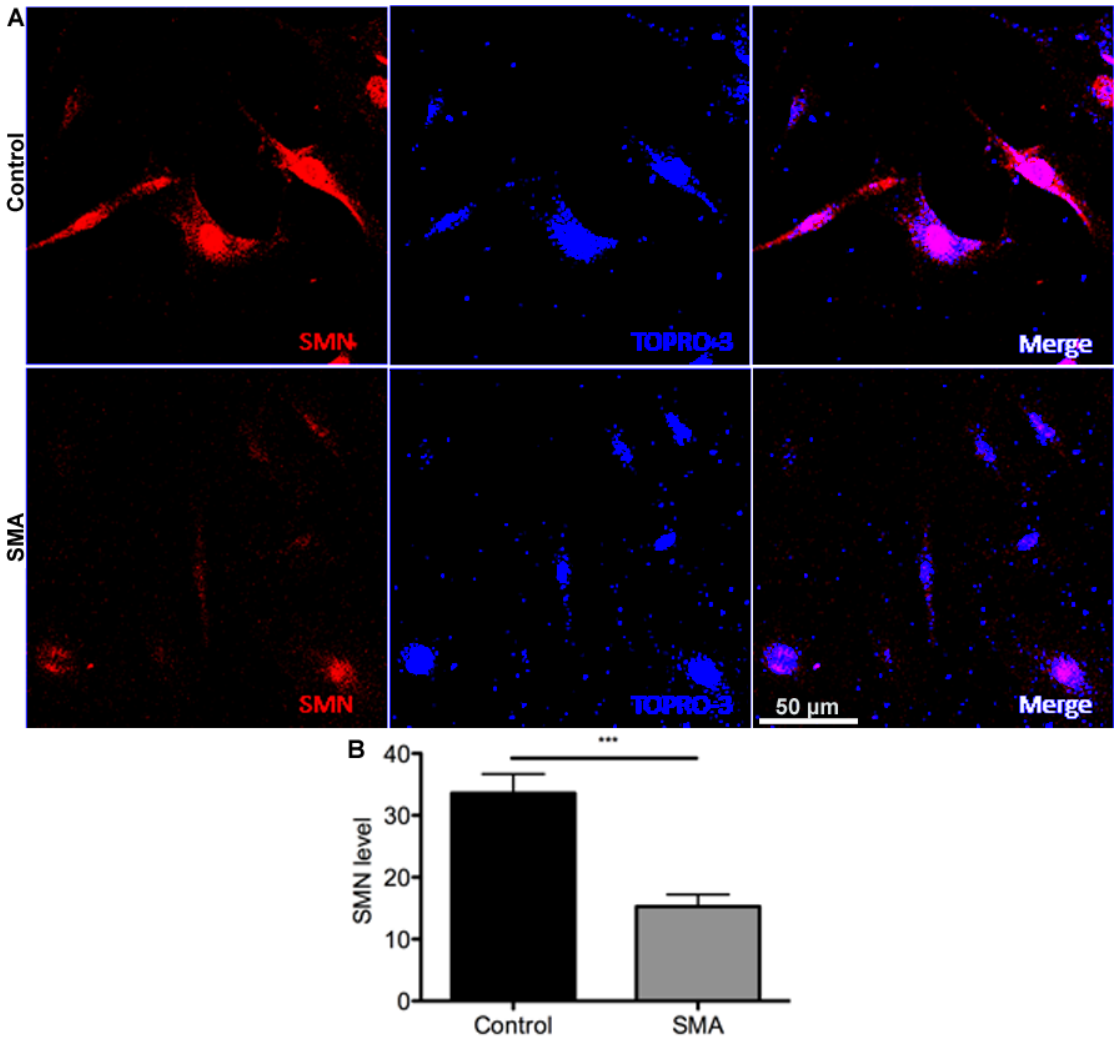

Figure 4.3 SMN expression levels. (A) Representative confocal micrographs of isolated Schwann cells from 'Taiwanese' SMA mice and littermate controls, immunolabelled to reveal SMN protein. SMN was strongly expressed in Schwann cells from control mice, but was markedly reduced in primary cultures of SMA-derived Schwann cells (B) (* P < 0.001; N = 4 subcultures from single preparation per genotype, 2 fields of view imaged per culture, > 150 cells quantified per field of view; unpaired two-tailed t-test, n = 4 readings).**

4.2.3 SMA-derived Schwann cells develop normally pre-differentiation

Several transcription factors control Schwann cell development and their transition from an undifferentiated to a myelinating phenotype. Examples of these transcription factors are SRY-box containing gene 10 (SOX10), SRY-box containing

gene 2 (SOX2), and POU domain class 3 transcription factor 1 (POU3F1 or OCT6). SOX10 is a lineage marker for Schwann cell development and is present at all stages of Schwann cell development (Britsch *et al*., 2001). Immature Schwann cell marker SOX2 is important for maintaining the undifferentiated state and is a negative regulator of myelination (Nam *et al*., 2005).

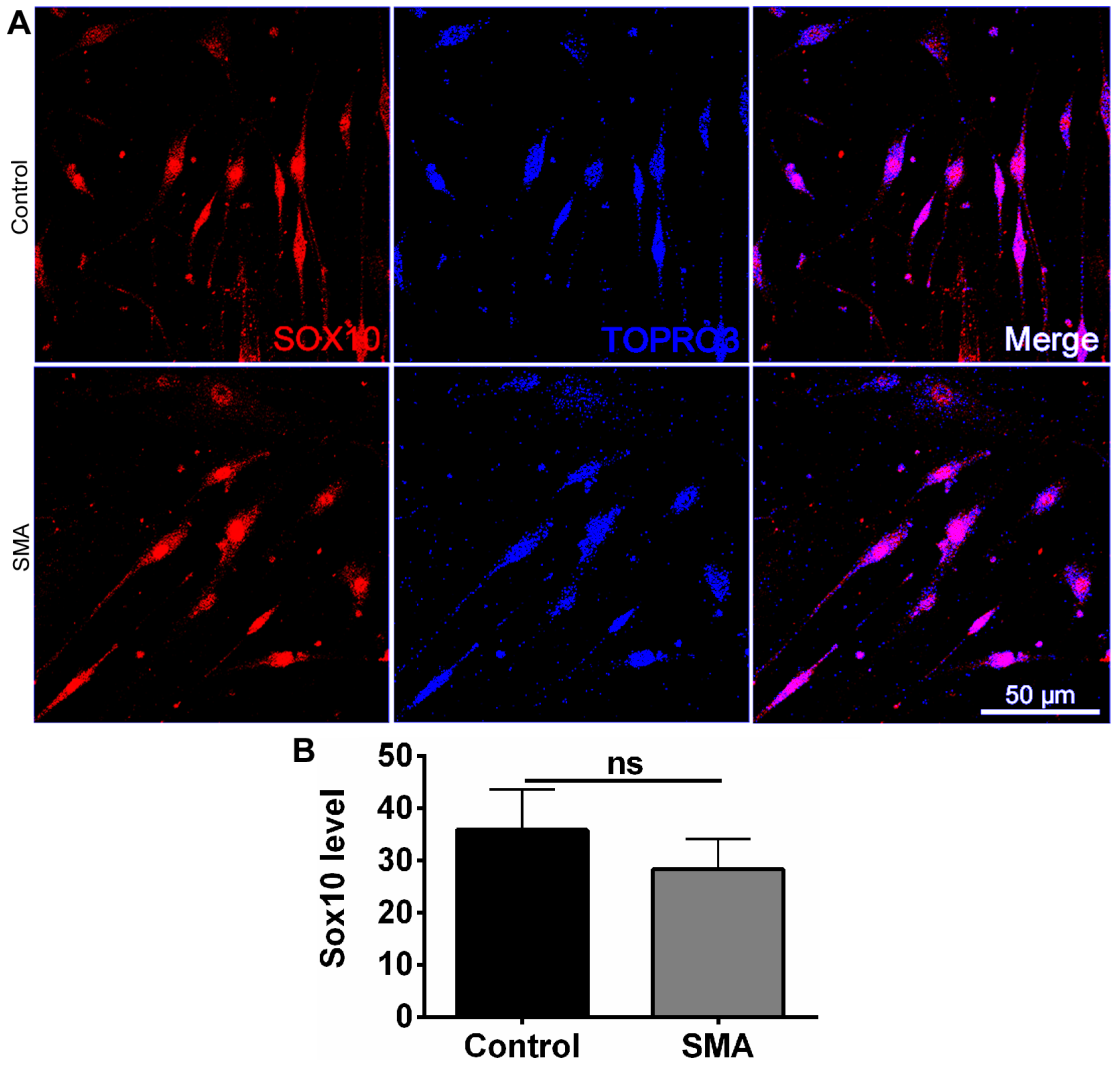

Figure 4.4 (A) Representative confocal micrographs of isolated Schwann cells showing no significant difference in Schwann cell marker, Sox10 in SMA-derived Schwann cells compared to cells from control littermates. (B) Bar graph showing no significant difference in SOX10 expression in SMA- and control-derived Schwann cells (Unpaired two-tailed t-test; N = 4 subcultures from single preparation per genotype, 2 fields of view imaged per culture > 150 cells quantified per field of view, n = 4 readings).

POU3F1 transiently increases before myelination to regulate early myelination transcription factors such as early growth response 2 (EGR2) (Jaegle *et al*., 2003). Prior to the induction of differentiation, transcription factor levels SOX10 (Figure 4.4), SOX2 (Figure 4.5), and POU3F1 (Figure 4.6) were similar between SMA-derived and control Schwann cells. These results show that pre-differentiated Schwann cells isolated from SMA mice expressed the normal complement of immature Schwann cell markers.

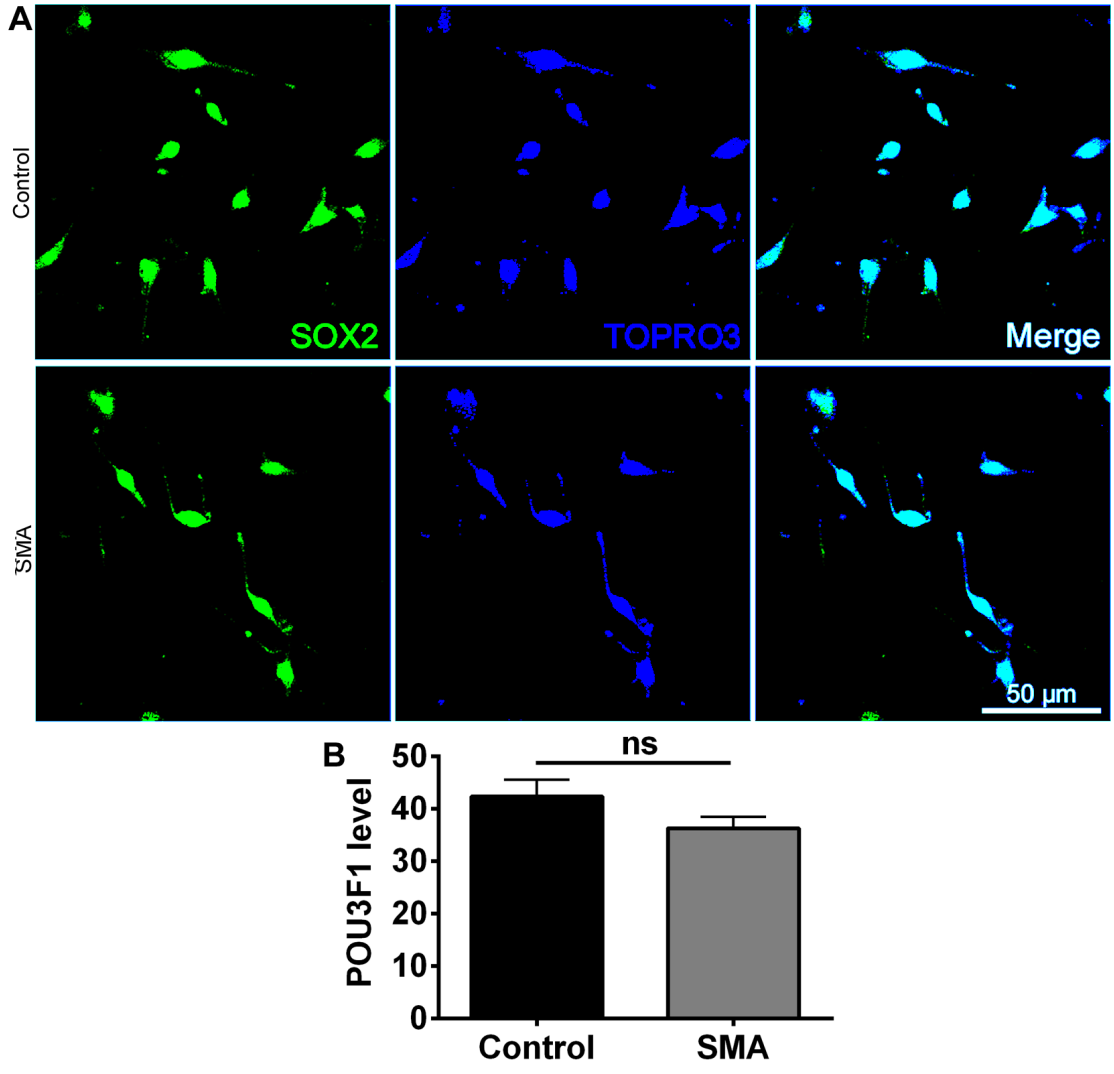

Figure 4.5 (A) Representative confocal micrographs of isolated Schwann cells showing no significant difference in late marker of Schwann cell differentiation, SOX2 in SMA-derived Schwann cells compared to cells from control littermates. (B) Bar graph showing no significant difference in SOX2 expression in SMA- and control-derived Schwann cells (Unpaired two-tailed

t-test; N = 4 subcultures from one preparation per genotype, 2 fields of view imaged per culture > 150 cells quantified per field of view, n = 4 readings).

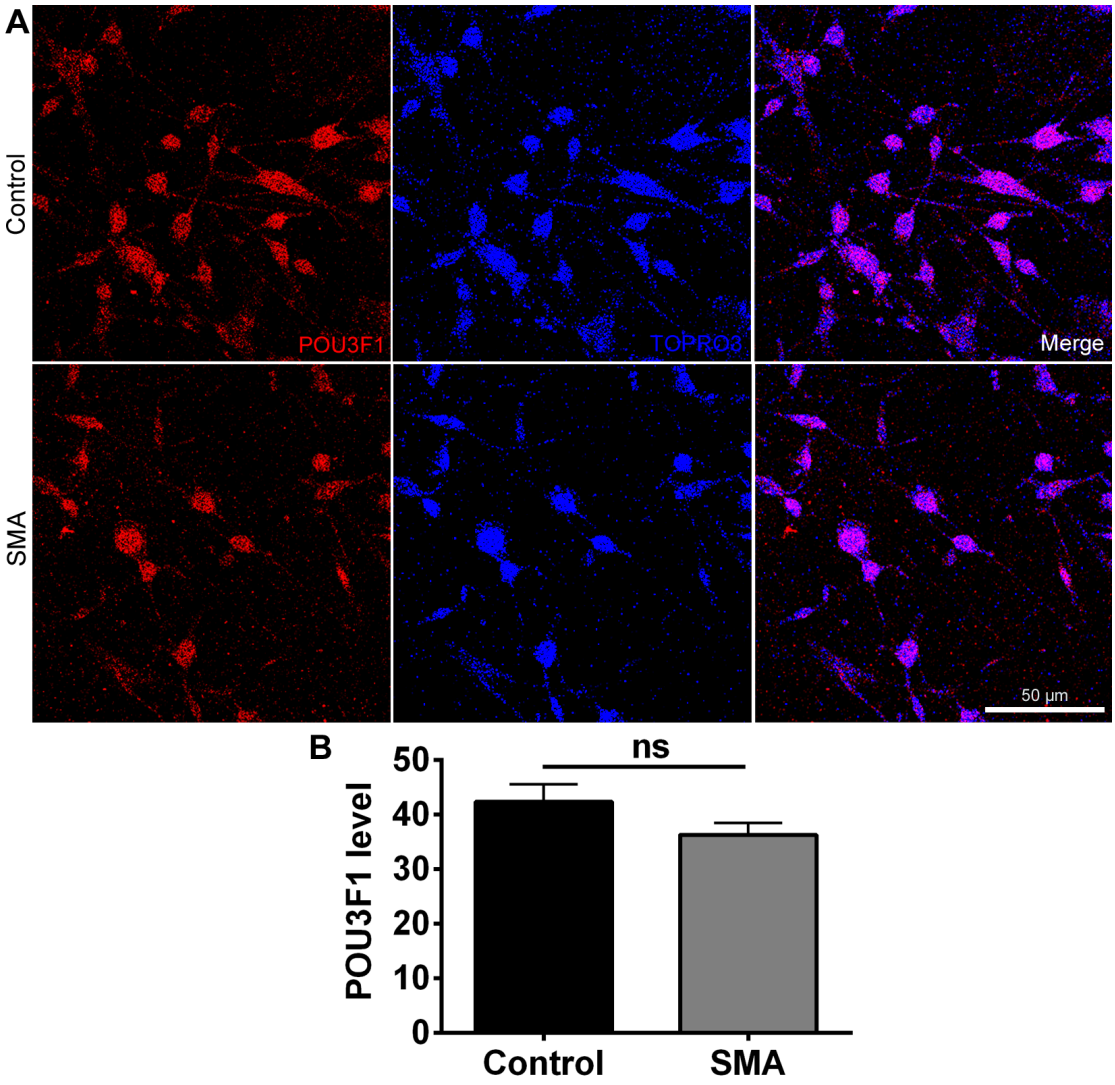

Figure 4.6 (A) Representative confocal micrographs of isolated Schwann cells showing no significant difference in Schwann cell differentiation marker, POU3F1 (red) in SMA-derived Schwann cells compared to cells from control littermates. (B) Bar graph showing no significant difference in POU3F1 expression in SMA- and control-derived Schwann cells (Unpaired two-tailed t-test; N = 4 subcultures from one preparation per genotype, 2 fields of view imaged per culture > 25 cells quantified per field of view, n = 4 readings).

4.2.4 SMA-derived Schwann cells fail to respond normally to myelination cues

Arthur-Farraj *et al* showed that immature Schwann cells could be differentiated *in vitro* by addition of dbCAMP and NRG1 to induce the myelinating Schwann cell

phenotype (Arthur-Farraj *et al*., 2011). They reported strong expression of myelin markers, such as early growth response 2 (EGR2 or Krox20) and myelin protein zero (MPZ) after 72 and 120 hours, respectively.

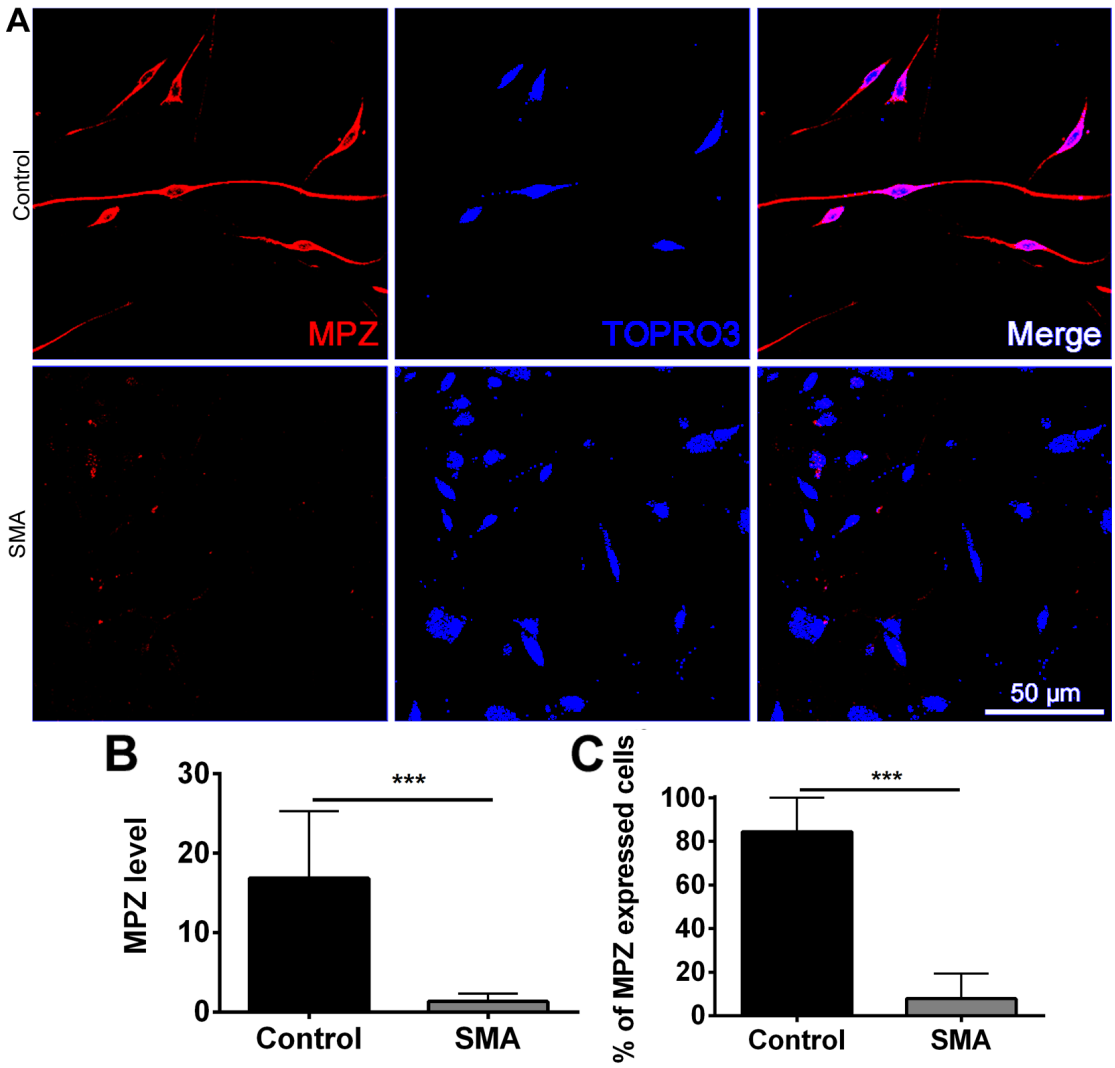

Figure 4.7 (A) Representative confocal micrographs of differentiated Schwann cells immunolabelled with antibodies against myelin protein MPZ. MPZ levels were noticeably lower in SMA-derived Schwann cells. (B) Bar graph showing significant reduction of MPZ level expression in SMA-derived Schwann cells 120 hours post-differentiation (* P < 0.001 ; two-tailed, unpaired t-test; N = 4 subcultures from one preparation per genotype, 2 fields of view imaged per culture, > 25 cells quantified per field of view, n = 4 readings). (C) Bar graph showing significant reduction in number of cells expressing MPZ in SMA-derived Schwann cells 120 hours post-differentiation (*** P < 0.001; two-tailed, unpaired nonparametric t-test; N = 4 subcultures from single preparation per genotype, 2 fields of view imaged per culture, > 25 cells quantified per field of view, n = 4 readings)**

I used this model to establish whether observed *in vivo* myelination defects in SMA mice were due to differences in the intrinsic ability of Schwann cells to respond to differentiation signals. MPZ levels were measured in SMA- and control-derived Schwann cells 120 hours after differentiation. MPZ levels were significantly less elevated in SMA-derived Schwann cells compared to control cells (Figure 4.7).

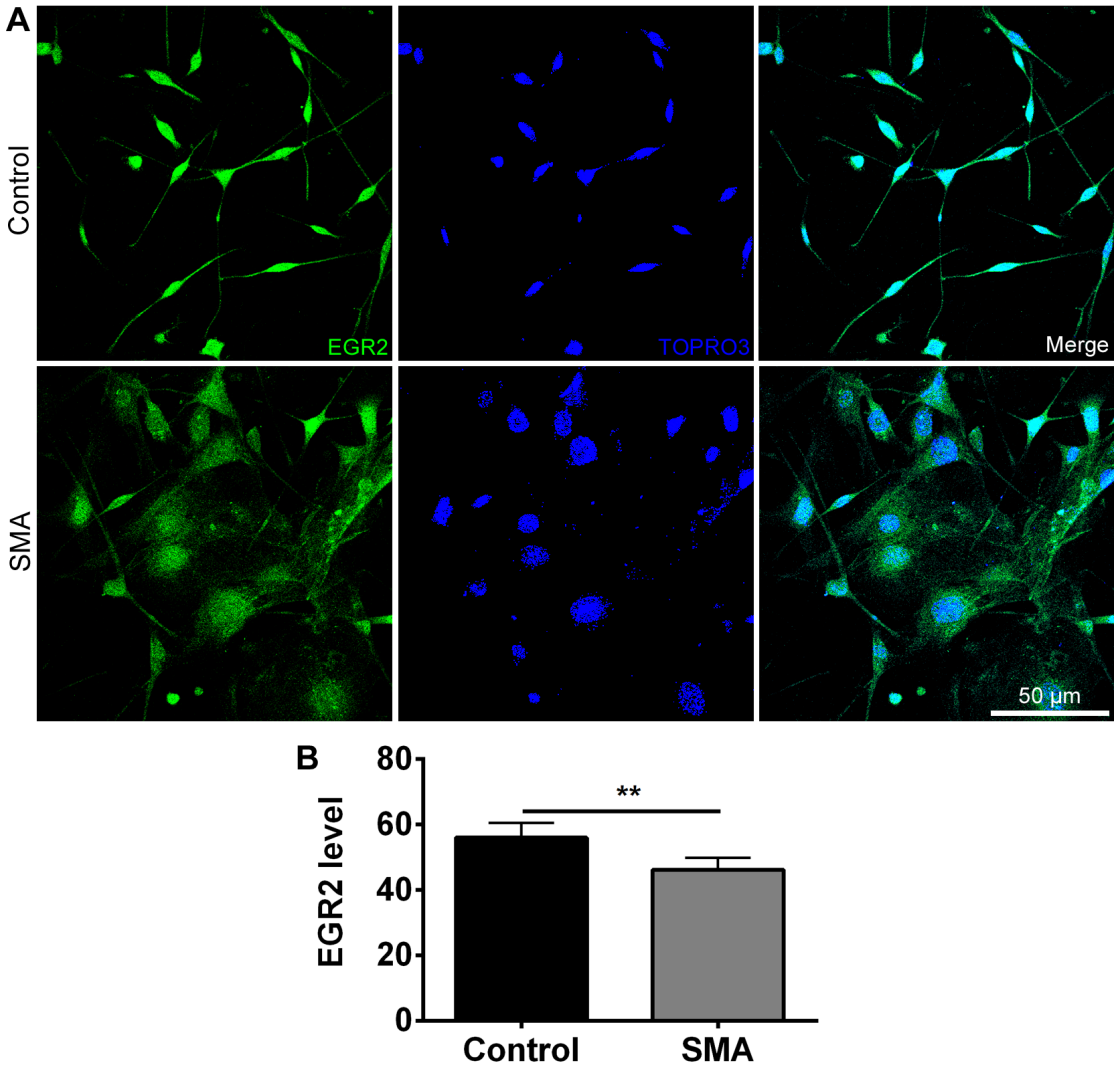

Figure 4.8 Significantly reduced EGR2 expression in isolated SMA-derived Schwann cells post-differentiation. (A) Representative confocal micrographs of differentiated Schwann cells immunolabelled with antibody against early myelin marker EGR2 (green) and nuclei staining TOPRO3 (blue). (B) Bar graph showing significant reduction of EGR2 expression in SMA-derived Schwann cells (P < 0.01; two-tailed, unpaired t-test; N = 2 cultures/ genotype, 2 fields of view imaged per culture, > 25 cells quantified per field of view, n = 8 readings)**

Similarly, EGR2 levels were significantly lower in SMA Schwann cells 72 hours after differentiation (Figure 4.8). The EGR2 immunostaining of SMA-derived Schwann cells revealed altered cell morphology compared to control Schwann cells. To ensure that the altered morphology was not due to experimental errors, the EGR2 immunostaining was repeated and the similar results were obtained. However, the underlying possible mechanisms are still unknown.

These data indicated intrinsic defects in SMA-derived Schwann cells, leading to a failure to respond normally to differentiation signals occurring in the absence of any influence from pathological neurons.

4.2.5 SMN-dependent myelination defects in SMA-derived Schwann cells

Next I wanted to determine whether Schwann cell differentiation defects were SMN dependent and reversible. SMA-derived Schwann cells were transfected with a SMN expression construct under the control of a Schwann cell specific promoter (pMPZ-SMN) (Shorer *et al*., 1995) and pEHHG (a GFP-expression, non-SMN carrying, control construct, see methods) (Hamilton *et al*., 2012) at 90 hours post-differentiation. Control and SMA-derived Schwann cells were also transfected with control pEHHG. Transfection efficiency was 100% for both control and SMA-derived Schwann cells. MPZ levels were quantified at 120 hours post-differentiation. MPZ levels in SMA-derived Schwann cells were restored to levels observed in healthy control Schwann cells. This result indicated that myelination defects in SMA-derived Schwann cells occurred as a direct result of reduced SMN levels. It

also demonstrated that these defects were reversible upon SMN restoration (Figure 4.9).

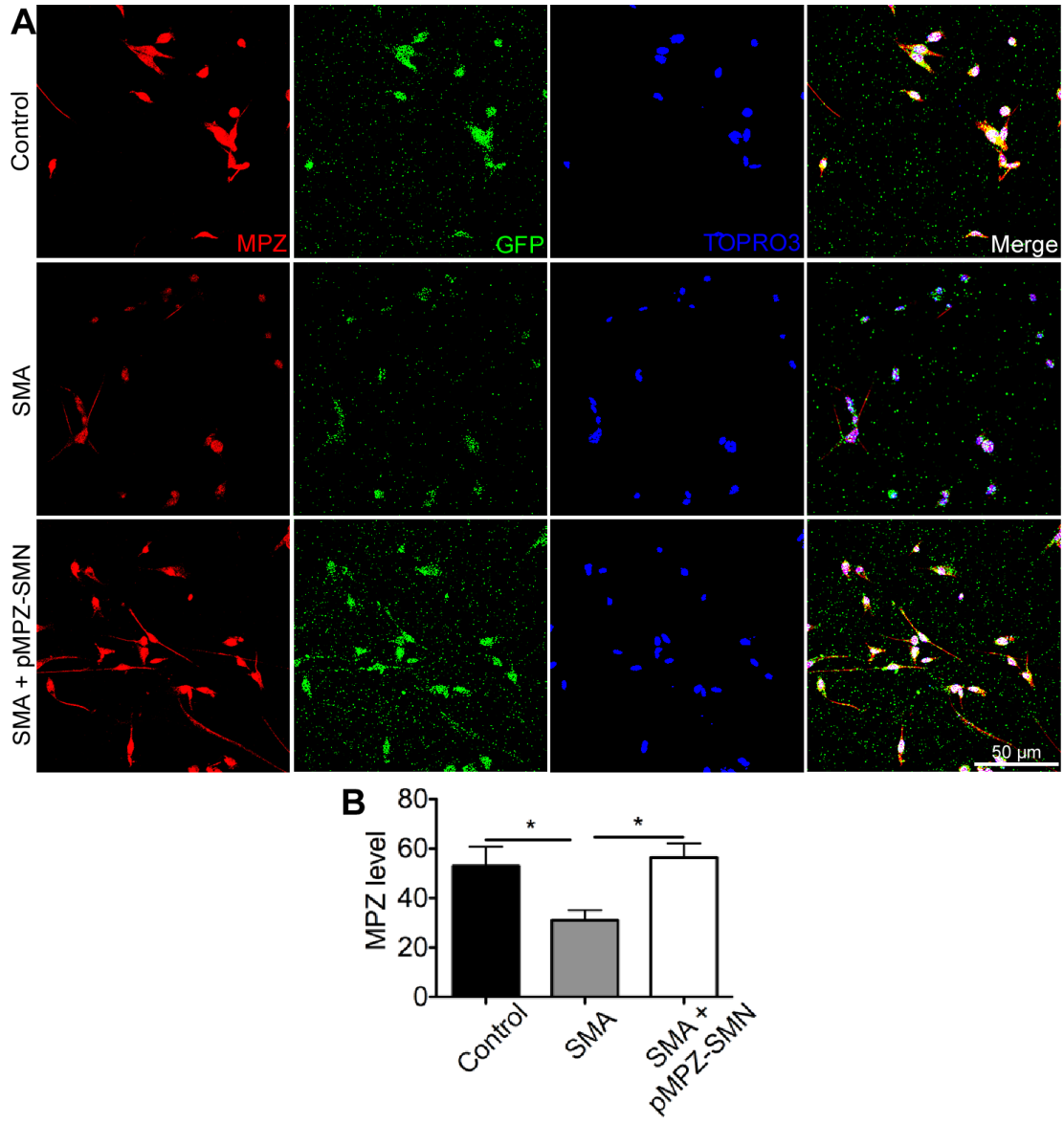

Figure 4.9 (A) Representative confocal micrographs of primary Schwann cell cultures transfected with pEHHG (non-SMN transgene) alone (Control and SMA) or pEHHG/pMPZ-SMN (SMA). Cells were immunolabelled with antibodies against MPZ (red) and cell nuclei were labeled with TOPRO3 (blue). GFP expression was used to confirm the expression from the pEHHG plasmid (green). (B) Bar chart showing a significant restoration of MPZ levels in SMA-derived Schwann cells transfected with pMPZ-SMN compared with pEHHG alone (* P ≤ 0.05;) (At 120 hours post-differentiation; two-tailed, unpaired t-test; N = 4 subcultures from single preparation per genotype, n = 4 readings).

It is interesting to observe SMN transfection effect on SMA Schwann cell differentiation at later time-points, when Schwann cell proliferation will dilute the

amount of SMN construct available to each cell. However Schwann cell's mechanism of action for differentiation has not been studied after 120 hours in wild-type cells (Arthur-Farraj *et al*., 2011) and therefore I did not check those time-points.

4.2.6 Perturbations in expression of myelination transcription factors

Levels of myelin gene transcription factors SOX10, SOX2, POU3F1 and NOTCH1 were quantified 72 hours post-differentiation to examine whether SMN-dependent defects in transcription were responsible for the observed changes in MPZ and EGR2 protein levels. SMA-derived Schwann cells expressed significantly lower SOX10 levels compared to control cells (Figure 4.10).

SOX2 levels were also significantly reduced in SMA-derived Schwann cells (Figure 4.11). In contrast, POU3F1 levels remained unchanged (Figure 4.12). The negative regulator of myelination, NOTCH1 levels were increased in SMA-derived Schwann cells (Figure 4.13). This data showed that perturbations in levels of several myelination regulating transcription factors were present in SMA Schwann cells. These may therefore contribute to low MPZ levels observed in SMA-derived Schwann cells.

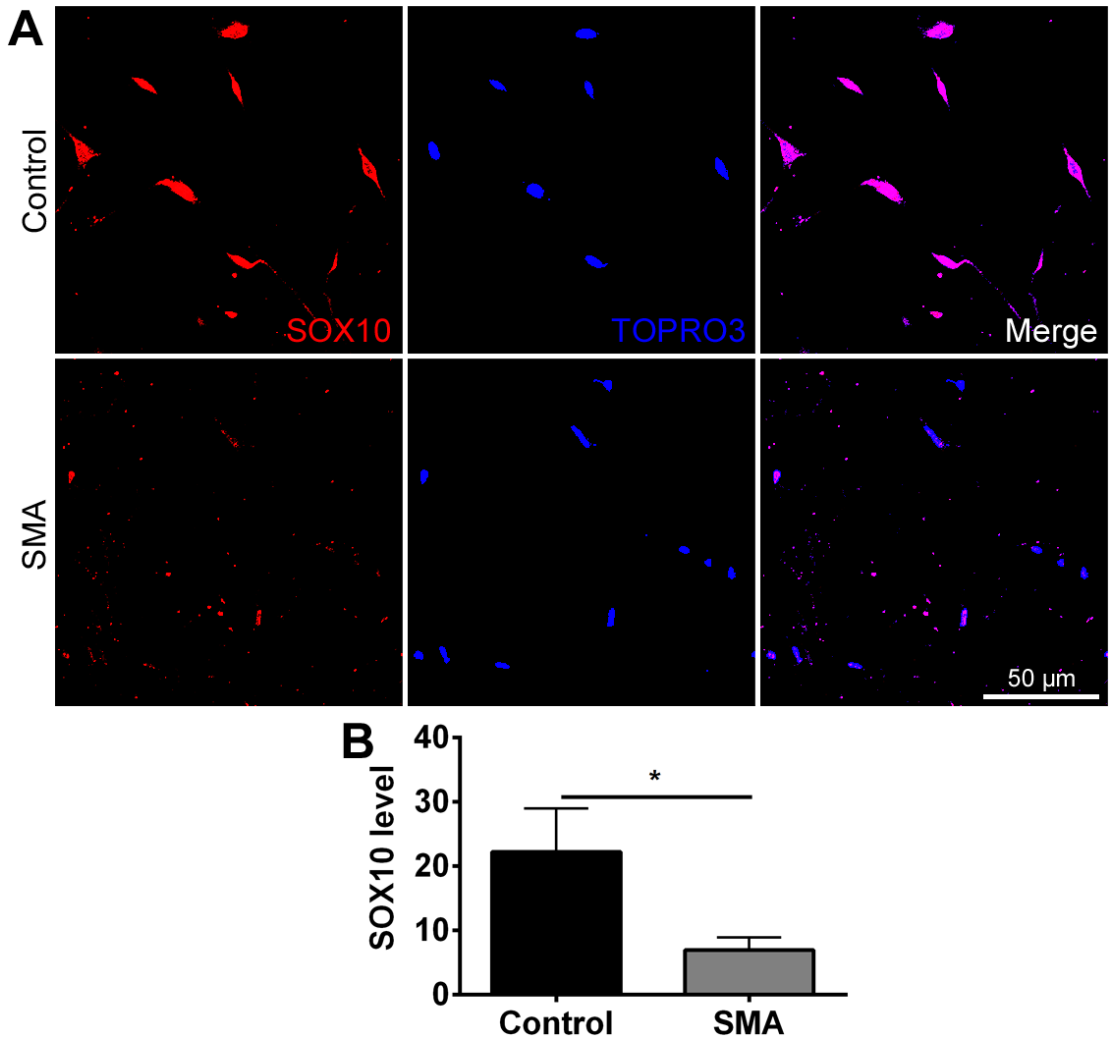

Figure 4.10 (A) Representative confocal micrographs of differentiated Schwann cells showing reduced levels of Schwann cell lineage marker SOX10 in SMA-derived Schwann cells. (B) Bar graph showing significant reduction in SOX10 expression levels in SMA-derived Schwann cells post-differentiation (* P < 0.05; at 72 hours post-differentiation; two-tailed, unpaired t-test; N = 4 subcultures from single preparation per genotype, 2 fields of view imaged per culture, > 25 cells quantified per field of view, n = 4 readings).

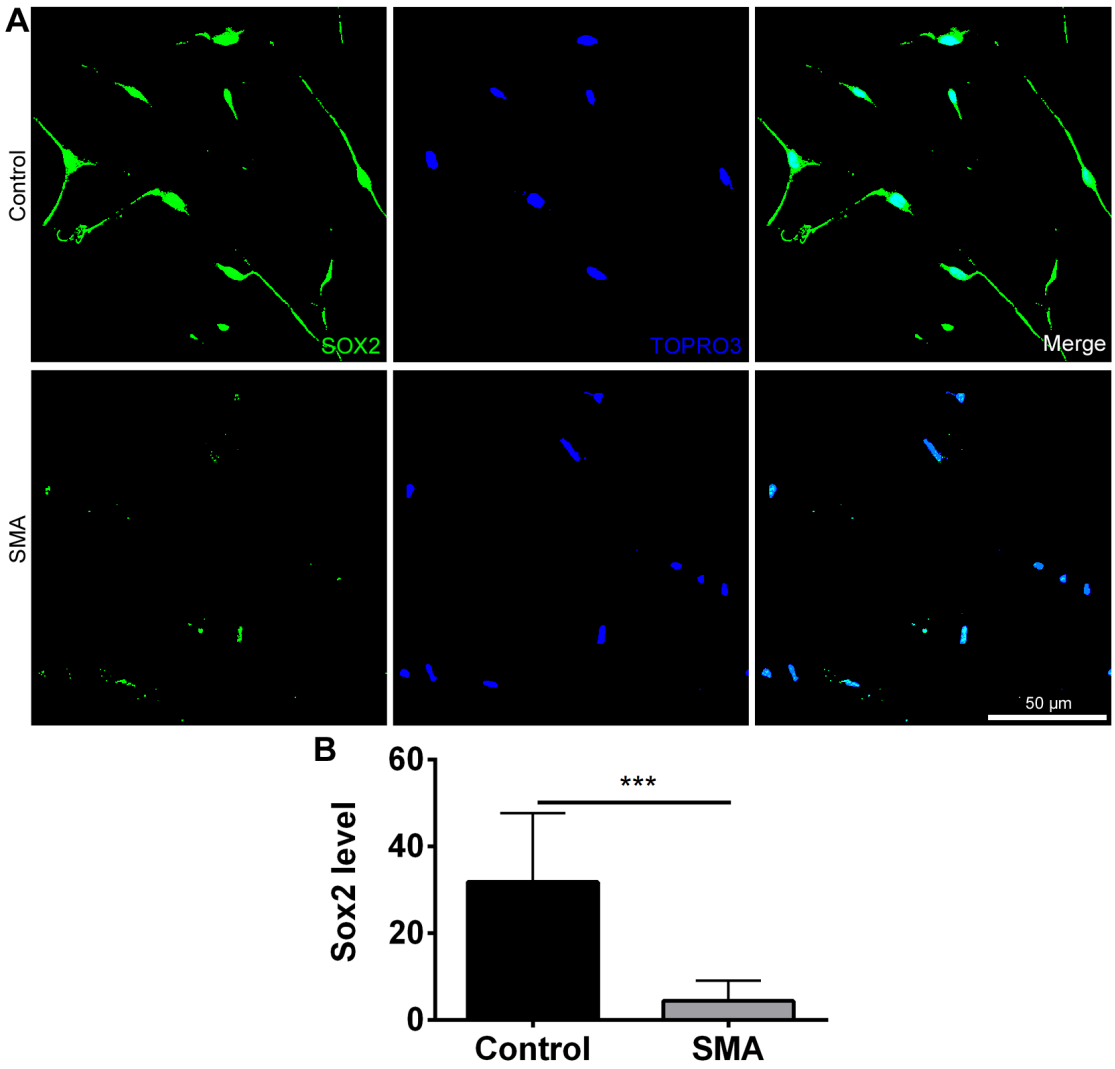

Figure 4.11 (A) Representative confocal micrographs of differentiated Schwann cells showing reduced levels of Schwann cell marker SOX2 in SMA derived-Schwann cells. (B) Bar graph showing significant reduction in SOX2 expression levels in SMA-derived Schwann cells post-differentiation (* P < 0.001 respectively; at 72 hours post-differentiation; two-tailed, unpaired t-test; N = 4 subcultures from single preparation per genotype, 2 fields of view imaged per culture, > 25 cells quantified per field of view, n = 4 readings).**

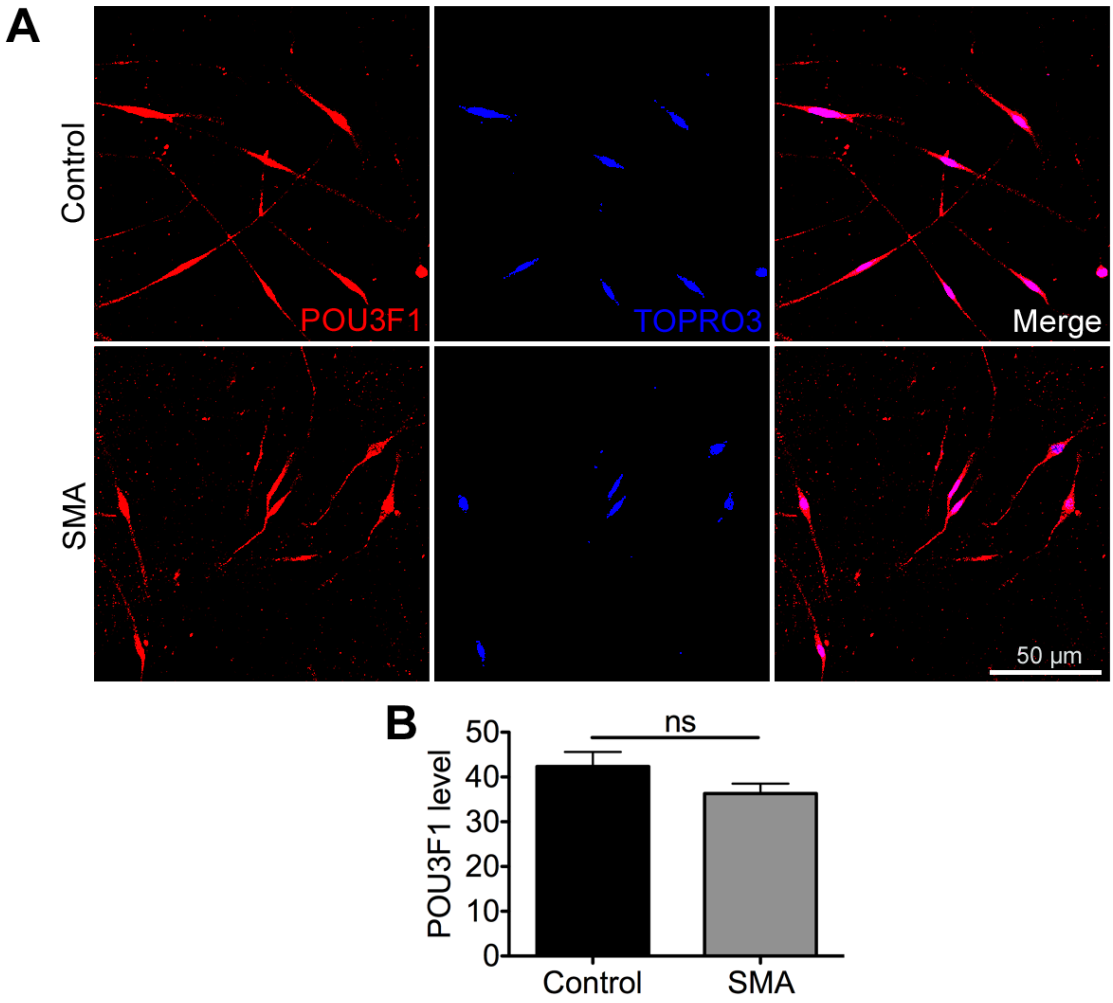

Figure 4.12 (A) Representative confocal micrographs of differentiated Schwann cells showing no change in levels of Schwann cell differentiation marker POU3F1 in SMA derived Schwann cells. (B) Bar graph showing no significant alterations in POU3F1 expression levels in SMA-derived Schwann cells post-differentiation (at 72 hours post-differentiation; two-tailed, unpaired t-test; N = N = 4 subcultures from single preparation per genotype, 2 fields of view imaged per culture, > 25 cells quantified per field of view, n = 4 readings).

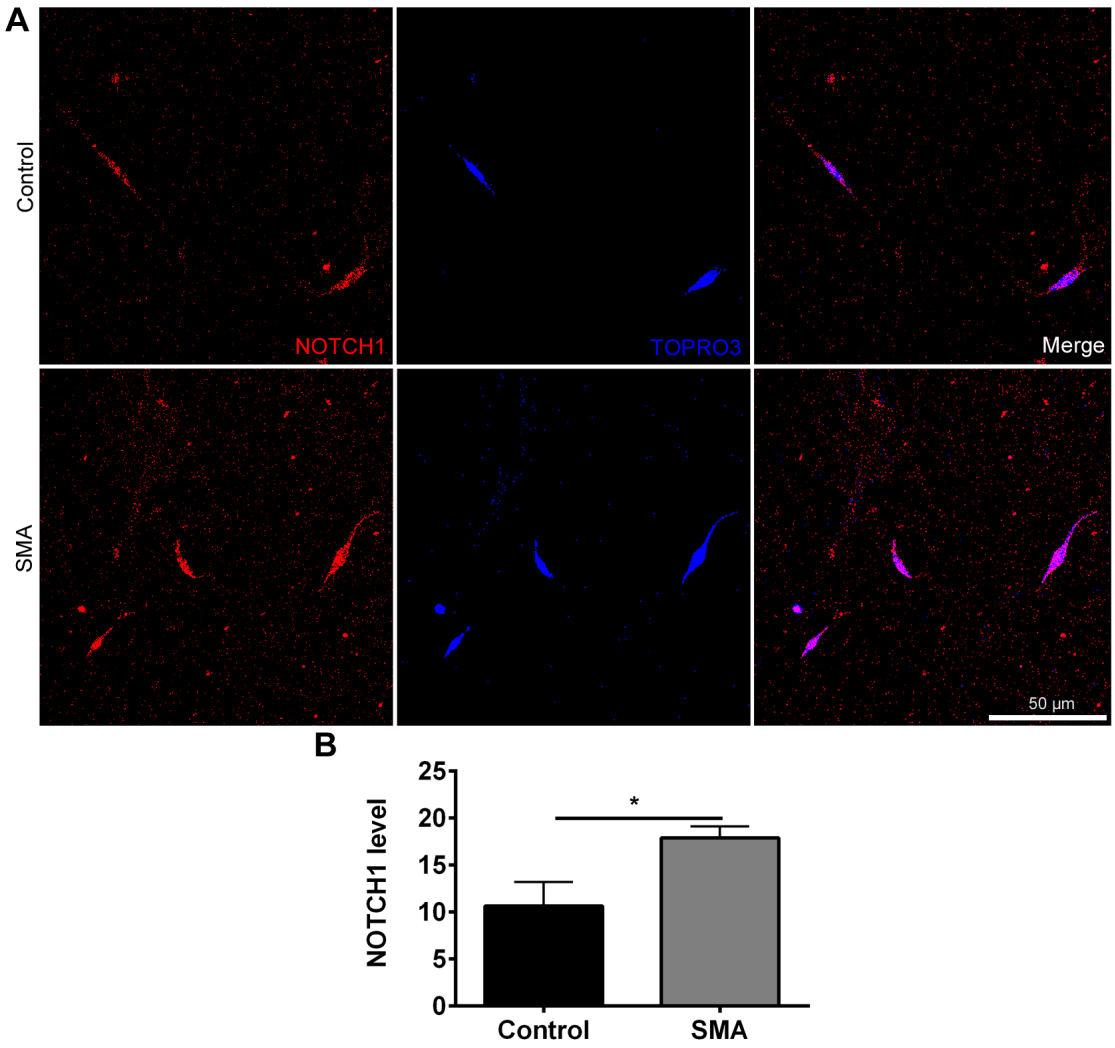

Figure 4.13 (A) Representative confocal micrographs of differentiated Schwann cells showing significant increase in Schwann cell differentiation marker NOTCH1 in SMA-derived Schwann cells. (B) Bar graph showing significant increase in NOTCH1 expression levels in SMA-derived Schwann cells post-differentiation (* P< 0.05; at 72 hours post-differentiation; two-tailed, unpaired t-test; N = 4 subcultures from single preparation per genotype, 2 fields of view imaged per culture, > 25 cells quantified per field of view, n = 4 readings).

4.2.7 Low MPZ levels were not due to transcriptional defects

Next, I wanted to establish whether the reduction in myelin marker MPZ levels in SMA-derived Schwann cells was a direct result of disruption in gene transcription. qPCR analysis of gene transcription at 120 hours post-differentiation revealed that MPZ mRNA levels were the same in SMA-derived Schwann cells compared with control cells (Figure 4.14). Therefore, low levels of SMN were not regulating MPZ

protein levels by modulating gene transcription. This data suggests that SMN likely mediates MPZ expression in Schwann cells by regulating protein translation and/or stability.

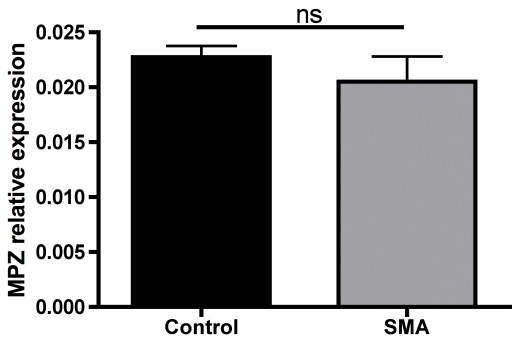

Figure 4.14 No significant difference in the MPZ gene expression levels in control and SMA differentiated Schwann cells (at 120 hours post-differentiation; two-tailed, unpaired t-test; N = 3 mice per genotype, each sample analysed in triplicate).

4.2.8 Deficient myelination of wild-type neurons by SMA-derived Schwann cells in vitro

Next, I used dorsal root ganglion (DRG) neuron-Schwann cell co-cultures (see methods) to establish whether intrinsic deficiencies observed in SMA-derived Schwann cells could induce defective myelination of healthy neurons. Motor neurons are severely affected in SMA, but alterations were also observed in sensory axons (Jablonka *et al*., 2006). Our previous data in a mixed population of motor and sensory neurons was shown defective myelination (Hunter *et al*., 2014). Myelination studies are frequently performed in well-established Schwann cell-sensory DRG neuron co-cultures (Honkanen *et al*., 2007) and we use this model for the myelination experiments instead of using motor neuron-Schwann cell co-cultures.

Myelination was induced in co-cultures for 40 days and cells were immunolabelled with antibodies against neurofilament medium protein (neurite marker) and myelin basic protein (MBP, compact myelin marker). It was observed that there was significant decrease in the percentage of neurites with corresponding myelin protein expressing in co-cultures of SMA-derived Schwann cells with wild-type neurons, compared to those with Schwann cells from littermate controls (Figure 4.15).

This observation suggested that myelination abnormalities observed in SMA mice *in vivo* were, at least in part, due to intrinsic defects in Schwann cells.

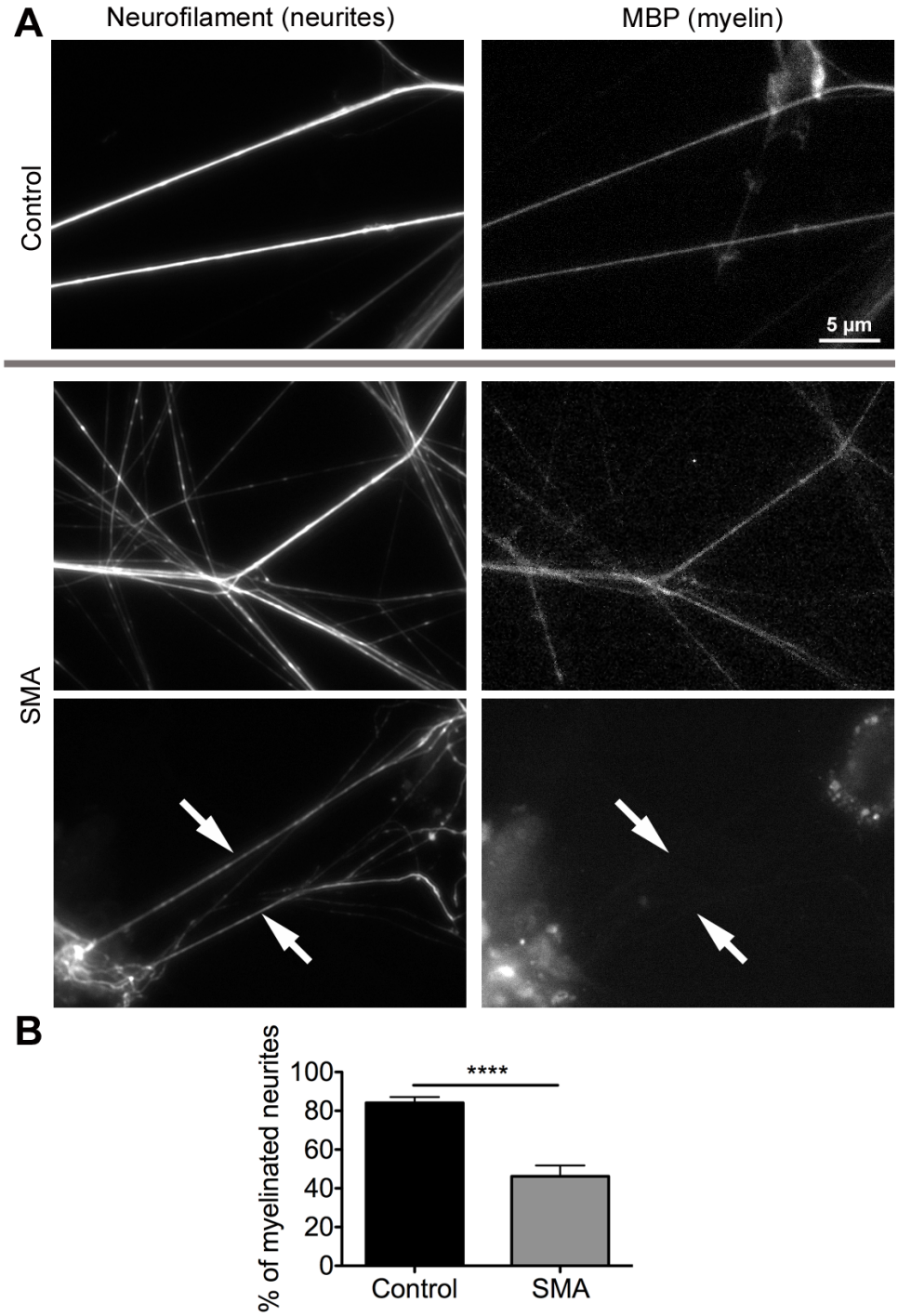

Figure 4.15 Defective ability of SMA-derived Schwann cells to generate myelin protein when co-cultured with healthy neurons. (A) Representative micrographs of DRG-Schwann cell co-cultures immunolabelled with antibodies against neurofilaments (NF-M; left panel) and a myelin marker MBP (right panel) 30 days after induction of myelination. Although some neurite processes were associated with a corresponding MBP signal from SMA-derived Schwann cells (indicating that myelination processes were not completely abolished), many neurite processes lacked a corresponding MBP signal compared with control littermates (white arrows). (B) Bar graph showing a significant reduction in the percentage of neurite processes with a corresponding MBP signal in co-cultures with SMA Schwann cells (** $P \leq 0.0001$; two-tailed, unpaired t-test; N=3 co-cultures per genotype, four fields of view imaged per culture, 5–20 neurites quantified per field of view).**

4.2.9 Influence of SMA Schwann cells on neuronal stability

Next, I wanted to examine whether SMA-derived Schwann cells influenced the stability of neighbouring healthy neurons. Neurite densities were quantified in DRG neuron-Schwann cell co-cultures established with SMA-derived Schwann cells-control DRG neurons and were compared to co-cultures with control cells (see methods). There was a significant reduction in neurite density in co-cultures established with SMA-derived Schwann cells (Figure 4.16). However no axonal fragmentation was observed suggesting a lack of Wallerian-like neurodegeneration. The reduction in neurite density was considered more likely to have happened gradually over time, as seen in dying-back pathways, which have been shown in SMA mice (Murray *et al*., 2008).

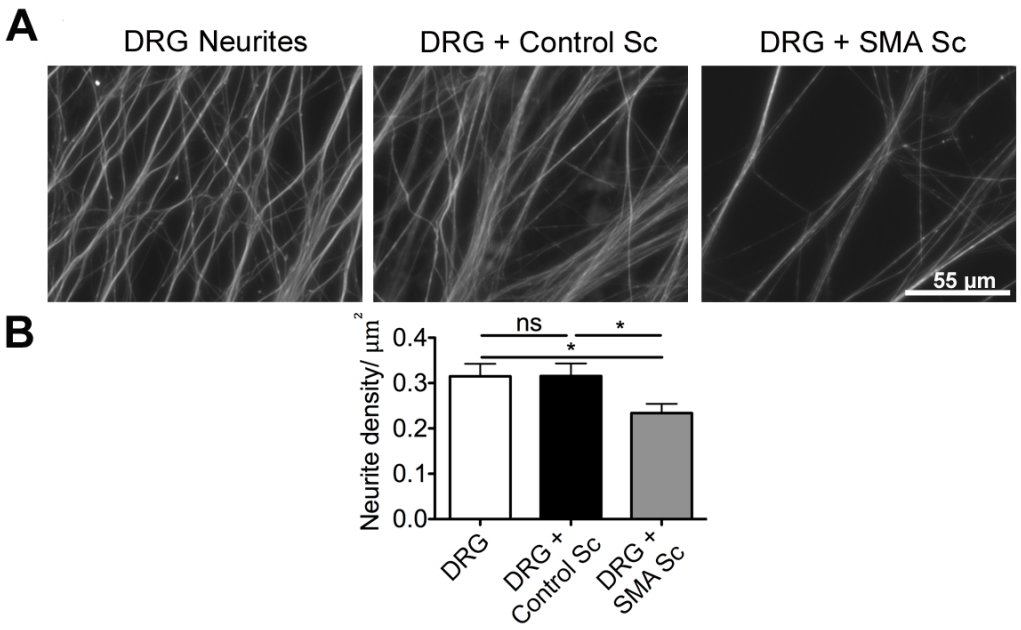

Figure 4.16 (A) Representative micrographs of purified DRG neurites (before addition of Schwann cells), DRG neurites from co-cultures with control Schwann cells and DRG neurites from co-cultures with SMA-derived Schwann cells. Neurites were immunolabelled with antibodies against NF-M. (B) Bar chart showing that neurite densities were maintained after 42 days of co-cultures when healthy DRG neurons were combined with control Schwann cells. In contrast, there was a significant reduction in neurite densities when healthy DRG neurons were cultured with SMA-derived Schwann cells (* P ≤ 0.05; N = 7 co-cultures per genotype, three independent fields of view quantified per culture).

I next investigated the mechanism through which SMA-derived Schwann cells might de-stabilise neighbouring healthy neurons. It has been shown that astrocytes regulate neuron stability by secreting neurotoxic factors in ALS (Lasiene & Yamanaka, 2011). Therefore I examined the ability of SMA-derived Schwann cells to produce neurotoxic factors. Healthy purified DRG neurons were exposed to conditioned medium (see methods) from isolated SMA and control Schwann cells. Phase-contrast pictures were taken at 6, 24 and 72 hours after addition of the conditioned medium. Neurite densities I measured for both cultures and no significant changes were observed (Figure 4.17). Thus, neuronal viability was not being modulated by secretion of a toxic factor from SMA Schwann cells.

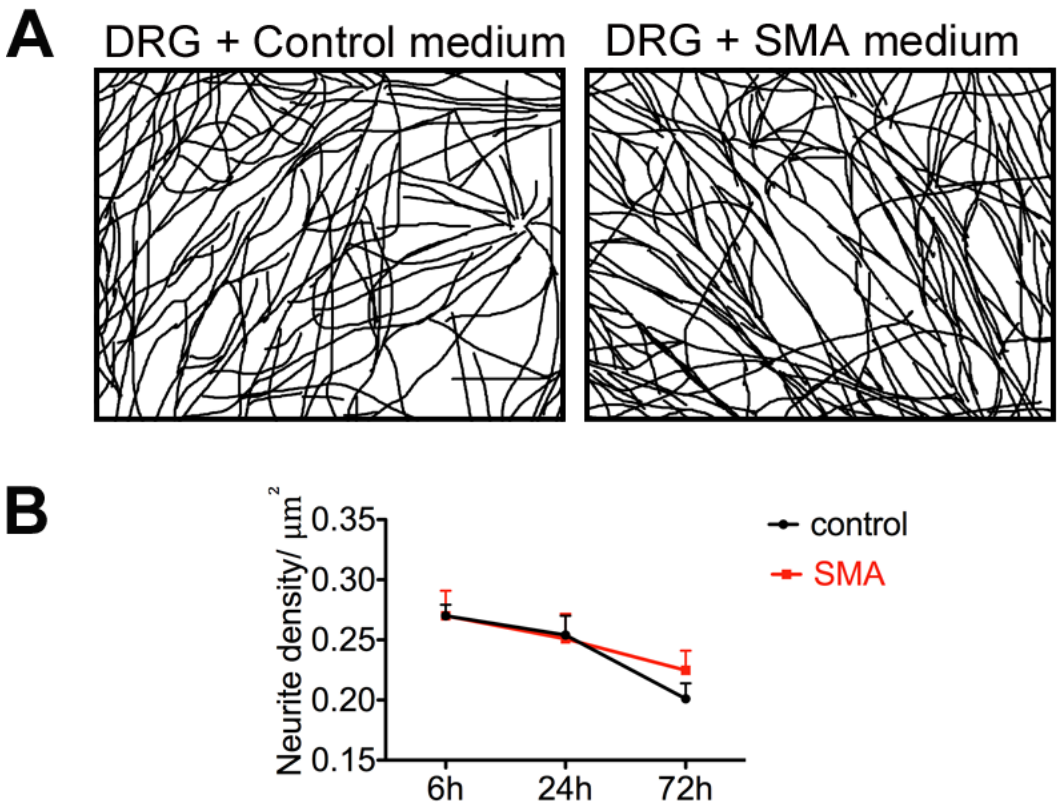

Figure 4.17 (A) Representative tracings from phase contrast micrographs of DRG neurites cultured for 72 hours with conditioned media from either control or SMA Schwann cells. (B) Time-course graph demonstrating no significant change in neurite densities following treatment with conditioned media derived from control (black) or SMA (red) Schwann cells at 6, 24 or 72 h ($P > 0.05$ at all time points; one-way ANOVA with Tukey's post hoc analyses; N = 10 co-cultures per genotype).

Schwann cells could also potentially influence neuronal stability in SMA via disruption to the extracellular matrix (ECM). Microarray analysis on post-symptomatic P5 SMA mouse spinal cord has shown perturbations in extracellular matrix components such as laminin alpha 2 (LAMA2) (Murray *et al*., 2010). Laminin signalling plays an important role in Schwann cell proliferation and differentiation (Chernousov *et al*., 2008). Laminin signalling has also reported to be disrupted in SMA motor neurons (Rathod *et al*., 2012). Local translation of β-actin in growth cones of motor neurons has shown to be regulated by laminin signalling, which is disturbed in SMA (Rathod et al., 2012).

Laminin protein expression was quantified both *in vivo* and *in vitro*. LAMA2 expression levels were examined in intercostal and sciatic nerves representing severely affected and less affected neurons, respectively. At early-symptomatic stage (P7), LAMA2 expression levels in SMA sciatic nerves did not show any difference with control littermates, but it was already significantly decreased in intercostal nerves. At a late symptomatic time point (P11), LAMA2 expression showed a modest reduction in SMA sciatic nerves compared to control nerves.

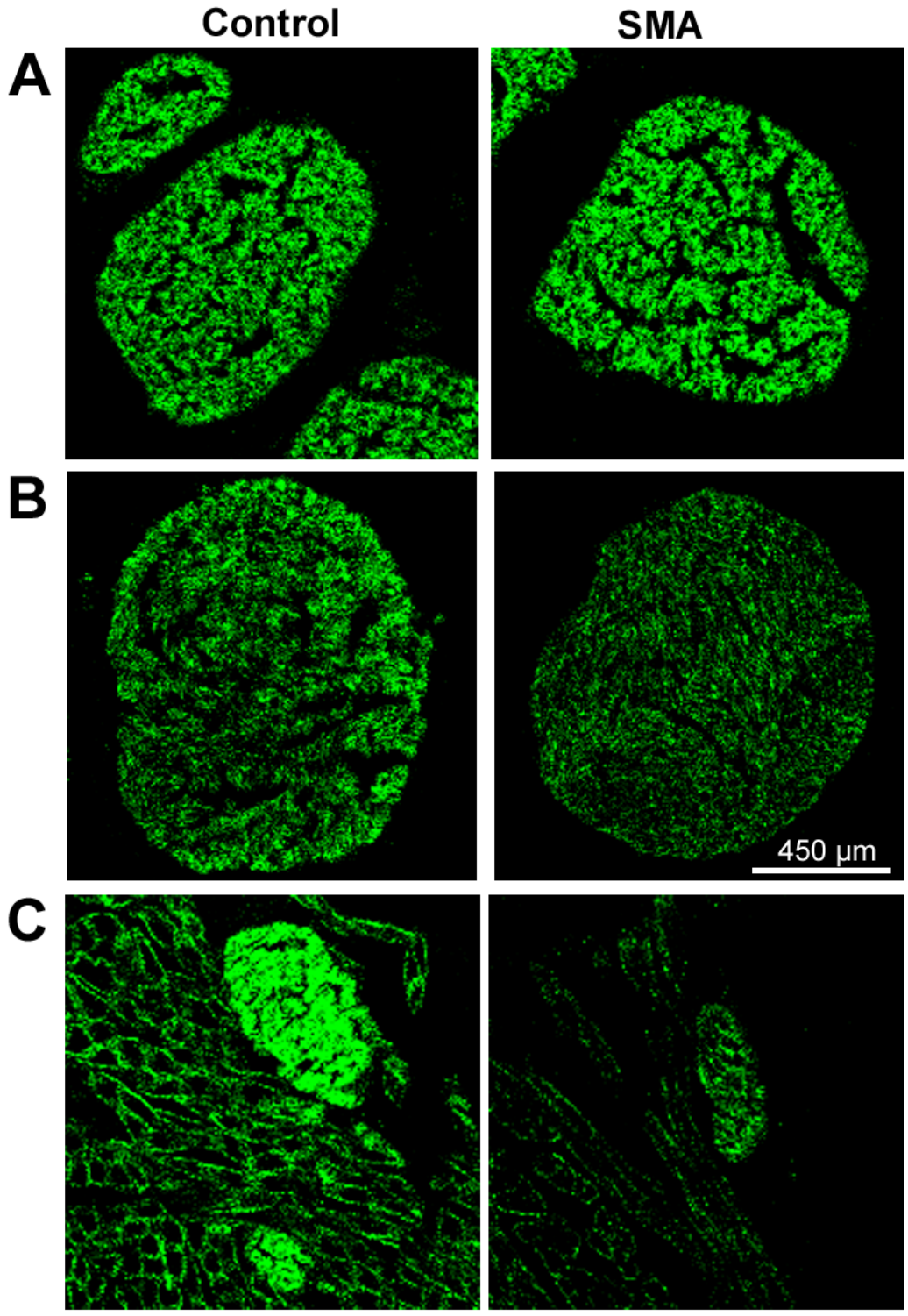

Figure 4.18 Representative fluorescence micrographs of sciatic (A and B) and intercostal (C) nerves from 'Taiwanese' SMA mice and littermate controls immunolabelled with antibodies against LAMA2. All panels were taken with identical microscope settings. (A) There was no difference in LAMA2 levels in sciatic nerve at an early-symptomatic (P7) time point, (B) but there was a modest reduction at P11 (late-symptomatic). LAMA2 levels were already notably reduced in intercostal nerves (white arrows) of SMA mice at an early-symptomatic (P7) time point (C). Note how LAMA2 levels were also reduced in surrounding intercostal muscle fibres in SMA mice.

Analysis of LAMA2 expression in isolated Schwann cells showed significant reduction in SMA-derived Schwann cells compared to control cells at both pre- and post-differentiation stages (Figure 4.19). Therefore reduction in LAMA2 expression in Schwann cells appears to be partly responsible for the LAMA2 deficits observed in peripheral nerve from SMA mice *in vivo*.

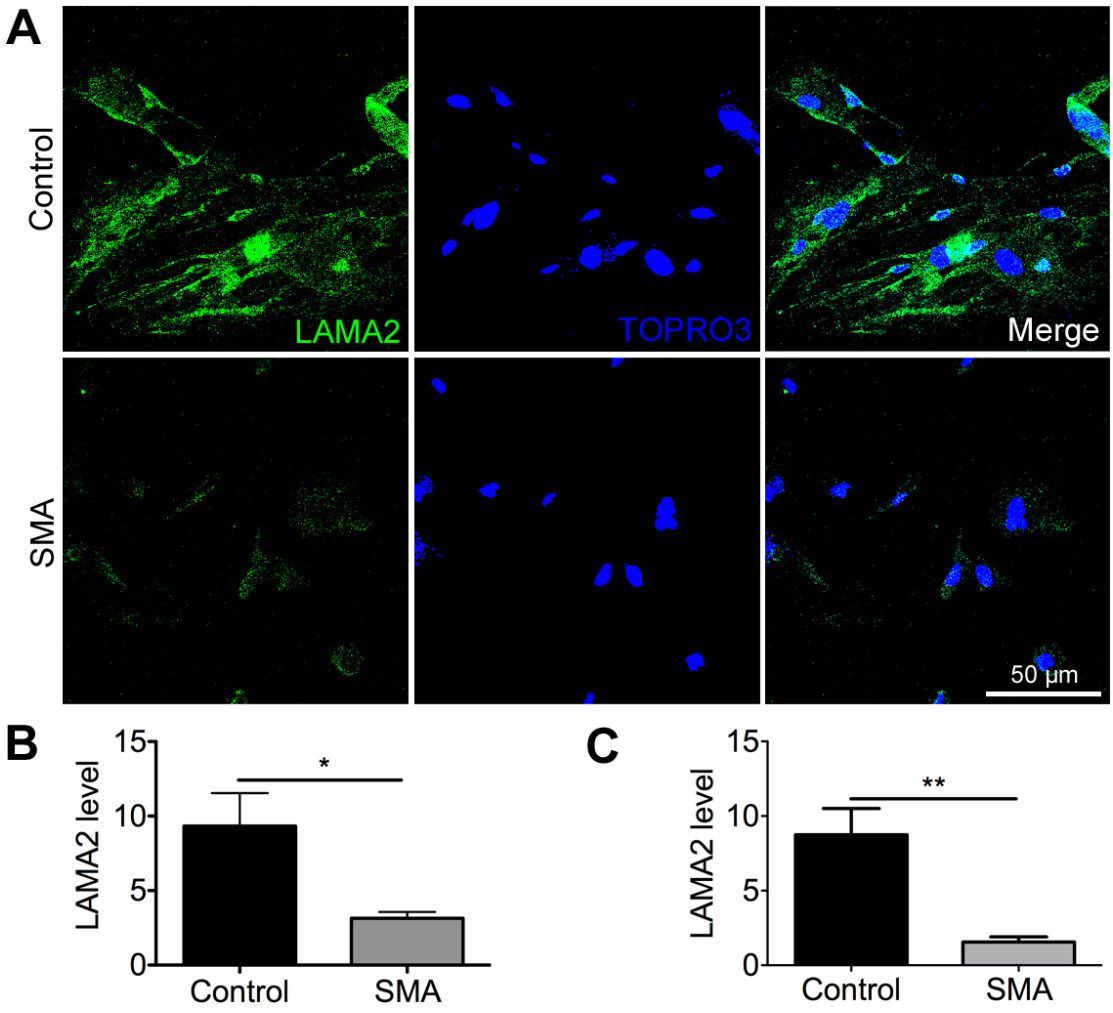

Figure 4.19 (A) Representative confocal micrographs of pre-differentiated Schwann cells immunolabelled with antibodies against LAMA2 (green) and nuclei labeled with TOPRO3 (blue). (B and C) Significant reduction in LAMA2 expression in SMA-derived Schwann cells both pre-differentiation (B) and post-differentiation (C) (* P<0.05, ** P<0.01, respectively; both tests two-tailed, unpaired t-test; N = 4 subcultures from single preparation per genotype, two fields of view imaged per culture, 150 cells quantified per field of view, n = 4 readings).

LAMA2 mRNA levels were also examined in 120 hours post-differentiated Schwann cells, but no significant reduction was observed in SMA-derived Schwann cells. As for MPZ, this suggests a role for translational regulation or stability of LAMA2.

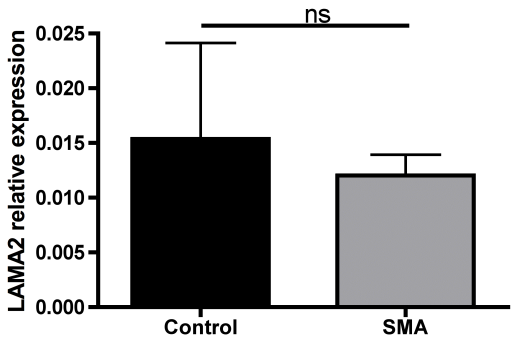

Figure 4.20 No significant difference in LAMA2 gene expression levels in control and SMA differentiated Schwann cells (at 120 hours post-differentiation; two-tailed, unpaired t-test; N = 3 mice per genotype, each sample analysed in triplicate).

These results suggest that defects in Schwann cell expression of ECM components could play a role in the observed reduced neurite stability in the co-cultures. Defective expression of ECM proteins in peripheral nerves in SMA may be mediated, at least in part by, defective expression of ECM proteins by Schwann cells.

4.3 Discussion

In this chapter I demonstrated that isolated SMA-derived Schwann cells developed normally prior to differentiation. However, they failed to respond normally to differentiation upon induction of myelination. Abnormal expression of a key myelin protein (MPZ) in SMA Schwann cells could be rescued by SMN restoration. It was shown that SMA-derived Schwann cells were unable to induce myelination in co-cultures with healthy neurons. SMA Schwann cells also influenced the stability of neighbouring wild-type neurons. This effect was not due to secretion of a neurotoxic factor, but was likely mediated by defects in the ECM core component, laminin. This study suggests that low SMN levels induce intrinsic defects in Schwann cells which lead to abnormal myelination, neurite instability and defective ECM.

Although low levels of SMN are often considered to selectively affect lower motor neurons in SMA, several recent lines of evidence have suggested that SMN depletion also influences other cells and tissues such as muscle, liver, brain, heart, pancreas, bones and vasculatures (Hamilton & Gillingwater, 2013). Therefore, SMA is in fact a multi-system disorder and it is essential to identify the targeted tissues and their pathological alterations in response to low levels of SMN. Our study also confirms this notion and adds Schwann cells to the list of cells that are affected by SMN depletion.

There are several promising therapies for SMA such as gene therapy to replace SMN1 or modification of SMN2 splicing, but the major challenge is to effectively target all cells and tissues contributing to the pathology. For instance, it has been shown that increasing SMN specifically in either motor neurons or skeletal muscle

was not sufficient to inhibit SMA pathology (Martinez *et al*., 2012). Another study compared systemic versus CNS restoration of SMN in severe SMA mouse model and showed that peripheral SMN restoration is essential for long-term rescue of SMA. Systemic SMN restoration improved liver function by increasing insulin-like growth factor (IGF1) to normal levels and extend lifespan by 25 fold (Hua *et al*., 2011). Schwann cells play an essential role in form and function of neurons and targeting Schwann cells alongside motor neurons may lead to more efficient treatments.

It could be still argued that some of the defects I observed in Schwann cells occurred as a secondary consequence of neuronal pathology. In order to further examine the consequence of neuronal pathology for Schwann cells and vice versa, co-cultures with healthy Schwann cells and SMA-derived DRG neurons may give more insight about their mutual interactions

Schwann cell differentiation and myelination have a complex machinery involving collaboration of several transcription factors. SOX10 and EGR2 are essential transcription factors to promote myelination by MPZ transcription (Svaren & Meijer, 2008). I showed perturbations in their levels in SMA-derived Schwann cells. However, our MPZ mRNA analysis indicated no significant difference in MPZ transcription between SMA and control differentiated Schwann cells. Therefore SMN reduction may exert its effect by regulating key myelin protein translation and/or protein stability. Interestingly, SMN has been shown recently to be a transcriptional regulator (Sanchez *et al*., 2013). SMN has been reported to be present along axonal projections of motor neurons and associates with granular foci, the

structures that mediate the transport of specific mRNAs and regulate mRNA localisation, stability and translation. It has been demonstrated that SMN acts through polyribosomes to regulate translation of mRNAs such as arginine methyltransferase CARM1. The mutations in the Tudor domain of SMN have been shown to inhibit translational repression (Sanchez *et al*., 2013). Similarly, SMN may inhibit translation of myelin gene mRNAs as well as laminin and induce intrinsic defects in Schwann cells.

The extracellular matrix plays an important role in Schwann cell development and myelination. Laminin, one major ECM component and its receptor integrins were shown to have fundamental effects on Schwann cell proliferation, survival, process extension and elongation (Chernousov *et al*., 2008). Neurons are also dependent on laminin for their development and stability, as previously reported in SMN-deficient motor neurons (Rathod *et al*., 2012). Our observation of LAMA2 reduction in both peripheral nerves and Schwann cells suggests potential ECM-dependent pathways through which Schwann cells influence neuronal development and stability in SMA. Reduction in LAMA2 levels was observed at a pre-differentiation stage, suggesting a core defect in the Schwann cells, regardless of their myelination status.

Although this study showed that a reduction in SMN levels leads to intrinsic defects in Schwann cells, the precise molecular mechanisms through which SMN exerts its effect remain unclear. For this reason, I analysed protein expression profiles of differentiated SMA and control Schwann cells in the next chapter.

Chapter 5: Label-free quantitative proteomic profiling identifies disruption of ubiquitin pathways as a key driver of intrinsic defects in SMA Schwann cells

5.1 Introduction

In Chapter 4, I demonstrated that depleted SMN levels led to intrinsic defects in Schwann cells from SMA mice. However, the molecular mechanisms through which SMN influenced Schwann cells remained unclear. To specifically address this question, protein expression profiles were quantified and compared in differentiated Schwann cells from SMA and littermate control mice, using label-free proteomics technology.

Proteomics, the large-scale analysis of protein expression, is routinely used to understand molecular alterations during development, pathogenesis and following drug treatments (Tyers & Mann, 2003). Proteomic analysis is important because proteins are the final products of genes that directly influence cell functions. Proteins are a product of mRNA translation, but mRNAs are not always translated into proteins (Adams, 2008). Proteins also undergo different post-translational modifications depending on the physiological state of the cell suggesting that proteomic analysis is a more sensitive approach to study biologically-relevant molecular events in cells and tissues.

Major quantitative proteomic techniques are currently based either on two-dimensional gel electrophoresis (2-DE) or liquid chromatography combined with mass spectrometry (LC-MS) (Messana *et al*., 2013). Proteins are separated from each other by their charge and molecular weight in 2-DE gel based techniques (Görg *et*

al., 2004). Recently, however there has been more interest in LC-MS methods because of their relative high-throughput and reproducibility compared to 2-DE approaches. In LC-MS methods, peptides are tagged by stable isotopes or remain label-free before separation with chromatography (Messana *et al*., 2013; Wang *et al*., 2012).

Proteomic analysis has been used in previous SMA studies. Proteomic analysis of embryonic stem (ES) cells derived from severe SMA mice revealed reduction in SMN-activated cellular stress pathways, disrupted energy metabolism and cytoskeletal stability upon differentiation to motor neurons (Wu *et al*., 2011). Proteomic analysis of the hippocampus in mice with severe SMA revealed widespread modifications in expression levels of proteins necessary for cellular proliferation, migration and development (Wishart *et al*., 2010). Proteomic analysis has also been used to identify drug targets in SMA. Proteomic screens have been performed on a SMA cell line treated with valproate, one potential drug for SMA treatment. It has been observed that valproate treatment reduced collagen I synthesis, resulting in bone loss (Fuller *et al*., 2010). Label-free proteomics have been also performed to identify molecular biomarkers in pathologically-affected skeletal muscle from SMA mice, revealing calreticulin and GRP75/mortalin as biomarkers for reporting on disease progress in samples of muscle and skin (Mutsaers *et al*., 2013). In another study, protein biomarkers have been identified in plasma by iTRAQ (isobaric tag for relative and absolute quantitation) proteomics in human patients (Finkel *et al*., 2012). Therefore, proteomic analysis is a powerful and established tool for examining the molecular pathogenesis of SMA.

Although proteomic experiments can identify specific proteins with altered expression profiles, details concerning protein interactions and the molecular pathways that they participate in require further bioinformatics approaches. For this purpose, Ingenuity Pathway Analysis (IPA) software has been developed. IPA collects data from the published literature and generates functional networks of proteins based on their interactions and/or shared molecular pathways (for more details see: http://www.ingenuity.com). *In silico* pathway analysis of proteomic data has been performed in other SMA studies to identify direct and indirect molecular interactions, pathway associations and functional assessments involving proteins of interest (Wishart *et al*., 2010).

SMN's best-characterised role is in RNA processing pathways (Pellizzoni *et al*., 2002; Lotti *et al*., 2012). However, whether defects in these pathways contribute directly to disease pathogenesis remains unclear (Bäumer *et al*., 2009; Praveen *et al*., 2012). Other potential non-canonical roles for SMN may therefore contribute to disease pathogenesis, including functions in translational regulation (Sanchez *et al*., 2013), axonogenesis (Rossoll *et al*., 2003; Rage *et al*., 2013), and modulation of ubiquitin homeostasis (Wishart *et al*., 2014). To determine the molecular consequences of SMN depletion in Schwann cells, proteomic analysis was used. Our proteomic analysis, unlike previous proteomic screens, was performed in a homogenous cell population and was cell type-specific. Another advantage of our system was that both SMA and healthy control Schwann cells were derived from the same litter and therefore, the experimental variability was reduced.

In this chapter, I undertook a label-free proteomic assessment of differentiated Schwann cells from SMA mice to identify proteins differentially expressed compared to control Schwann cells. Using Ingenuity Pathway Analysis (IPA), I showed that differentially expressed proteins contributed to known muscular and neurological disorders, by influencing cell death and survival pathways as well as glucose metabolism and ubiquitination pathways. Next, I confirmed that ubiquitination pathways were disrupted in differentiated Schwann cells from SMA mice by examining UBA1 levels. I showed that, unlike in the neuromuscular system, UBA1 disruption in Schwann cells did not lead to downstream defects in β-catenin signalling. Finally, I demonstrated that inhibition of UBA1 protein in healthy Schwann cells reduced expression of myelin protein, phenocopying SMA Schwann cells.

5.2 Results

5.2.1 Label-free proteomic analysis of Schwann cells revealed molecular differences in SMA-derived Schwann cells

Label-free proteomic analysis was used to quantify the molecular composition of Schwann cells isolated from control and SMA mice 72-hours post-differentiation (n=3 cultures per genotype, n=5 mice per culture; for detailed description of label-free proteomics see Chapter 2). Briefly, the raw mass spectrometry data was uploaded to Progenesis software for analysis. For each genotype three replicate runs were performed. Sample number 3 from SMA Schwann cells was selected as a reference dataset, based on its minimum distortion pattern. All other runs were initially aligned with the reference run automatically by the software and then manually where required. All ions with retention time of less than 19.589 and more than 138.961 minutes were excluded. The runs were grouped into control and SMA datasets.

The MS/MS data of candidate peptides were exported to the Mascot database for comparison to known peptides and identification of corresponding proteins. 663 proteins were identified and were re-imported to Progenesis software for further filtering by removing data with conflicts (see chapter 2). 195 proteins identified by two or more unique peptides and more than 20% up- or down-regulated in SMA Schwann cells were selected for further analysis. Figure 5.1 shows the filtering process performed on proteomics data from differentiated Schwann cells. 83 proteins out of 195 filtered proteins were up regulated, whereas 112 proteins were down

regulated more than 20% compared to control Schwann cells (Table 5.1 & Table 5.2).

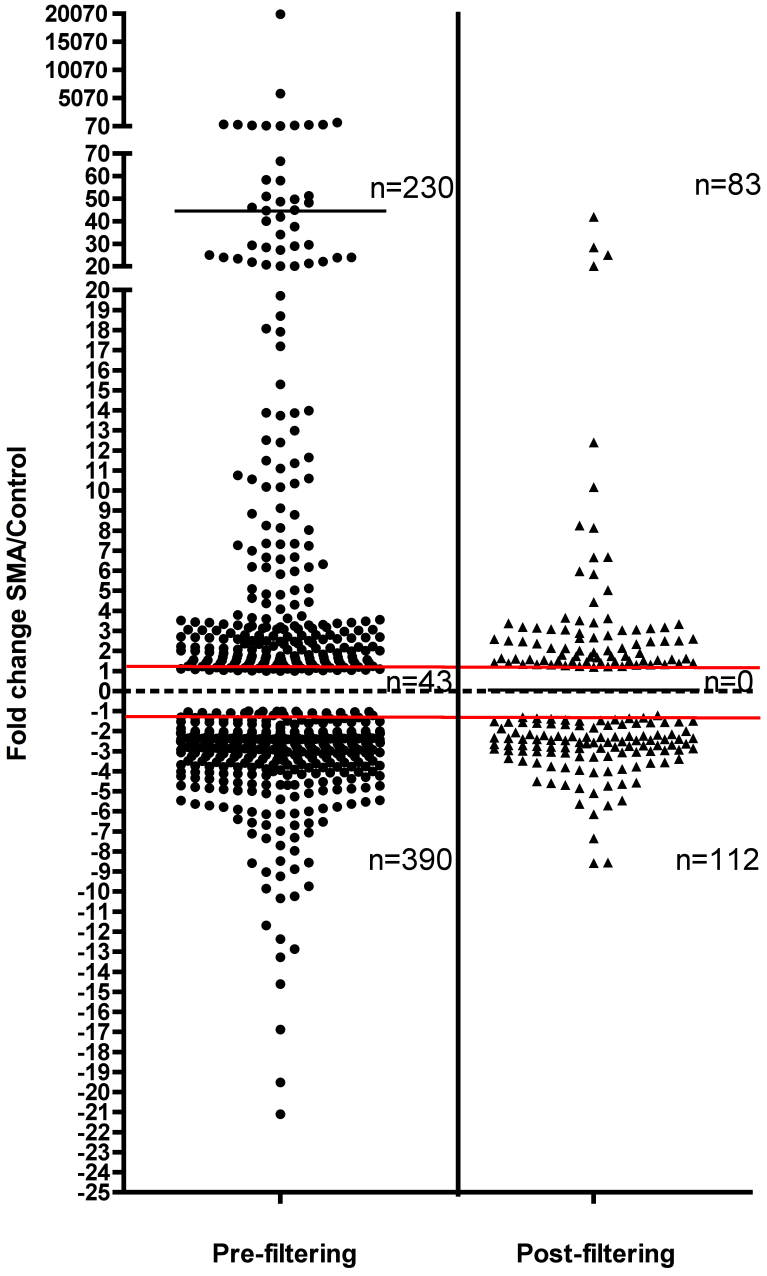

Figure 5.1 Scatter plot showing the process of filtering on the raw label-free proteomics data. 663 proteins were initially identified (left panel) in control and SMA Schwann cells, with the fold change in expression levels between samples represented as a ratio (SMA/Control). 195 proteins were identified after resolving conflicts and filtering based on peptide counts of more than 1 and more than 1.2 fold (20%) change in the expression profile in SMA versus control (right panel). Red lines indicate the 20% cut off threshold for being up- or down regulation in SMA-derived Schwann cells compared to controls. 83 proteins were more than 20% up regulated, whereas 112 proteins down-regulated in SMA compared to control Schwann cells.

Table 5.1 Schwann cell proteins that were up regulated by >20% in SMA mice compared with littermate controls (all peptide counts are >1)

Gene name	Protein name	Accession number	Peptides	Fold change	Anova (P-value)
Rab11b	Ras-related protein Rab-11B	IPI00135869	2	41.92432611	2.25E-06
Ptrf	Polymerase I and transcript release factor	IPI00117689	2	28.47467306	1.29E-05
Me1	NADP-dependent malic enzyme	IPI00128857	3	25.09088637	9.71E-07
Histh2bj Hist1h2bn Hist1h2bf Hist1h2bl	Histone H2B type 1-F/J/L	IPI00114642	3	20.20495492	1.10E-07
Nap1l1	Nucleosome assembly protein 1-like 1	IPI00123199	4	12.40327996	3.38E-05
Surf4	Surfeit locus protein 4	IPI00133249	2	10.1735082	7.08E-05
Crlf1	Cytokine receptor-like factor 1	IPI00408751	2	8.2599662	6.22E-06
Cald1	caldesmon 1	IPI00122450	6	8.135485259	2.29E-05
Uchl1	Ubiquitin carboxyl-terminal hydrolase isozyme L1	IPI00313962	3	6.6846993	2.89E-06
Prdx1	Peroxiredoxin-1	IPI00121788	7	6.674709044	4.52E-06
Hyou1	Hypoxia up-regulated protein 1	IPI00123342	2	5.972535207	0.000311039
S100a10	Protein S100-A10	IPI00222555	2	5.835460334	0.000119939
Cct2	T-complex protein 1 subunit beta	IPI00320217	3	5.033899684	4.44E-05
Kpnb1	Importin subunit beta-1	IPI00323881	2	4.438902892	3.72E-05
Hspa9	Stress-70 protein, mitochondrial	IPI00133903	4	3.66186703	0.000129191
Inf2	Isoform 1 of Inverted formin-2	IPI00678133	3	3.624115204	0.000613975
Sod1	Superoxide dismutase [Cu-Zn]	IPI00130589	2	3.525442066	7.83E-06
Sorbs2	Uncharacterized protein	IPI00177047	2	3.420079863	0.000185545
Dbn1	Isoform A of Drebrin	IPI00135475	4	3.385909332	0.001227799
S100a4	Protein S100-A4	IPI00124096	2	3.33814045	0.000426471
Hadha	Trifunctional enzyme subunit alpha, mitochondrial	IPI00223092	3	3.198565292	3.97E-05
Gpi1	Glucose-6-phosphate isomerase	IPI00228633	2	3.1833332	0.000124524
Dnaja2	DnaJ homolog subfamily A member 2	IPI00136251	3	3.158031031	0.0018338
Psmc1	26S protease regulatory subunit 4	IPI00133428	3	3.136066408	9.42E-05
Rtn4	Isoform 1 of Reticulon-4	IPI00469392	6	3.086615884	0.00015073
Mtap	S-methyl-5'-thioadenosine phosphorylase	IPI00132096	2	3.072450003	0.000287106
Aldh1a1	Retinal dehydrogenase 1	IPI00626662	6	3.060914815	4.87E-05
Anxa1	Annexin A1	IPI00230395	5	3.034787054	7.18E-05
Spna2	Isoform 2 of Spectrin alpha chain, brain	IPI00753793	15	2.901825983	6.87E-05
Col1a2	Collagen alpha-2(I) chain	IPI00222188	2	2.771122421	0.000191984

Gene name	Protein name	Accession number	Peptides	Fold change	Anova (P-value)
Gnb2	Guanine nucleotide-binding protein G(I)/G(S)/G(T) subunit beta-2	IPI00162780	2	2.666925059	5.53E-05
Alb	Serum albumin	IPI00131695	3	2.652972168	4.69E-05
Capg	Macrophage-capping protein	IPI00136906	4	2.612293025	1.23E-05
Fmr1	Isoform ISO3 of Fragile X mental retardation protein 1 homolog	IPI00227005	2	2.598339962	0.0021798
Lasp1	LIM and SH3 domain protein 1	IPI00125091	2	2.515416379	0.000184415
Txnrd1	Isoform 2 of Thioredoxin reductase 1, cytoplasmic	IPI00469251	2	2.511175994	0.019966376
Hk1	Isoform HK1-SA of Hexokinase-1	IPI00283611	2	2.508571096	0.000119071
Serpinb6a	Serpin B6	IPI00121471	4	2.476229472	8.35E-07
Cfl1	Putative uncharacterized protein	IPI00407543	2	2.471950687	0.000588488
Ctnna1	Catenin alpha-1	IPI00112963	2	2.369663732	0.000663734
Plod2	Procollagen-lysine,2-oxoglutarate 5-dioxygenase 2 isoform 1	IPI00123758	2	2.34678508	0.000104885
Hspd1	Isoform 1 of 60 kDa heat shock protein, mitochondrial	IPI00308885	4	2.146343945	0.000931687
Lamc1	laminin subunit gamma-1 precursor	IPI01027808	2	2.145005815	0.000143953
Dnaja1	DnaJ homolog subfamily A member 1	IPI00132208	2	2.135632218	0.000199456
Spnb2	Isoform 1 of Spectrin beta chain, brain 1	IPI00319830	18	2.0347355	7.28E-05
Actr3	Actin-related protein 3	IPI00115627	4	2.012104304	5.79E-05
Atp5a1	ATP synthase subunit alpha, mitochondrial	IPI00130280	4	1.936860813	4.07E-05
Aldoa	fructose-bisphosphate aldolase A isoform 1	IPI00856379	6	1.893735544	2.87E-05
Txnl1	Thioredoxin-like protein 1	IPI00266281	2	1.813438628	0.000853125
Rpn2	Dolichyl-diphosphooligosaccharide-protein glycosyltransferase subunit 2	IPI00475154	3	1.749661854	0.000237411
Clic1	Chloride intracellular channel protein 1	IPI00130344	2	1.747078355	0.003417362
Asah1	Acid ceramidase	IPI00125266	3	1.739801778	0.001747757
Hist1h4[1]	Histone H4	IPI00407339	4	1.712462933	0.000218369
LOC100047183	Protein AHNAK2-like	IPI00988375	5	1.681956919	0.002009435
Col1a1	Isoform 1 of Collagen alpha-1(I) chain	IPI00329872	10	1.635632601	4.97E-05
Gstp1	Glutathione S-transferase P 1	IPI00555023	2	1.617550528	0.000770036

[1] Proteins included are: *Hist1h4m; Hist1h4c; Hist1h4k; Hist1h4h; Hist2h4; Hist1h4b; Hist1h4j; Hist1h4i; Hist1h4d; Hist1h4a; Hist1h4f; Hist4h4; Hist1h4n*

Gene name	Protein name	Accession number	Peptides	Fold change	Anova (P-value)
Cdc42	Isoform 2 of Cell division control protein 42 homolog	IPI00113849	2	1.606802482	0.00205437
Dhx9	Uncharacterized protein	IPI00339468	2	1.587679615	0.008874274
Anxa2	Annexin A2	IPI00468203	10	1.580207437	0.000108256
Hnrnpm	Uncharacterized protein	IPI00918137	3	1.546543537	0.000598341
Anxa6	Annexin A6	IPI00554894	11	1.544715439	0.000874632
Eif4a1	Eukaryotic initiation factor 4A-I	IPI00118676	4	1.513761013	0.000196588
Cct8	T-complex protein 1 subunit theta	IPI00469268	2	1.505322427	0.004745693
Anxa5	Annexin A5	IPI00317309	6	1.501770651	0.021745556
Pfn1	Profilin-1	IPI00224740	4	1.466299712	0.000268083
Gsn	Isoform 1 of Gelsolin	IPI00117167	6	1.458467523	0.000563686
Atp5b	ATP synthase subunit beta, mitochondrial	IPI00468481	7	1.447429818	0.000256396
Ywhag	14-3-3 protein gamma	IPI00230707	2	1.419361866	0.00209086
Plec	Plectin isoform 1b2alpha	IPI00229509	27	1.414294926	0.000882755
Pgd	6-phosphogluconate dehydrogenase, decarboxylating	IPI00466919	4	1.402272187	0.002044674
Rpsa LOC100 505031	40S ribosomal protein SA	IPI00123604	2	1.384561569	0.000822485
Nedd4	E3 ubiquitin-protein ligase NEDD4	IPI00462445; IPI00403303	4	1.370075293	0.004040821
Calm2 Calm1 Calm3	Uncharacterized protein	IPI00467841	3	1.353000447	0.000384019
Akap12	Isoform 1 of A-kinase anchor protein 12	IPI00123709	11	1.33846113	0.002122168
-	36 kDa protein	IPI00988228	3	1.333575392	0.002495454
Hnrnpk	Isoform 2 of Heterogeneous nuclear ribonucleoprotein K	IPI00224575	2	1.323203786	0.000885776
Lmna	Isoform A of Prelamin-A/C	IPI00620256	8	1.321923792	0.001971639
Canx	Calnexin	IPI00119618	2	1.314824795	0.000676768
Tcp1	Isoform 1 of T-complex protein 1 subunit alpha	IPI00459493	5	1.282134418	0.013821566
Rab1	Ras-related protein Rab-1A	IPI00114560	1	1.247558101	0.004760429
Flna	Isoform 1 of Filamin-A	IPI00131138	11	1.240737269	0.018528294
Serpinh1	Serpin H1	IPI00114733	7	1.227110277	0.00120822
Hspa5	Isoform 1 of General vesicular transport factor p115	IPI00319992	8	1.206477959	0.019930791

Table 5.2 Schwann cell proteins that were down regulated by >20% in SMA mice compared with littermate controls (all peptide counts are >1)

Gene name	Protein name	Accession number	Peptides	Fold change	Anova (P-value)
Krt78	Keratin Kb40	IPI00348328	2	8.580116604	1.79E-08
Wdr1	WD repeat-containing protein 1	IPI00314748	3	8.555523292	6.40E-05
Adh5	Alcohol dehydrogenase class-3	IPI00555004	2	7.343104438	6.56E-06
Gorasp2	Isoform 1 of Golgi reassembly-stacking protein 2	IPI00165716	2	6.142796566	9.25E-05
Dsg1b	Desmoglein-1-beta	IPI00380460	3	5.704337338	5.19E-05
Rps8	40S ribosomal protein S8	IPI00466820	2	5.622876477	0.000365601
Jup	Junction plakoglobin	IPI00229475	7	5.454108812	2.30E-07
Rnh1	Ribonuclease inhibitor	IPI00313296	3	5.092790463	1.92E-06
Pgam1	Phosphoglycerate mutase 1	IPI00457898	4	4.834587974	7.21E-07
Dsp	Desmoplakin	IPI00553419	10	4.724196176	2.39E-06
Psap	Sulfated glycoprotein 1	IPI00321190	4	4.687623262	3.80E-06
Rpl10	60S ribosomal protein L10	IPI00474637	3	4.634438831	8.18E-05
Fhl2	Four and a half LIM domains protein 2	IPI00118205	3	4.593067921	0.000239729
Eef1g	Elongation factor 1-gamma	IPI00318841	3	4.569295108	6.51E-07
Rpl12	60S ribosomal protein L12	IPI00849793	5	4.493647854	3.39E-06
Pls3	Plastin-3	IPI00115528	2	4.055721326	0.000240097
Prmt1	Isoform 1 of Protein arginine N-methyltransferase 1	IPI00120495	2	3.999241168	8.71E-05
Sqstm1	Isoform 1 of Sequestosome-1	IPI00133374	2	3.937072326	0.001039479
Glud1	Glutamate dehydrogenase 1, mitochondrial	IPI00114209	3	3.881609805	6.57E-06
Uggt1	UDP-glucose:glycoprotein glucosyltransferase 1	IPI00762897	2	3.800575965	0.000201465
Gnb2l1	Guanine nucleotide-binding protein subunit beta-2-like 1	IPI00317740	3	3.759440568	0.000123855
Hsph1	Isoform HSP105-alpha of Heat shock protein 105 kDa	IPI00123802	4	3.752562932	0.000109693
Gfpt1	Isoform 1 of Glucosamine--fructose-6-phosphate aminotransferase [isomerizing] 1	IPI00406371	2	3.582872971	0.007213633
Vdac2	Voltage-dependent anion-selective channel protein 2	IPI00122547	2	3.565192632	0.000291753
Vwa5a	Von Willebrand factor A domain-containing protein 5A	IPI00221817; IPI00460122	4	3.556067789	0.000116706
Add1	Isoform 1 of Alpha-adducin	IPI00136000	3	3.47734116	2.58E-05
Rps4x	40S ribosomal protein S4, X isoform	IPI00331092	2	3.380730413	0.000224641

Gene name	Protein name	Accession number	Peptides	Fold change	Anova (P-value)
Sugt1	Suppressor of G2 allele of SKP1 homolog	IPI00408957	2	3.349300452	0.000699473
Mtap1b	Microtubule-associated protein 1B	IPI00130920	3	3.280621143	0.00036261
Coro1c	Coronin-1C	IPI00124820	2	3.248513565	0.000236454
Fn1	Fibronectin	IPI00113539	2	3.235657278	0.000460348
Dnm2	Isoform 1 of Dynamin-2	IPI00131445	3	3.064780713	0.00018545
Stat3	Isoform Stat3B of Signal transducer and activator of transcription 3	IPI00227814	2	3.053813233	0.000131014
Copg	Coatomer subunit gamma	IPI00223437	2	3.02780233	0.000368061
Nars	Asparaginyl-tRNA synthetase, cytoplasmic	IPI00223415	5	3.02573343	1.38E-05
Aldh7a1	Isoform 1 of Alpha-aminoadipic semialdehyde dehydrogenase	IPI00230084	2	3.002360735	5.72E-05
Sacm1l	Phosphatidylinositide phosphatase SAC1	IPI00109221	2	2.987224133	0.005108555
Lta4h	Leukotriene A-4 hydrolase	IPI00229527	2	2.980163218	0.005458829
Slc25a12	Calcium-binding mitochondrial carrier protein Aralar1	IPI00308162; IPI00135651	2	2.957860267	0.000128222
Eif2s3x	Eukaryotic translation initiation factor 2 subunit 3, X-linked	IPI00230415; IPI00230416	2	2.952531868	1.90E-05
Rpl10a	60S ribosomal protein L10a	IPI00849927	2	2.928729656	1.82E-07
Hnrnpu	Heterogeneous nuclear ribonucleoprotein U	IPI00458583	2	2.867782152	3.16E-06
Ddah2	N(G),N(G)-dimethylarginine dimethylaminohydrolase 2	IPI00336881	2	2.865538719	5.08E-05
Pcbp1	Poly(rC)-binding protein 1	IPI00128904	2	2.853011693	2.86E-06
Cttn	Src substrate cortactin	IPI00118143	2	2.838307296	4.32E-05
Ap2a2	AP-2 complex subunit alpha-2	IPI00310131	2	2.814409781	0.00049384
Mdh1	Malate dehydrogenase, cytoplasmic	IPI00336324	3	2.787307843	7.42E-05
Npc2	Epididymal secretory protein E1	IPI00129186	2	2.784195535	6.63E-06
Adam10	Disintegrin and metalloproteinase domain-containing protein 10	IPI00131881	2	2.748016221	8.39E-05
Capzb	Isoform 2 of F-actin-capping protein subunit beta	IPI00269481	3	2.739484682	1.11E-05
Sncg	Gamma-synuclein	IPI00271440	3	2.7130939	1.58E-06
Sec23a	Protein transport protein Sec23A	IPI00123349	4	2.707184398	7.27E-05
Fkbp10	Peptidyl-prolyl cis-trans isomerase FKBP10	IPI00122493	2	2.704312293	0.000135942
Lepre1	Isoform 1 of Prolyl 3-hydroxylase 1	IPI00109205	2	2.699075181	7.44E-05
Ctsb	Cathepsin B	IPI00113517	3	2.677051162	4.55E-05

Gene name	Protein name	Accession number	Peptides	Fold change	Anova (P-value)
Ass1	Argininosuccinate synthase	IPI00134746	6	2.654662427	1.17E-06
Sucla2	Succinyl-CoA ligase [ADP-forming] subunit beta, mitochondrial	IPI00261627	2	2.622878616	7.02E-06
Psma4	Proteasome subunit alpha type-4	IPI00277001	2	2.61647652	4.78E-06
P4ha2	Isoform IIb of Prolyl 4-hydroxylase subunit alpha-2	IPI00120100	5	2.564663288	2.28E-05
Itgb1	Integrin beta-1	IPI00132474	2	2.551411055	7.82E-05
Copa	Coatomer subunit alpha	IPI00229834	3	2.547852787	0.003549081
Eif3c	Eukaryotic translation initiation factor 3 subunit C	IPI00321647	3	2.503656699	0.0003898
Eif2s2	Eukaryotic translation initiation factor 2 subunit 2	IPI00116302	3	2.459285924	0.000170835
Tpp2	Isoform Short of Tripeptidyl-peptidase 2	IPI00227843	2	2.45657187	0.002863989
Erp44	Endoplasmic reticulum resident protein 44	IPI00134058	2	2.442842887	0.00046811
Rpl4	60S ribosomal protein L4	IPI00111412	3	2.441677869	0.000305099
Myl6	Isoform Smooth muscle of Myosin light polypeptide 6	IPI00354819	3	2.402047476	2.18E-06
Nsf	Vesicle-fusing ATPase	IPI00656325	2	2.401586278	0.000115937
Epb4.1l2	Band 4.1-like protein 2	IPI00309481	3	2.390794065	0.000285233
Sec31a	Isoform 2 of Protein transport protein Sec31A	IPI00853859	2	2.38311104	9.61E-06
Igf2r	Cation-independent mannose-6-phosphate receptor	IPI00308971	2	2.346499417	0.004459201
Pdcd6ip	Isoform 3 of Programmed cell death 6-interacting protein	IPI00323483	2	2.345054217	6.97E-06
Ap2a1	Isoform A of AP-2 complex subunit alpha-1	IPI00108780	2	2.325042415	0.001261129
Gapdh	Glyceraldehyde-3-phosphate dehydrogenase	IPI00273646	5	2.300796427	2.01E-05
Golgb1	Golgi autoantigen, golgin subfamily b, macrogolgin 1	IPI00929857	2	2.285155195	0.001018217
Rplp2	60S acidic ribosomal protein P2	IPI00139795	2	2.275680059	6.98E-05
Anxa7	Annexin A7	IPI00114017	2	2.261234738	6.06E-05
Nucks1	Nuclear ubiquitous casein and cyclin-dependent kinases substrate	IPI00341869	2	2.243500575	0.000103702
Rps3	40S ribosomal protein S3	IPI00134599	2	2.240970509	0.002182785
Rplp0	60S acidic ribosomal protein P0	IPI00314950	4	2.230476629	2.44E-05
Tufm	Isoform 1 of Elongation factor Tu,	IPI00274407	2	2.204020021	0.002895051

Gene name	Protein name	Accession number	Peptides	Fold change	Anova (P-value)
	mitochondrial				
Prx	Isoform 1 of Periaxin	IPI00469952	2	2.180933796	0.000278402
Uso1	Isoform 1 of General vesicular transport factor p115	IPI00128071	4	2.156768388	0.000698575
P4ha1	Isoform 2 of Prolyl 4-hydroxylase subunit alpha-1	IPI00399959	6	2.15164726	0.001068814
Hnrnpa3	Isoform 1 of Heterogeneous nuclear ribonucleoprotein A3	IPI00269661	2	2.056178629	0.001598363
Uba1	Ubiquitin-like modifier-activating enzyme 1	IPI00123313	4	1.990801394	4.40E-05
Gnb1	Guanine nucleotide-binding protein G(I)/G(S)/G(T) subunit beta-1	IPI00120716	3	1.870269364	0.000958904
Rps17	40S ribosomal protein S17	IPI00465880	3	1.825844017	0.000914371
Nomo1	Nodal modulator 1	IPI00222429	2	1.711952764	0.000377668
Prdx2	Peroxiredoxin-2	IPI00117910	2	1.699377508	0.001276595
Rab6	Isoform 1 of Ras-related protein Rab-6A	IPI00116697	2	1.653058678	0.004742902
Vcp	Transitional endoplasmic reticulum ATPase	IPI00622235	7	1.635592784	4.81E-05
Txndc5	Thioredoxin domain-containing protein 5	IPI00163011	4	1.612167497	0.002283254
Eef1b2	Elongation factor 1-beta	IPI00320208	3	1.59498509	0.0016289
Mvp	Major vault protein	IPI00111258	2	1.590509535	0.00508647
Copb1	Coatomer subunit beta	IPI00120503	3	1.562702879	0.000186958
Sept2	Septin-2	IPI00114945	4	1.549793666	1.64E-05
Tkt	Transketolase	IPI00137409	3	1.547902755	1.32E-05
Psmd1	26S proteasome non-ATPase regulatory subunit 1	IPI00267295	3	1.538023248	0.000101076
Pdia4	Protein disulfide-isomerase A4	IPI00271951	4	1.518737235	2.50E-05
Gdi2	Isoform 1 of Rab GDP dissociation inhibitor beta	IPI00122565	3	1.506890798	0.002116667
Ywhaz	14-3-3 protein zeta/delta	IPI00116498	5	1.485200853	0.000535741
Hsp90b1	Endoplasmin	IPI00129526	4	1.478765174	0.002531193
Hspa4	Heat shock 70 kDa protein 4	IPI00331556	4	1.460867498	0.000924191
Rcn2	Putative uncharacterized protein	IPI00474959	2	1.427991178	0.019124064
Pgk1	Phosphoglycerate kinase 1	IPI00555069	6	1.411842176	0.000262416
Eef2	Elongation factor 2	IPI00466069	10	1.374994769	0.000209352
Myo1c	Isoform 2 of Myosin-Ic	IPI00467172	2	1.351928536	0.003620869
Krt79	Keratin, type II cytoskeletal 79	IPI00124499	1	1.347811428	0.00352169
Col3a1	Collagen alpha-1(III) chain	IPI00129571	9	1.331787626	0.000753896

Gene name	Protein name	Accession number	Peptides	Fold change	Anova (P-value)
Vdac1	Isoform Pl-VDAC1 of Voltage-dependent anion-selective channel protein 1	IPI00122549	2	1.305955275	0.005548413
Pcyox1	Prenylcysteine oxidase	IPI00460063	2	1.206665779	0.01029442

5.2.2 Ingenuity Pathway Analysis (IPA) revealed differentially expressed proteins in SMA-derived Schwann cells are implicated in muscular and neurological disorders

To establish any functional clustering of differentially expressed proteins in Schwann cells isolated from SMA mice, a systems level analysis of the proteomics data was performed using Ingenuity Pathway Analysis (IPA) software. This software collects data from the published scientific literature to analyse proteins of interest with respect to their known functions in biological systems (Wishart *et al*., 2010). 183 out of 195 proteins were mapped for data mining of published literature to establish functional clustering. IPA analysis revealed that approximately 43% of identified proteins modified in SMA Schwann cells were previously implicated in skeletal and muscular disorders and 37% of mapped proteins were known to contribute to neurological pathologies. These data indicate that many of the differentially expressed proteins in Schwann cells from SMA mice are known "pathological" proteins contributing to myopathies and neurological disorders (Table 5.3).

Name	P-value	# Proteins
Neurological Diseases	2.13E-10 - 4.03E-03	64
Developmental Disorder	1.34E-09 - 4.03E-03	39
Hereditary Disorder	1.34E-09 - 4.03E-03	32
Skeletal and Muscular Disorders	1.34E-09 - 4.03E-03	75
Dermatological Diseases and Conditions	1.28E-08 - 3.47E-03	43

Table 5.3 Top ranked diseases and disorders that are associated with differentially expressed proteins identified in SMA-derived Schwann cells by IPA analysis

5.2.3 Functional clustering analysis revealed disruption of cellular assembly, death and survival pathways in Schwann cells from SMA mice

Approximately half of the proteins with more than a 20% change in their expression in SMA Schwann cells were identified to participate in cell assembly and organisation pathways (84 proteins). The laminin receptor, β1 integrin (ITGB1) was shown to be down-regulated in SMA Schwann cells (Feltri *et al*., 2002) (Table 5.2). As shown earlier in this thesis, defective laminin protein production is an important intrinsic defect observed in SMA Schwann cells. Therefore, reduction in SMN levels may exert its effect on laminin expression through modulation of β1 integrin signalling. This further supports the hypothesis that extracellular matrix defects contribute to SMA pathology (Table 5.4, for detailed tables of each molecular function see Appendices 1-5).

Name	**P-value**	**# Proteins**
Cellular Growth and Proliferation	1.10E-13 - 3.31E-03	96
Cell Death and Survival	6.60E-13 - 4.03E-03	95
Molecular Transport	2.29E-11 - 3.40E-03	52
Protein Trafficking	2.29E-11 - 8.60E-04	28
Cellular Assembly and Organisation	3.44E-11 - 4.03E-03	84

Table 5.4 Molecular and cellular functions that altered significantly in Schwann cells from SMA mice

IPA analysis also revealed that 95 differentially expressed proteins are involved in cell death pathways. Apoptotic cell death has previously been reported in SMN-depleted neuroblastoma hybrid (NSC-34) cell lines (Parker *et al*., 2008), muscle satellite cells in a severe SMA mouse model (Dachs *et al*., 2011), and lower motor neurons in SMA fetuses (Ito *et al*., 2011). Similarly it has been shown that human

SMN protein prolonged cell survival in PC12 cells deprived of trophic support (Vyas *et al*., 2002).

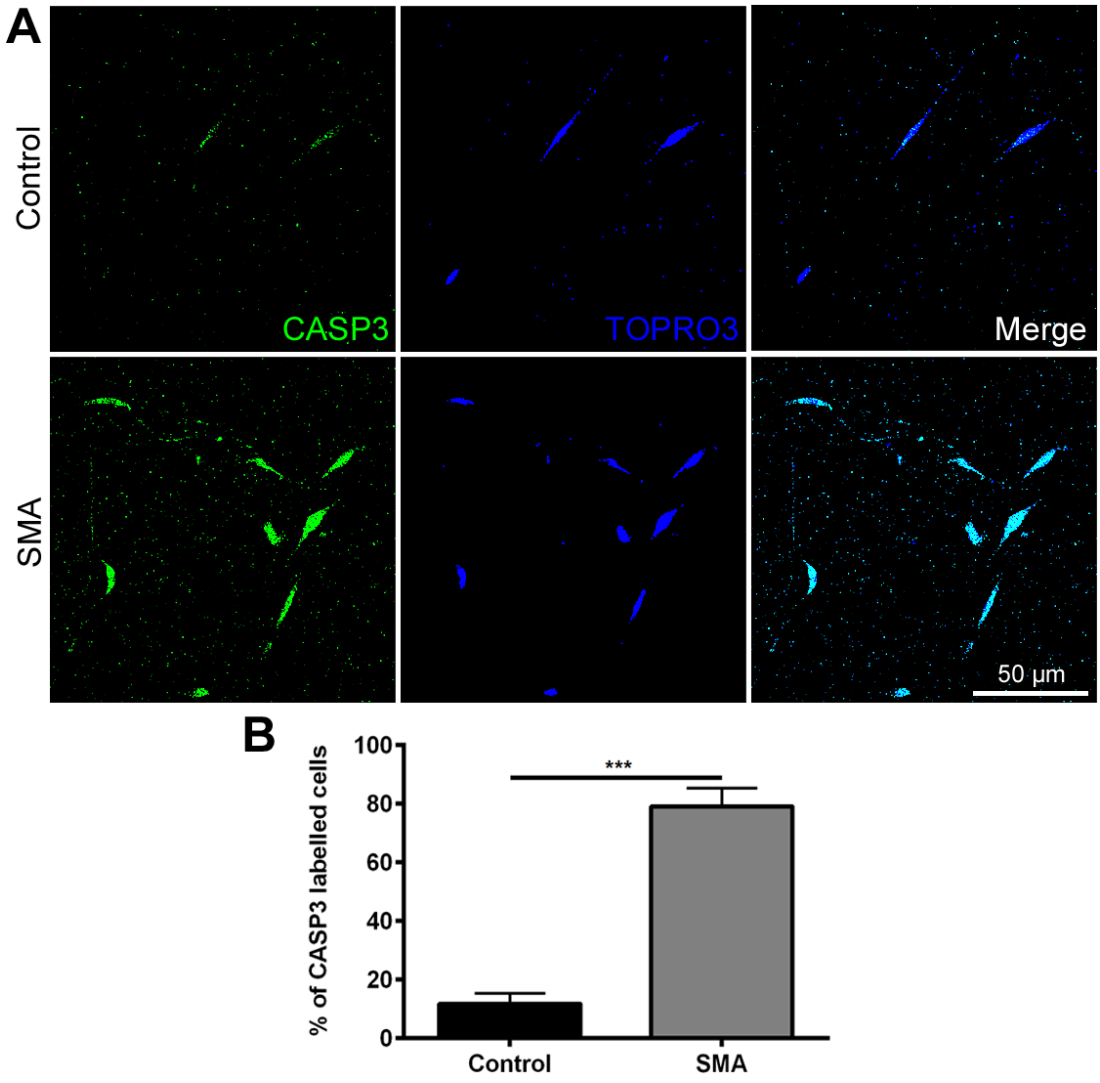

Figure 5.2 (A) Representative confocal micrographs of isolated Schwann cells immunolabelled with antibodies against the apoptotic marker CASP3 (green) and nuclei labeled with TOPRO3 (blue), showing significant increase in CASP3 expression levels in SMA-derived Schwann cells compared to littermate controls 120 hours post-differentiation. (B) Bar graph showing significant increase in levels of CASP3 in SMA-derived Schwann cells compared to control cells 120 hours post-differentiation (* P< 0.001; two-tailed, unpaired non-parametric t-test; N = 4 subcultures from single preparation per genotype, 2 fields of view imaged per culture, > 150 cells quantified per field of view, n = 4 readings).**

To confirm that apoptosis pathways were being activated in SMA Schwann cells, CASP3 immunostaining was performed on SMA and control Schwann cells 120 hours post-differentiation. CASP3 levels were significantly increased in SMA-

derived Schwann cells representing activation of apoptosis pathways (Figure 5.2). These data therefore validate the IPA results suggesting apoptosis pathway activation in differentiated SMA Schwann cells.

5.2.4 Molecular perturbations in glucose metabolism and ubiquitination pathways in Schwann cells from SMA mice

IPA analysis also revealed modifications in several canonical functional pathways in SMA Schwann cells. Disruption in glucose metabolism was identified as one of these pathways (Table 5.5). Perturbations in glucogenesis have previously been observed in both SMA mouse models and type I SMA patients (Bowerman *et al*., 2012; Bruce *et al*., 1995; Kunkel *et al*., 2011).

Name	P-value	Ratio	Proteins
Gluconeogenesis I	1.75E-07	6/48 (0.125)	ALDOA, GP1, MDH1, ME1, PGAM1, PGK1
Protein Ubiquitination Pathway	8.03E-07	14/270 (0.052)	DNAJA1, HSP90B1, HSPA4, HSPA5, HSPA9, HSPD1, HSPH1, PSMA4, PSMC1, PSMD1, SUGT1, UBA1, UCHL1, USO1
Caveolar-mediated Endocytosis Signalling	1.38E-06	8/85 (0.094)	ALB, COPA, COPB1, COPG1, DNM2, FLNA, ITGB1, PTRF
Huntington's Disease Signalling	3.39E-05	11/252 (0.044)	AP2A2, ATP5B, CTSD, DNM2, GNB1, GNB2, GNB2L1, HSPA4, HSPA5, HSPA9, NSF
EIF2 Signalling	3.42E-05	10/201 (0.05)	EIF2S2, EIF3C/EIF3CL, EIF4A1, RPL4, RPL12, RPL10A, RPLP0, RPLP2, RPS3, RPS4X

Table 5.5 Top canonical pathways containing significant numbers of mapped differentially expressed proteins; Ratio represents the ratio of differentially expressed proteins number to the total number of proteins that contribute to the pathway in the IPA database.

Similarly, 14 proteins were identified in our analysis contributing to ubiquitination pathways (Table 5.5). In eukaryotic cells, proteins are degraded by the ubiquitin-proteasome system (UPS), but ubiquitination also regulates different cellular functions such as cell signalling and post-translational modifications (Rubinsztein, 2006). Ubiquitin, a 76 amino acid polypeptide, is activated by E1 enzymes in an ATP-dependent manner. The ubiquitin-conjugating enzyme E2, binds to activated ubiquitin and E3 ubiquitin ligases catalyse ubiquitin transfer to protein substrates. Finally, ubiquitinated protein is degraded by the 26S proteasome (Hershko & Ciechanover, 1998; Kleiger & Mayor, 2014).

Previous studies have reported that ubiquitination pathways are important drivers of disease pathogenesis in SMA (Wishart et al., 2014) with additional contributions to SMN protein turnover (Kwon *et al*., 2013; Han *et al*., 2012; Chang *et al*., 2004; Burnett *et al*., 2009). It has also been reported that ubiquitination regulates neuromuscular junction development (Liu et al., 2009) as well as synaptic growth and function (DiAntonio et al., 2001), processes known to be disrupted in SMA (Murray *et al*., 2008; Kariya *et al*., 2008).

IPA analysis of ubiquitination pathway proteins indicated that ubiquitin carboxyl-terminal hydrolase L1 (UCHL1) was up-regulated in SMA Schwann cells, while ubiquitin activator-like modifier E1 (UBA1) was down regulated (Figure 5.3). Interestingly, SMN expression levels have been shown to be directly regulated by UCHL1 in primary SMA fibroblasts, where over-expression of UCHL1 reduced SMN expression levels (Hsu et al., 2010). Mutations in the UBA1 gene also cause X-linked spinal muscular atrophy (SMAX2), which is characterised by motor neuron

impairments similar to SMN-dependent SMA (Ramser *et al*., 2008; Dlamini *et al*., 2013). Importantly, a recent study has revealed major perturbations in ubiquitination pathways in *Drosophila*, mouse and zebrafish models of SMA (Wishart et al., 2014).

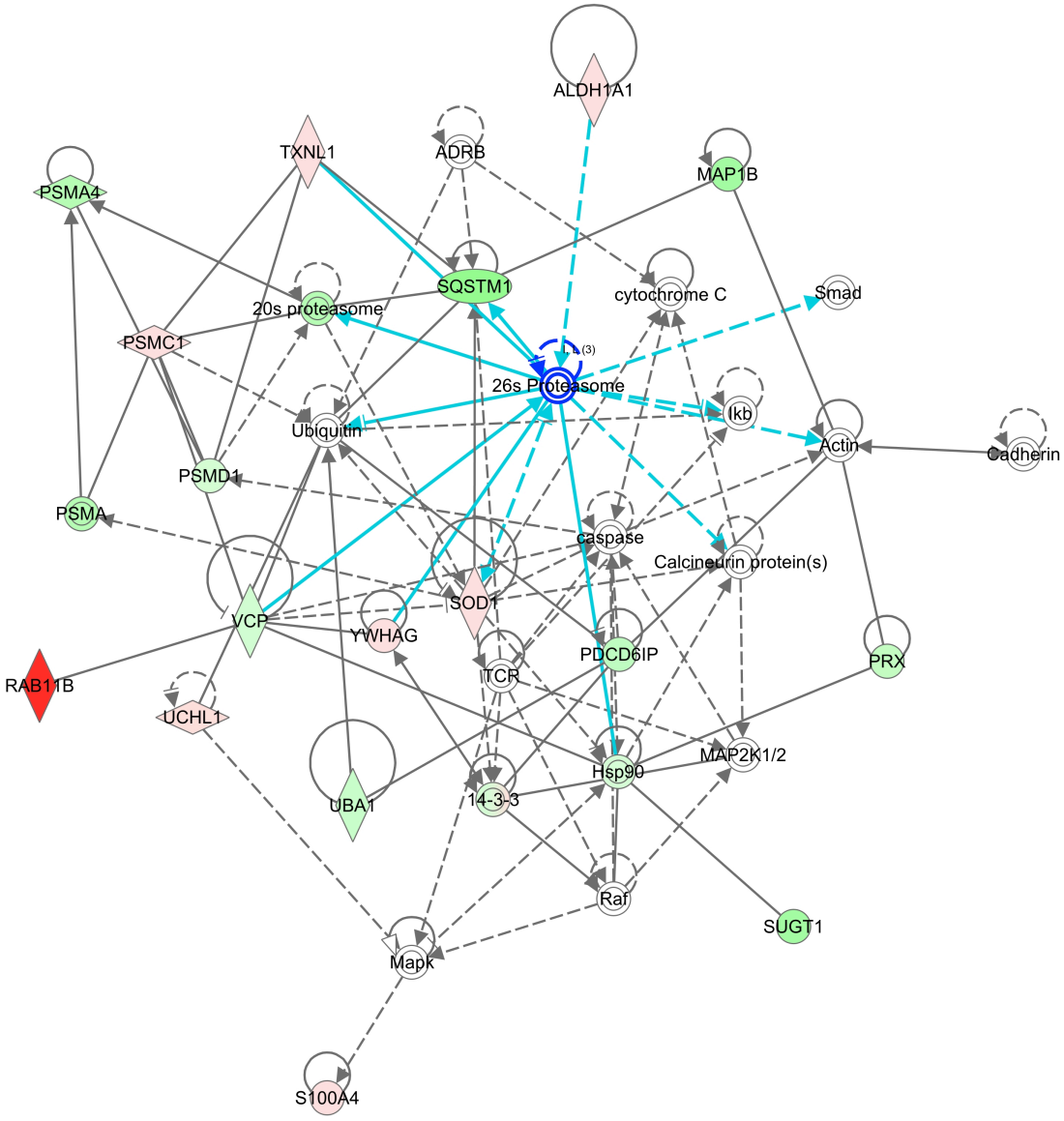

Figure 5.3 Protein-interactions of ubiquitination pathways in SMA derived-Schwann cells. Red nodes represented up-regulated proteins in SMA mice compared to littermate controls, while green nodes represented down-regulated proteins. Grey nodes represented proteins that either not changed in SMA Schwann cells or unidentified in our proteomic screen due to filtering process.

This study showed that reduction in UBA1 levels induced SMA neuromuscular pathology by modulating beta-catenin signalling. The ubiquitin-proteasome system

has also been shown to mediate a variety of cellular physiological events in Schwann cells. For instance, Schwann cell differentiation and myelination have been reported to be mediated by proteasome inhibition after nerve injury (Lee et al., 2009).

5.2.5 Disruption in UBA1 protein levels following SMN depletion exerts its effect on SMA Schwann cells via ß-catenin independent pathways

As discussed earlier, UBA1 protein levels have been shown to decrease significantly in animal models of SMA (Wishart et al., 2014). Therefore I wanted to validate and extend our proteomic data showing reduced levels of UBA1 in differentiated SMA Schwann cells. Schwann cells were differentiated for 72 hours and immunostained with anti-UBA1 antibody. UBA1 protein levels were significantly reduced in SMA-derived Schwann cells compared to littermate controls (Figure 5.4), thereby confirming and validating the proteomic data. These data confirm that reduction in SMN protein levels disrupts ubiquitination pathways, at least in part by reducing levels of UBA1.

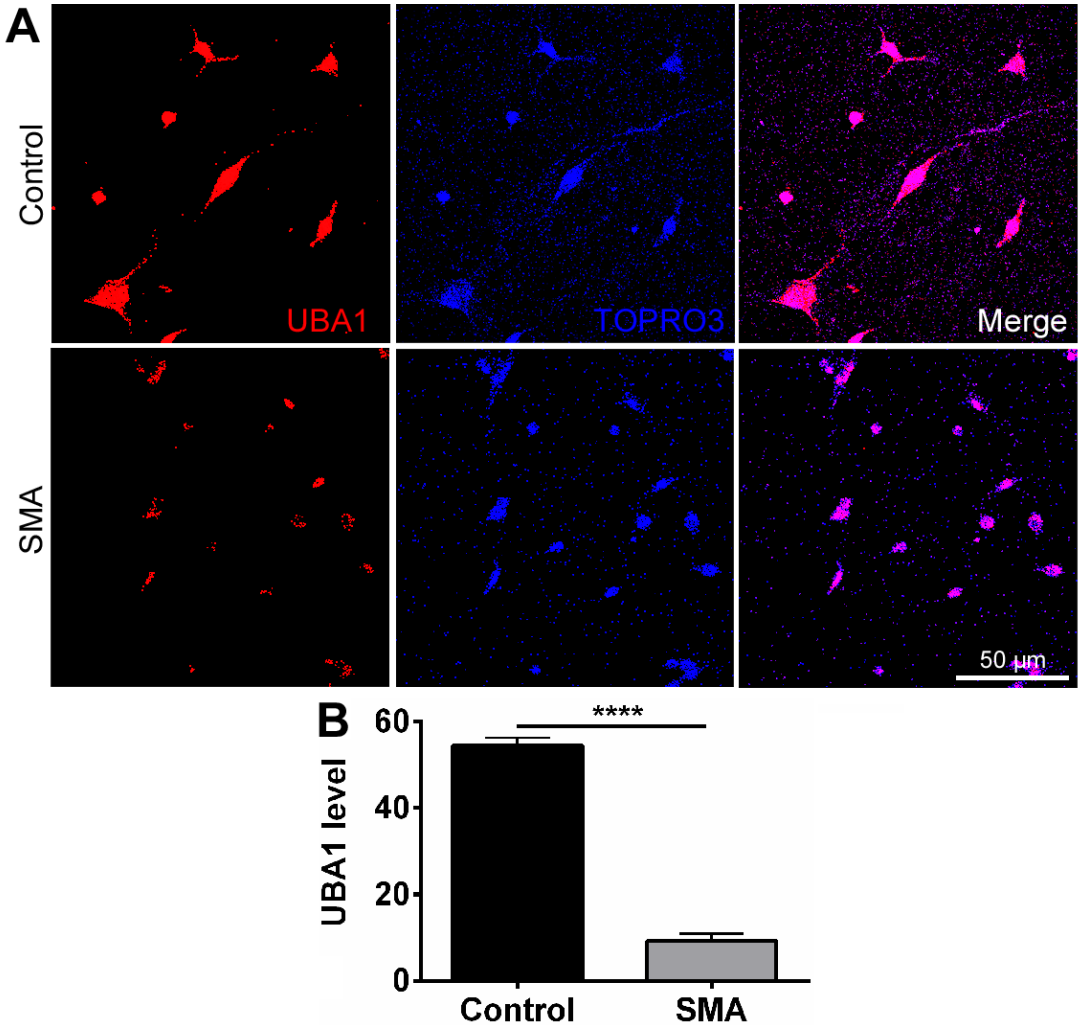

Figure 5.4 (A) Representative confocal micrographs of Schwann cells showing reduced levels of UBA1 in SMA derived Schwann cells compared to control cells 72 hours post-differentiation. (B) Bar graph showing significant reduction in UBA1 expression levels in SMA-derived Schwann cells 72 hours post-differentiation (* P < 0.001; at 72 hours post-differentiation; two-tailed, unpaired t-test; N = 4 subcultures from single preparation per genotype, 2 fields of view imaged per culture, > 25 cells quantified per field of view, n = 4 readings).**

Previous studies in the neuromuscular system have demonstrated that UBA1 levels caused neuromuscular pathology in SMA, at least in part, by modulating beta-catenin dependent pathways (Wishart et al., 2014). Beta-catenin is one of the downstream targets of ubiquination pathways (Clevers & Nusse, 2012) and beta-catenin has been reported to accumulate in both spinal cord and skeletal muscles in SMA mice (Wishart et al., 2014). Pharmacological inhibition of beta-catenin also has been

shown to robustly ameliorate neuromuscular pathology in zebrafish, *Drosophila* and mouse models of SMA (Wishart *et al*., 2014). Therefore, Schwann cells were immunostained with beta-catenin antibody 72 hours post-differentiation to determine whether reduction in UBA1 protein levels exerted its effect through modulating levels of beta-catenin protein.

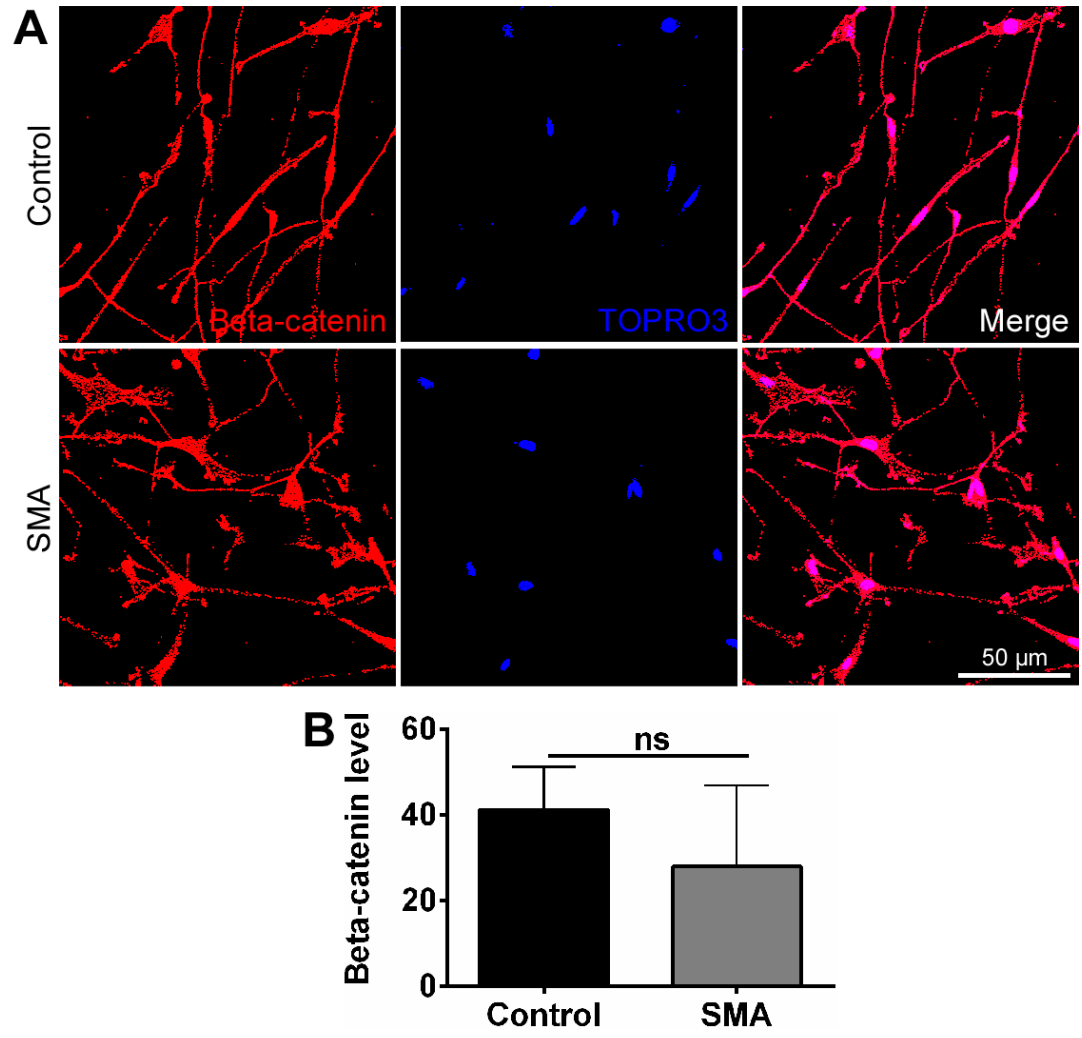

Figure 5.5 (A) Representative confocal micrographs of differentiated Schwann cells showing no significant change in beta-catenin levels in SMA derived Schwann cells compared to control Schwann cells. (B) Bar graph showing no significant difference in Beta-catenin expression levels in SMA-derived Schwann cells compared to littermate controls post-differentiation (at 72 hours post-differentiation; two-tailed, unpaired t-test; N = 4 subcultures from single preparation per genotype, 2 fields of view imaged per culture, > 25 cells quantified per field of view, n = 4 readings).

No significant difference in beta-catenin protein levels were observed in control and SMA Schwann cells (Figure 5.5) suggesting the reduction in UBA1 did not lead to corresponding modifications in beta-catenin pathways, similar to other non-neuronal tissues and organs (Wishart *et al*., 2014).

5.2.6 UBA1 inhibition phenocopied SMA by reducing myelin protein expression levels

To identify whether the disruption to ubiqutination pathways I identified, contributed directly to intrinsic defects I observed in Schwann cells from SMA mice, UBA1 protein was pharmacologically inhibited in healthy Schwann cells by treatment with 10 μM UBEI-41 96 hours post-differentiation (see methods). Myelin marker MPZ expression decreased significantly in healthy Schwann cells after inhibition of UBA1 protein compared to control cells, with MPZ levels similar to those observed in untreated SMA Schwann cells (Figure 5.6). Therefore, pharmacological inhibition of UBA1 phenocopied the post-differentiation myelination defects observed in SMA Schwann cells.

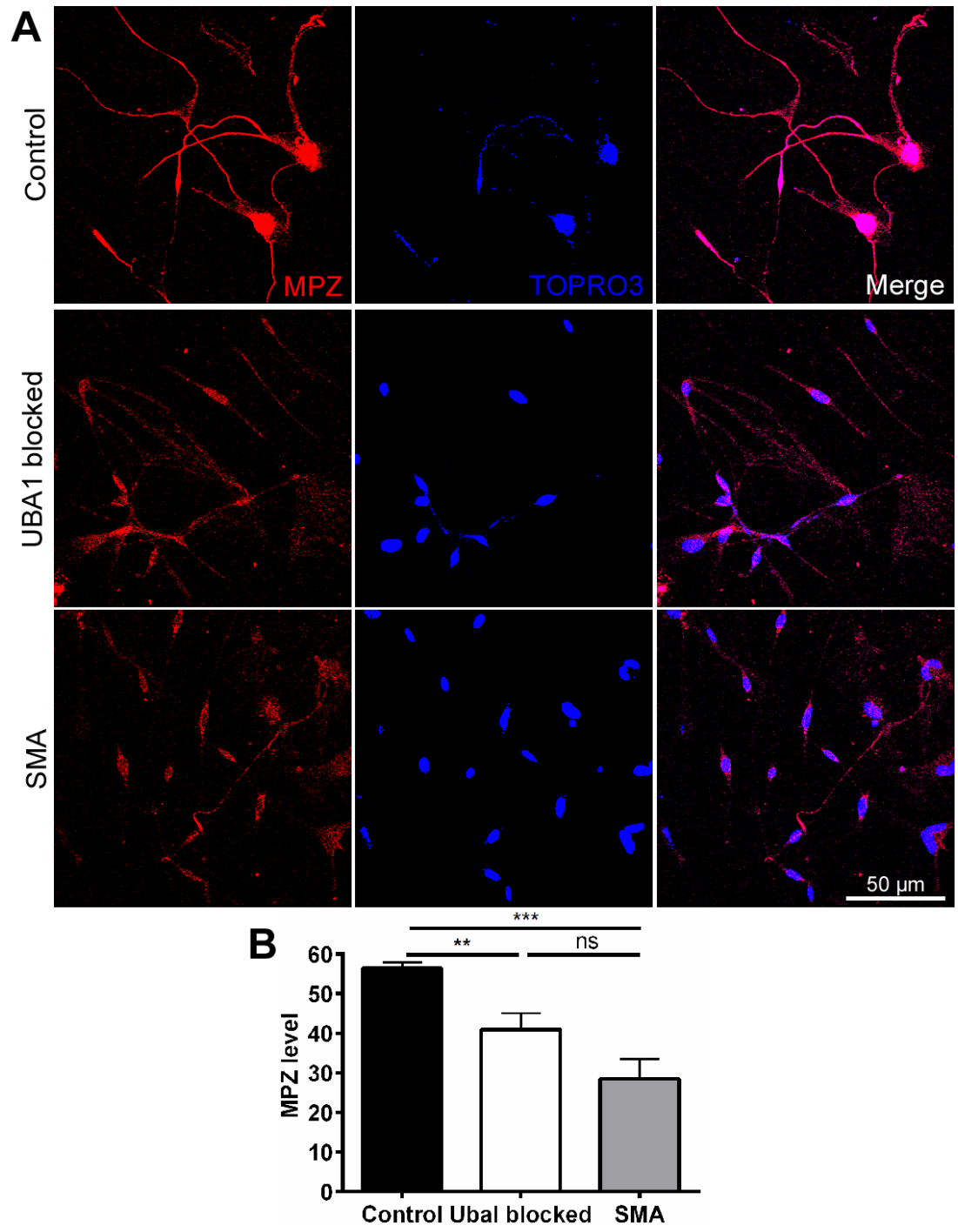

Figure 5.6 (A) Representative confocal micrographs of differentiated Schwann cells showing reduced levels of MPZ in SMA derived Schwann cells. UBA1 blocking of healthy Schwann cells reduced significantly the MPZ level (B) Bar graph showing significant reduction in MPZ expression levels in healthy Schwann cells treated with UBA1 blocker post-differentiation (*P<0.001 and **P<0.01; at 72 hours post-differentiation; two-tailed, unpaired t-test; N = 4 subcultures from single preparation per genotype, 2 fields of view imaged per culture, >25 cells quantified per field of view, n = 4 readings).**

5.3 Discussion

In this chapter, I used highly sensitive label-free proteomics technology to identify differentially expressed proteins in SMA-derived Schwann cells. Using Progenesis software, 195 proteins were identified with > 1.2-fold change in their expression compared to control Schwann cells. Proteins were functionally clustered by IPA analysis. Identified proteins were predicted to be involved in muscular and neurological disorders. Differentially expressed proteins were demonstrated to contribute to cellular functions such as cell proliferation, death and assembly. I also demonstrated that apoptosis was increased in SMA-derived Schwann cells and revealed that proteins contributing to glucogenesis and ubiquitination pathways were modified in SMA-derived Schwann cells. I examined whether disruption in ubiquitination pathways influenced intrinsic defects I observed in Schwann cells from SMA mice. Differentiated SMA Schwann cells showed reduction in UBA1 levels, which induced its effect on SMA Schwann cells via beta-catenin independent signalling. I showed that UBA1 inhibition reduced myelin protein expression in healthy Schwann cells. I conclude that reduction in SMN levels perturbs ubiquitination pathways, and UBA1 in particular, leading to intrinsic defects in Schwann cells from SMA mice.

The extracellular matrix component LAMA2 was shown in Chapter 4 to have decreased expression in SMA-derived Schwann cells. Laminins act as signals to influence Schwann cell survival, proliferation and myelination (Yu *et al*., 2005). Laminins can exert their effects through their receptors such as integrins (Chernousov *et al*., 2008). Interestingly, β1 integrin (ITGB1) was identified in our

proteomics data to be down-regulated 2.5-fold in SMA-derived Schwann cells. Schwann cells lacking laminin-β1 integrin signals are unable to extend processes to interdigitate between axonal bundles (axonal sorting) for proper myelination (Feltri *et al*., 2002). β1 integrins have also shown to be a key factor in axo-glia interactions in central nervous system (CNS) myelination (Câmara *et al*., 2009). Similarly, axo-glia interactions have been shown to be disrupted in SMA mice (Hunter *et al*., 2014) suggesting a likely role for β1 integrin in normal axo-glial maturation observed in SMA mice.

The ability of Laminins to induce β-actin mRNA translation has been shown to be disrupted in SMN-deficient motor neurons (Rathod *et al*., 2012). Inverted formin-2 (INF2) protein is one of the actin mediators with dual functions of accelerating both polymerisation and depolymerisation (Chhabra & Higgs, 2006). INF2 was significantly increased (3.6-fold) in SMA Schwann cells compared to control cells. It has been shown that mutations in *INF2* induce a rare form of Charcot-Marie-Tooth (CMT) disease with renal dysfunction. Abnormal accumulation of β-actin in Schwann cell cytoplasm induced myelination abnormalities (Mathis *et al*., 2014). Therefore, further studies may be warranted to examine the influence of INF2 on β-actin polymerisation and subsequent myelination in SMA pathology.

The actin-binding protein plastin-3 (PLS3) was also down-regulated 4-fold in Schwann cells from SMA mice. Oprea *et al*. demonstrated that PLS3 acts as a protective modifier of SMA through increasing F-actin levels (Oprea *et al*., 2008). PLS3 protein levels have been shown to be SMN-dependent in a zebrafish model of SMA (Hao le *et al*., 2012). SMN exerted its effect by regulating PLS3 translation

(Hao le *et al*., 2012). Overexpression of PLS3 in SMA mice has been shown to stabilize axons and increase muscle fiber size (Ackermann *et al*., 2013). F-actin has been observed to regulate the Schwann cell cytoskeleton and myelination (Susuki *et al*., 2011). This suggests a potential mechanism through which a reduction in SMN levels decreases PLS3 levels in SMA Schwann cells, resulting in defects in the cytoskeleton and myelination through perturbations in F-actin levels.

37% of the proteins I identified with altered expression in SMA Schwann cells have previously been shown to contribute to neurological disorders. Superoxide dismutase 1 (SOD1) protein, a genetic cause of ALS, was one of the altered proteins in our proteomic analysis. It was down-regulated by 2.1-fold in SMA-derived Schwann cells. It has been demonstrated that mutant SOD1 alters the localization of SMN protein by preventing its recruitment to Cajal bodies (Kariya *et al*., 2012). SMN protein was also shown to protect cells against oxidative stress and subsequent cell death caused by mutant SOD1 *in vitro* (Zou *et al*., 2007). This suggests that SMN and SOD1 proteins may interact, through still unknown mechanisms, to induce motor neuron disorders. Reductions in SMN could therefore be causing perturbations in SOD1 protein levels in Schwann cells from SMA mice.

Glucogenesis pathways were also shown to be disrupted in our proteomics data. Metabolism abnormalities such as hyperglycemia have been observed in SMA patients (Crawford *et al*., 1999). It was reported that SMA type I patients display more pancreatic glucagon-producing cells and abnormal glucose levels (Bowerman *et al*., 2012). Bowerman *et al*. reported that SMN-depleted mice showed increased hepatic insulin and glucagon sensitivity (Bowerman *et al*., 2014). Malic enzyme 1

(ME1) was among the differentially expressed proteins in glucogenesis pathways with a significant 25-fold decrease in expression in SMA-derived Schwann cells. ME1 has been shown to regulate adiposity and insulin sensitivity (Al-Dwairi *et al*., 2012), suggesting that reductions in ME1 may lead to metabolism defects observed in SMA pathology.

Functional clustering analyses revealed that more than half of the proteins with altered expression are involved in regulating cell death and survival pathways. One of these proteins was acid ceramidase (ASAH1), with 3-fold down-regulation in Schwann cells from SMA mice. SMA with progressive myoclonic epilepsy (SMA-PME) is a rare form of SMA caused by mutations in *ASAH1* (Zhou *et al*., 2012). Mutations in *ASAH1* cause defects in motor neuron axonal branching and a dramatic increase in apoptosis in the spinal cord of zebrafish (Zhou *et al*., 2012). In human patients, motor deficits were observed around three years of age after normal developmental milestones. Lower motor neurons are known to be affected, leading to respiratory muscle involvement and severe handicap or death occurring before 20 years of age (Zhou *et al*., 2012). The finding that ASAH1 levels were altered in Schwann cells deficient in SMN protein suggests potential shared molecular mechanisms linking SMN-dependent and SMN-independent forms of SMA.

Previous studies have shown an important regulatory role for the ubiquitin-proteasome system in SMN protein stability (Burnett *et al*., 2009; Chang *et al*., 2004; Kwon *et al*., 2013), as well as pathogenesis of a genetically distinct form of SMA, X-linked spinal muscular atrophy (Ramser *et al*., 2008). In addition, a direct role for dysregulation of ubiquitin homeostasis has recently been reported in SMA, where

SMN reduction induced neuromuscular pathology through targeting of UBA1 levels (Wishart *et al*., 2014). Our study extends our understanding of the role of ubiquitination pathways in SMA pathology by showing a specific role in Schwann cells.

As well as UBA1, the E3 ubiquitin ligase NEDD4 (neural precursor cell expressed developmentally down-regulated gene 4) has been shown to regulate form and function of neuromuscular junctions in mice (Liu *et al*., 2009). NEDD4 deficient mice die prenatally with reduced skeletal muscle fibre size and motor neuron numbers. Although ultrastructural analysis of NEDD4 mutants revealed an increase in pre-synaptic nerve terminal branches, nerve diameters were decreased compared to littermate controls (Liu *et al*., 2009). Interestingly, our proteomic analysis revealed that NEDD4 protein expression was increased 1.4-fold in SMA-derived Schwann cells. It has been observed that NEDD4 is not expressed in motor neurons, but is strongly expressed in Schwann cells and skeletal muscles and exerts its regulatory effect on NMJs via non-cell autonomous mechanisms (Liu *et al*., 2009). NEDD4 has also been reported to induce axon branching through PTEN (phosphatase and tensin homolog deleted on chromosome ten) down-regulation in developing xenopus retinal ganglion cells (Drinjakovic *et al*., 2010). Reduction in PTEN levels has been shown to rescue axonal growth defects and restore beta-actin levels in axonal growth cones of SMN-deficient motor neurons (Ning *et al*., 2010), This suggests that NEDD4 up-regulation in SMA-derived Schwann cells could influence NMJ form and function through PTEN degradation.

I found that UBA1 disruption in SMA Schwann cells did not lead to downstream changes in beta-catenin signalling, confirming the findings of previous study in which UBA1-associated disruption of β-catenin was shown to be restricted to the neuromuscular system in SMA mice (Wishart *et al*., 2014). Inactive beta-catenin is in complex with APC (adenomatous polyposis coli), axin and GSK3 beta (glycogen synthase kinase-3). Upon binding of Wnt to its receptor frizzled, an associated protein dishevelled 2 (Dvl2) releases beta-catenin from the complex (Yost *et al*., 1996). An isoform of NEDD4, NEDD4L has also been shown to induce poly-ubiquitination and degradation of Dvl2 (Ding *et al*., 2013). Increase in NEDD4 protein levels may inhibit beta-catenin accumulation in the SMA Schwann cells through Dvl2 degradation. More studies are therefore required to characterise NEDD4 function and its effect on inhibition of beta-catenin accumulation in Schwann cells from SMA mice.

Heat shock proteins (HSPs) are involved in folding, maintenance and degradation of proteins in response to cell stresses including hyperthermia, oxygen radicals and heavy metals (De Maio, 1999). HSPs are known to contribute to protein degradation induced by ubiquitination pathways. Our proteomics screen revealed differential expression in several heat shock proteins such as HSP70 and HSP90 in SMA-derived Schwann cells compared to control cells. HSP90, which localises on the cell surface in the nervous system, has been shown to be involved in cell migration (Sidera *et al*., 2004). Inhibition of HSP90 in migrating Schwann cells in culture revealed that HSP90 is associated with lamellipodia formation and actin cytoskeleton organisation (Sidera *et al*., 2004). *In vitro* studies have also shown HSP90 binds directly to fibronectin in breast cancer cells and HSP90ß inhibition increases formation of

extracellular fibronectin matrix (Hunter *et al*., 2014). Interestingly, fibronectin expression levels were shown to decrease 3.2-fold in SMA Schwann cells. HSP90 reduction in SMA Schwann cells (1.48-fold) may therefore influence abnormal myelination by inhibiting proper migration of Schwann cells and their ability to form extracellular matrix, as we observed in chapter three.

HSP70 induction has been reported to promote degradation of the negative regulator of myelination, c-Jun, in neuregulin-associated demyelination (Li *et al*., 2012). Proteasome inhibition has also been reported to inhibit Schwann cells from inducing dedifferentiation markers such as P75 nerve growth factor receptor and glial fibrillary acidic protein both *in vitro* and *in vivo* (Lee *et al*., 2009). Heat-shock proteins also actively contribute to the myelination disorder Charcot-Marie-Tooth disease type 1A (CMT1A), which is caused by duplication or point mutations in peripheral myelin protein 22 (PMP22) (Rangaraju *et al*., 2008; Chittoor *et al*., 2013). In neuropathic Schwann cells, reduction in PMP22 degradation leads to formation of cytosolic aggregates. Induction of cytosolic HSP70 has shown to improve myelin formation and processing of PMP22 (Rangaraju *et al*., 2008). These studies suggest that perturbations in heat-shock protein levels and proteasome system in SMA Schwann cells can induce myelination deficits through myelin transcription factors regulation and degradation.

In this chapter, I showed that proteomics is a powerful tool to identify differentially expressed proteins in Schwann cells from SMA mice and functional clustering of these proteins can reveal potential mechanisms contributing to SMA pathology. Ubiquitination pathway dysregulation, in particular UBA1 reduction, was shown to

be one of the mechanisms that causes intrinsic defects in Schwann cells from SMA mice. Therefore, targeting UPS components, specifically UBA1 can be considered as a potential treatment for SMA.

Chapter 6: General discussion

6.1 Overview of results

In this thesis I first developed an *in vitro* model system to allow the isolation of Schwann cells from postnatal SMA mice. This offers a solution to one major challenge in neurobiology by facilitating *in vitro* analyses of a sufficient number of purified myelin-competent Schwann cells from a mouse model of neuromuscular disease. Previous mouse Schwann cell protocols were not efficient for such quantitative studies in SMA mouse models. By undertaking modifications to the substrata, medium composition, number of pups, and the age of animals used, I obtained approximately 400,000 cells per preparation with 95-98% purity from 8-day-old 'Taiwanese' SMA mice. I also showed that these Schwann cells were capable of inducing myelination responses in DRG neuron-Schwann cell co-cultures.

In this study, three important questions were then addressed, using the new *in vitro* model system:

1) **Are there any intrinsic defects in SMA Schwann cells?**

I confirmed that SMN protein levels were significantly reduced in SMA-derived Schwann cells. I showed that Schwann cells from SMA mice developed normally pre-differentiation. In contrast, SMA-derived Schwann cells did not respond normally to myelination cues, as a significant reduction in expression levels of key myelin proteins was observed. Restoring SMN levels was shown to rescue these myelination defects, suggesting that deficient myelination was SMN-dependent.

2) **Do intrinsic defects in Schwann cells contribute to SMA pathogenesis?**

Using co-cultures of wild-type DRG neurons with SMA-derived Schwann cells, I showed that neurons were abnormally myelinated. SMA-derived Schwann cells also promoted instability in neighbouring healthy neurons. I demonstrated that neurite instability was not due to the generation of a neurotoxic agent secreted from SMA Schwann cells. Rather, I showed that the extracellular matrix was disrupted in SMA Schwann cells both *in vitro* and *in vivo,* providing a possible explanation for the observed neurite instability.

3) **Can molecular pathways driving SMA Schwann cell defects be identified?**

Using label-free proteomics, 195 proteins were identified in SMA Schwann cells with > 20% up- or down-regulation in their expression levels compared to control Schwann cells. Functional clustering analyses revealed that the majority of these proteins are known pathological proteins contributing to myopathies and neurological disorders. Differentially expressed proteins were demonstrated to contribute to several cellular functions, including cell proliferation, death and assembly. I verified that apoptosis was increased in Schwann cells from SMA mice. Proteins contributing to glucogenesis and ubiquitination pathways were also shown to be modified in SMA-derived Schwann cells. Reduction in expression levels of UBA1 in SMA-derived Schwann cells verified the ubiquitination disruption observed in functional clustering analysis. Pharmacological inhibition of UBA1 in healthy Schwann cells reduced myelin protein expression and phenocopied Schwann cell defects in SMA mice. Thus, I showed that disruption to ubiquitination pathways

was responsible, at least in part, for intrinsic defects in Schwann cells from SMA mice.

6.2 Contribution of cells and tissues other than motor neurons to SMA pathogenesis

Although SMA is traditionally known as neuromuscular and lower motor neuron disease, it has become increasingly clear that other cells and tissues are also involved (Hamilton & Gillingwater, 2013). The identification of Schwann cell pathology in this thesis supports the hypothesis that it is not only motor neurons that are affected. The important finding of this study is that Schwann cell pathology can occur independently of axonopathy and neurodegeneration. Rather, I found that SMA Schwann cells induced neurite instability and contributed directly to defective myelination. Interestingly, Schwann cells appeared to promote neurite instability, at least in part, by producing a disrupted extracellular matrix. However, although intrinsic Schwann cell defects may contribute to SMA pathogenesis in mouse models, their relative contribution to the overall disease status of human patients with SMA remains unclear and will need further investigation.

Several therapeutic approaches are currently under investigation, but there is still no cure for SMA. The identification of new target cells for SMN, such as Schwann cells, will hopefully lead to the design of more efficient and better-targeted treatments for the disease. Recently, it has been proposed that therapies which aimed to increase SMN levels, should be delivered systematically due to the involvement of non-neuromuscular tissues in SMA pathogenesis (Sleigh *et al*., 2011). However, different cell types and tissues have differential susceptibility to SMN reduction (the

threshold hypothesis of SMA) and therefore, it is important to achieve a maintenance level of SMN in all affected cells (Sleigh *et al*., 2011). Also the developmental time point in which SMN delivery could inhibit pathology is a key factor for efficient treatment. For instance, it has been reported that SMN delivery with scAAV9 at P1 in SMAΔ7 mice improved lifespan to 250 days, whereas SMN administration at P10 had little effect, indicating that earlier SMN replacement leads to better survival (Foust *et al*., 2010). Thus, differently affected cells may require delivery of therapy at different developmental time windows to achieve the optimal treatment for SMA.

This study confirms an important role for SMN in regulating ubiquitination pathways. A recent study has shown that SMN reduction disrupts the ubiquitination pathway, and UBA1 in particular (Wishart *et al*., 2014). Beta-catenin was found to be a downstream mediator of UBA1-dependent pathology in spinal cord and muscle, but still unknown effectors mediated non-neuromuscular pathology (Wishart *et al*., 2014). Similarly, I demonstrate that beta-catenin is not responsible for mediating ubiquitination pathway-dependent disruption in SMA Schwann cells. Therefore, SMA treatments targeting beta-catenin are unlikely to ameliorate Schwann cell pathology. However, targeting UBA1 would be likely to have therapeutic effects for Schwann cells as well as the neuromuscular system.

6.3 *In vitro* analysis of peripheral neuropathies

Several protocols have been proposed for the isolation and purification of Schwann cells from neonatal mice (Seilheimer *et al*., 1989; Dong *et al*., 1999; Nicholson *et al*., 2001). However, these publications have not reported the number of Schwann cells they obtained and their ability to produce myelin. Recently Honkanen *et al*.

published a protocol in which they isolated 1.9-3.3 X 10^6 of 95% pure myelin-competent Schwann cells from 12-15 4-day-old mouse pups (Honkanen *et al*., 2007). Using this protocol in 'Taiwanese' SMA mice, I showed that the number of Schwann cells obtained was not sufficient for quantitative analysis. I therefore developed the protocol in order to obtain higher number of Schwann cells, as well as using older pups to allow me to distinguish between healthy and SMA mice before pooling their sciatic nerves for experiments.

The new protocol I have developed might now be considered useful for *in vitro* studies of Schwann cells in other peripheral neuropathies, such as Charcot-Marie-Tooth disease. To my knowledge, most *in vitro* CMT studies have been performed either using DRG neuron-Schwann cell co-cultures from rat models (Nobbio *et al*., 2006) or using mouse DRG explants (Liu *et al*., 2005). The potential of rat DRG neuron-Schwann cell co-culture is severely compromised by the lack of rat myelin mutants with the exception of the rat model of human CMT1A disease (Nobbio *et al*., 2006). In DRG explant culture models, neurons and Schwann cells are necessarily derived from the same animal and studies are thus restricted to a single genotype expressed by both neurons and Schwann cells. In order to dissect complex interactions between peripheral neuron and Schwann cell, co-cultures of mixed genotype are useful. For instance, in our study Schwann cells from SMA mice induce instability and abnormal myelination in healthy DRG neurons from wild-type mice, indicating that the myelination defects I observed are not just the consequence of neurodegeneration, a result that cannot have been determined by using DRG explant cultures.

6.4 Proteomic analysis in neurodegenerative disorders

Proteomics, the large-scale analysis of protein expression, is routinely used to understand molecular alterations during development, pathogenesis and drug treatments (Tyers & Mann, 2003). The proteome is not as uniform and static as the genome (Adams, 2008). In addition, post-transcriptional modifications, such as methylation, phosphorylation, glycosylation and ubiquitination add extra complexity to the proteome (Jensen, 2006). Therefore, studying proteomics has been suggested to be more beneficial than genomic analysis to understand complex cellular functions and their alterations in development and pathologies (Adams, 2008).

Proteomic analysis has previously been used in SMA studies. Proteomic analysis of embryonic stem (ES) cells derived from severe SMA mice revealed that SMN depletion activated cellular stress pathways, disrupted energy metabolism and cytoskeletal stability (Wu *et al*., 2011). Widespread molecular changes have also been observed by proteomic analysis of the hippocampus in SMA mice (Wishart *et al*., 2010). Proteomic analysis has also been used to identify drug targets and their potential side effects in SMA. Valproate treatment has reported to reduce collagen I synthesis, resulting in bone loss (Fuller *et al*., 2010). Label-free proteomics has also identified calreticulin and GRP75/mortalin as biomarkers for reporting on SMA disease progress in samples of muscle and skin (Mutsaers *et al*., 2013). In another study, protein biomarkers have been identified in plasma by iTRAQ proteomics in human patients (Finkel *et al*., 2012). Therefore, proteomic analysis is a powerful tool for identification of SMA biomarkers. In this study, I performed proteomics screen in isolated Schwann cells. Unlike previous proteomic screens, I used homogenous cell

population and therefore was able to identify cell type-specific molecular changes in SMA pathogenesis. In the system I have used, both control and SMA Schwann cells were extracted from the same litter, which introduced less variability to the proteomic results. These experimental refinements meant that I also obtained a larger coverage of proteins than in the previous proteomic studies discussed above. In order to interpret such a large amount of data, differentially expressed proteins were clustered using IPA analysis with respect to their known functions in biological systems (Wishart *et al*., 2010). Therefore, proteomic analysis combined with bioinformatics enabled me to identify the molecular pathways that may contribute to intrinsic defects in Schwann cells. This suggests that the same approach should perhaps now be used in other isolated cell populations affected in SMA to unravel the molecular pathways contributing to disease pathogenesis.

Proteomic analysis has previously been shown to provide insights into other neurodegenerative disorders. For instance, the glial contribution to neuroprotection has recently been investigated in ALS primary cultured mouse astrocytes. Isotope labelling quantitative proteomics has been performed to identify secreted factors from astrocyte in response to motor neuron-derived angiogenin (ANG) stimulation (Skorupa *et al*., 2013). ANG induces astrocytes to secrete neuroprotective factors and its mutation has been observed in ALS patients (Skorupa *et al*., 2013). The proteomic analysis identified a set of astrocyte-derived proteins that may have a neuroprotective role and can slow ALS progression (Skorupa *et al*., 2013). Therefore, proteomic analysis is a powerful platform to study glial contribution not only in SMA but also in other neuromuscular disorders.

6.5 Ubiquitin-proteasome system disruption in neurodegeneration

In section 6.2, I discussed how ubiquitination pathways were disrupted in SMA Schwann cells. However, SMA is not the only neurological disorder that exhibits ubiquitination-proteasome disruption. Several other neurodegenerative diseases are associated with the formation of ubiquitinated conjugates that are unable to be degraded by a compromised proteasome system and in response form aggregates in cell bodies (Rubinsztein, 2006). Some examples of such ubiquitinated aggresomes are PMP22 aggregates in CMT1A (Fortun *et al*., 2006), neurofibrillary tangles in Alzheimer's disease, Lewy bodies in Parkinson's disease and Bunina bodies in amyotrophic lateral sclerosis (Shaw, 2005; Schmitt, 2006; Fortun *et al*., 2006). Duplication in the *PMP22* gene in CMT1A leads to overexpression of PMP22 protein. Faulty proteins are ubiquitinated, but excess PMP22 overloads the proteasome system, leading to disruption in Schwann cell intracellular sorting of PMP22 and other proteins. Interestingly, PMP22 aggresome formation induces demyelination that occurs before onset of neurodegeneration (Fortun *et al*., 2006). It is still not known whether disruption to the ubiquitin-proteasome system in SMA Schwann cells forms any aggregates in the cytoplasm. Therefore, further work on the consequences of disruption in ubiquitination pathway in Schwann cells is required.

6.6 Conclusion

Taken together, I have shown here that Schwann cells may contribute to the pathogenesis of SMA. First, I demonstrate intrinsic defects in SMA Schwann cells, leading to abnormal myelination and neurite instability. Next, SMA Schwann cell defects have been shown to be independent of neuronal degeneration. Finally, I show

that ubiquitin homeostasis is disrupted in SMA Schwann cells, contributing to pathology via pathways independent of beta-catenin. These new insights extend our knowledge of SMA pathogenesis as a multi-system disorder and will hopefully lead to new treatment approaches that targ*et al*l affected cells and tissues.

Bibliography

Ackermann, B. *et al*., 2013. Plastin 3 ameliorates spinal muscular atrophy via delayed axon pruning and improves neuromuscular junction functionality. *Hum Mol Genet.*, 22(7), pp.1328-47.

Adams, J., 2008. The proteom: Discovering the structure and function of proteins. *Nature education*, 1(3), p.6.

Adlkofer, K., Naef, R. & Suter, U., 1997. Analysis of compound heterozygous mice reveals that the Trembler mutation can behave as a gain-of-function allele. *J Neurosci Res.*, 49(6), pp.671-80.

Alberti, S., Gregório, E.A., Spadella, C.T. & Cojocel, C., 2007. Localization and irregular distribution of Na,K-ATPase in myelin sheath from rat sciatic nerve. *Tissue Cell.*, 39(3), pp.195-201.

Al-Dwairi, A., Pabona, J.M., Simmen, R.C. & Simmen, F.A., 2012. Cytosolic malic enzyme 1 (ME1) mediates high fat diet-induced adiposity, endocrine profile, and gastrointestinal tract proliferation-associated biomarkers in male mice. *PLoS One.*, 7(10), p.e46716.

Andrews, H. *et al*., 2006. Increased axonal mitochondrial activity as an adaptation to myelin deficiency in the Shiverer mouse. *J Neurosci Res.*, 83(8), pp.1533-9.

Araujo, A.P., Araujo, M. & Swoboda, K.J., 2009. Vascular perfusion abnormalities in infants with spinal muscular atrophy. *J Pediatr.*, 155(2), pp.292-4.

Arnold, A.S. *et al*., 2004. Reduced expression of nicotinic AChRs in myotubes from spinal muscular atrophy I patients. *Lab Invest.*, 84(10), pp.1271-8.

Arthur-Farraj, P. et al., 2011. Mouse schwann cells need both NRG1 and cyclic AMP to myelinate. *Glia*, 59(5), pp.720-33.

Aszódi, A., Legate, K.R., Nakchbandi, I. & Fässler, R., 2006. What mouse mutants teach us about extracellular matrix function. *Annu Rev Cell Dev Biol.*, 22, pp.591-621.

Avila, A.M. *et al*., 2007. Trichostatin A increases SMN expression and survival in a mouse model of spinal muscular atrophy. *J Clin Invest.*, 117(3), pp.659-71.

Azzouz, M. *et al*., 2004. Lentivector-mediated SMN replacement in a mouse model of spinal muscular atrophy. *J Clin Invest.*, 114(12), pp.1726-31.

Barbarese, E. *et al*., 1999. RNA on the road to myelin. *J Neurocytol.*, 28(4-5), pp.263-70.

Bebee, T.W., Dominguez, C.E. & Chandler, D.S., 2012. Mouse models of SMA: tools for disease characterization and therapeutic development. *Hum Genet.*, 131(8), pp.1277-93.

Beck, K.D. *et al*., 1995. Mesencephalic dopaminergic neurons protected by GDNF from axotomy-induced degeneration in the adult brain. *Nature.*, 373(6512), pp.339-41.

Beers, D.R. *et al*., 2006. Wild-type microglia extend survival in PU.1 knockout mice with familial amyotrophic lateral sclerosis. *Proc Natl Acad Sci U S A.*, 103(43), pp.16021-6.

Beirowski, B., 2013. Concepts for regulation of axon integrity by enwrapping glia. *Front Cell Neurosci.*, 7, p.256.

Berger, P., Niemann, A. & Suter, U., 2006. Schwann cells and the pathogenesis of inherited motor and sensory neuropathies (Charcot-Marie-Tooth disease). *Glia*, 54(4), pp.243-57.

Bevan, A.K. *et al*., 2010. Early heart failure in the SMNDelta7 model of spinal muscular atrophy and correction by postnatal scAAV9-SMN delivery. *Hum Mol Genet.*, 19(20), pp.3895-905.

Bäumer, D. *et al*., 2009. Alternative splicing events are a late feature of pathology in a mouse model of spinal muscular atrophy. *PLoS Genet*, 5(12), p.e1000773.

Bäumer, D., Talbot, K. & Turner, M.R., 2014. Advances in motor neurone disease. *J R Soc Med.*, 107(1), pp.14-21.

Boillée, S., Vande Velde, C. & Cleveland, D.W., 2006. ALS: a disease of motor neurons and their nonneuronal neighbors. *Neuron.*, 52(1), pp.39-59.

Boucher, T.J. *et al*., 2000. Potent analgesic effects of GDNF in neuropathic pain states. *Science.*, 290(5489), pp.124-7.

Bowerman, M. *et al*., 2009. SMN, profilin IIa and plastin 3: a link between the deregulation of actin dynamics and SMA pathogenesis. *Mol Cell Neurosci.*, 42(1), pp.66-74.

Bowerman, M. *et al*., 2014. Defects in pancreatic development and glucose metabolism in SMN-depleted mice independent of canonical Spinal Muscular Atrophy neuromuscular pathology. *Hum Mol Genet.,* 23(13), pp.3432-44.

Bowerman, M., Shafey, D. & Kothary, R., 2007. Smn depletion alters profilin II expression and leads to upregulation of the RhoA/ROCK pathway and defects in neuronal integrity. *J Mol Neurosci.*, 32(2), pp.120-31.

Bowerman, M. *et al*., 2012. Glucose metabolism and pancreatic defects in spinal muscular atrophy. *Ann Neurol.*, 72(2), pp.256-68.

Brand-Saberi, B., 2005. Genetic and epigenetic control of skeletal muscle development. *Ann Anat.*, 187(3), pp.199-207.

Braun, S. *et al*., 1997. Degeneration of cocultures of spinal muscular atrophy muscle cells and rat spinal cord explants is not due to secreted factors and cannot be prevented by neurotrophins. *Muscle Nerve.*, 20(8), pp.953-60.

Brett, D. *et al*., 2002. Alternative splicing and genome complexity. *Nat Genet.*, 30(1), pp.29-30.

Briese, M. *et al*., 2009. Deletion of smn-1, the Caenorhabditis elegans ortholog of the spinal muscular atrophy gene, results in locomotor dysfunction and reduced lifespan. *Hum Mol Genet.*, 18(1), pp.97-104.

Britsch, S., 2007. The neuregulin-I/ErbB signaling system in development and disease. *Adv Anat Embryol Cell Biol.*, 190, pp.1-65.

Britsch, S. *et al*., 2001. The transcription factor Sox10 is a key regulator of peripheral glial development. *Genes Dev.*, 15(1), pp.66-78.

Britsch, S. *et al*., 2001. The transcription factor Sox10 is a key regulator of peripheral glial development. *Genes Dev.*, 15(1), pp.66-78.

Brockes, J.P. & Raff, M.C., 1979. Studies on cultured rat Schwann cells. II. Comparison with a rat Schwann cell line. *In Vitro.*, 15(10), pp.772-8.

Bruce, A.K., Jacobsen, E., Dossing, H. & Kondrup, J., 1995. Hypoglycaemia in spinal muscular atrophy. *Lancet.*, 346(8975), pp.609-10.

Brzustowicz, L.M. *et al*., 1995. Linkage disequilibrium and haplotype analysis among Polish families with spinal muscular atrophy. *Am J Hum Genet.*, 56(1), pp.210-15.

Burghes, A.H. & Beattie, C.E., 2009. Spinal muscular atrophy: why do low levels of survival motor neuron protein make motor neurons sick? *Nat Rev Neurosci.*, 10(8), pp.597-609.

Burnett, B.G. *et al*., 2009. Regulation of SMN protein stability. *Mol Cell Biol.*, 29(5), pp.1107-15.

Câmara, J. *et al*., 2009. Integrin-mediated axoglial interactions initiate myelination in the central nervous system. *J Cell Biol.*, 185(4), pp.669-712.

Carpenter, S. *et al*., 1978. Pathological involvement of primary sensory neurons in Werdnig-Hoffmann disease. *Acta Neuropathol.*, 42(2), pp.91-7.

Cartegni, L. & Krainer, A., 2002. Disruption of an SF2/ASF-dependent exonic splicing enhancer in SMN2 causes spinal muscular atrophy in the absence of SMN1. *Nat Genet.*, 30(4), pp.377-84.

Casella, G.T., Bunge, R.P. & Wood, P.M., 1996. Improved method for harvesting human Schwann cells from mature peripheral nerve and expansion in vitro. *Glia.*, 17(4), pp.327-38.

Chang, H.C. *et al*., 2008. Modeling spinal muscular atrophy in Drosophila. *PLoS One.*, 3(9), p.e3209.

Chang, H.C., Hung, W.C., Chuang, Y.J. & Jong, Y.J., 2004. Degradation of survival motor neuron (SMN) protein is mediated via the ubiquitin/proteasome pathway. *Neurochem Int.*, 45(7), pp.1107-12.

Chan, J.R. *et al*., 2006. The polarity protein Par-3 directly interacts with p75NTR to regulate myelination. *Science.*, 314(5800), pp.832-6.

Chan, Y.B. *et al*., 2003. Neuromuscular defects in a Drosophila survival motor neuron gene mutant. *Hum Mol Genet.*, 12(12), pp.1367-76.

Chan, J.R. *et al*., 2004. NGF controls axonal receptivity to myelination by Schwann cells or oligodendrocytes. *Neuron.*, 43(2), pp.183-91.

Chao, M.V., Rajagopal, R. & Lee, F.S., 2006. Neurotrophin signalling in health and disease. *Clin Sci (Lond).*, 110(2), pp.167-73.

Chen, Z.L. & Strickland, S., 2003. Laminin gamma1 is critical for Schwann cell differentiation, axon myelination, and regeneration in the peripheral nerve. *J Cell Biol.*, 163(4), pp.889-99.

Chernousov, M.A. *et al*., 2006. Glypican-1 and alpha4(V) collagen are required for Schwann cell myelination. *J Neurosci.*, 26(2), pp.508-17.

Chernousov, M.A., Stahl, R.C. & Carey, D.J., 1998. Schwann cells use a novel collagen-dependent mechanism for fibronectin fibril assembly. *J Cell Sci.,* 111(Pt 18), pp.2763-77.

Chernousov, M.A., Stahl, R.C. & Carey, D.J., 2001. Schwann cell type V collagen inhibits axonal outgrowth and promotes Schwann cell migration via distinct adhesive activities of the collagen and noncollagen domains. *J Neurosci.*, 21(16), pp.6125-35.

Chernousov, M.A. *et al*., 2008. Regulation of Schwann Cell Function by the Extracellular Matrix. *Glia.*, 56(14), pp.1498-507.

Chhabra, E.S. & Higgs, H.N., 2006. INF2 Is a WASP Homology 2 Motif-containing Formin That Severs Actin Filaments and Accelerates Both Polymerization and Depolymerization. *J. Biol. Chem.*, 281(36), pp. 26754-26767.

Chien, Y.Y. & Nonaka, I., 1989. Peripheral nerve involvement in Werdnig-Hoffmann disease. *Brain Dev.*, 11(4), pp.221-9.

Chittoor , V.G. *et al*., 2013. Biochemical characterization of protein quality control mechanisms during disease progression in the C22 mouse model of CMT1A. *ASN Neuro.*, 5(5), p.pii: e00128.

Cifuentes-Diaz, C. *et al*., 2002. Neurofilament accumulation at the motor endplate and lack of axonal sprouting in a spinal muscular atrophy mouse model. *Hum Mol Genet.*, 11(12), pp.1439-47.

Clement, A.M. *et al*., 2003. Wild-type nonneuronal cells extend survival of SOD1 mutant motor neurons in ALS mice. *Science.*, 302(5642), pp.113-7.

Clevers, H. & Nusse, R., 2012. Wnt/β-catenin signaling and disease. *Cell.*, 149(6), pp.1192-205.

Corti, S. *et al*., 2009. Motoneuron transplantation rescues the phenotype of SMARD1 (spinal muscular atrophy with respiratory distress type 1). *J Neurosci.*, 29(38), pp.11761-71.

Corti, S. *et al*., 2010. Embryonic stem cell-derived neural stem cells improve spinal muscular atrophy phenotype in mice. *Brain.*, 133(Pt2), pp.465-81.

Cosgaya, J.M., Chan, J.R. & Shooter, E.M., 2002. The neurotrophin receptor p75NTR as a positive modulator of myelination. *Science.*, 298(5596), pp.1245-8.

Court, F.A. *et al*., 2008. Identity, developmental restriction and reactivity of extralaminar cells capping mammalian neuromuscular junctions. *J Cell Sci.*, 121(Pt 23), pp.3901-11.

Court, F.A. *et al*., 2004. Restricted growth of Schwann cells lacking Cajal bands slows conduction in myelinated nerves. *Nature.*, 431(7005), pp.191-5.

Crawford, T.O. *et al*., 1999. Abnormal fatty acid metabolism in childhood spinal muscular atrophy. *Ann Neurol.*, 45(3), pp.337-43.

Dachs, E. *et al*., 2011. Defective neuromuscular junction organization and postnatal myogenesis in mice with severe spinal muscular atrophy. *J Neuropathol Exp Neurol.*, 70(6), pp.444-61.

D'Amico, A., Mercuri, E., Tiziano, F.D. & Bertini, E., 2011. Spinal muscular atrophy. *Orphanet J Rare Dis.*, 6(71).

De Maio, A., 1999. Heat shock proteins: facts, thoughts, and dreams. *Shock.*, 11(1), pp.1-12.

Di Giorgio, F.P. *et al*., 2007. Non-cell autonomous effect of glia on motor neurons in an embryonic stem cell-based ALS model. *Nat Neurosci.*, 10(5), pp.608-14.

DiAntonio, A. *et al*., 2001. Ubiquitination-dependent mechanisms regulate synaptic growth and function. *Nature.*, 412(6845), pp.449-52.

Ding, Y. *et al*., 2013. HECT domain-containing E3 ubiquitin ligase NEDD4L negatively regulates Wnt signaling by targeting dishevelled for proteasomal degradation. *J Biol Chem.*, 288(12), pp.8289-98.

Dlamini, N. *et al*., 2013. Clinical and neuropathological features of X-linked spinal muscular atrophy (SMAX2) associated with a novel mutation in the UBA1 gene. *Neuromuscul Disord.*, 23(5), pp.391-8.

Dominguez, E. *et al*., 2011. Intravenous scAAV9 delivery of a codon-optimized SMN1 sequence rescues SMA mice. *Hum Mol Genet.*, 20(4), pp.681-93.

Dominguez, E. *et al*., 2011. Intravenous scAAV9 delivery of a codon-optimized SMN1 sequence rescues SMA mice. *Hum Mol Genet.*, 20(4), pp.681-93.

Dong, Z. *et al*., 1995. Neu differentiation factor is a neuron-glia signal and regulates survival, proliferation, and maturation of rat Schwann cell precursors. *Neuron.*, 15(3), pp.585-96.

Dong, Z. *et al*., 1999. Schwann cell development in embryonic mouse nerves. *J Neurosci Res.*, 56(4), pp.334-48.

Drinjakovic, J. *et al*., 2010. E3 ligase Nedd4 promotes axon branching by downregulating PTEN. *Neuron.*, 65(3), pp.341-57.

Dubowitz, V., 1999. Very severe spinal muscular atrophy (SMA type 0): an expanding clinical phenotype. *Eur J Paediatr Neurol.*, 3(2), pp.49-51.

Dykes, I.M., Lanier, J., Eng, S.R. & Turner, E.E., 2010. Brn3a regulates neuronal subtype specification in the trigeminal ganglion by promoting Runx expression during sensory differentiation. *Neural Dev.*, 5, p.3.

Eggert, C., Chari, A., Laggerbauer, B. & Fischer, U., 2006. Spinal muscular atrophy: the RNP connection. *Trends Mol Med.*, 12(3), pp.113-21.

Eldridge, C.F., Bunge, M.B. & Bunge, R.P., 1989. Differentiation of axon-related Schwann cells in vitro: II. Control of myelin formation by basal lamina. *J Neurosci.*, 9(2), pp.625-38.

Eng, S.R. *et al*., 2001. Defects in sensory axon growth precede neuronal death in Brn3a-deficient mice. *J Neurosci.*, 21(2), pp.541-9.

Ernsberger, U., 2009. Role of neurotrophin signalling in the differentiation of neurons from dorsal root ganglia and sympathetic ganglia. *Cell Tissue Res.*, 336(3), pp.349-84.

Esper, R.M. & Loeb, J.A., 2004. Rapid axoglial signaling mediated by neuregulin and neurotrophic factors. *J Neurosci.*, 27(27), pp.6218-27.

Fabricius, C., Berthold, C.H. & Rydmark, M., 1993. Axoplasmic organelles at nodes of Ranvier. II. Occurrence and distribution in large myelinated spinal cord axons of the adult cat. *J Neurocytol.*, 22(11), pp.941-54.

Fan, L. & Simard, L.R., 2002. Survival motor neuron (SMN) protein: role in neurite outgrowth and neuromuscular maturation during neuronal differentiation and development. *Hum Mol Genet.*, 11(14), pp.1605-14.

Farrar, M.A. *et al*., 2011. Dysfunction of axonal membrane conductances in adolescents and young adults with spinal muscular atrophy. *Brain.*, 134(Pt 11), pp.3185-97.

Felderhoff-Mueser, U. *et al*., 2002. Severe spinal muscular atrophy variant associated with congenital bone fractures. *J Child Neurol.*, 17(9), pp.718-21.

Feldkötter, M. *et al*., 2002. Quantitative analyses of SMN1 and SMN2 based on real-time lightCycler PCR: fast and highly reliable carrier testing and prediction of severity of spinal muscular atrophy. *Am J Hum Genet.*, 70(2), pp.358-68.

Fellner, L., Jellinger, K.A., Wenning, G.K. & Stefanova, N., 2011. Glial dysfunction in the pathogenesis of a-synucleinopathies: emerging concepts. *Acta Neuropathol*, 121(6), p.675–693.

Feltri, M.L. *et al*., 2002. Conditional disruption of B1 integrin in Schwann cells impedes interactions with axons. *J Cell Biol.*, 156(1), pp.199-209.

Feltri, M.L. *et al*., 2002. Conditional disruption of beta 1 integrin in Schwann cells impedes interactions with axons. *J Cell Biol.*, 156(1), pp.199-209.

Feng, Z. & Ko, C.P., 2008. The role of glial cells in the formation and maintenance of the neuromuscular junction. *Ann N Y Acad Sci.*, 1132, pp.19-28.

Fields, R.D., 2006. Nerve impulses regulate myelination through purinergic signalling. *Novartis Found Symp.*, 276, pp.158-61.
Finkel, R.S. *et al*., 2012. Candidate Proteins, Metabolites and Transcripts in the Biomarkers for Spinal Muscular Atrophy (BforSMA) Clinical Study. *PLoS One.*, 7(4), p.e35462.
Fortun, J. *et al*., 2006. Alterations in degradative pathways and protein aggregation in a neuropathy model based on PMP22 overexpression. *Neurobiol Dis.*, 22(1), pp.153-64.
Foust, K.D. *et al*., 2009. Intravascular AAV9 preferentially targets neonatal neurons and adult astrocytes. *Nat Biotechnol.*, 27(1), pp.59-65.
Foust, K.D. *et al*., 2010. Rescue of the spinal muscular atrophy phenotype in a mouse model by early postnatal delivery of SMN. *Nat Biotechnol.*, 28(3), pp.271-4.
Fuller, H.R. *et al*., 2010. Valproate and bone loss: iTRAQ proteomics show that valproate reduces collagens and osteonectin in SMA cells. *J Proteome Res.*, 9(8), pp.4228-33.
Görg, A., Weiss, W. & Dunn, M.J., 2004. Current two-dimensional electrophoresis technology for proteomics. *Proteomics.*, 4(12), pp.3665-85.
Gall, J.G., 2003. The centennial of the Cajal body. *Nat Rev Mol Cell Biol.*, 4(12), pp.975-80.
Gatzinsky, K.P. *et al*., 2003. Early onset of degenerative changes at nodes of Ranvier in alpha-motor axons of Cntf null (-/-) mutant mice. *Glia.*, 42(4), pp.340-9.
Gillespie, C.S. *et al*., 2000. Peripheral demyelination and neuropathic pain behavior in periaxin-deficient mice. *Neuron.*, 26(2), pp.523-31.
Glascock, J.J. *et al*., 2012. Decreasing disease severity in symptomatic, Smn(-/-);SMN2(+/+), spinal muscular atrophy mice following scAAV9-SMN delivery. *Hum Gene Ther.*, 23(3), pp.330-5.
Gogliotti, R.G. *et al*., 2012. Motor neuron rescue in spinal muscular atrophy mice demonstrates that sensory-motor defects are a consequence, not a cause, of motor neuron dysfunction. *J Neurosci.*, 32(11), pp.3818-29.
Greenwood, A.L., Turner, E.E. & Anderson, D.J., 1999. Identification of dividing, determined sensory neuron precursors in the mammalian neural crest. *Development.*, 126(16), pp.3545-59.
Gubitz, A.K., Feng, W. & Dreyfuss, G., 2004. The SMN complex. *Exp Cell Res.*, 296(1), pp.51-6.
Höke, A. *et al*., 2003. Glial cell line-derived neurotrophic factor alters axon schwann cell units and promotes myelination in unmyelinated nerve fibers. *J Neurosci.*, 23(2), pp.561-7.
Haaker, G. & Fujak, A., 2013. Proximal spinal muscular atrophy: current orthopedic perspective. *Appl Clin Genet.*, 6(11), pp.113-20.
Haddad, H. *et al*., 2003. Riluzole attenuates spinal muscular atrophy disease progression in a mouse model. *Muscle Nerve.*, 28(4), pp.432-7.
Hamilton, G. & Gillingwater, T.H., 2013. Spinal muscular atrophy: going beyond the motor neuron. *Trends in Molecular Medicine*, 19(1), pp.40-50.
Hamilton, G. *et al*., 2012. Functional and genetic analysis of haplotypic sequence variation at the nicastrin genomic locus. *Neurobiol. Aging*, 33(8), pp.1848.e1-13.

Han, K.J. *et al*., 2012. Ubiquitin-specific protease 9x deubiquitinates and stabilizes the spinal muscular atrophy protein-survival motor neuron. *J Biol Chem.*, 287(52), pp.43741-52.

Haney, C.A. *et al*., 1999. Heterophilic binding of L1 on unmyelinated sensory axons mediates Schwann cell adhesion and is required for axonal survival. *J Cell Biol.*, 146(5), pp.1173-84.

Han, K.J. *et al*., 2012. Ubiquitin-specific protease 9x deubiquitinates and stabilizes the spinal muscular atrophy protein-survival motor neuron. *J Biol Chem.*, 287(52), pp.43741-52.

Hao le, T., Wolman, M., Granato, M. & Beatie, C.E., 2012. Survival motor neuron affects plastin 3 protein levels leading to motor defects. *J Neurosci.*, 32(15), pp.5074-84.

Hayhurst, M. *et al*., 2012. A cell-autonomous defect in skeletal muscle satellite cells expressing low levels of survival of motor neuron protein. *Dev Biol.*, 368(2), pp.323-34.

Heier, C.R. & DiDonato, C.J., 2009. Translational readthrough by the aminoglycoside geneticin (G418) modulates SMN stability in vitro and improves motor function in SMA mice in vivo. *Hum Mol Genet.*, 18(7), pp.1310-22.

Heier, C.R., Satta, R., Lutz, C. & DiDonato, C.J., 2010. Arrhythmia and cardiac defects are a feature of spinal muscular atrophy model mice. *Hum Mol Genet.*, 19(20), pp.3906-18.

Helbling-leclerc, A. *et al*., 1995. Mutations in the laminin alpha 2-chain gene (LAMA2) cause merosin-deficient congenital muscular dystrophy. *Nat Genet.*, 11(2), pp.216-8.

Henderson, C.E. *et al*., 1987. Extracts of muscle biopsies from patients with spinal muscular atrophies inhibit neurite outgrowth from spinal neurons. *Neurology.*, 37(8), pp.1361-4.

Henderson, C.E. *et al*., 1994. GDNF: a potent survival factor for motoneurons present in peripheral nerve and muscle. *Science.*, 266(5187), pp.1062-4.

Hershko, A. & Ciechanover, A., 1998. The Ubiquitin System. *Annu. Rev. Biochem.*, 67, pp.425-79.

Hess, D.M. *et al*., 2007. Localization of TrkC to Schwann cells and effects of neurotrophin-3 signaling at neuromuscular synapses. *J Comp Neurol.*, 501(4), pp.465-82.

Hofmann, Y. *et al*., 2000. Htra2-beta 1 stimulates an exonic splicing enhancer and can restore full-length SMN expression to survival motor neuron 2 (SMN2). *Proc Natl Acad Sci U S A.*, 97(17), pp.9618-23.

Hollenbeck, P.J. & Saxton, W.M., 2005. The axonal transport of mitochondria. *J Cell Sci.*, 118(Pt23), pp.5411-9.

Honkanen, H. *et al*., 2007. Isolation, purification and expansion of myelination-competent, neonatal mouse Schwann cells. *Eur J Neurosci.*, 26(4), pp.953-64.

Hsieh-Li, H. *et al*., 2000. A mouse model for spinal muscular atrophy. *Nature genetics*, 24(1), pp.66-70.

Hsu, S.H. *et al*., 2010. Ubiquitin carboxyl-terminal hydrolase L1 (UCHL1) regulates the level of SMN expression through ubiquitination in primary spinal muscular atrophy fibroblasts. *Clin Chim Acta.*, 211(23-24), pp.1920-8.

Hua, Y. *et al*., 2010. Antisense correction of SMN2 splicing in the CNS rescues necrosis in a type III SMA mouse model. *Genes Dev.*, 24(15), pp.1634-44.
Hua, Y. *et al*., 2011. Peripheral SMN restoration is essential for long-term rescue of a severe spinal muscular atrophy mouse model. *Nature.*, 478(7367), pp.123-6.
Hubbard, S.R. & Gnanasambandan, K., 2013. Structure and activation of MuSK, a receptor tyrosine kinase central to neuromuscular junction formation. *Biochim Biophys Acta.*, 1834(10), pp.2166-9.
Hunter, G. *et al*., 2014. SMN-dependent intrinsic defects in Schwann cells in mouse models of spinal muscular atrophy. *Hum Mol Genet.*, 23(9), pp.2235-50
Hunter, M.C. *et al*., 2014. Hsp90 Binds Directly to Fibronectin (FN) and Inhibition Reduces the Extracellular Fibronectin Matrix in Breast Cancer Cells. *PLoS One.*, 9(1), p.e86842.
Hyden, H. & McEwen, B., 1966. A glial protein specific for the nervous system. *Proc Natl Acad Sci U S A.*, 55(2), pp.354-58.
Imlach, W.L. *et al*., 2012. SMN is required for sensory-motor circuit function in Drosophila. *Cell.*, 151(2), pp.427-39.
Inoue, K. *et al*., 2002. Runx3 controls the axonal projection of proprioceptive dorsal root ganglion neurons. *Nat Neurosci.*, 5(10), pp.946-54.
Ito, Y. *et al*., 2004. Thalamic lesions in a long-surviving child with spinal muscular atrophy type I: MRI and EEG findings. *Brain Dev.*, 26(1), pp.53-6.
Ito, Y. *et al*., 2011. New insights into the pathogenesis of spinal muscular atrophy. *Brain Dev.*, 33(4), pp.321-31.
Jablonka, S. *et al*., 2006. Distinct and overlapping alterations in motor and sensory neurons in a mouse model of spinal muscular atrophy. *Hum Mol Genet.*, 15(3), pp.511-8.
Jaegle, M. *et al*., 2003. The POU proteins Brn-2 and Oct-6 share important functions in Schwann cell development. *Genes Dev.*, 17(11), pp.1380-91.
Jagalur, N.B. *et al*., 2011. Functional dissection of the Oct6 Schwann cell enhancer reveals an essential role for dimeric Sox10 binding. *J Neurosci.*, 31(23), pp.8585-94.
Jensen, O.N., 2006. Interpreting the protein language using proteomics. *Nat Rev Mol Cell Biol.*, 7(6), pp.391-403.
Jessen, K. *et al*., 1994. The Schwann cell precursor and its fate: a study of cell death and differentiation during gliogenesis in rat embryonic nerves. *Neuron.*, 12(3), pp.509-27.
Jessen, K.R. & Mirsky, R., 2005. The origin and development of glial cells in peripheral nerves. *Nat Rev Neurosci.2005*, 6(9), pp.671-82.
Jessen, K.R., Morgan, L., Stewart, H.J. & Mirsky, R., 1990. Three markers of adult non-myelin-forming Schwann cells, 217c(Ran-1), A5E3 and GFAP: development and regulation by neuron-Schwann cell interactions. *Development*, 109(1), pp.91-103.
Johnson, D.G. & Dent, S.Y., 2013. Chromatin: receiver and quarterback for cellular signals. *Cell.*, 152(4), pp.685-9.
Juárez, P. & Palau, F., 2012. Neural andMolecular Features on Charcot-Marie-Tooth Disease Plasticity and Therapy. *Neural Plast.*, 2012, p.171636.
Kaewkhaw, R., Scutt, A.M. & Haycock, J.W., 2012. Integrated culture and purification of rat Schwann cells from freshly isolated adult tissue. *Nat Protoc.*, 7(11), pp.1996-2004.

Kang, H., Tian, L. & Thompson, W., 2003. Terminal Schwann cells guide the reinnervation of muscle after nerve injury. *J Neurocytol.*, 32(5-8), pp.975-85.
Kariya, S. *et al*., 2008. Reduced SMN protein impairs maturation of the neuromuscular junctions in mouse models of spinal muscular atrophy. *Hum Mol Genet.*, 17(16), pp.2552-69.
Kariya, S. *et al*., 2012. Mutant superoxide dismutase 1 (SOD1), a cause of amyotrophic lateral sclerosis, disrupts the recruitment of SMN, the spinal muscular atrophy protein to nuclear Cajal bodies. *Hum Mol Genet.*, 21(15), pp.3421-34.
Katoh-Semba, R. *et al*., 2002. Riluzole enhances expression of brain-derived neurotrophic factor with consequent proliferation of granule precursor cells in the rat hippocampus. *FASEB J.*, 16(10), pp.1328-30.
Kerr, D.A. *et al*., 2000. Survival motor neuron protein modulates neuron-specific apoptosis. *Proc Natl Acad Sci U S A.*, 97(24), pp.13312-7.
Kim, H.A., Ling, B. & Ratner, N., 1997. Nf1-deficient mouse Schwann cells are angiogenic and invasive and can be induced to hyperproliferate: reversion of some phenotypes by an inhibitor of farnesyl protein transferase. *Mol Cell Biol.* , 17(2), pp.862-72.
Kleiger, G. & Mayor, T., 2014. Perilous journey: a tour of the ubiquitin-proteasome system. *Trends Cell Biol.* 24(6), pp.352-9.
Kleinman, H.K. & Martin, G.R., 2005. Matrigel: basement membrane matrix with biological activity. *Semin Cancer Biol.*, 15(5), pp.378-86.
Kleitman, N., Wood, P.M. & Bunge , R.P., 1997. Tissue culture methods for the study of myelination. In In Cowan, W.M., Jessell, T.M. & Zipursky, S.L. *Molecular and Cellular Approaches to Neural Development*. Newyork/ Axford: Oxford University Press. pp.337-77.
Kong, L. *et al*., 2009. Impaired synaptic vesicle release and immaturity of neuromuscular junctions in spinal muscular atrophy mice. *J Neurosci.*, 29(3), pp.842-51.
Krajewski, K.M. *et al*., 2000. Neurological dysfunction and axonal degeneration in Charcot-Marie-Tooth disease type 1A. *Brain.*, 123(Pt 7), pp.1516-27.
Kummer, T.T., Misgeld, T. & Sanes, J.R., 2006. Assembly of the postsynaptic membrane at the neuromuscular junction: paradigm lost. *Curr Opin Neurobiol.*, 16(1), pp.74-82.
Kunkel, S.D. *et al*., 2011. mRNA expression signatures of human skeletal muscle atrophy identify a natural compound that increases muscle mass. *Cell Metab.*, 13(6), pp.627-38.
Kwon, D.Y. *et al*., 2013. The E3 ubiquitin ligase mind bomb 1 ubiquitinates and promotes the degradation of survival of motor neuron protein. *Mol Biol Cell.* , 24(12), pp.1863-71.
Lasiene, J. & Yamanaka, K., 2011. Glial Cells in Amyotrophic Lateral Sclerosis. *Neurol Res Int.*, 2011, pp.1-7.
LeBlanc, S.E., Ward, R.M. & Svaren, J., 2007. Neuropathy-associated Egr2 mutants disrupt cooperative activation of myelin protein zero by Egr2 and Sox10. *Mol Cell Biol.*, 27(9), pp.3521-19.
Lee, H.Y. *et al*., 2004. Instructive role of Wnt/beta-catenin in sensory fate specification in neural crest stem cells. *Science.*, 303(5660), pp.1020-3.

Lee, H.K. *et al*., 2009. Proteasome inhibition suppresses Schwann cell dedifferentiation in vitro and in vivo. *Glia.*, 57(16), pp.1825-34.
Lefebvre, S. *et al*., 1995. Identification and characterization of a spinal muscular atrophy-determining gene. *Cell.*, 80(1), pp.155-65.
Le, N. *et al*., 2005. Analysis of congenital hypomyelinating Egr2Lo/Lo nerves identifies Sox2 as an inhibitor of Schwann cell differentiation and myelination. *Proc Natl Acad Sci U S A.*, 102(7), pp.2596-601.
Lesbordes, J.C. *et al*., 2003. Therapeutic benefits of cardiotrophin-1 gene transfer in a mouse model of spinal muscular atrophy. *Hum Mol Genet.*, 12(11), pp.1233-9.
Levanon, D. *et al*., 2001. Spatial and temporal expression pattern of Runx3 (Aml2) and Runx1 (Aml1) indicates non-redundant functions during mouse embryogenesis. *Mech Dev.*, 109(2), pp.413-7.
Lichtman, j.W. & Colman, H., 2000. Synapse elimination and indelible memory. *Neuron.*, 25(2), pp.269-78.
Li, S., Jiang, Q. & Stys, P.K., 2000. Important role of reverse Na(+)-Ca(2+) exchange in spinal cord white matter injury at physiological temperature. *J Neurophysiol.*, 84(2), pp.1116-9.
Li, C. *et al*., 2012. Induction of heat shock protein 70 (Hsp70) prevents neuregulin-induced demyelination by enhancing the proteasomal clearance of c-Jun. *ASN Neuro.*, 4(7), p.e00102.
Ling, K.K., Gibbs, R.M., Feng, Z. & Ko, C.P., 2012. Severe neuromuscular denervation of clinically relevant muscles in a mouse model of spinal muscular atrophy. *Hum Mol Genet.*, 21(1), pp.185-95.
Lin, W. *et al*., 2000. Aberrant development of motor axons and neuromuscular synapses in erbB2-deficient mice. *Proc Natl Acad Sci U S A.*, 97(3), pp.1299-304.
Liu, Q. & Dreyfuss, G., 1996. A novel nuclear structure containing the survival of motor neurons protein. *EMBO J.*, 15(14), pp.3555-65.
Liu, Y., Oppenheim, R.W., Sugiura, Y. & Lin, W., 2009. Abnormal development of the neuromuscular junction in Nedd4-deficient mice. *Dev Biol.*, 330(1), pp.153-66.
Liu, N., Varma, S., Shooter, E.M. & Tolwani, R.J., 2005. Enhancement of Schwann cell myelin formation by K252a in the Trembler-J mouse dorsal root ganglion explant culture. *J Neurosci Res.*, 79(3), pp.310-7.
Liu, X.F., Wang, D.X. & Ma, D., 2011. Using General Anesthesia plus Muscle Relaxant in a Patient with Spinal Muscular Atrophy Type IV: A Case Report. *Case Rep Anesthesiol.*, 2011, p.743587.
Lobsiger, S.C. *et al*., 2009. Schwann cells expressing dismutase active mutant SOD1 unexpectedly slow disease progression in ALS mice. *Proc Natl Acad Sci U S A.*, 106(11), pp.4465-70.
Lobsiger, C.S. & Cleveland, D.W., 2007. Glial cells as intrinsic components of non-cell-autonomous neurodegenerative disease. *Nat. Neurosci.*, 10(11), p.1355 – 1360.
Lo, L., Dormand, E., Greenwood, A. & Anderson, D.J., 2002. Comparison of the generic neuronal differentiation and neuron subtype specification functions of mammalian achaete-scute and atonal homologs in cultured neural progenitor cells. *Development.*, 129(7), pp.1553-67.

Lorson, C.L. & Androphy, E.J., 2000. An exonic enhancer is required for inclusion of an essential exon in the SMA-determining gene SMN. *Hum Mol Genet.*, 9(2), pp.259-65.

Lorson, C.L., Hahnen, E., Androphy, E.J. & Wirth, B., 1999. A single nucleotide in the SMN gene regulates splicing and is responsible for spinal muscular atrophy. *Proc Natl Acad Sci U S A.*, 96(11), pp.6307-11.

Lotti, F. *et al*., 2012. An SMN-dependent U12 splicing event essential for motor circuit function. *Cell.*, 151(2), pp.440-54.

Lubischer, J.L. & Bebinger, D.M., 1999. Regulation of terminal Schwann cell number at the adult neuromuscular junction. *J Neurosci.*, 19(24), p.RC46.

Lupski, J.R. *et al*., 1991. DNA duplication associated with Charcot-Marie-Tooth disease type 1A. *Cell.*, 66(2), pp.219-32.

Ma, Q., Fode, c., Guillemot, F. & Anderson, D.J., 1999. Neurogenin1 and neurogenin2 control two distinct waves of neurogenesis in developing dorsal root ganglia. *Genes Dev.*, 13(13), pp.1717-28.

Marchetto, M.C. *et al*., 2008. Non-cell-autonomous effect of human SOD1 G37R astrocytes on motor neurons derived from human embryonic stem cells. *Cell Stem Cell.*, 3(6), pp.649-57.

Martinez, T.L. *et al*., 2012. Survival motor neuron protein in motor neurons determines synaptic integrity in spinal muscular atrophy. *J Neurosci.*, 32(25), pp.8703-15.

Martinou, J.C. & Merlie, J.P., 1991. Nerve-dependent modulation of acetylcholine receptor epsilon-subunit gene expression. *J Neurosci.*, 11(5), pp.1291-9.

Martínez-Hernández, R. *et al*., 2013. Synaptic defects in type I spinal muscular atrophy in human development. *J Pathol.*, 229(1), pp.49-61.

Martínez-Hernández, R. *et al*., 2009. The developmental pattern of myotubes in spinal muscular atrophy indicates prenatal delay of muscle maturation. *J Neuropathol Exp Neurol.*, 68(5), pp.474-81.

Mathis, S. *et al*., 2014. Neuropathologic Characterization of INF2-Related Charcot-Marie-Tooth Disease: Evidence for a Schwann Cell Actinopathy. *J Neuropathol Exp Neurol.* 73(3), pp.223-33.

Mattis, V.B. *et al*., 2009. Delivery of a read-through inducing compound, TC007, lessens the severity of a spinal muscular atrophy animal model. *Hum Mol Genet.*, 18(20), pp.3906-13.

Maurel, P. *et al*., 2007. Nectin-like proteins mediate axon Schwann cell interactions along the internode and are essential for myelination. *J Cell Biol.*, 178(5), pp.861-74.

Maurel, P. & Salzer, J.L., 2000. Axonal regulation of Schwann cell proliferation and survival and the initial events of myelination requires PI3-kinase activity. *J Neurosci.*, 20(12), pp.4635-45.

McGovern, V.L., Gavrilina, T.O., Beattie, C.E. & Burghes, A.H., 2008. Embryonic motor axon development in the severe SMA mouse. *Hum Mol Genet.*, 17(18), pp.2900-9.

McWhorter, M.L., Monani, U.R., Burghes, A.H. & Beattie, C.E., 2003. Knockdown of the survival motor neuron (Smn) protein in zebrafish causes defects in motor axon outgrowth and pathfinding. *J Cell Biol.*, 162(5), pp.919-31.

Meier, C. *et al*., 1999. Developing Schwann cells acquire the ability to survive without axons by establishing an autocrine circuit involving insulin-like growth

factor, neurotrophin-3, and platelet-derived growth factor-BB. *J Neurosci.*, 19(10), pp.3847-59.
Melki, J. *et al*., 1994. De novo and inherited deletions of the 5q13 region in spinal muscular atrophies. *Science.*, 264(5164), pp.1474-7.
Mentis, G.Z. *et al*., 2011. Early functional impairment of sensory-motor connectivity in a mouse model of spinal muscular atrophy. *Neuron.*, 69(3), pp.453-67.
Messana, I. *et al*., 2013. Unraveling the different proteomic platforms. *J Sep Sci.*, 36(1), pp.128-39.
Michailov, G.V. *et al*., 2004. Axonal neuregulin-1 regulates myelin sheath thickness. *Science.*, 304(5671), pp.700-3.
Monani, U.R., 2005. Spinal muscular atrophy: a deficiency in a ubiquitous protein; a motor neuron-specific disease. *Neuron.*, 48(6), pp.885-96.
Monani, U.R. *et al*., 1999. A single nucleotide difference that alters splicing patterns distinguishes the SMA gene SMN1 from the copy gene SMN2. *Hum Mol Genet.*, 8(7), pp.1177-83.
Monani, U.R. *et al*., 2000. The human centromeric survival motor neuron gene (SMN2) rescues embryonic lethality in Smn(-/-) mice and results in a mouse with spinal muscular atrophy. *Hum Mol Genet.*, 9(3), pp.333-9.
Morrissey, T.K. *et al*., 1995. Axon-induced mitogenesis of human Schwann cells involves heregulin and p185erbB2. *Proc Natl Acad Sci U S A.*, 92(5), pp.1431-5.
Munsat, T.L. & Davies, K.E., 1992. International SMA consortium meeting. (26-28 June 1992, Bonn, Germany). *Neuromuscul Disord.*, 2(5-6), pp.423-8.
Murray, L.M. *et al*., 2008. Selective vulnerability of motor neurons and dissociation of pre- and post-synaptic pathology at the neuromuscular junction in mouse models of spinal muscular atrophy. *Human Molecular Genetics*, 17(7), pp.949-62.
Murray, L.M. *et al*., 2010. Pre-symptomatic development of lower motor neuron connectivity in a mouse model of severe spinal muscular atrophy. *Hum Mol Genet.*, 19(3), pp.420-33.
Murray, L.M., Talbot, K. & Gillingwater, T.H., 2010. Review: neuromuscular synaptic vulnerability in motor neurone disease: amyotrophic lateral sclerosis and spinal muscular atrophy. *Neuropathol Appl Neurobiol.*, 36(2), pp.133-56.
Mutsaers, C.A. *et al*., 2013. Label-free proteomics identifies Calreticulin and GRP75/Mortalin as peripherally accessible protein biomarkers for spinal muscular atrophy. 5(10), pp.1-13.
Mutsaers, C.A. *et al*., 2011. Reversible molecular pathology of skeletal muscle in spinal muscular atrophy. *Hum Mol Genet.*, 20(22), pp.4334-44.
Nagele, R.G. *et al*., 2004. Contribution of glial cells to the development of amyloid plaques in Alzheimer's disease. *Neurobiology of Aging*, 25(5), p.663–674.
Nam, L. *et al*., 2005. Analysis of congenital hypomyelinating Egr2Lo/Lo nerves identifies Sox2 as an inhibitor of Schwann cell differentiation and myelination. *Proc Natl Acad Sci U S A.*, 102(7), pp.2596-601.
Nave, K.A. & Trapp, B.D., 2008. Axon-glial signaling and the glial support of axon function. *Annu Rev Neurosci.*, 31, pp.535-61.
Nicholson, S.M., Gomès, D., de Néchaud, B. & Bruzzone, R., 2001. Altered gene expression in Schwann cells of connexin32 knockout animals. *J Neurosci Res.*, 66(1), pp.23-36.

Nilsen, T.W., 2003. The spliceosome: the most complex macromolecular machine in the cell? *Bioessays.*, 25(12), pp.1147-9.

Ning, K. *et al*., 2010. PTEN depletion rescues axonal growth defect and improves survival in SMN-deficient motor neurons. *Hum Mol Genet.*, 19(16), pp.3159-68.

Nishimura, A. *et al*., 2004. A mutation in the vesicle-trafficking protein VAPB causes late-onset spinal muscular atrophy and amyotrophic lateral sclerosis. *Am J Hum Genet.*, 75(5), pp.822-31.

Nobbio, L. *et al*., 2006. Axonal damage and demyelination in long-term dorsal root ganglia cultures from a rat model of Charcot-Marie-Tooth type 1A disease. *Eur J Neurosci.*, 23(6), pp.1445-52.

Nodari, A. *et al*., 2007. Beta1 integrin activates Rac1 in Schwann cells to generate radial lamellae during axonal sorting and myelination. *J Cell Biol.*, 177(6), pp.1063-75.

Ogata, T. *et al*., 2004. Opposing extracellular signal-regulated kinase and Akt pathways control Schwann cell myelination. *J Neurosci.*, 24(30), pp.6724-32.

Ogg, S.C. & Lamond, A.I., 2002. Cajal bodies and coilin-moving towards function. *J Cell Biol.*, 159(1), pp.17-21.

Ogino, S. *et al*., 2002. Genetic risk assessment in carrier testing for spinal muscular atrophy. *Am J Med Genet.*, 110(4), pp.301-7.

Oppenheim, R.W. *et al*., 2001. Cardiotrophin-1, a muscle-derived cytokine, is required for the survival of subpopulations of developing motoneurons. *J Neurosci.*, 21(4), pp.1283-91.

Oprea, G.E. *et al*., 2008. Plastin 3 is a protective modifier of autosomal recessive spinal muscular atrophy. *Science.*, 320(5875), pp.524-7.

Osman, E.Y., Yen, P.F. & Lorson, C.L., 2012. Bifunctional RNAs targeting the intronic splicing silencer N1 increase SMN levels and reduce disease severity in an animal model of spinal muscular atrophy. *Mol Ther.*, 20(1), pp.119-26.

Pan, B. *et al*., 2005. Myelin-associated glycoprotein and complementary axonal ligands, gangliosides, mediate axon stability in the CNS and PNS: neuropathology and behavioral deficits in single- and double-null mice. *Exp Neurol.*, 195(1), pp.208-17.

Parker, G.C. *et al*., 2008. Survival motor neuron protein regulates apoptosis in an in vitro model of spinal muscular atrophy. *Neurotox Res.*, 13(1), pp.39-48.

Parkinson, D.B. *et al*., 2008. c-Jun is a negative regulator of myelination. *J Cell Biol.*, 181(4), pp.625-37.

Parkinson, D.B. *et al*., 2004. Krox-20 inhibits Jun-NH2-terminal kinase/c-Jun to control Schwann cell proliferation and death. *J Cell Biol.*, 164(3), pp.385-94.

Passini, M.A. *et al*., 2011. Antisense oligonucleotides delivered to the mouse CNS ameliorate symptoms of severe spinal muscular atrophy. *Sci Transl Med.*, 3(72), p.72ra18.

Pavan, W.J. & Raible, D.W., 2012. Specification of neural crest into sensory neuron and melanocyte lineages. *Dev Biol.*, 366(1), pp.55-63.

Pellizzoni, L., Yong, J. & Dreyfuss, G., 2002. Essential role for the SMN complex in the specificity of snRNP assembly. *Science.*, 298(5599), pp.1775-9.

Perez, S.E., Rebelo, S. & Anderson, D.J., 1999. Early specification of sensory neuron fate revealed by expression and function of neurogenins in the chick embryo. *Development.*, 126(8), pp.1715-28.

Päiväläinen, S. *et al*., 2008. Myelination in mouse dorsal root ganglion/Schwann cell cocultures. *Mol Cell Neurosci.*, 37(3), pp.568-78.
Pinard, A., Lévesque, S., Vallée, J. & Robitaille, R., 2003. Glutamatergic modulation of synaptic plasticity at a PNS vertebrate cholinergic synapse. *Eur J Neurosci.*, 18(12), pp.3241-50.
Praveen, K., Wen, Y. & Matera, A.G., 2012. A Drosopholia model of spinal muscular atrophy uncouples snRNP biogenesis functions of survival motor neuron from locomation and viability defects. *Cell Rep.*, 1(6), pp.624-31.
Previtali, S.C. *et al*., 2003. Expression of laminin receptors in Schwann cell differentiation: evidence for distinct roles. *J Neurosci.*, 23(13), pp.5520-30.
Prockop, D.J. & Kivirikko, K.I., 1995. Collagens: molecular biology, diseases, and potentials for therapy. *Annu Rev Biochem.*, 64, pp.403-34.
Rage, F. *et al*., 2013. Genome-wide identification of mRNAs associated with the protein SMN whose depletion decreases their axonal localization. *RNA.*, 19(12), pp.1755-66.
Ramser, J. *et al*., 2008. Rare missense and synonymous variants in UBE1 are associated with X-linked infantile spinal muscular atrophy. *Am J Hum Genet.*, 82(1), pp.188-93.
Rangaraju, S. *et al*., 2008. Pharmacological induction of the heat shock response improves myelination in a neuropathic model. *Neurobiol Dis.*, 32(1), pp.105-15.
Rasband, M.N., 2011. Composition, assembly, and maintenance of excitable membrane domains in myelinated axons. *Semin Cell Dev Biol.*, 22(2), pp.178-84.
Rasminsky, M., Kearney, R.E., Aguayo, A.J. & Bray, G.M., 1978. Conduction of nervous impulses in spinal roots and peripheral nerves of dystrophic mice. *Brain Res.*, 143(1), pp.71-85.
Rathod, R. *et al*., 2012. Laminin induced local axonal translation of β-actin mRNA is impaired in SMN-deficient motoneurons.. *Histochem Cell Biol.*, 138(5), pp.737-48.
Reynolds, M.L. & Woolf, c.J., 1992. Terminal Schwann cells elaborate extensive processes following denervation of the motor endplate. *J Neurocytol.*, 21(1), pp.50-66.
Rezania, K. & Roos, R.P., 2013. Spinal cord: motor neuron diseases. *Neurol Clin.*, 31(1), pp.219-39.
Riessland, M. *et al*., 2010. SAHA ameliorates the SMA phenotype in two mouse models for spinal muscular atrophy. *Hum Mol Genet.*, 19(8), pp.1492-506.
Robitaille, R., 1998. Modulation of synaptic efficacy and synaptic depression by glial cells at the frog neuromuscular junction. *Neuron.*, 21(4), pp.847-55.
Rochon, D., Rousse, I. & Robitaille, R., 2001. Synapse-glia interactions at the mammalian neuromuscular junction. *J Neurosci.*, 21(11), pp.3819-29.
Rosenberg, S.S., Ng, B.K. & Chan, J.R., 2006. The quest for remyelination: a new role for neurotrophins and their receptors. *Brain Pathol.*, 16(4), pp.288-94.
Rossoll, W. *et al*., 2003. Smn, the spinal muscular atrophy-determining gene product, modulates axon growth and localization of beta-actin mRNA in growth cones of motoneurons. *J Cell Biol.*, 163(4), pp.801-12.
Rothstein, J.D. *et al*., 2005. Beta-lactam antibiotics offer neuroprotection by increasing glutamate transporter expression. *Nature.*, 433(7021), pp.73-7.

Rousse, I. & Robitaille, R., 2006. Calcium signaling in Schwann cells at synaptic and extra-synaptic sites: active glial modulation of neuronal activity. *Glia.*, 54(7), pp.691-9.

Rubinsztein, D.C., 2006. The roles of intracellular protein-degradation pathways in neurodegeneration. *Nature.*, 443(7113), pp.780-6.

Rudnik-Schöneborn, S., Arning, L., Epplen, J. & Zerres, K., 2012. SETX gene mutation in a family diagnosed autosomal dominant proximal spinal muscular atrophy. *Neuromuscul Disord.*, 22(3), pp.258-62.

Rudnik-Schöneborn, S. *et al*., 2003. Classical infantile spinal muscular atrophy with SMN deficiency causes sensory neuronopathy. *Neurology.*, 60(6), pp.983-7.

Rudnik-Schöneborn, S. *et al*., 2008. Congenital heart disease is a feature of severe infantile spinal muscular atrophy. *J Med Genet.*, 45(10), pp.635-8.

Sanchez, G. *et al*., 2013. A novel function for the survival motoneuron protein as a translational regulator. *Hum Mol Genet.*, 22(4), pp.668-84.

Sanes, J.R. & Lichtman, J.W., 1999. Development of the vertebrate neuromuscular junction. *Annu Rev Neurosci.*, 22, pp.389-442.

Sanes, J.R. & Lichtman, J.W., 2001. Induction, assembly, maturation and maintenance of a postsynaptic apparatus. *Nat Rev Neurosci.*, 2(11), pp.791-805.

Schmitt, H.P., 2006. Protein ubiquitination, degradation and the proteasome in neuro-degenerative disorders: no clear evidence for a significant pathogenetic role of proteasome failure in Alzheimer disease and related disorders. *Med Hypotheses.*, 67(2), pp.311-7.

Schrank, B. *et al*., 1997. Inactivation of the survival motor neuron gene, a candidate gene for human spinal muscular atrophy, leads to massive cell death in early mouse embryos. *Proc Natl Acad Sci U S A.*, 94(18), pp.9920-5.

Seilheimer, B., Persohn, E. & Schachner, M., 1989. Antibodies to the L1 adhesion molecule inhibit Schwann cell ensheathment of neurons in vitro. *J Cell Biol.*, 109(6 Pt 1), pp.3095-103.

Shababi, M. *et al*., 2010. Cardiac defects contribute to the pathology of spinal muscular atrophy models. *Hum Mol Genet.*, 19(20), pp.4059-71.

Shafey, D., Côté, P.D. & Kothary, R., 2005. Hypomorphic Smn knockdown C2C12 myoblasts reveal intrinsic defects in myoblast fusion and myotube morphology. *Exp Cell Res.*, 311(1), pp.49-61.

Shafey, D., MacKenzie, A.E. & Kothary, R., 2008. Neurodevelopmental abnormalities in neurosphere-derived neural stem cells from SMN-depleted mice. *J Neurosci Res.*, 86(13), pp.2839-47.

Shah, N., Groves, A. & Anderson, D., 1996. Alternative neural crest cell fates are instructively promoted by TGFbeta superfamily members. *Cell.*, 85(3), pp.331-43.

Shaw, P.J., 2005. Molecular and cellular pathways of neurodegeneration in motor neurone disease. *J Neurol Neurosurg Psychiatry.*, 76(8), pp.1046-57.

Sherman, D.L., Fabrizi, C., Gillespie, C.S. & Brophy, P.J., 2001. Specific disruption of a schwann cell dystrophin-related protein complex in a demyelinating neuropathy. *Neuron.*, 30(3), pp.677-87.

Shorer, z. *et al*., 1995. Demyelinating peripheral neuropathy in merosin-deficient congenital muscular dystrophy. *J Child Neurol*, 10(6), pp.472-5.

Shy, M.E. *et al*., 2004. Phenotypic clustering in MPZ mutations. *Brain.*, 127(Pt 2), pp.371-84.
Sidera, K. *et al*., 2004. Involvement of cell surface HSP90 in cell migration reveals a novel role in the developing nervous system. *J Biol Chem.*, 279(44), pp.45379-88.
Simons, M. *et al*., 2000. Assembly of myelin by association of proteolipid protein with cholesterol- and galactosylceramide-rich membrane domains. *J Cell Biol.*, 151(1), pp.143-54.
Simons, M. & Trotter, J., 2007. Wrapping it up: the cell biology of myelination. *Curr Opin Neurobiol.*, 17(5), pp.533-40.
Singh, N., Singh, N., Androphy, E. & Singh, R., 2006. Splicing of a critical exon of human Survival Motor Neuron is regulated by a unique silencer element located in the last intron. *Mol Cell Biol*, 26(4), pp.1333-46.
Skeie, G.O. *et al*., 2010. Guidelines for treatment of autoimmune neuromuscular transmission disorders. *Eur J Neurol.*, 17(7), pp.893-902.
Skorupa, A. *et al*., 2013. Angiogenin induces modifications in the astrocyte secretome: relevance to amyotrophic lateral sclerosis. *J Proteomics.*, 91, pp.274-85.
Sleigh, N.J., Gillingwater, T.H. & Talbot, K., 2011. The contribution of mouse models to understanding the pathogenesis of spinal muscular atrophy. *Dis Model Mech.*, 4(4), pp.457-67.
Smith, I.W., Mikesh, M., Lee, Y.I. & Thompson, W.J., 2013. Terminal Schwann cells participate in the competition underlying neuromuscular synapse elimination. *J Neurosci.*, 33(45), pp.17724-36.
Somers, E. *et al*., 2013. creasing SMN levels using the histone deacetylase inhibitor SAHA ameliorates defects in skeletal muscle microvasculature in a mouse model of severe spinal muscular atrophy. *Neurosci Lett.*, 544, pp.100-4.
Somers, E. *et al*., 2012. Density, Calibre and ramification of muscle capillaries are altered in a mouse model of severe spinal muscular atrophy. *Neuromuscul Disord.*, 22(5), pp.435-42.
Sondell, M., Fex-Svenningsen, A. & Kanje, M., 1997. The insulin-like growth factors I and II stimulate proliferation of different types of Schwann cells. *Neuroreport.*, 8(13), pp.2871-6.
Son, Y.J., Trachtenberg, J.T. & Thompson, W.J., 1996. Schwann cells induce and guide sprouting and reinnervation of neuromuscular junctions. *Trends Neurosci.*, 19(7), pp.280-5.
Stewart, h.J. *et al*., 1996. Regulation of rat Schwann cell Po expression and DNA synthesis by insulin-like growth factors in vitro. *Eur J Neurosci.* , 8(3), pp.553-64.
Stewart, H., Morgan, L., Jessen, K. & Mirsky, R., 1993. Changes in DNA synthesis rate in the Schwann cell lineage in vivo are correlated with the precursor--Schwann cell transition and myelination. *Eur J Neurosci.*, 5(9), pp.1136-44.
Stirling, C.A., 1975. Abnormalities in Schwann cell sheaths in spinal nerve roots of dystrophic mice. *J Anat.*, 119(Pt 1), pp.169-80.
Sugiura, Y. & Lin, W., 2011. Neuron-glia interactions: the roles of Schwann cells in neuromuscular synapse formation and function. *Biosci Rep.*, 31(5), pp.295-302.

Sun, Y. *et al*., 2008. A central role for Islet1 in sensory neuron development linking sensory and spinal gene regulatory programs. *Nat Neurosci.*, 11(11), pp.1283-93.

Susuki, K. *et al*., 2011. Schwann cell spectrins modulate peripheral nerve myelination. *Proc Natl Acad Sci U S A.*, 108(19), pp.8009-14.

Svaren, J. & Meijer, D., 2008. The molecular machinery of myelin gene transcription in Schwann cells. *Glia.*, 56(14), pp.1541-51.

Takahashi, R. *et al*., 1994. A null mutation in the human CNTF gene is not causally related to neurological diseases. *Nat Genet.*, 7(1), pp.79-84.

Taveggia, C. *et al*., 2005. Neuregulin-1 type III determines the ensheathment fate of axons. *Neuron.*, 47(5), pp.681-94.

Thomas, P.K., 1963. The connective tissue of peripheral nerve: an electron microscope study. *J Anat.*, 97, pp.35-44.

Thomas, S. & Robitaille, R., 2001. Differential frequency-dependent regulation of transmitter release by endogenous nitric oxide at the amphibian neuromuscular synapse. *J Neurosci.*, 21(4), pp.1087-95.

Thomson, S.R. *et al*., 2012. Morphological characteristics of motor neurons do not determine their relative susceptibility to degeneration in a mouse model of severe spinal muscular atrophy. *PLoS One.*, 7(12), p.e52605.

Thomson, S.R. *et al*., 2012. Using induced pluripotent stem cells (iPSC) to model human neuromuscular connectivity: promise or reality? *J Anat.*, 220(2), pp.122-30.

Topp, K.S. & Boyd, B.S., 2006. Structure and biomechanics of peripheral nerves: nerve responses to physical stresses and implications for physical therapist practice. *Phys Ther.*, 86(1), pp.92-109.

Tyers, M. & Mann, M., 2003. From genomics to proteomics. *Nature.*, 422(6928), pp.193-7.

Valori, C.F. *et al*., 2010. Systemic delivery of scAAV9 expressing SMN prolongs survival in a model of spinal muscular atrophy. *Sci Transl Med.*, 2(35), p.35ra42.

Van Vught, P.W. *et al*., 2007. Ciliary neurotrophic factor null alleles are not a risk factor for Charcot-Marie-Tooth disease, hereditary neuropathy with pressure palsies and amyotrophic lateral sclerosis. *Neuromuscul Disord.*, 17(11-12), pp.964-7.

Verdú, E. *et al*., 2000. Expansion of adult Schwann cells from mouse predegenerated peripheral nerves. *J Neurosci Methods.*, 30(1-2), pp.111-7.

Vitriol, E.A. & Zheng, J.Q., 2012. Growth cone travel in space and time: the cellular ensemble of cytoskeleton, adhesion, and membrane. *Neuron.*, 73(6), pp.1068-81.

Vitte, J.M. *et al*., 2004. Deletion of murine Smn exon 7 directed to liver leads to severe defect of liver development associated with iron overload. *Am J Pathol.*, 165(5), pp.1731-41.

Vyas, S. *et al*., 2002. Involvement of survival motor neuron (SMN) protein in cell death. *Hum Mol Genet.*, 11(22), pp.2751-64.

Wang, H., Alvarez, S. & Hicks, L.M., 2012. Comprehensive comparison of iTRAQ and label-free LC-based quantitative proteomics approaches using two Chlamydomonas reinhardtii strains of interest for biofuels engineering. *J Proteome Res.*, 11(1), pp.487-501.

Wang, J. & Dreyfuss, G., 2001. Characterization of functional domains of the SMN protein in vivo. *J Biol Chem.*, 276(48), pp.45387-93.
Wanner, I. *et al*., 2006. Role of N-cadherin in Schwann cell precursors of growing nerves. *Glia.*, 54(5), pp.439-59.
Will, C.L. & Lührmann, R., 2001. Spliceosomal UsnRNP biogenesis, structure and function. *Curr Opin Cell Biol.*, 13(3), pp.290-301.
Wishart, T.M. *et al*., 2010. SMN deficiency disrupts brain development in a mouse model of severe spinal muscular atrophy. *Hum Mol Genet.*, 19(21), pp.4216-28.
Wishart, T.M. *et al*., 2014. Dysregulation of ubiquitin homeostasis and β-catenin signalling promote spinal muscular atrophy. *J Clin Invest.*, 124(4), pp1821-34
Wolpowitz, D. *et al*., 2000. Cysteine-rich domain isoforms of the neuregulin-1 gene are required for maintenance of peripheral synapses. *Neuron.*, 25(1), pp.79-91.
Woodhoo , A. *et al*., 2009. Notch controls embryonic Schwann cell differentiation, postnatal myelination and adult plasticity. *Nat Neurosci.*, 12(7), pp.839-47.
Woodhoo, A. & Sommer, L., 2008. Development of the Schwann cell lineage: from the neural crest to the myelinated nerve. *Glia.*, 56(14), pp.1481-90.
Workman, E., Kolb, S.J. & Battle, D.J., 2012. Spliceosomal small nuclear ribonucleoprotein biogenesis defects and motor neuron selectivity in spinal muscular atrophy. *Brain Res.*, 1462, pp.93-9.
Workman, E., Kolb, S.J. & Battle, D.J., 2012. Spliceosomal small nuclear ribonucleoprotein biogenesis defects and motor neuron selectivity in spinal muscular atrophy. *Brain Res.*, 1462, pp.93-99.
Wu, C.Y. *et al*., 2011. Proteomic assessment of a cell model of spinal muscular atrophy. *BMC Neurosci.*, 12(25), pp.1-13.
Xiao, J. *et al*., 2009. BDNF exerts contrasting effects on peripheral myelination of NGF-dependent and BDNF-dependent DRG neurons. *J Neurosci.*, 29(13), pp.4016-22.
Yamada, H., Komiyama, A. & Suzuki, K., 1995. Schwann cell responses to forskolin and cyclic AMP analogues: comparative study of mouse and rat Schwann cells. *Brain Res.*, 681(1-2), pp.97-104.
Yamanaka, K. *et al*., 2008. Astrocytes as determinants of disease progression in inherited amyotrophic lateral sclerosis. *Nat Neurosci.*, 11(3), pp.251-3.
Yang, D. *et al*., 2005. Coordinate control of axon defasciculation and myelination by laminin-2 and -8. *J Cell Biol.*, 168(4), pp.655-66.
Yonekawa, T. *et al*., 2013. Peripheral nerve abnormalities in pediatric patients with spinal muscular atrophy. *Brain Dev.*, 35(2), pp.165-71.
Yost, C. *et al*., 1996. The axis-inducing activity, stability, and subcellular distribution of beta-catenin is regulated in Xenopus embryos by glycogen synthase kinase 3. *Genes Dev.*, 10(12), pp.1443-54.
Yu, W.M. *et al*., 2005. Schwann cell-specific ablation of laminin gama1 causes apoptosis and prevents proliferation. *J Neurosci.*, 25(18), pp.4463-72.
Yusuf, F. & Brand-Saberi, B., 2012. Myogenesis and muscle regeneration. *Histochem Cell Biol.*, 138(2), pp.187-99.
Zanetta, C. *et al*., 2014. Molecular, genetic and stem cell-mediated therapeutic strategies for spinal muscular atrophy (SMA). *J Cell Mol Med.*, 18(2), pp.187-96.

Zhou, J. *et al*., 2012. Spinal muscular atrophy associated with progressive myoclonic epilepsy is caused by mutations in ASAH1. *Am J Hum Genet.*, 91(1), pp.5-14.
Zou, T. *et al*., 2007. SMN protects cells against mutant SOD1 toxicity by increasing chaperone activity. *Biochem Biophys Res Commun.*, 364(4), pp.850-5.

Appendices

Appendix 1: Functional clustering revealed cellular growth and proliferation were significantly affected in Schwann cells from SMA mice

Disease or function annotation	P-value	Molecules
Proliferation of cells	1.10E-13	ADAM10, AKAP12, ALB, ALDH1A1, ANXA1, ANXA2, ANXA7, ASAH1, ATP5A1, ATP5B, CCT2, CDC42, CFL1, CLIC1, COL1A1, COL1A2, CRLF1, CTNNA1, CTSB, CTSD, CTTN, DBN1, DNAJA1, DNAJA2, DNM2, DSP, EEF1B2, EIF3C/EIF3CL, EIF4A1, FHL2, FLNA, FMR1, FN1, FSCN1, GNB1, GNB2L1, GPI, GSN, GSTP1, HADHA, HK1, HNRNPK, HNRNPM, HNRNPU, HSP90B1, HSPA5, HSPD1, IGF2R, ITGB1, JUP, LAMC1, LASP1, LEPRE1, LGALS1, LMNA, MTAP, MVP, NAP1L1, P4HA2, PCYOX1, PDCD6IP, PFN1, PGK1, PLEC, PRDX1, PRDX2, PRMT1, PSAP, PSMC1, RAB1A, RNH1, RPS4X, S100A10, S100A4, SEC23A, SERPINH1, SNCG, SND1, SOD1, SPTAN1, SPTBN1, SQSTM1, STAT3, SUGT1, SURF4, TCP1, TPP2, TXNDC5, TXNL1, TXNRD1, UBA1, UCHL1, VCP, VDAC1, YWHAG, YWHAQ
Proliferation of breast cancer cell lines	9.19E-08	ANXA2, ASAH1, CTSD, EEF1B2, EIF3C/EIF3CL, FN1, GNB2L1, HNRNPK, HSPA5, ITGB1, LGALS1, MTAP, PFN1, PRDX2, S100A4, SNCG, SND1, STAT3, UBA1, YWHAQ
Proliferation of tumor cell lines	3.38E-07	AKAP12, ALDH1A1, ANXA1, ANXA2, ANXA7, ASAH1, CDC42, COL1A1, CTSB, CTSD, CTTN, EEF1B2, EIF3C/EIF3CL, EIF4A1, FHL2, FLNA, FN1, FSCN1, GNB2L1, HK1, HNRNPK, HSPA5, IGF2R, ITGB1, JUP, LGALS1, MTAP, PDCD6IP, PFN1, PRDX2, PRMT1, S100A10, S100A4, SNCG, SND1, SOD1, SPTAN1, STAT3, TCP1, TPP2, UBA1, UCHL1, YWHAG, YWHAQ
Metastasis of tumor cell lines	2.69E-05	ASAH1, CTSB, CTTN, FN1, PRDX2, S100A4, SNCG, SND1
Metastasis of breast cancer cell lines	4.15E-05	CTSB, PRDX2, S100A4, SNCG, SND1
Proliferation of carcinoma cell lines	3.05E-04	ANXA1, ANXA2, FHL2, FSCN1, HK1, IGF2R, ITGB1, JUP, S100A10, SOD1, STAT3, UCHL1
Neoplasia of tumor cell lines	3.72E-04	ASAH1, CTSB, CTTN, FN1, JUP, PDCD6IP, PRDX2, S100A4, SNCG, SND1
Proliferation of	9.08E-04	AKAP12, ALDH1A1, ANXA7, ASAH1, FSCN1, HK1, IGF2R, ITGB1,

Disease or function annotation	P-value	Molecules
prostate cancer cell lines		SND1, STAT3
Proliferation of squamous-cell carcinoma	1.15E-03	ADAM10, STAT3
Metastasis of carcinoma cell lines	1.26E-03	CTTN, FN1, S100A4
Colony formation of leukemia cell lines	1.91E-03	ALDH1A1, CTSB, SQSTM1
Colony formation of cells	2.98E-03	AKAP12, ALDH1A1, ANXA1, ANXA7, CDC42, CTSB, CTSD, JUP, LEPRE1, S100A10, SOD1, SQSTM1, STAT3, SUGT1
Colony formation of tumor cell lines	3.31E-03	ALDH1A1, ANXA1, ANXA7, CTSB, CTSD, S100A10, SOD1, SQSTM1, STAT3

Appendix 2: Functional clustering revealed cell death and survival were significantly affected in Schwann cells from SMA mice

Disease or function annotation	P-value	Molecules
Cell death	7.22E-13	ADH5, AKAP12, ALB, ALDH1A1, ALDOA, ANXA1, ANXA2, ANXA5, ANXA7, AP2A2, ASAH1, ASS1, ATP5A1, CANX, CCT2, CCT8, CDC42, CFL1, COL1A1, CRLF1, CTNNA1, CTSB, CTSD, CTTN, DDAH2, DHX9, DNAJA1, DNM2, DSG1, DSP, EIF3C/EIF3CL, FHL2, FLNA, FN1, GFPT1, GLUD1, GNB2, GNB2L1, GPI, GSN, GSTP1, HADHA, HK1, HNRNPK, HSP90B1, HSPA4, HSPA5, HSPA9, HSPD1, HSPH1, HYOU1, IGF2R, ITGB1, JUP, LGALS1, LMNA, MAP1B, MDH1, MVP, NSF, PDCD6IP, PLEC, PRDX1, PRDX2, PSAP, PSMC1, Rpl10, RPLP0, RPS3, RTN4, S100A10, S100A4, SNCG, SND1, SOD1, SORBS2, SPTBN1, SQSTM1, STAT3, TCP1, TPP2, TUFM, TXNDC5, TXNRD1, UBA1, UCHL1, VCP, VDAC1, VDAC2, YWHAG, YWHAQ, YWHAZ
Apoptosis	1.10E-12	ADH5, AKAP12, ALB, ALDH1A1, ALDOA, ANXA1, ANXA2, ANXA5, ANXA7, AP2A2, ASAH1, ASS1, CANX, CCT2, CDC42, CFL1, COL1A1, CRLF1, CTNNA1, CTSB, CTSD, CTTN, DDAH2, DHX9, DNM2, DSG1, DSP, EIF3C/EIF3CL, FHL2, FN1, GFPT1, GLUD1, GNB2, GNB2L1, GPI, GSN, GSTP1, HK1, HNRNPK, HSP90B1, HSPA4, HSPA5, HSPA9, HSPD1, HSPH1, HYOU1, IGF2R, ITGB1, JUP, LGALS1, LMNA, MAP1B, MDH1, PDCD6IP, PRDX1, PRDX2, PSAP, Rpl10, RPLP0, RPS3, RTN4, S100A10, S100A4, SNCG, SND1, SOD1, SORBS2, SPTBN1, STAT3, TCP1, TPP2, TXNDC5, UBA1, UCHL1, VCP, VDAC1, VDAC2, YWHAQ, YWHAZ
Necrosis	6.60E-13	AKAP12, ALB, ALDH1A1, ALDOA, ANXA1, ANXA2, AP2A2, ASAH1, ASS1, ATP5A1, CCT2, CCT8, CDC42, COL1A1, CRLF1, CTNNA1, CTSB, CTSD, CTTN, DNM2, DSG1, DSP, EIF3C/EIF3CL, FHL2, FLNA, FN1, GFPT1, GLUD1, GNB2, GNB2L1, GPI, GSN, GSTP1, HADHA, HK1, HNRNPK, HSPA4, HSPA5, HSPA9, HSPD1, HSPH1, HYOU1, IGF2R, ITGB1, JUP, LGALS1, LMNA, MAP1B, MDH1, MVP, PDCD6IP, PLEC, PRDX1, PRDX2, PSAP, Rpl10, RPLP0, RPS3, RTN4, S100A10, S100A4, SND1, SOD1, SPTBN1, SQSTM1, STAT3, TCP1, TPP2, TUFM, TXNRD1, UBA1, UCHL1, VCP, VDAC1, VDAC2, YWHAG, YWHAQ, YWHAZ
Cell death of tumor cell lines	1.90E-11	AKAP12, ALB, ANXA2, AP2A2, ASAH1, ATP5A1, CCT2, CCT8, CDC42, COL1A1, CTSB, CTSD, CTTN, DNM2, DSG1, FN1, GNB2L1, GPI, GSN, GSTP1, HK1, HNRNPK, HSPA4, HSPA5, HSPA9, HSPD1, IGF2R, ITGB1, JUP, LGALS1, LMNA, PDCD6IP, PRDX1, PRDX2,

Disease or function annotation	P-value	Molecules
		PSAP, RPLP0, RPS3, RTN4, S100A4, SND1, SOD1, SQSTM1, STAT3, TCP1, TPP2, TUFM, TXNRD1, UCHL1, VCP, VDAC1, VDAC2, YWHAG, YWHAZ
Apoptosis of tumor cell lines	6.10E-09	AKAP12, ALB, ANXA2, AP2A2, CCT2, CDC42, COL1A1, CTSB, CTSD, CTTN, DNM2, DSG1, FN1, GNB2L1, GSN, GSTP1, HNRNPK, HSPA4, HSPA5, HSPA9, HSPD1, IGF2R, ITGB1, JUP, LGALS1, PDCD6IP, PRDX1, PSAP, RPLP0, RPS3, RTN4, S100A4, SND1, SOD1, STAT3, TCP1, UCHL1, VCP, VDAC1, VDAC2, YWHAZ
Cell survival	2.84E-05	ASAH1, ASS1, CDC42, COL1A1, CTSB, DHX9, DNM2, EEF2, EIF3C/EIF3CL, FLNA, FN1, GLUD1, GNB2L1, GSTP1, HNRNPU, HSP90B1, HSPA4, HSPA5, HSPD1, HYOU1, IGF2R, ITGB1, JUP, LMNA, MVP, PRDX2, PSMA4, S100A4, SND1, SOD1, SQSTM1, STAT3, TCP1, TXNDC5, VCP, VDAC1, YWHAZ
Cell viability	7.07E-05	ASAH1, ASS1, CDC42, COL1A1, CTSB, DNM2, EEF2, EIF3C/EIF3CL, FLNA, FN1, GLUD1, GNB2L1, GSTP1, HNRNPU, HSP90B1, HSPA5, HSPD1, HYOU1, IGF2R, ITGB1, LMNA, MVP, PRDX2, PSMA4, S100A4, SND1, SOD1, SQSTM1, STAT3, TCP1, TXNDC5, VCP, VDAC1, YWHAZ
Neuronal cell death	2.13E-05	ASAH1, CDC42, CRLF1, CTSB, CTSD, FN1, GLUD1, GPI, HSPA5, HSPD1, HSPH1, HYOU1, ITGB1, LGALS1, MAP1B, PDCD6IP, PRDX2, RPS3, SOD1, STAT3, TCP1, UCHL1, YWHAZ
Cell death of connective tissue cells	1.44E-05	ASAH1, CDC42, CTSB, CTSD, EIF3C/EIF3CL, FLNA, FN1, GNB2, GPI, GSN, GSTP1, HSPA5, HSPD1, IGF2R, ITGB1, LMNA, Rpl10, STAT3, TPP2, UBA1, VCP, YWHAZ
Cell viability of tumor cell lines	2.24E-04	ASAH1, COL1A1, DNM2, EEF2, EIF3C/EIF3CL, FLNA, FN1, GLUD1, GNB2L1, GSTP1, HSP90B1, HSPA5, IGF2R, ITGB1, PRDX2, PSMA4, S100A4, SOD1, SQSTM1, STAT3, TCP1, VCP
Apoptosis of neurons	2.10E-05	ASAH1, CDC42, CRLF1, CTSB, FN1, GLUD1, GPI, HSPA5, HSPD1, HSPH1, HYOU1, LGALS1, MAP1B, PDCD6IP, PRDX2, RPS3, SOD1
Cell death of fibroblast cell lines	1.46E-04	ASAH1, CTSB, CTSD, EIF3C/EIF3CL, FN1, GNB2, GPI, GSN, GSTP1, HSPA5, HSPD1, ITGB1, Rpl10, UBA1, VCP, YWHAZ
Cell death of kidney cells	1.24E-04	ALB, CDC42, GFPT1, GNB2, GSN, GSTP1, HK1, HSPA5, HYOU1, ITGB1, SOD1, VCP, VDAC1, YWHAQ
Cell death of cervical cancer cell lines	1.27E-04	CTSB, HNRNPK, LMNA, PDCD6IP, PRDX2, SOD1, SQSTM1, STAT3, TCP1, TXNRD1, UCHL1, VCP, VDAC1
cell death of kidney cell lines	3.49E-04	CDC42, GNB2, GSN, GSTP1, HK1, HSPA5, HYOU1, ITGB1, SOD1, VCP, VDAC1, YWHAQ
Cell death of colon cancer cell lines	2.97E-04	AP2A2, CDC42, GSN, GSTP1, HSPD1, IGF2R, ITGB1, LMNA, SQSTM1, TXNRD1, VCP

Disease or function annotation	P-value	Molecules
Cell death of neuroblastoma cell lines	5.35E-05	ATP5A1, CCT2, CCT8, CDC42, ITGB1, PRDX2, SOD1, SQSTM1, STAT3, TCP1
Cell death of central nervous system cells	2.71E-03	ALB, CDC42, CTSD, HSPA5, HSPD1, HYOU1, MAP1B, RPS3, SOD1, TCP1
Cell death of cerebral cortex cells	1.18E-03	CDC42, CTSD, HSPA5, HSPD1, HYOU1, MAP1B, RPS3, SOD1, TCP1
Cell death of fibroblasts	3.39E-03	CDC42, CTSD, FLNA, GPI, IGF2R, ITGB1, LMNA, STAT3, TPP2
Cellular degradation	6.70E-04	CTSB, CTSD, PSAP, PSMC1, SOD1, SQSTM1, STAT3, UCHL1
Cell death of carcinoma cell lines	2.95E-03	AP2A2, CTTN, GPI, HK1, HSPA5, SOD1, STAT3, UCHL1
Cell death of lymphoma cell lines	2.95E-03	ALB, ANXA2, LGALS1, RPLP0, STAT3, TPP2, YWHAG, YWHAZ
Degeneration of neurons	2.14E-03	CTSB, CTSD, PSAP, PSMC1, SOD1, STAT3, UCHL1
Apoptosis of prostate cancer cell lines	3.71E-03	AKAP12, FN1, HSPA5, HSPD1, ITGB1, LGALS1, STAT3
Cell death of pheochromocytoma cell lines	2.57E-03	CDC42, PSAP, RPS3, SOD1, STAT3, VCP
Cell viability of brain cancer cell lines	2.27E-04	DNM2, EEF2, GLUD1, HSPA5, STAT3
Cell viability of myeloma cell lines	1.70E-03	EIF3C/EIF3CL, HSP90B1, PSMA4, SOD1, STAT3
Apoptosis of pheochromocytoma Cell lines	3.16E-03	CDC42, PSAP, RPS3, SOD1, STAT3
Cell death of endothelial cell lines	2.62E-03	CTSD, FN1, HYOU1, SOD1
Delay in apoptosis of fibroblast cell lines	1.72E-03	FN1, GSN
Killing of cervical cancer cell lines	4.03E-03	GSTP1, HNRNPK
Cell death	7.22E-13	ADH5, AKAP12, ALB, ALDH1A1, ALDOA, ANXA1, ANXA2, ANXA5, ANXA7, AP2A2, ASAH1, ASS1, ATP5A1, CANX, CCT2, CCT8, CDC42, CFL1, COL1A1, CRLF1, CTNNA1, CTSB, CTSD,

Disease or function annotation	P-value	Molecules
		CTTN, DDAH2, DHX9, DNAJA1, DNM2, DSG1, DSP, EIF3C/EIF3CL, FHL2, FLNA, FN1, GFPT1, GLUD1, GNB2, GNB2L1, GPI, GSN, GSTP1, HADHA, HK1, HNRNPK, HSP90B1, HSPA4, HSPA5, HSPA9, HSPD1, HSPH1, HYOU1, IGF2R, ITGB1, JUP, LGALS1, LMNA, MAP1B, MDH1, MVP, NSF, PDCD6IP, PLEC, PRDX1, PRDX2, PSAP, PSMC1, Rpl10, RPLP0, RPS3, RTN4, S100A10, S100A4, SNCG, SND1, SOD1, SORBS2, SPTBN1, SQSTM1, STAT3, TCP1, TPP2, TUFM, TXNDC5, TXNRD1, UBA1, UCHL1, VCP, VDAC1, VDAC2, YWHAG, YWHAQ, YWHAZ
Apoptosis	1.10E-12	ADH5, AKAP12, ALB, ALDH1A1, ALDOA, ANXA1, ANXA2, ANXA5, ANXA7, AP2A2, ASAH1, ASS1, CANX, CCT2, CDC42, CFL1, COL1A1, CRLF1, CTNNA1, CTSB, CTSD, CTTN, DDAH2, DHX9, DNM2, DSG1, DSP, EIF3C/EIF3CL, FHL2, FN1, GFPT1, GLUD1, GNB2, GNB2L1, GPI, GSN, GSTP1, HK1, HNRNPK, HSP90B1, HSPA4, HSPA5, HSPA9, HSPD1, HSPH1, HYOU1, IGF2R, ITGB1, JUP, LGALS1, LMNA, MAP1B, MDH1, PDCD6IP, PRDX1, PRDX2, PSAP, Rpl10, RPLP0, RPS3, RTN4, S100A10, S100A4, SNCG, SND1, SOD1, SORBS2, SPTBN1, STAT3, TCP1, TPP2, TXNDC5, UBA1, UCHL1, VCP, VDAC1, VDAC2, YWHAQ, YWHAZ
Necrosis	6.60E-13	AKAP12, ALB, ALDH1A1, ALDOA, ANXA1, ANXA2, AP2A2, ASAH1, ASS1, ATP5A1, CCT2, CCT8, CDC42, COL1A1, CRLF1, CTNNA1, CTSB, CTSD, CTTN, DNM2, DSG1, DSP, EIF3C/EIF3CL, FHL2, FLNA, FN1, GFPT1, GLUD1, GNB2, GNB2L1, GPI, GSN, GSTP1, HADHA, HK1, HNRNPK, HSPA4, HSPA5, HSPA9, HSPD1, HSPH1, HYOU1, IGF2R, ITGB1, JUP, LGALS1, LMNA, MAP1B, MDH1, MVP, PDCD6IP, PLEC, PRDX1, PRDX2, PSAP, Rpl10, RPLP0, RPS3, RTN4, S100A10, S100A4, SND1, SOD1, SPTBN1, SQSTM1, STAT3, TCP1, TPP2, TUFM, TXNRD1, UBA1, UCHL1, VCP, VDAC1, VDAC2, YWHAG, YWHAQ, YWHAZ
Cell death of tumor cell lines	1.90E-11	AKAP12, ALB, ANXA2, AP2A2, ASAH1, ATP5A1, CCT2, CCT8, CDC42, COL1A1, CTSB, CTSD, CTTN, DNM2, DSG1, FN1, GNB2L1, GPI, GSN, GSTP1, HK1, HNRNPK, HSPA4, HSPA5, HSPA9, HSPD1, IGF2R, ITGB1, JUP, LGALS1, LMNA, PDCD6IP, PRDX1, PRDX2, PSAP, RPLP0, RPS3, RTN4, S100A4, SND1, SOD1, SQSTM1, STAT3, TCP1, TPP2, TUFM, TXNRD1, UCHL1, VCP, VDAC1, VDAC2, YWHAG, YWHAZ
Delay in apoptosis of fibroblast cell lines	6.10E-09	AKAP12, ALB, ANXA2, AP2A2, CCT2, CDC42, COL1A1, CTSB, CTSD, CTTN, DNM2, DSG1, FN1, GNB2L1, GSN, GSTP1, HNRNPK, HSPA4, HSPA5, HSPA9, HSPD1, IGF2R, ITGB1, JUP, LGALS1, PDCD6IP, PRDX1, PSAP, RPLP0, RPS3, RTN4, S100A4, SND1, SOD1, STAT3, TCP1, UCHL1, VCP, VDAC1, VDAC2, YWHAZ

Disease or function annotation	P-value	Molecules
Killing of cervical cancer cell lines	2.84E-05	ASAH1, ASS1, CDC42, COL1A1, CTSB, DHX9, DNM2, EEF2, EIF3C/EIF3CL, FLNA, FN1, GLUD1, GNB2L1, GSTP1, HNRNPU, HSP90B1, HSPA4, HSPA5, HSPD1, HYOU1, IGF2R, ITGB1, JUP, LMNA, MVP, PRDX2, PSMA4, S100A4, SND1, SOD1, SQSTM1, STAT3, TCP1, TXNDC5, VCP, VDAC1, YWHAZ

Appendix 3: Functional clustering revealed molecular transport was significantly affected in Schwann cells from SMA mice

Disease or function annotation	P-value	Molecules
Transport of molecule	7.44E-09	ALB, ANXA1, ANXA2, ANXA6, AP2A1, AP2A2, ASAH1, ATP5A1, ATP5B, CANX, CDC42, CFL1, CLIC1, COL1A1, DNAJA1, DNAJA2, FMR1, FN1, GDI2, GSN, HNRNPA3, HSPA9, IGF2R, ITGB1, JUP, KPNB1, LASP1, LGALS1, MAP1B, MYO1C, NPC2, NSF, PCYOX1, PDIA4, PSAP, RAB1A, RAB6A, RTN4, SEC23A, SEPT2, SNCG, SOD1, SPTBN1, SQSTM1, STAT3, USO1, VDAC1, VDAC2, YWHAZ
Transport of protein	2.29E-11	AP2A1, AP2A2, CFL1, COL1A1, DNAJA1, DNAJA2, GDI2, HSPA9, IGF2R, JUP, KPNB1, MAP1B, NSF, RAB1A, RAB6A, SEC23A, SOD1, SPTBN1, SQSTM1, STAT3, USO1
Secretion of molecule	1.71E-04	ANXA1, ANXA2, ANXA6, ASAH1, CANX, CDC42, FN1, GSN, LGALS1, MYO1C, NSF, PDIA4, RTN4, SEC23A, SNCG, SOD1, STAT3, YWHAZ
Internalization of protein	7.23E-06	CFL1, DNAJA1, DNAJA2, DNM2, JUP, KPNB1, SPTBN1, STAT3
Import of protein	8.10E-06	CFL1, DNAJA1, DNAJA2, JUP, KPNB1, SPTBN1, STAT3
Secretion of protein	8.60E-04	ANXA1, ANXA2, CANX, CDC42, MYO1C, PDIA4, SEC23A
Quantity of hydrogen peroxide	3.40E-03	PRDX1, PRDX2, SOD1
Redistribution of phosphatidylserine	3.51E-04	GSN, LGALS1
Accumulation of lactosylceramide	1.72E-03	NPC2, PSAP
Accumulation of glucosylceramide	2.39E-03	NPC2, PSAP
Quantity of lactosylceramide	3.16E-03	ASAH1, PSAP

Appendix 4: IPA analysis showed protein trafficking was significantly affected in Schwann cells from SMA mice

Disease or function annotation	P-value	Molecules
Transport of protein	2.29E-11	AP2A1, AP2A2, CFL1, COL1A1, DNAJA1, DNAJA2, GDI2, HSPA9, IGF2R, JUP, KPNB1, MAP1B, NSF, RAB1A, RAB6A, SEC23A, SOD1, SPTBN1, SQSTM1, STAT3, USO1
Internalization of protein	7.23E-06	CFL1, DNAJA1, DNAJA2, DNM2, JUP, KPNB1, SPTBN1, STAT3
Import of protein	8.10E-06	CFL1, DNAJA1, DNAJA2, JUP, KPNB1, SPTBN1, STAT3
Secretion of protein	8.60E-04	ANXA1, ANXA2, CANX, CDC42, MYO1C, PDIA4, SEC23A

Appendix 5: Functional clustering indicated cellular assembly and organisation were significantly affected in Schwann cells from SMA mice

Disease or function annotation	P-value	Molecules
Organization of cytoplasm	1.13E-08	ACTR3 ADD1, AKAP12, ALDOA, ANXA1, CANX, CAPG, CAPZB, CDC42, CFL1, CORO1C, CTTN, DBN1, DNM2, DSP, EPB41L2, FHL2, FLNA, FMR1, FN1, FSCN1, GOLGB1, GORASP2, GSN, ITGB1, JUP, KPNB1, LAMC1, LASP1, MAP1B, PFN1, PLS3, PRMT1, RAB6A, RTN4, S100A4, SEPT2, SOD1, SPTAN1, SPTBN1, STAT3, SURF4, TLN1, UCHL1
Organization of cytoskeleton	8.50E-08	ACTR3, ADD1, AKAP12, ALDOA, ANXA1, CANX, CAPG, CAPZB, CDC42, CFL1, CORO1C, CTTN, DBN1, DNM2, DSP, EPB41L2, FHL2, FLNA, FMR1, FN1, FSCN1, GSN, ITGB1, JUP, KPNB1, LAMC1, LASP1, MAP1B, PFN1, PLS3, PRMT1, RTN4, S100A4, SEPT2, SOD1, SPTAN1, SPTBN1, STAT3, TLN1, UCHL1
Microtubule dynamics	1.93E-05	ACTR3, AKAP12, CANX, CAPG, CAPZB, CDC42, CFL1, CTTN, DBN1, DNM2, DSP, FLNA, FMR1, FN1, FSCN1, GSN, ITGB1, KPNB1, LAMC1, LASP1, MAP1B, PFN1, PRMT1, RTN4, S100A4, SEPT2, SOD1, SPTBN1, STAT3, TLN1, UCHL1
Organization of organelle	2.18E-10	ALDOA, ANXA2, CAPZB, CDC42, CFL1, COL1A1, COL1A2, COL3A1, CTNNA1, DBN1, DSP, FLNA, FN1, GOLGB1, GORASP2, ITGB1, JUP, LMNA, P4HA1, PLS3, RAB6A, SERPINH1, SOD1, SPTBN1, SURF4
Formation of cellular protrusions	5.08E-05	ACTR3, AKAP12, CAPG, CAPZB, CDC42, CFL1, CTTN, DBN1, DNM2, FLNA, FMR1, FN1, FSCN1, ITGB1, LAMC1, LASP1, MAP1B, PFN1, PRMT1, RTN4, S100A4, SEPT2, SPTBN1, UCHL1
Development of cytoplasm	3.41E-07	ACTR3, ADD1, ANXA1, Cald1, CAPZB, CDC42, CFL1, CORO1C, CTSD, CTTN, FLNA, FN1, GNB1, GPI, GSN, ITGB1, MAP1B, PDCD6IP, PFN1, STAT3
Formation of filaments	3.38E-07	ACTR3, ADD1, Cald1, CAPZB, CDC42, CFL1, CTTN, FN1, GNB1, GPI, GSN, HSPA5, ITGB1, MAP1B, PDCD6IP, PFN1, SERPINH1, STAT3, TCP1
Formation of cytoskeleton	2.96E-07	ACTR3, ADD1, Cald1, CAPZB, CDC42, CFL1, CORO1C, CTTN, FLNA, FN1, GNB1, GPI, GSN, ITGB1, MAP1B, PDCD6IP, PFN1, STAT3
Organization of filaments	3.44E-11	ALDOA, ANXA2, CDC42, CFL1, COL1A1, COL1A2, COL3A1, DBN1, DSP, FLNA, FN1, ITGB1, JUP, P4HA1, PLS3, SERPINH1, SOD1

Disease or function annotation	P-value	Molecules
Formation of actin filaments	7.56E-06	ACTR3, ADD1, Cald1, CDC42, CFL1, CTTN, FN1, GNB1, GPI, GSN, ITGB1, PDCD6IP, PFN1, STAT3
Outgrowth of neurites	5.97E-04	ADAM10, CDC42, CORO1B, FN1, ITGB1, LGALS1, MAP1B, PSAP, RTN4, S100A4, SOD1, SPTBN1, STAT3, YWHAZ
Neuritogenesis	2.74E-03	ACTR3, CAPZB, CDC42, DBN1, FMR1, ITGB1, LAMC1, MAP1B, PFN1, PRMT1, RTN4, SEPT2, SPTBN1, UCHL1
Morphogenesis of neurites	7.95E-04	ACTR3, CAPZB, CDC42, DBN1, FMR1, ITGB1, LAMC1, MAP1B, PFN1, PRMT1, RTN4, SEPT2
Quantity of filaments	1.79E-07	CDC42, CFL1, DNM2, DSP, FN1, GNB2L1, MAP1B, PLEC, SERPINH1, SPTAN1, STAT3
Quantity of cellular protrusions	1.12E-06	CANX, CAPZB, CDC42, CTTN, FN1, FSCN1, GSN, MAP1B, SOD1, STAT3, TLN1
Organization of actin cytoskeleton	3.53E-05	AKAP12, CDC42, CFL1, CORO1C, EPB41L2, FLNA, FN1, FSCN1, SEPT2, SPTAN1, TLN1
Assembly of cell-cell contacts	3.98E-05	CTNNA1, DSG1, DSP, FMR1, GNB2L1, ITGB1, JUP, LAMC1, RTN4, TLN1, YWHAG
Assembly of intercellular junctions	1.89E-04	CTNNA1, DSG1, DSP, FMR1, ITGB1, JUP, LAMC1, RTN4, TLN1, YWHAG
Organization of actin filaments	5.31E-07	ALDOA, CDC42, CFL1, DBN1, FLNA, FN1, ITGB1, JUP, PLS3
Reorganization of cytoskeleton	1.74E-04	AKAP12, CDC42, CFL1, DSP, FLNA, FN1, JUP, PLS3, SPTAN1
Formation of actin stress fibers	1.18E-03	Cald1, CDC42, FN1, GNB1, GPI, ITGB1, PDCD6IP, PFN1, STAT3
Formation of plasma membrane	1.21E-03	CDC42, CTNNA1, DNM2, FMR1, ITGB1, JUP, LAMC1, RTN4, YWHAG
Quantity of actin stress fibers	1.78E-07	CDC42, CFL1, DNM2, FN1, GNB2L1, PLEC, SPTAN1, STAT3
Organization of cellular membrane	2.88E-05	ANXA1, CAPZB, CDC42, CFL1, CTNNA1, DSP, LMNA, SPTBN1
Formation of cellular inclusion bodies	4.21E-05	CTSB, DNAJA1, HSPA4, PSAP, SOD1, SQSTM1, UCHL1
Formation of vesicles	1.50E-04	ANXA2, ANXA5, AP2A2, DNM2, FLNA, NSF, PDCD6IP
Polymerization of filaments	1.59E-04	ACTR3, ADD1, CAPZB, CDC42, CFL1, GSN, MAP1B
Stabilization of filaments	1.69E-04	CFL1, CTTN, DSP, FLNA, FMR1, MAP1B, STAT3

Disease or function annotation	P-value	Molecules
Formation of focal adhesions	7.25E-04	AKAP12, Cald1, CDC42, FN1, GNB1, ITGB1, NSF
Formation of lamellipodia	1.39E-03	ACTR3, CAPZB, CDC42, CFL1, DNM2, FN1, LASP1
Formation of filopodia	1.80E-03	ACTR3, AKAP12, CDC42, FN1, FSCN1, ITGB1, MAP1B
Organization of collagen fibrils	1.10E-06	ANXA2, COL1A1, COL1A2, COL3A1, P4HA1, SERPINH1
Quantity of focal adhesions	4.33E-06	Cald1, FLNA, FN1, GNB2L1, ITGB1, SPTAN1
Fusion of cellular membrane	2.06E-05	ANXA1, ANXA7, MYO1C, NSF, PSAP, USO1
Fusion of vesicles	5.68E-05	ANXA1, ANXA2, ANXA7, MYO1C, NSF, VCP
Organization of plasma membrane	1.92E-04	CAPZB, CDC42, CFL1, CTNNA1, DSP, SPTBN1
Reorganization of actin cytoskeleton	5.04E-04	AKAP12, CDC42, CFL1, FLNA, FN1, SPTAN1
Polymerization of actin filaments	8.09E-04	ACTR3, ADD1, CDC42, CFL1, GSN
Rearrangement of cytoskeleton	8.09E-04	ANXA1, ANXA2, CDC42, FN1, ITGB1
Quantity of intercellular junctions	8.66E-04	CAPZB, DSP, FMR1, JUP, SOD1
Retraction of cellular protrusions	1.90E-03	CDC42, FN1, GPI, GSN, MAP1B
Quantity of plasma membrane projections	2.73E-03	CANX, CDC42, FN1, MAP1B, SOD1
Growth of Golgi cisternae	6.73E-08	GOLGB1, NSF, USO1, VCP
Formation of actin cytoskeleton	1.25E-05	CORO1C, FLNA, FN1, ITGB1
Formation of podosomes	7.03E-05	Cald1, CDC42, CTTN, GSN
Disruption of cell-cell contacts	1.68E-04	ANXA1, GNB2L1, ITGB1, SOD1
Disruption of cytoskeleton	3.40E-04	GSN, ITGB1, LMNA, PLEC
Formation of actin	4.88E-04	ADD1, Cald1, CDC42, FSCN1

Disease or function annotation	P-value	Molecules
bundles		
Organization of Golgi apparatus	6.77E-04	GOLGB1, GORASP2, RAB6A, SURF4
Reorganization of filaments	6.77E-04	CDC42, DSP, JUP, PLS3
Formation of desmosomes	1.27E-06	DSG1, DSP, JUP
Stabilization of actin filaments	2.60E-04	CFL1, CTTN, FLNA
Formation of fibronectin matrix	3.35E-04	FN1, ITGB1, PDCD6IP
Size of focal adhesions	6.40E-04	Cald1, FLNA, NSF
Transport of mitochondria	6.40E-04	MAP1B, SOD1, UCHL1
Length of dendritic spines	7.71E-04	CDC42, DBN1, FMR1
Organization of cellular protrusions	7.71E-04	CAPZB, CFL1, FSCN1
Organization of actin stress fibers	1.26E-03	FN1, ITGB1, PLS3
Trafficking of vesicles	1.46E-03	ANXA5, AP2A2, RAB6A
Release of granules	3.06E-03	FN1, LGALS1, NSF
Extension of peripheral lamellae	1.18E-04	GSN, ITGB1
Fusion of vesicle membrane	1.18E-04	ANXA7, PSAP
Stabilization of hemidesmosomes	1.18E-04	ITGB1, PLEC
Transport of nucleus	1.18E-04	FN1, GPI
Assembly of axon initial segments	3.51E-04	SPTAN1, SPTBN1
Quantity of podosomes	3.51E-04	Cald1, CDC42
Retraction of filopodia	3.51E-04	CDC42, GSN
Binding of actin	6.97E-04	EPB41L2, YWHAZ
Formation of basal	6.97E-04	ITGB1, LAMC1

Disease or function annotation	P-value	Molecules
membrane		
Quantity of desmosomes	6.97E-04	DSP, JUP
Retraction of pseudopodia	6.97E-04	FN1, GPI
Depolymerization of actin	1.15E-03	CFL1, PLEC
Quantity of hemidesmosomes	1.15E-03	ITGB1, PLEC
Branching of nerves	1.72E-03	ITGB1, RTN4
Formation of multivesicular bodies	2.39E-03	ANXA2, PDCD6IP
Binding of ribosome	3.16E-03	EEF1B2, HSPA5
Elongation of actin filaments	3.16E-03	INF2, PFN1
Fusion of liposome	3.16E-03	ANXA1, ANXA2
Localization of vesicles	3.16E-03	CTTN, MYO1C
Modification of cytoskeleton	3.16E-03	GSN, S100A4
Quantity of membrane ruffles	3.16E-03	ADD1, SORBS2
Size of dendritic trees	3.16E-03	ITGB1, RTN4
Formation of caveolae	4.03E-03	ANXA6, PTRF

Appendix 6: List of publications, posters and presentations

List of Publications

Hunter G., **Aghamaleky Sarvestany A.**, Roche S.L., Symes R.C., Gillingwater T.H., 2014. SMN-dependent intrinsic defects in Schwann cells in mouse models of spinal muscular atrophy. *Hum Mol Genet.* (In press)

Aghamaleky Sarvestany A., Hunter G., Tavendale A., Lamont D.J., Llavero Hurtado M., Graham L., Wishart T.M., Gillingwater T.H., Label-free quantitative profiling identifies disruption of ubiquitin homeostasis as a key driver of Schwann cell defects in spinal muscular atrophy (In press)

Anatomical Society Summer Meeting 2013-Talk

Intrinsic defects in Schwann cells in spinal muscular atrophy

Euan MacDonald Centre Post-Graduate Seminar 2013-Talk

Intrinsic defects in Schwann cells in spinal muscular atrophy

Edinburgh University Neuroscience Day 2013

Intrinsic, SMN-dependent defects in Schwann cells in spinal muscular atrophy (SMA)